Plant Life Management
Midterm status of a R&D project

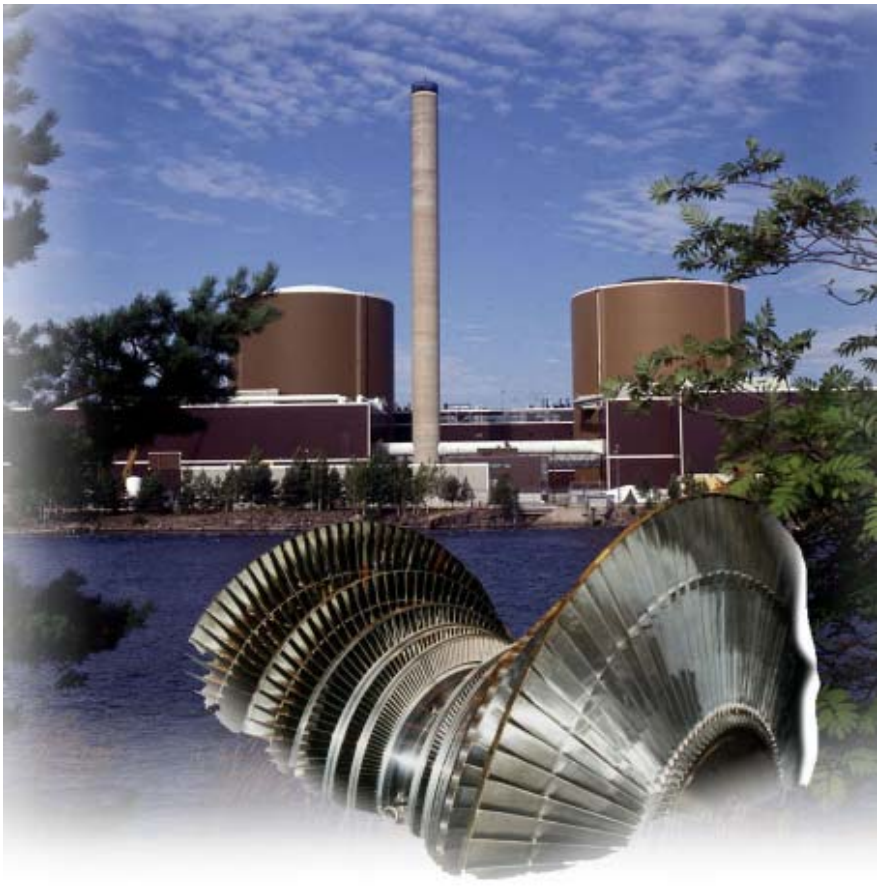

TECHNICAL RESEARCH CENTRE OF FINLAND ESPOO 2001

VTT SYMPOSIUM 218

Keywords: nuclear power plants, service life, life (durability), structures, stress corrosion cracking, aging (metallurgy), piping, vibrations, reliability

Plant Life Management
Midterm status of a R&D project

Edited by

Jussi Solin

VTT Manufacturing technology

Organised by

Technical Research Centre of Finland

TECHNICAL RESEARCH CENTRE OF FINLAND
ESPOO 2001

ISBN 951–38–5727–1 (soft back ed.)
ISSN 0357–9387 (soft back ed.)

ISBN 951–38–5728–X (URL:http://www.inf.vtt.fi/pdf/)
ISSN 1455–0873 (URL:http://www.inf.vtt.fi/pdf/)

JULKAISIJA – UTGIVARE – PUBLISHER

Valtion teknillinen tutkimuskeskus (VTT), Vuorimiehentie 5, PL 2000, 02044 VTT
puh. vaihde (09) 4561, faksi 456 4374

Statens tekniska forskningscentral (VTT), Bergsmansvägen 5, PB 2000, 02044 VTT
tel. växel (09) 4561, fax 456 4374

Technical Research Centre of Finland (VTT)
Vuorimiehentie 5, P.O.Box 2000, FIN–02044 VTT, Finland
phone internat. + 358 9 4561, fax + 358 9 456 4374

VTT Valmistustekniikka, Voimalaitosten materiaalitekniikka, Kemistintie 3, PL 1704, 02044 VTT
puh. vaihde (09) 4561, faksi (09) 456 7002, (09) 456 5875

VTT Tillverkningsteknik, Material och strukturell integritet, Kemistvägen 3, PB 1704, 02044 VTT
tel. växel (09) 4561, fax (09) 456 7002, (09) 456 5875

VTT Manufacturing Technology, Materials and Structural Integrity,
Kemistintie 3, P.O.Box 1704, FIN–02044 VTT, Finland
phone internat. + 358 9 4561, fax + 358 9 456 7002, + 358 9 456 5875

Otamedia Oy, Espoo 2001

Preface

A project on plant life management was started in 1999 for four years. The main activities during the first project year (from May 1999 to April 2000) were reported in VTT Research notes 2077, Plant life managemet (XVO) report 1999. This symposium describes subsequent results during the second project year in the two parallel projects: Rakenteellisen käyttöiän hallinta (XVO, Tekes dnro 171/401/00) and Ydinvoimalaitosten rakenteellisen käytettävyyden kehittäminen (YKK, Tekes dnro 278/480/00).

The papers in this symposium do not cover the project as a whole, but are selected to give an overview of the main achievements and challenges of the research and development efforts. Most papers have been presented in the project seminars in Olkiluoto, Loviisa, Helsinki and Porvoo during spring 2001. Additional papers have been edited on the basis of work reports and scientific publications prepared in this project. The first paper gives an overview of the project and Appendix A lists all public reports within this project.

The current compilation gives main emphasis to two topics: three inter-linked papers on life management of VVER reactor pressure vessels on pages 107 to 158 and four papers focusing on monitoring of water chemistry and assessing the influences on oxidation, cracking susceptibility and activity build-up on pages 169 to 240. However, all other papers are also closely related and the large activities on management of piping vibration and integrity, NDE and environment assisted ageing of stainless steels and superalloys shall not be overlooked.

The authors and research teams have done a great job. This would not have been possible without a rigid funding basis and open communication between the researchers and experts in industry. The funding organisations, Tekes, TVO, Fortum Power and Heat, Fortum Nuclear Services, Neste Engineering and VTT, the project steering group chaired by Mr. Juho Hakala of TVO, all experts and altogether about hundred people are gratefully acknowledged of their valuable contributions.

Espoo 20.6.2001
Jussi Solin

Contents

Joint research for operability and life management of NPP components

Jussi Solin, Rauno Rintamaa
VTT Manufacturing Technology, Espoo, Finland

Juho Hakala
Teollisuuden Voima Oy, Olkiluoto, Finland

Antero Tamminen, Jyrki Kohopää
Fortum, Finland

Abstract

Experimental and analytical research is being carried out in an industrially oriented project cluster dealing with estimating and managing lifetime of critical structures and components in energy industry. The research topics include systematic component lifetime management, lifetime of pressure bearing components, piping vibrations and integrity management, management of materials ageing, non-destructive inspection, water chemistry, oxide films and their role in service reliability and build-up of activity levels, stress corrosion cracking in Inconel welds, irradiation assisted stress corrosion cracking of core components, development of crack growth testing methods as well as the mechanisms of environmentally assisted cracking.

1. Introduction

With the support of the National Technology Agency (Tekes), VTT launched together with the Finnish nuclear power utilities – TVO and Fortum – an R&D project cluster to be performed in 1999–2002. Thanks to a small but powerful consortium having a lot of experience on mutual co-operation, together with the constructive attitude and help of Tekes, the first project was started fast and successfully [1].

To keep the project in focus, the initial work plans were based on current and anticipated challenges of the Finnish nuclear power plants. Broadening of the consortium and finalisation of the project structure was to be continued parallel to the execution. Technology transfer across the industry sectors is an important target. The nuclear industry may benefit of adopting approaches tested in other industry. On the other hand, part of the advances in conceptual solutions, materials science and other generic technology are transferable to other capital-intensive industry sectors where avoiding of unplanned outages is equally important.

The projects deal with systematic component lifetime management, piping vibrations and integrity, NDE, materials ageing, environmentally assisted cracking and interactions of process water and materials. This presentation gives an overview of the project cluster and discusses some generic approaches for component life management being developed within the project. The point of view is related to nuclear power.

2. Motivation of R&D for life management

2.1 Industrial experience

All four Finnish nuclear plant units – two boiling water reactors (BWR) at TVO Olkiluoto plant and two pressurised water reactors (VVER) at Fortum Loviisa plant – have operated with excellent usage factors for more than 20 years without any significant outages due to materials or structural integrity problems. The utilities are obviously very much interested to be able to continue this record and efficient operation long in the future.

The fact that the Finnish nuclear reactors have performed so well is a good proof of high technology and expertise in operation and preventive maintenance. Significant research efforts on critical components' ageing, structural integrity and lifetime management are continuously invested to maintain the excellent usage factors and to be able to continue operation long in future. VTT carries out important parts of this research.

2.2 Safety and economy points of view

In the case of nuclear power plants, safety and operability are never seen as competing demands for two reasons. Firstly, safety is never compromised. Secondly, the component life management and preventive maintenance actions performed due to safety can usually be justified by economic arguments as well.

Even small incidents and deviations from normal operation may lead to shutdown of the reactor. The time span for re-starting of the reactor is long and the minimum loss of production is large. Actually, the usage factors are so high that unscheduled outages must be rare events. Component ageing and maintenance needs shall be anticipated well in advance.

2.3 Continuous improvement strategy

The idea of continuous improvement was adopted to the nuclear regulation principles in Finland. In stead of getting a licence for 30 or 40 years in a time, the Finnish NPP's operate on shorter operation licences. Each renewal of operation licence is based on a safety review. The regulatory body requires that the utilities follow the international state of the art and adopt all feasibly available means to maintain and improve the safety.

On the other hand, continuous improvement is also needed for effective and long term utilisation of the primary capital investment to the plant, which is a major concern to the utility. The common interest to continuous improvements forms a good platform for co-operation between the authority and utilities. The continuous improvement strategy has already proven its benefits from both safety and operability points of view. The in-depth assessments and various safety improvements performed in relation to the Loviisa RPV safety case are a good example of this strategy.

3. Outline of the research activities

3.1 Project cluster

The development of the "XVO-YKK-RKK" project cluster is illustrated in Fig. 1. In 1999 a jointly funded research project was launched for one year under co-ordination of VTT. The following year the project was split into two parts. The more generic research containing parts were continued as the joint research project. Another halve was re-structured as an industry group R&D project under co-ordination of TVO and concentrating solely on nuclear components. Most of the R&D work was commissioned from VTT.

This year both projects were put together as an industrial R&D project. The industry group was expanded beyond nuclear industry and is comprised of six companies under co-ordination of TVO. Additional research suppliers were invited to join the team, but VTT still performs majority of the work. Some tasks are continued in separated research projects by the Helsinki University of Technology (HUT) and VTT.

3.2 Project organisation and co-operation

The total volume of work is about 2 M€ per annum. A few young researchers and students are occupied for the full time, but most of the work is shared between about 100 experts each contributing a couple of months, weeks or just days into the projects. Seventy people are involved at VTT, more than twenty at TVO and Fortum and a few at HUT.

The research teams of VTT are continuously in close contact to the experts in industry. Open communication between the researchers and utility staff is an essential success factor. It helps to guide the work and to obtain a balanced mix of long term research and problem-solving activities. The innovations become focused to issues having direct relevance to practice and the experts in industry can utilise the results in real time.

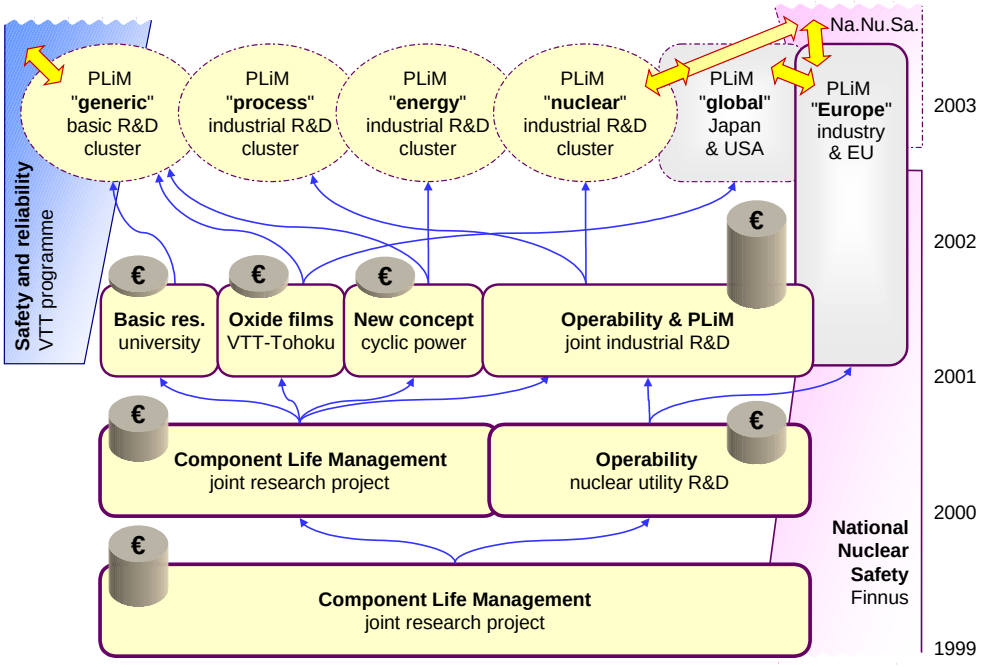

Figure 1. Development and a vision of the future of XVO-YKK-RKK project cluster since launching the XVO project in 1999.

Transparency and openness for co-operation and criticism are important values for all our activities on nuclear safety and operability. The project cluster has strong links to the national research programme on nuclear safety (Finnus) and the fifth framework programme of European Union, where generic technology is being developed from the safety point of view. VTT has also related activities funded by other industry in Europe and Japan. This is an important point, because the volume of this cluster is still insufficient for developing and running advanced experimental facilities needed for nuclear component life management.

Fortunately, transparency is still widely applied in the international research community. It makes synergistic co-ordination possible and enables efficient technology transfer through intensive networking.

3.3 Research topics

The projects are divided into subprojects and tasks. All of them aim to industrial applications, but with different time perspectives, Fig. 2. Development of capabilities and experience is funded by the industry – with the support of Tekes. The long term building of core competence is mainly funded by VTT. This has recently become possible through VTT's new internal funding instruments for strategic research.

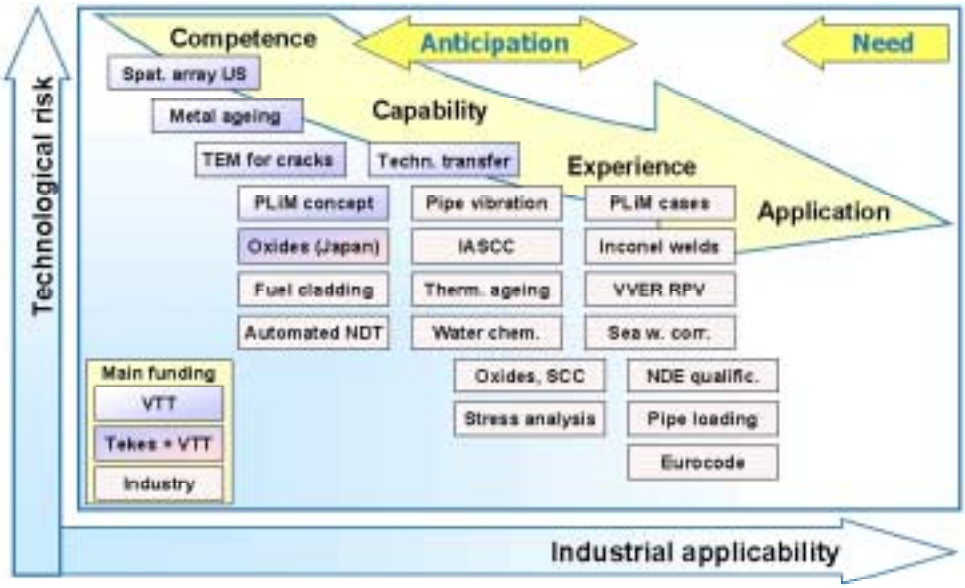

Figure 2. Mapping of current research tasks within the XVO-YKK-RKK project cluster (in 2001).

Furthermore, VTT and HUT receive Tekes funding also to certain projects. HUT develops and verifies theoretical models for explaining and managing environment assisted ageing and cracking of metals. VTT has sent a researcher to Japan for a post-doctorial exchange and co-operates with the Tohoku University's center of excellence on environment assisted fracture to model and measure behaviour of oxide films, which control the material ageing in NPP coolant loops.

The other papers in this proceedings describe in more detail the R&D efforts within the project. Some remarks on the research on corrosion, stress corrosion

cracking, pressure vessel integrity, NDE, piping vibrations, data base system for management of piping integrity and general methodology for component life management are given in the following.

4. Water chemistry and corrosion R&D

Nuclear reactors are designed to last for decades. This is being achieved e.g. by selecting the best materials and careful control of the water chemistry of the plant. Highly alloyed stainless steels and nickel-based alloys are employed for some of the reactor internal components to improve their corrosion resistance in high temperature water. [2, 3]

4.1 In situ monitoring of water chemistry

Control of water chemistry is an important topic for the power plants. VTT has developed and installed in situ monitoring cells to primary circuits of both Finnish NPP's. The cells contain special probes capable to monitor essential corrosion related parameters in high temperature water, Fig. 3. In addition, tens of material samples are deposited in another cell. The oxide films on the material samples are periodically investigated to clarify the oxide growth and properties together with the activity contamination during the plant operation cycles [4, 5].

4.2 Transpassive corrosion

The susceptibility of steels to localised corrosion is generally suppressed by alloying with high amounts of chromium. However, it renders the steel much more susceptible to general (transpassive) corrosion in highly oxidising environments. So far, transpassive corrosion has been investigated in other processes known to be highly oxidising, but a current question is, whether it can occur also in the reactor core area. The reason for his suspect is the hydrogen peroxide produced in the radiolysis reactions. The amount of H_2O_2 or occurrence of transpassive corrosion has not yet been measured in situ, but it should be possible in near future.

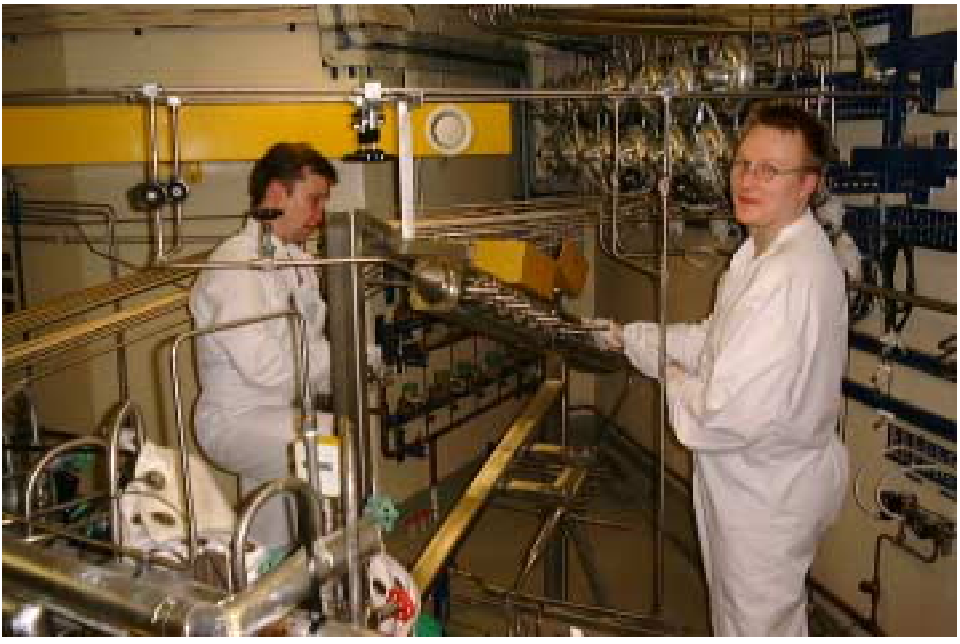

Figure 3. Installation of primary circuit water chemistry and oxide behaviour monitoring cells at theLoviisa plant.

4.3 Oxides and cracks

For estimation of corrosion rate and for determination of optimal content of the alloying elements, a quantitative model is needed for the behaviour of oxide films on the metal surfaces, Fig. 4. Investigations on behaviour of oxide films concentrated in stainless steels [6, 7] and zirconium alloys [8].

For corrosion to occur, species have to be transported through the oxide film and the rate of transport plays an important role in all corrosion phenomena. VTT researchers have developed a quantitative kinetic model of oxide films and, interestingly, the description of passive films is also compatible with recent findings on environment assisted cracking. The corrosion model predicts transport of atomic holes (vacancies) into the metal. On the other hand, diffusion of vacancies contributes to the crack growth according to the Selective Dissolution Vacancy Creep model of stress corrosion cracking [9].

So far, experimental findings support these two models separately. When combined, the models may explain initiation of cracks in BWR internal components.

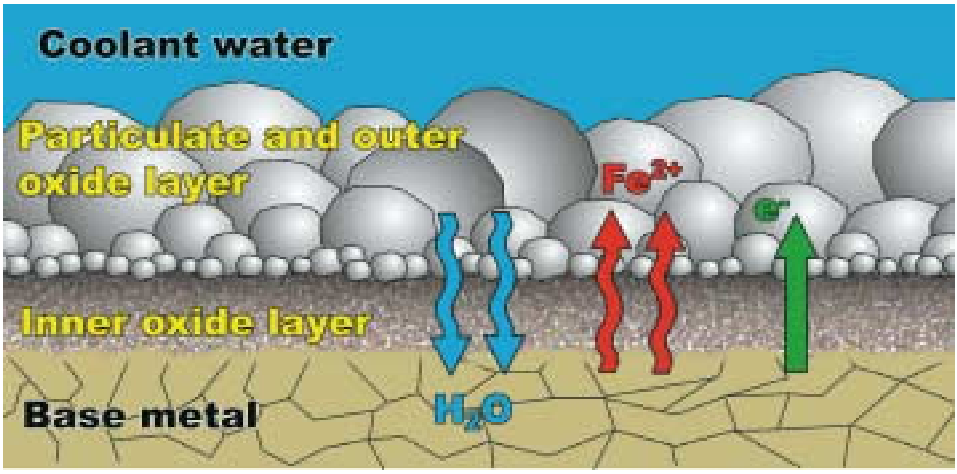

Figure 4. A scheme of typical oxide layers growing on metal surfaces.

5. VVER reactor pressure vessel life management

5.1 Radiation embrittlement

In light water reactors part of the fast neutrons escape outside the reactor core and hit the reactor pressure vessel (RPV) wall. These fast neutrons cause atomic scale defects in the crystallographic structure of the steel. The formed vacancies and displaced atoms may migrate and/or interact with the alloying elements and impurities present in the solution. Small precipitates, impurity clusters and grain boundary segregation may result. The hardness and strength of the steel are increased, but simultaneously the ductility decreases.

This radiation embrittlement of the RPV steel is a common problem in many pressurised water reactors (PWR), in particular in the Russian VVER designs from 70'ies. If suitable countermeasures were not introduced, embrittlement would become a life limiting factor for safe operation of the plant.

The circumferential welds in the Loviisa RPV have significantly higher copper and phosphorus contents than the base metal. These impurities influence the embrittlement mechanism and rate. Unfortunately, one of these welds is near the reactor core area and gets a notable fluence of neutrons during normal operation, Fig. 5.

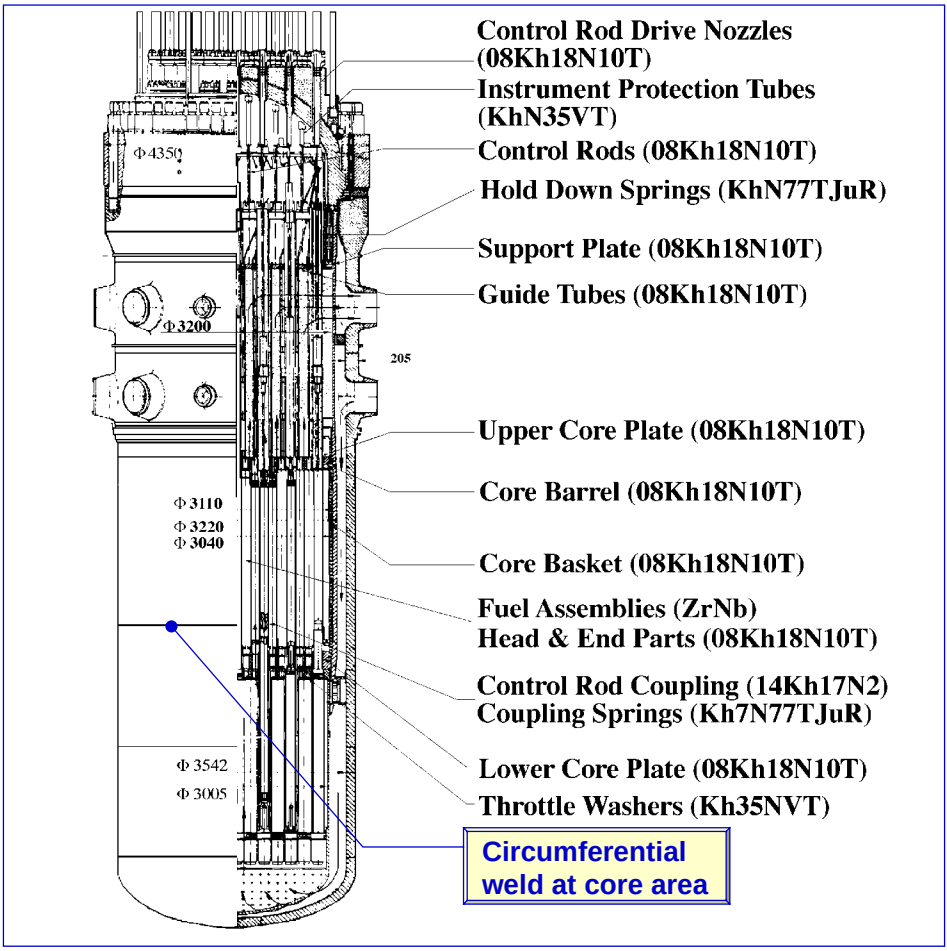

Figure 5. VVER 440 Reactor pressure vessel and location of the critical weld.

5.2 Mitigation methods and structural safety analyses

In order to maintain adequate safety level, several backfitting measures have been performed in Loviisa. The neutron flux and embrittlement rate was reduced

after receiving the first indications of anticipated problems. An increase of emergency core cooling water temperature and other process related changes followed to eliminate and reduce potential transients. Finally, the core weld of Loviisa 1 was successfully annealed in 1996. A current concern is to verify the post-annealing embrittlement rate in order to enable safe and economic life management of the RPV.

The structural safety analysis of the RPV is a comprehensive process leading to a fracture mechanics based integrity assessment. All input data and methodologies must be carefully verified, Fig. 6.

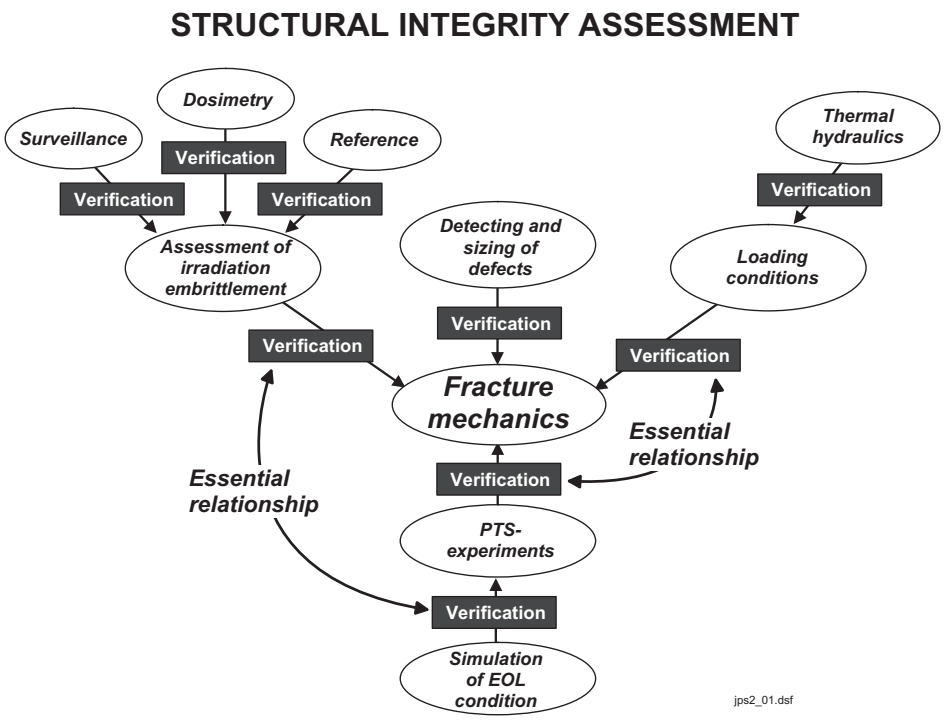

Figure 6. Methods and data for the RPV structural safety analysis.

5.3 Material annealing and re-irradiation behaviour

It is clear that shortage of time and relevant materials limits the creation of a data base for post-annealing material behaviour. A reliable model and verified data is

needed and extrapolations have to be made. As a first stage, vessel annealing required sufficient data on the material annealing behaviour. Later on re-irradiation behaviour has been the dominating goal for defining the material properties.

The material shortage problem was tackled by two different ways. Reconstitution of the broken surveillance specimens was introduced and used in the annealing and re-embrittlement studies since the middle of 1980s. Additionally, so called "tailored" weld material, which has similar chemical composition and initial transition temperature as the beltline weld of the Loviisa 1 RPV, was purchased.

The material research programmes supporting the annealing and post-annealing operation of Loviisa 1 are described in other papers in this proceedings.

5.4 Prediction of re-embrittlement rate

There are currently three main approaches proposed for predicting the post-annealing re-embrittlement rate: lateral, vertical or conservative shift approach, Fig. 7. All three approaches are based on the assumption that the re-embrittlement follows the same path as the embrittlement during the first irradiation cycle. The approaches differ by the definition of the beginning of the re-embrittlement in relation to the original embrittlement path.

The test results on re-embrittlement indicate that none of the approaches is physically correct. Based on the currently available results, a new tentative approach to describe the post-annealing re-embrittlement behaviour of Cr-Mo-V weld metals has been proposed by Dr. Kohopää and better described in other papers in this proceedings [10, 11, 12].

The new approach is based on the hypothesis that in the studied weld metals, the solute phosphorus content rather than the copper content is the governing factor in the post-annealing re-embrittlement. If the hypothesis can be verified, the total post-annealing embrittlement can be modelled by simply adding the residual embrittlement and the re-embrittlement due to phosphorus precipitation, and possibly also the embrittlement caused by matrix defect mechanism.

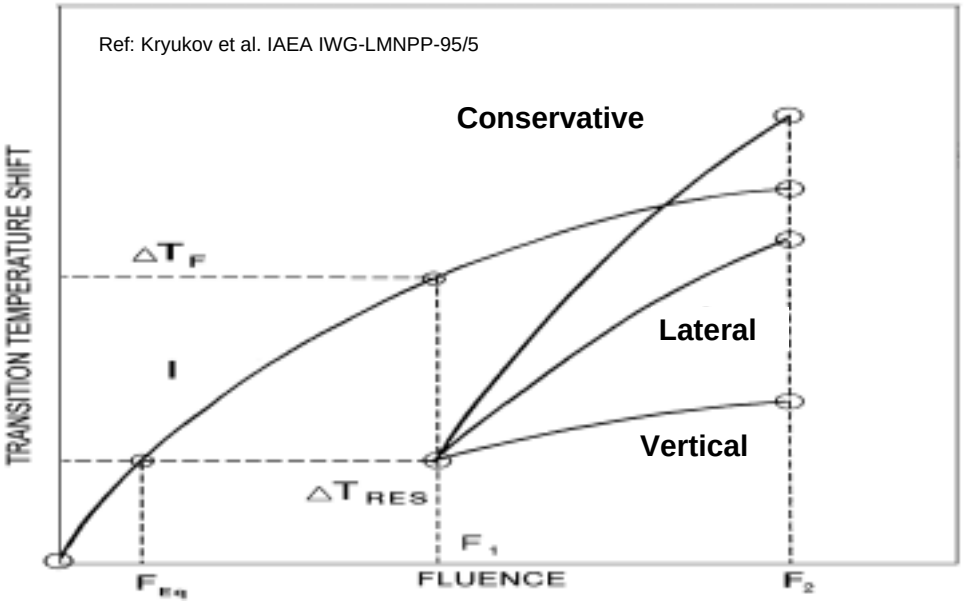

Figure 7. Currently available re-embrittlement models.

6. Developments in mechanised ultrasonic inspection and qualification of NDE

Reliability of non-destructive testing results has a direct influence on structural integrity assessment and safety of the inspected structures, e.g., NPP primary circuit pressure boundaries. Advanced technology together with highly skilled and experienced personnel is required.

One of the current trends is automation. Mechanised equipment can replace tedious manual work in positioning and moving of the transducers. Large areas can be scanned, analysed and numerically documented for direct comparison of eventual later repeated inspections. Another major trend is qualification, which aims to ensure that the inspection results are correct and fit for the purpose. The suitability and proper operation of equipment, methods and personnel, i.e. the whole chain, shall be proven. [13, 14]

6.1 A mechanised scanner for ultrasonic inspection

The long term motivation and main objectives of this development work are the following:

- Reduction in irradiation doses during inservice inspections at NPPs.
- Development of scanners for different components.
- Increased reliability of inspection.
- Enhanced possibilities for analysing the results.
- Qualification of the inspection.

In 1999 a new type of mechanised scanner for ultrasonic inspection of piping welds was constructed and first pilot inspections were performed at the Olkiluoto plant. Based on the experience gained in the inspection of piping welds the development of the scanner was continued in 2000. The target of the work was to develop further the applicability of the scanner to different inspection areas where the access is limited and the working conditions in manual inspection are difficult.

6.2 Novel features of the SC 2000 scanner

The novelty of the new scanner design is the positioning system that allows very rapid positioning on the inspection object. Furthermore, the height of the scanner was again reduced to enhance the applicability on inspection items where free space around the piping is lacking and the height of the scanner is a critical dimension limiting the access. Due to the lightness, compact structure and easy assembly of the scanner on inspection area the SC2000 scanner provides substantial benefits in environments where access or working time is restricted, e.g., due to irradiation doses in "hot parts of" NPP's. Different types of sensors can be attached to the scanner and also adaptation to various NDT-methods is possible. The new scanner with its positioning system is shown in Fig. 8.

Figure 8. SC2000 scanner for mechanised ultrasonic inspection of pipings.

6.3 Pilot inspections

The scanner SC2000 was used in pilot in-service inspections of piping welds in Olkiluoto plant. In addition, the scanner was adapted to the inspection of safe-end welds in the emergency cooling nozzles of reactor pressure vessel in the Loviisa plant. Both inspections were successful and demonstrated that the main targets of the scanner development were achieved.

6.4 Qualification of mechanised inspection

In order to improve the reliability of inspection the complete inspection system (equipment, personnel, procedure) was qualified following the Finnish Qualification practise described in the document The qualification of inservice inspections. This document is based on the European Methodology for Inspection Qualification (ENIQ). The inspection procedure and its technical justifications were evaluated by a Qualification Body formed by several experts of ultrasonic testing. Furthermore, the capability of the inspection technique was demonstrated in practise by arranging an open test with test block containing representative reference reflectors.

6.5 Development of Finnish practise for qualification of NDT

The development of the Finnish practise for inspection qualification is continued in co-operation with the utilities and major inspection companies. First pilot-qualifications were carried out connected to the in-service inspections of Finnish NPPs. One of these was the above mentioned qualification of the mechanised inspection of piping welds in Olkiluoto plant.

A document describing the structure of the qualification examination and the validity of qualification has been prepared for the Finnish Steering Committee for inspection qualification. This document gives the general outlines of the qualification examinations (content of theoretical and practical examinations) and describes the rules according which a qualification successfully performed for certain inspection item can be accepted to cover other inspection items of the same type. This practise is an important approach to reduce the number of expensive qualifications without reducing the reliability of the inspection.

As another pilot qualification the mechanised ultrasonic inspection of the shell welds of reactor pressure vessel of Loviisa NPP was performed. For this inspection a detailed inspection procedure and technical justifications were drafted. These documents were the first complete qualification documents prepared for Finnish NPPs and form a basis for further qualifications in the future.

7. Piping vibrations and piping integrity management

Traditional design and condition monitoring of piping is mainly based on postulated events and on the application of allowable vibration levels. This approach gives only indirect information on the loading at the critical locations and generally leads to over conservative assessments.

7.1 Piping vibration management

Relevant information about the actual loading state and condition of the piping could be obtained by comprehensive direct measurements, but in practice, the amount of measurement points must be strictly limited. Therefore, a practical method based on measurements accompanied by detailed finite element (FE) analyses is being sought for. The target is to be able to manage piping vibrations and related integrity concerns by using a minimum number of fixed continuous measurements and on an adequate numerical model. [15]

Many actual structural details can be rather difficult to model or they may deviate significantly from design documents. So, often an iterative process is needed to obtain adequate agreement between computational and experimental results. This goal may be achieved using special purpose tools designed to update Finite Element analysis models with experimental data (modal correlation). Probably several iteration cycles are needed to come up to an adequately working FE model, Fig. 9.

7.2 Analysis of pilot pipelines

The R&D work is realised through studying selected pipelines supported by the general development needed. Another special feature of the R&D work is that the modelling work will utilise the piping and loading database systems being developed in parallel - as described in another paper in this proceedings.

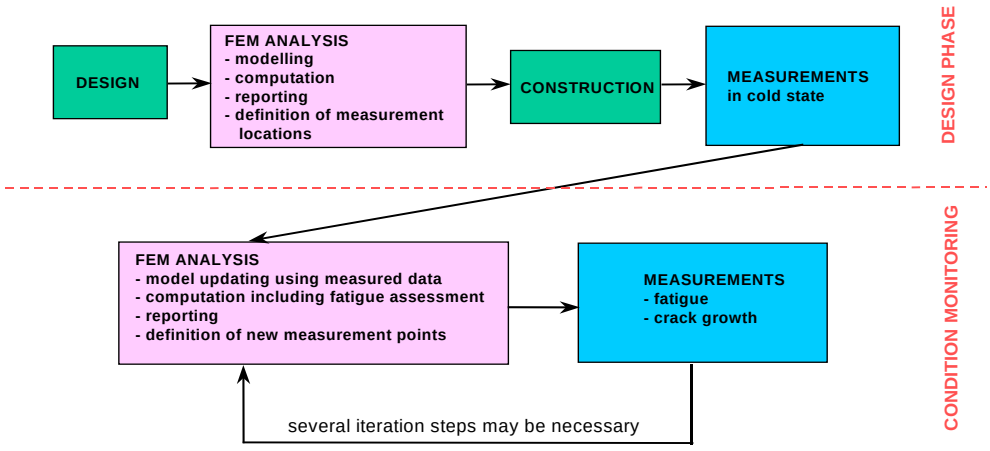

Figure. 9. An approach to come to an adequate model to monitor the vibration behaviour of a piping system.

Finite element analyses are carried out using the ABAQUS code. For the first pilot piping, one model was built according to the available design drawings. In the following cases (2 and 3) the geometry of the model was modified according to the observations and measurements carried out at the plant. For case 3 the water level was corrected to correspond to the expected vacuum.

The FEMtools code was used to compare the measured and calculated results and in updating the model (case 4) but the automatic updating procedure was not yet used. The FEMtools code is found to be an effective tool in comparing and studying measured and numerical data. The modeling of the supports according to the inspection clearly improved the numerical results whereas the effect of the measured wall thickness variation was of minor importance.

Manual updating improved the results further. The use of the automatic updating available in FEMtools is successful only when the original model is already relatively close to the measured data. One possible reason for differences is that at certain measurement points only the displacements in both horizontal directions were measured and the vertical ones had to be interpolated. The effect of the mesh used in the model should be carefully studied before any further updating. It is also necessary to continue the work by describing the supports in the model with beam elements instead of springs so that their vibration properties

can be described more realistically. The final updated model will be loaded using the excitation calculated by a special purpose code. Further work will be performed with two other piping cases.

7.3 Integrated database system for managing piping integrity

To make fitness, safety and lifetime related assessments for class 1 nuclear piping, the amount of necessary input data is considerable. At the same time it is essential that the data is reliable and up-to-date. Often it has to be collected in a very short time.

A relational database system, consisting of separate geometrical, material, loading and reference document databases is being developed by TVO and VTT. The system is developed to facilitate effective analyses of the piping and generation of the associated documentation, Fig. 10.

The system is meant to contain all up-to-date information necessary to analyse and monitor piping systems for an existing and operating plant. The system is basically an "as built" system and is not meant as a design tool although parameter studies should be possible. All data in the system will be accompanied by the necessary information with regard to dates, version and validity. For the sake of updating, it is very important that data is never duplicated. Use of relational database architecture provides a possibility to share any information without duplicating. For example, in case a load definition is changed, the system will "know" that the subsequent strength analysis and the associated results are not valid anymore. It is very important that subsequent analysis, like fatigue and fracture analysis, uses up-to-date input.

The system will be built up of separate and stand-alone databases and program modules. Thus, different parts can be used for their own purpose without the whole system having to be completed or in use. Commercially available programs will be used as much as possible, but for special purposes, customised programs will be developed. [16]

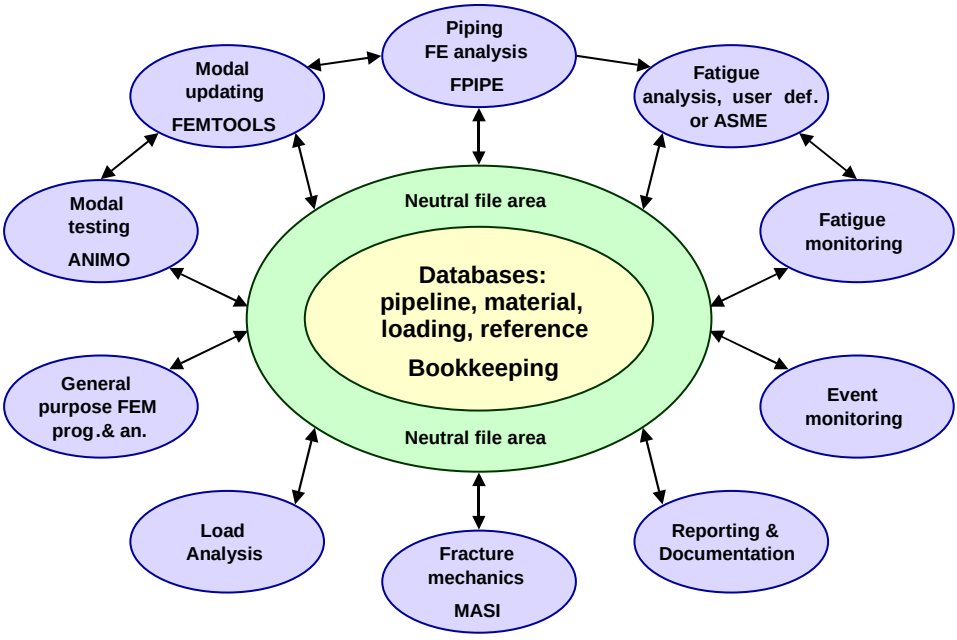

Figure 10. Relational database and program system being developed for TVO piping systems.

8. Systematic component life management

Many power and process industries are currently developing preventive maintenance and plant life management systems for their own use. Consideration of plant specific design and integrity problems support use of tailored programs and/or data bases for plant life management. The final applications will be developed on plant type, utility, plant or system level. However, common features can be included in the systems.

The project cluster, as a whole, deals with systematic component lifetime management, piping vibrations and integrity, NDE, materials ageing, interactions of coolant and materials, environmentally assisted cracking and ageing of reactor internals. The aim of one subproject is to define, how the results can be combined and applied in practice in an efficient way. The parallel disciplines shall be integrated such that quantitative assessments on remaining safe life and failure risks are possible. Fig. 11 shows a general scheme of component lifetime management followed in the current project.

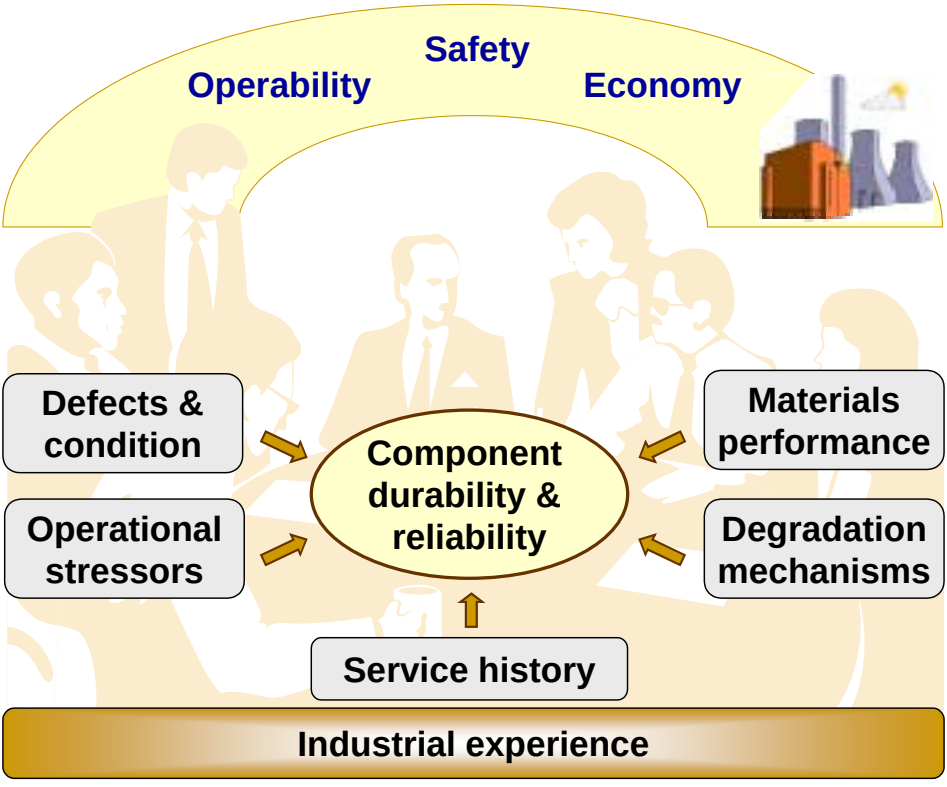

Figure 11. A general scheme for component lifetime management.

Systematic component lifetime management serves two parallel needs. The safety requirements set a mandatory basis for all operations. Operability needs originate from economical interests and market restrains.

Knowledge is needed on

- relevant ageing mechanisms and their impact on the selected components,
- materials performance in the process environment and subjected to the operational loads,
- condition of the materials and components,
- operational stressors in normal steady state operation and in transients,
- service history of the particular component, and
- general industrial experience in similar plants.

8.1 System design

Quantitative safety assessments can only be achieved through probabilistic approaches. For that purpose correct models on ageing mechanisms and the influencing factors are needed, but well-founded simplifications are also necessary. Another point is user friendliness. If the utility staff is supposed to input a huge amount of data and knowledge in the system, it must be fully compatible with the existing data management systems. The additional work shall be minimised and kept simple to be able hire temporary staff, e.g. students, for data input.

One possibility is to utilise modularity in a similar way as in the development of a database and program system for piping integrity assessment, Fig. 10. Actually, the TVO approach for piping integrity has turned out very successful and the development has reached phase enabling to consider expansion of the activity to cover other components as well.

8.2 Safety margins

The western nuclear safety relies on multiple barrier philosophy. The probability of abnormal transients and events is minimised as close to zero as possible. However, the plant must still be designed and maintained to tolerate even such events without causing a severe accident. This means that in addition to their normal operational function, components like fuel cladding tubes, reactor pressure vessel (RPV) and containment also act as physical barriers in case of accidents.

Both functions set high requirements on the integrity and ageing management of these components. All relevant stressors[1] must be considered in both cases. Ageing of materials and structures depends on the stressors acting during normal operation, start-up, shut-down and other normal transients. But in most cases the safety margins are more critical in the postulated abnormal conditions. In other words, the ageing rate and acceptance criteria may be based on totally different loading cases.

---

[1] "stressors" has a meaning broader than stresses, mechanical, thermal, chemical and other factors are included

8.3 Probabilistic ageing management

Quantitative safety assessments can only be achieved through probabilistic approaches. For that purpose accurate models on ageing mechanisms and the influencing factors are needed.

The Master Curve approach [ASTM E 1921-1997] has been developed by Kim Wallin of VTT for statistical analysis and application of fracture mechanics test data for quantitative assessment of RPV embrittlement and fracture risk. Similar approaches for other ageing mechanisms are sought for. It has been realised that statistical modelling of environment assisted cracking will be a big challenge. However, modelling of fatigue would be a reasonable target. A lot of suitable input can be found in literature on automotive and aircraft fatigue. Relevant solutions have been developed also at VTT in collaboration of other industries [17]. So far, development in fatigue assessment has targeted on the design phase and further work would be needed to adapt it suitable to post-design phases - and eventually to other failure mechanisms.

8.3.1 Statistically defined design criteria

Statistically defined fatigue design criteria are already used in automotive industry, where quantitative failure probabilities are of great importance. For example, the allowable failure probabilities for different components in Wärtsilä diesel engines are defined based on the importance of the component and the fatigue design curves are matched to fulfil these criteria [18].

One important lesson learnt in relation to determination of those design curves has been the – not so surprising fact – that the normally used experimental testing programs suitable for determining mean curves can be quite ineffective for determining the design curve. If the target is a design curve for a failure probability of 10^{-3} (which is still quite moderate), the value and uncertainty of standard deviation affect three times more than the value or uncertainty of the mean fatigue strength. But with a certain number of specimens, the mean value can be easily measured with a higher precision, at least for high cycle fatigue applications.

8.3.2 Unified approach for design and life management

Component design and life management are sometimes seen as different disciplines. However, they can also be integrated as illustrated in Figs. 12 and 13. The above, for fatigue in design phase discussed, probabilistic analysis could perhaps be generalised for component life management. For critical components in-service probabilistic assessment provides a significant saving potential at reasonable cost.

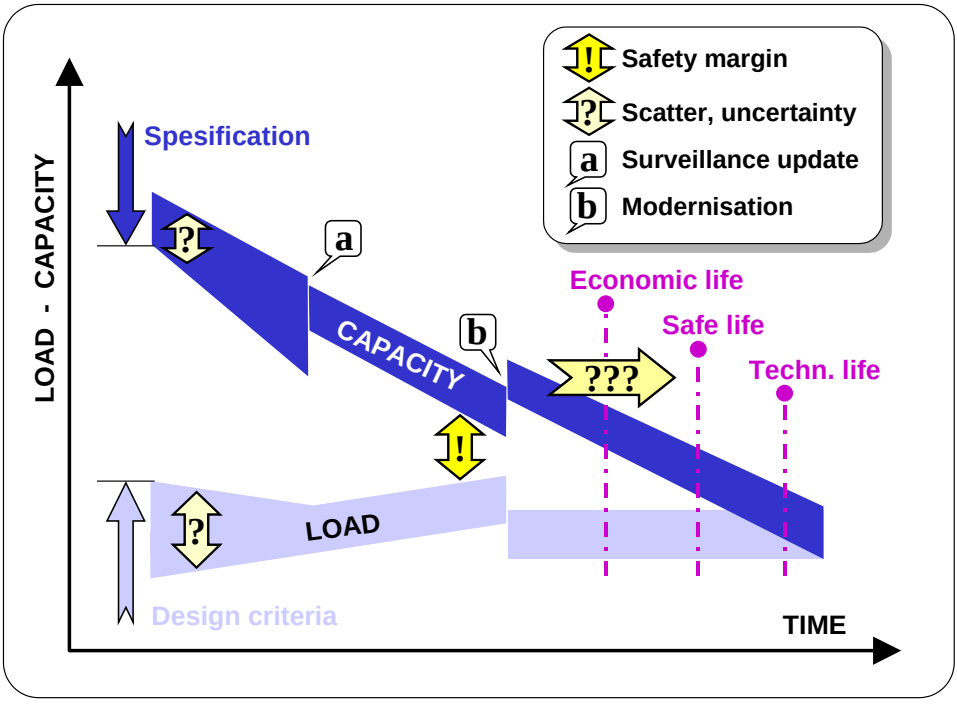

Figure 12. A schematic model for probabilistic component life management.

Monitoring of temperature transients and other stressors can reduce the uncertainty in the required capacity of component or material. On the other hand, surveillance studies may give reason to reduce the assumed uncertainty of material performance, i.e. scatter band of the capacity, see (a) in Fig. 13. In case the assessment results in an insufficient prediction of remaining economic or safe life, modernisation is needed, see (b) in Fig. 13.

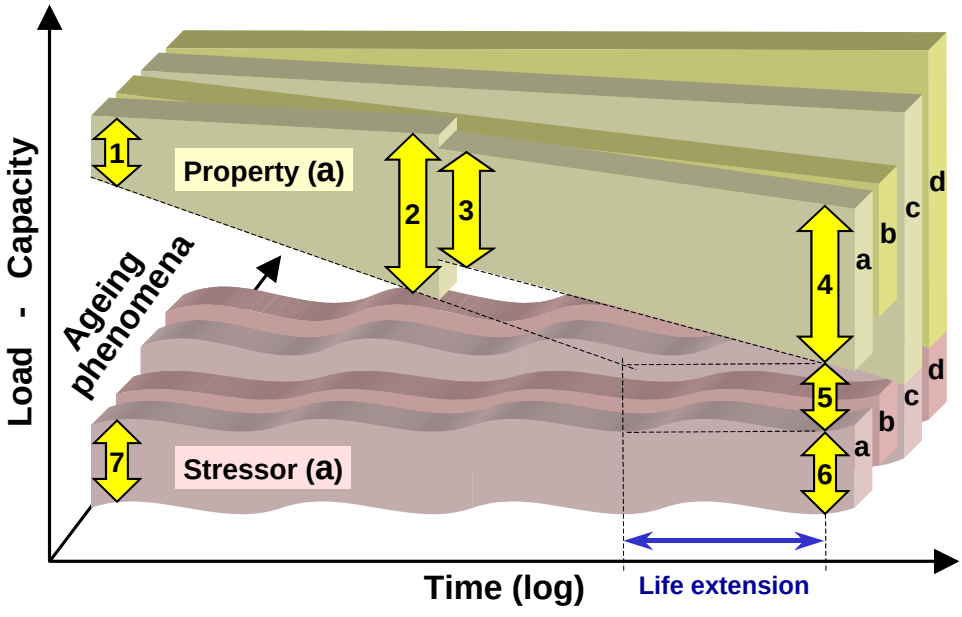

Figure 13. A schematic model for integrated component life management.

The above outlined model is not complete. A couple additional aspects are illustrated in Fig. 13. Firstly, the component – or plant – life does not depend on one single load-capacity pair. A similar analysis should be performed for all relevant components and all relevant stressor-property pairs. Fortunately, most of the possible life limiting factors can easily be excluded or shown non-critical. It may still be worth of noting that if a power plant is operated, e.g., for 60 years, there will come another generation of engineers. Also the non-critical considered failure models and basic arguments to exclude them from a deeper study should be documented to be easily available in future. The second aspect brought up in Fig. 13 is the link between design and life management. They should not be separated, as shown for the stressor-property pair (a).

Theoretically, the first input for a design project is the required safety margin (5), which shall remain at the end-of-life (EOL) condition. Next step could be searching of a material (or other) solution providing a good EOL property (4) at a reasonable cost. The selection gives the property specification (lower bound of 1) to be set for the manufacturer. By fixing a design life and an allowable ageing rate, the lower bound of EOL property (4) can be refined. By applying the safety margin (5), a criterion for the EOL stressor (6) upper bound is obtained. Fur-

thermore, by considering the eventual in-service changes of the stressor, the design criterion (7) can be set.

Component specific stressor and property values, scatter bands and ageing rates can be re-addressed during the operation phase. Added knowledge ($2 \rightarrow 3$) and eventual modifications can increase safety and extend the anticipated life.

9. Conclusions

Condition and life management of nuclear power plant components is a broad topic requiring systematic research and development. The industrial experience and innovations generated along the R&D activities show a good record in Finland. However, the future will bring new challenges. At least part of them can be anticipated and relevant capabilities are already being developed. Maintaining of safe and economic operability of the Finnish NPP's long in future requires continuous research and development. The current team work models are recommended for effective planning and execution of the joint research.

Acknowledgements

This presentation is prepared within the project Structural operability and plant life management (RKK), which is coordinated by Teollisuuden Voima Oy. The work has been funded by the National Technology Agency (Tekes), Teollisuuden Voima Oy (TVO), Fortum Power and Heat Oy, Fortum Nuclear Services Ltd., FEMdata Oy, Neste Engineering Oy, Fortum Oil and Gas Ltd. and VTT Manufacturing Technology. Their funding is gratefully acknowledged.

References

1. Solin, J. (ed.) Plant life managemet (XVO) Report 1999. VTT Research Notes 2077. Technical Research Centre of Finland, Espoo 2000. 68 p. + app. 3 p.

2. Muttilainen, E., Hietanen, O., Aaltonen, P. & Ehrnstén, U. 2001. Prevention of stress corrosion cracking in piping welds. In this book. Pp. 159–168.

3. Toivonen, A., Aaltonen, P., Nenonen, P., Ehrnstén, U., Käki, A., Valo, M., Kukkonen, A. & Hietanen, O. Irradiation assisted stress corrosion cracking of core components. In this book. Pp. 241–253.

4. Bojinov,M., Ehrnstén, U., Kinnunen, P., Laitinen, T., Mäkelä, K., Saario, T., Sirkiä, P., Taivalaho, L., Buddas, T, Halin, M. & Tompuri, K. Activity incorporation into the oxide films on stainless steel samples exposed to primary coolant in Loviisa 1 unit. In this book. Pp. 211–240.

5. Bojinov, M., Kinnunen, P., Laitinen, T., Mäkelä, K., Saario, T., Sirkiä, P., Helin, M., Muttilainen, E., Nousiainen, P. & Reinvall, A. Monitoring of BWR water chemistry and oxide films at Olkiluoto 1. In this book. Pp. 179–194.

6. Bojinov, M, Laitinen, T., Mäkelä, K., Mäkelä, M., Saario, T., Sirkiä, P., Buddas, T., Halin, M. & Tompuri, K. Stability of oxides on stainless steel during simulated PWR shutdown and start-up. In this book. Pp. 195–210.

7. Bojinov, M., Laitinen, T., Mäkelä, K., Saario, T., Sirkiä P., Toivonen, A., Muttilainen, E., Reinvall, A. & Balachov, I. Protectiveness of oxide films in simulated BWR crack conditions, SO_4^{2-} enrichment and cracking susceptibility. In this book. Pp. 169–178.

8. Bojinov, M., Hansson-Lyyra, L., Laitinen, T., Mäkelä, K. & Saario, T. In-situ Studies of the Oxide Film Properties on BWR Fuel Cladding Materials. In this book. Pp. 255–264.

9. Jagodzinski, Yu. & Hänninen, H. Modelling of Material Ageing. In this book. Pp. 265–268.

10. Kohopää, J., Tamminen, A., Valo, M. & Solin, J. Innovations on life management of VVER reactor pressure vessels. In this book. Pp. 107–126.

11. Valo, M., Shtrombakh, Y., Kryukov, A., Vodenicharov, St. & Kohopää, J. Tentative re-embrittlement analysis for WWER-440 welds after annealing. In this book. Pp. 127–140.

12. Valo, M. The year 2000 contribution towards quantitative estimation of irradiation and re-irradiation effects on material toughness. In this book. Pp. 141–158.

13. Kauppinen, P., Pitkänen, J. & Kuusinen, P. Developments in mechanised ultrasonic inspection and qualification of NDE. In this book. Pp. 91–96.

14. Paussu, R., Pitkänen, J., Särkiniemi, P., Jeskanen, H. & Elsing, B. Ultrasonic inspection of a reactor pressure vessel from outside surface. In this book. Pp. 97–106.

15. Smeekes, P., Talja, H., Saarenheimo, A. & Haapaniemi, H. Piping Vibration Management Combining Measurements and Numerical Simulation. In this book. Pp. 55–66.

16. Smeekes , P., Lipponen, A., Talja, H. & Raiko, H. Integrated Approach and Database System for Managing Load Cases and Integrity of Piping Systems. In this book. Pp. 35–54.

17. Marquis, G. & Solin, J. Thermal fatigue of NPP components: potential multiaxial, environmental and small cycle effects. In this book. Pp. 67–89.

18. Rabb, R. 1998. Life time evaluation of spectrum loaded machine parts. VTT Symposium 181. Fatigue Design 1998. Vol. 1. Pp. 85–96.

Integrated Approach and Database System for Managing Load Cases and Integrity of Piping Systems

Paul Smeekes
Teollisuuden Voima Oy, Olkiluoto, Finland
Aarne Lipponen, Heli Talja
VTT Manufacturing Technology, Espoo, Finland
Heikki Raiko
VTT Energy, Espoo, Finland

Abstract

To make fitness, safety and lifetime related assessments for class 1 nuclear piping, the amount of necessary input data is considerable. At the same time it is essential that the data is reliable and up-to-date. Often it has to be collected in a very short time.

This paper outlines the contents of the database system, consisting of separate geometrical, material, loading and reference document databases, which is being developed by TVO and VTT. The system is developed to facilitate the analyses of class 1 piping and generation of the associated documentation.

1. Introduction

In existing power plants, the number of people responsible for load, structural and vibration related projects might be very limited. This means that tasks related to obtaining starting points, performing an analysis and preparing documentation might be the responsibility of just one person. This person will be asked questions like:

- We want to make a change, what are the implications?
- We had an abnormal event, what are the implications?

- We want to make a risk assessment, where do we get the starting points?
- We need up-to-date information to order a new valve, please supply?
- During the inspection we found a crack, can we run until next year's outage?

These are short questions with often not much longer answers, but a lot of work and an adequate and up-to-date documentation is necessary to give the answer. The latter may be a real problem for several reasons, such as:

- Load and strength analyses for different systems have been done over tens of years time span.
- These analyses may have been performed and documented by different persons in different ways using different tools and have even been archived in different ways and at different locations.
- During the lifetime of the plant, there may have been a power uprate, major piping and equipment exchanges and modernization projects. The documentation may not have always been fully updated.
- Changes performed in the plant may not affect the as build structures, but may affect future changes.

Some or all of the above reasons may have led to a difficult-to-use load and strength archive.

Still there may be many situations where reliable and up-to-date information is needed fast. For this reason, the development of the pipeline and monitoring system was started

2. General information with regard to the system

The system presently under development is meant to contain all up-to-date information necessary to analyze and monitor piping systems for an existing and operating plant [1]. For a start only the TVO OL1 and OL2 plant will be entered into the system. The system is basically an "as built" system and is not meant as a design tool although parameter studies should be possible. All data in the

system will be accompanied by the necessary information with regard to dates, version and validity. It will be possible for instance to keep an "as-designed/standard" version and an "as-built/measured" version. The latter could for instance contain updated support information that has been acquired through vibration measurements and modal correlation [2]. Other versions could be kept as well.

In case a load definition is changed, the system will "know" that the subsequent strength analysis and the associated results are not valid anymore. It is very important that subsequent analysis, like fatigue and fracture analysis, uses up-to-date input. In that way, the remaining lifetime can be estimated and the need for actions determined. And with a growing importance of parameter studies and probabilistic analysis, like for instance analysis related to Risk Informed In-Service Inspection (RIISI), it is more and more important to have the input data to the analyses in a flexible and readily available electronic format.

A data organization like this requires a lot of bookkeeping. The bookkeeping routines have not yet been developed, but the necessary facilities are available. The development has been started and will be one of the main issues in the year 2001.

The system will be built up of separate and stand-alone databases and program modules. Thus, different parts can be used for their own purpose without the whole system having to be completed or in use. Commercially available programs will be used as much as possible (database development, piping structural and hydraulic analysis, FEM, CFD, etc.). For special purposes, customized programs will be developed (crack growth, event monitoring etc.).

When ready, the system can be logically divided into three main areas of databases, application programs and interfaces, Fig. 1.

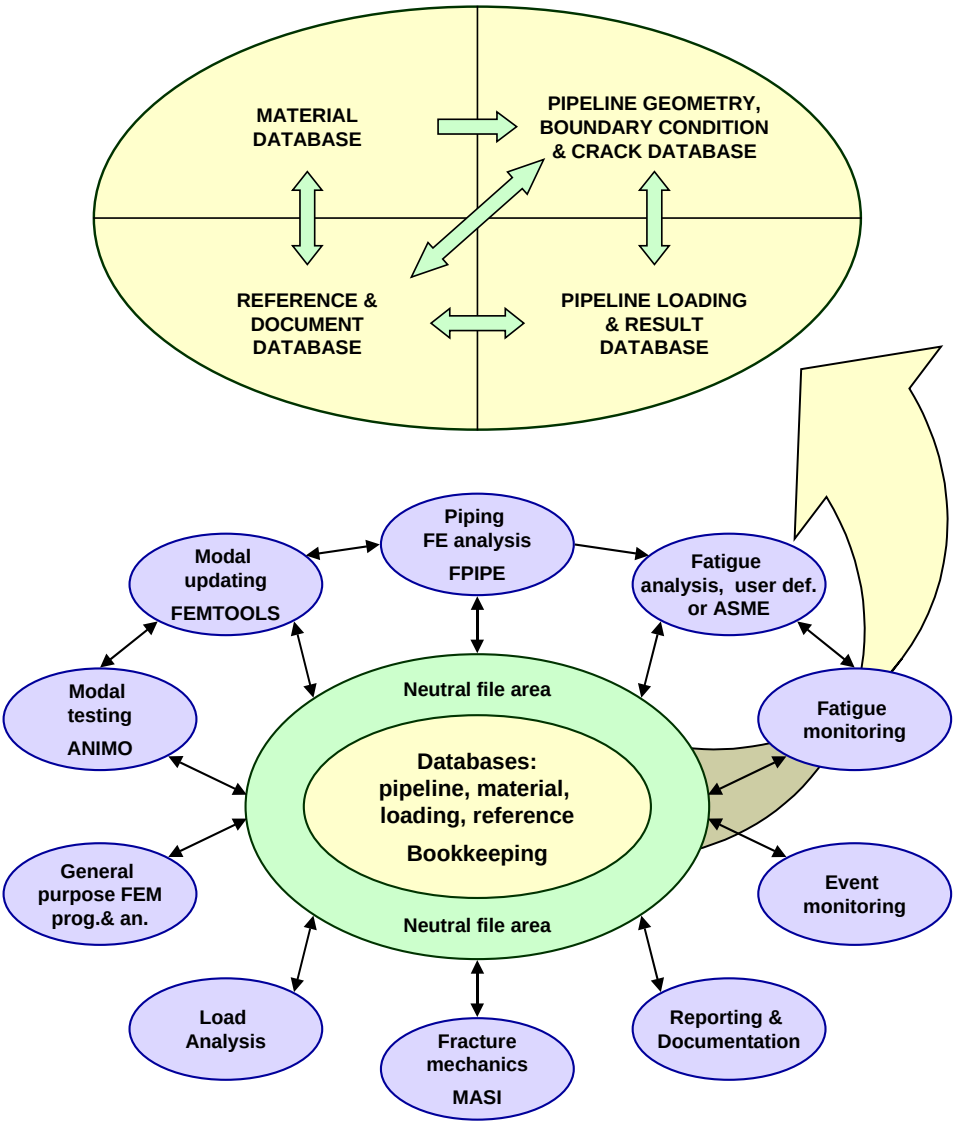

Figure 1. Structure of the pipeline analysis and monitoring system.

2.1 Interconnected databases

The core of the system consists of several interconnected databases and their user interfaces, and is called the database area. The contents of some of these databases are described in more detail in the next section. The different databases are edited with their own user interfaces that are designed to give

visual information alongside alphanumerical. According to the present plans, control and navigation is, as far as possible, handled from this level. For the moment the database area contains the following five databases:

1. The piping database, containing information like geometry, material, contents, isolation, loading, boundary conditions, detected cracks etc.
2. The material database, containing all information with regard to the materials referred to in the piping database. These properties may be standard properties or measured ones.
3. The loading database containing all information with regard to loads, loading combinations, ASME design and service limits, design events and occurred events. This database is very complex. It has been described in more detail in [3].
4. The result database containing all significant information with regard to the analysis results like stresses, displacements etc. The presence of the analysis results in the database gives the possibility to perform subsequent analysis without first having to go through the stress analysis.
5. The report database containing the documentation that is related to the previous items. Input made to and documentation produced by the technical databases will refer to the relevant documents from this database.

2.2 Application programs

At the outer border of the system are the application programs. This is called the application program area. As far as possible these programs shall use data from the databases and run in batch mode. However, if necessary, data from external sources can be used. This may be the case when some new data for the database is obtained with special purpose programs. Basically, the application programs can be of two types:

1. Commercially available analysis programs to perform structural, flow, thermal, fatigue, fracture mechanical and/or other analyses.
2. Tailor made analysis modules to perform post processing of previously obtained results, event monitoring, fatigue monitoring, crack growth monitoring, definition of inspection intervals etc.

2.3 Database interfaces

“Neutral” files are used as interface between the databases and the application programs. A neutral file is typically a batch-input file to control the flow of the analysis modules and to supply the input for the subsequent analysis. This means that an interface module is necessary to write the necessary data from the database into the neutral file and in the right format. Than either this file shall be submitted to the application program. Similar interface modules are made to extract significant data from the analysis program results into the database.

Although information is divided over several databases, one of the main principles in this project is that no information that may be used as input to an analysis is allowed to occur more than once. Another main principle is that all data shall be accompanied by a date, a validity indication and if possible a source reference.

Every part of the system will be completely documented. The documentation will consist of a user manual and a reference manual.

3. Elements of the database system

3.1 Piping database

The piping database consists of the piping geometry and all other information necessary to perform analysis. Therefore, it also contains information on welds and equipment, boundary conditions and the materials of, in and around the piping. The organization of piping geometry in the database is similar to the organization of piping systems and related drawings at TVO. This organization is as follows:

- At the first level, the system is found with the system identification number. Examples of systems are the feed water system (system 312) and the relief system (system 314). Drawings at this level are called system isometrics.
- At the second level, the main parts of the system are found. The feed water system for instance is divided into parts called 312 BAA-1, 312

BAA-2, 312 BCA-1 and 312 BCA-2. There are no separate drawing series at this level.

- At the third level, the piping geometry is divided into isometrics and associated part lists. At this level, the drawings have a part name followed by a sequential number, like 312 BCA-2-1, 312 BCA-2-2 and 312 BCA-2-3. This is the lowest and most detailed level of piping drawings available at TVO. There is one input table for every isometric.

The above choices were made to make organization of the database easy and recognizable for all possible users at TVO. Furthermore, possible future electronic drawings will be organized in the same way and this will ease the data exchange between the systems.

Further division was made according to normal FEM convention. This means that the database contains nodes and elements with all sorts of associated properties. In this context "elements" refer to geometrical elements like straight piping parts or pipe bends and "nodes" to the points connecting these elements. This means that a new element starts whenever there is a change of any of the element properties. Separate nodes will also be appointed to welds or nodes that shall be analyzed later on. Taking these rules into account is the work of the person entering data into the system and is very important when designing and building the database model.

However, the database model is not meant to be equal to the associated finite element model. It is meant to contain an as-build representation of the actual geometry inclusive main equipment, see also Fig. 2. This means that for instance additional nodes, necessary to perform a sound dynamic analysis will not be added in the database building stage. For this case the FPIPE program [6] will be further developed. It will be enhanced with routines to automatically change the model and, by the use of an iterative solution method, come to an optimum solution.

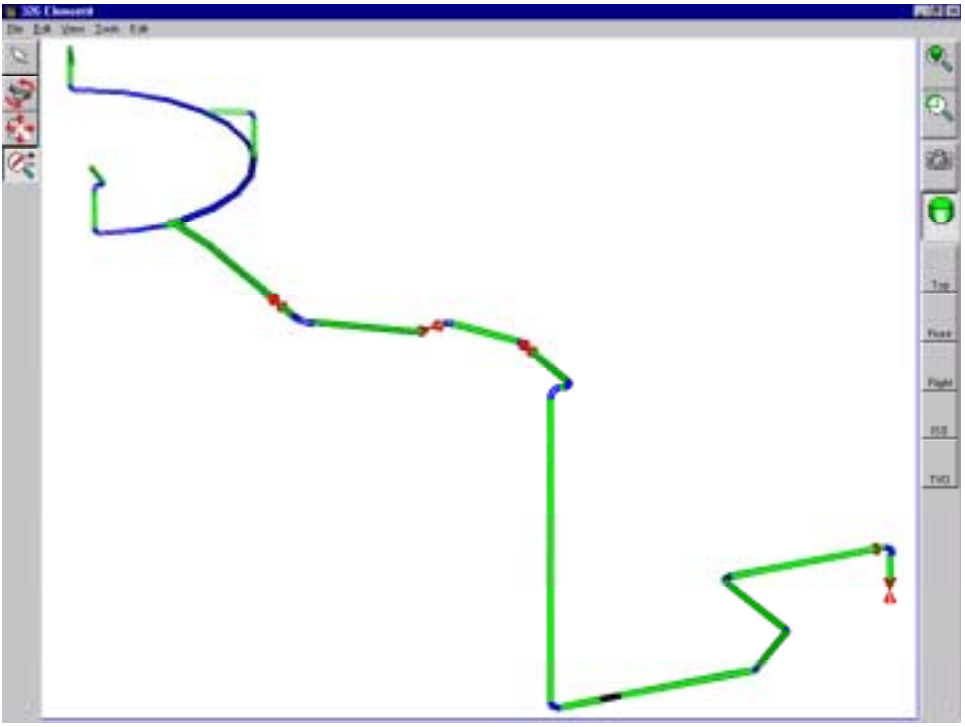

Figure 2. Visualization of piping using the piping database user interface.

Examples of information associated with a node are:

- The node number, co-ordinates in the plant coordinate system and isometric number (document database reference)
- Node element information like mass and associated stiffness and center of gravity
- Support information like stiffness, pipe whip restraint, stiffness matrix, gap or damping
- Reference to weld drawings inclusive weld (repair) information and dates
- Information as to what type of analysis shall be performed at the node (stress check, crack growth, fatigue etc.)

Examples of information associated with an element are:

- The element number, the nodes at the end of the elements and the isometric(s) to which the element belongs. As the isometrics can be found from the document database only a link to this database will be made.
- Cross sectional information like material designation, diameter and thickness of the pipe, the content designation and the isolation material designation. It should be noted that the designation of the material, contents and isolation is not more than a link to the material database. In this way the one of the most important rules of database design, namely “no data shall occur more than once in the database system”, is again fulfilled.
- Element type information like straight pipe, bend, T, expansion joint etc.
- Even very specific information like detected or postulated cracks can be entered into the database, see Fig. 3. In this way the system can also be used to perform bookkeeping of all the findings made during the inspections. Furthermore, it will be immediately available to perform subsequent analysis. During the, nowadays very short, outage speed of analysis and adequate documentation is of great importance. As all the related starting points for such a subsequent analysis will be in the system the analysis is in fact not more than a press-on-the-button.

3.2 The material database

The material properties of the normally used materials at TVO are gathered in a database called MATDBS. A typical view of the program interface display is shown in Fig. 4. As can be seen, many different material properties, if necessary as function of a second variable, can be saved. In addition, the source of the information is input. A link to the document database, see section 4.4, is still missing because the material database is elder then the document database and has not been updated with regard to this item. However, the source document is referenced from a reference list.

Note that the material identification, the content identification and the isolation identification mentioned in section 3.1 have to be chosen from the TVO material

database and as such cannot be freely chosen. Either an existing material has to be chosen or a new material has to be first introduced into the material database. This in fact shows another basic principle in the database development project where data may only occur once and user are helped/forced to use sound data. A possibility will be incorporated to calculate either with standard values or with alternative ones, for instance measured values.

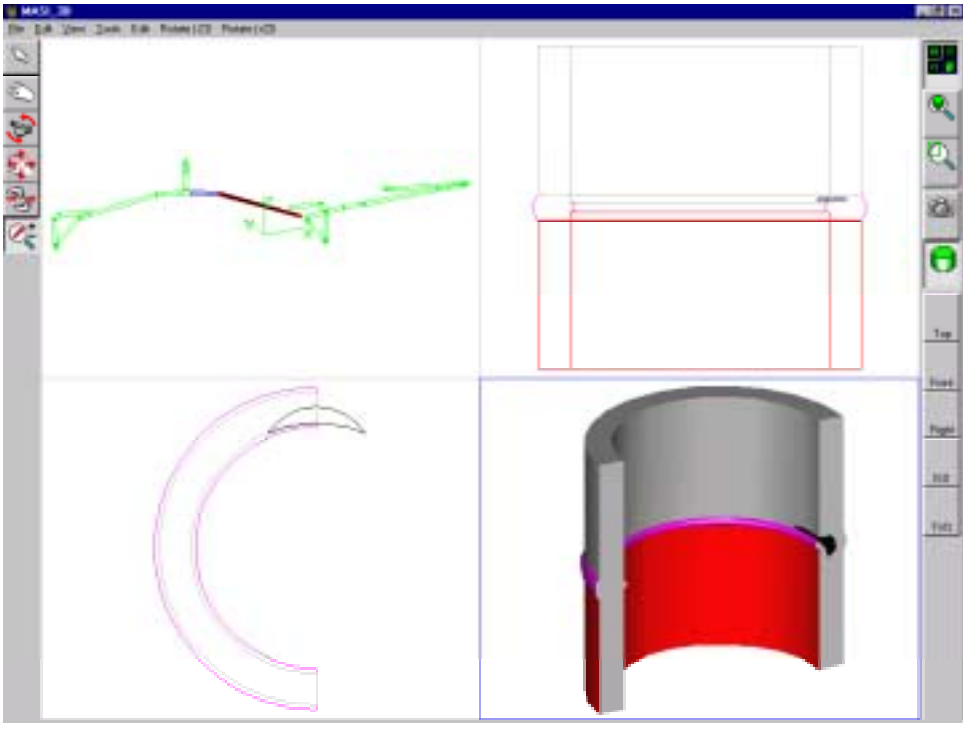

Figure 3. Visualization of a crack.

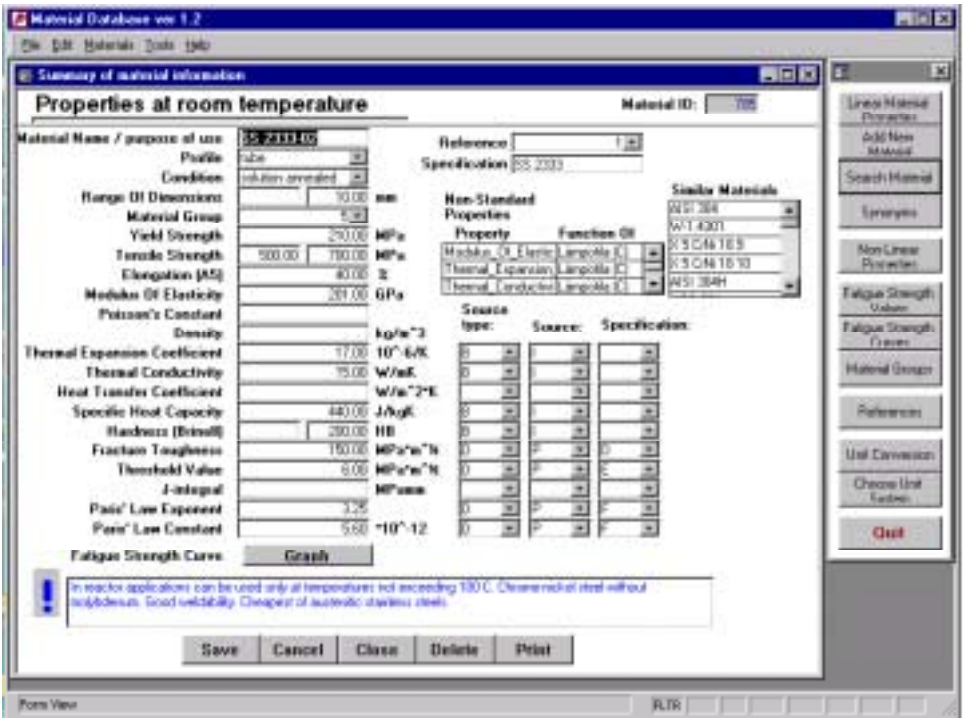

Figure 4. Contents of the material database.

3.3 The loading database

The loads, combinations, events and everything else related to it will as far as reasonable be saved in a loading database. This database is described in more detail in [3]. The load database is designed to:

1. Contain and document the actually valid design load specification inclusive service limits
2. Act as an input database to perform stress, flexibility, fatigue and/or crack analyses
3. Monitor and document the annual cumulative thermal transient events
4. Perform book-keeping of the load-cases and -combinations that are valid at a time and contain the connection between old and new data
5. Give the structure for the result database where the significant results of analyses are stored.

The loading database is part of the pipeline analysis and monitoring system that will be used for nuclear power plant piping systems and connected equipment at 2 Finnish nuclear power plants. These plants are situated in Olkiluoto and operated by Teollisuuden Voima OY (TVO). For a start the system will be used for class 1 piping systems only, but later on it may be extended to other systems where it is useful. The system will comprise a large set of process systems and components. Piping components, geometry, materials and systems are defined in an associated pipeline database [1]. Like the pipeline database, also the load-database will have a combined alphanumerical and graphical user-interface to show the user what the actual state is and what changes are made. The database system runs on a PC using commercially available database software.

The loading database system is being developed by TVO and VTT to facilitate the condition monitoring, aging and thermal transient follow-up, load history bookkeeping, documentation for component load specifications and related analyses for class 1 piping. The load specification system applied is shown in Fig. 5.

Basic dimensioning and necessary checks are made according to design standards like the ASME Code [5]. This code defines allowable stress/strain levels in applicable service limits and rules how to estimate the usage factor of the cyclic loads. Normally those standards are applied that were valid when designing the plant or component. When ordering new components, they have to be compatible with the rules valid at that moment. This is the practice, at least in Finland. This means that in one plant different acceptance systems may exist simultaneously. This makes it difficult to find the applicable load data at a time.

Load-cases and -combinations are fully user configurable. In the present application either static or dynamic pressures, temperatures, weights, and forced displacements can be included as basic loads. These are included in the database or coupled as structured files in case of large data quantities. Presently, the database structure has been designed and is implemented. The items 1, part of item 2 and item 3 of the above list are implemented and test runs have been made for a piping system for at least part of the analysis types described under item 2. Most of the basic programming work on the loading database will be finalized within one year. During the presentation the present status of the databases and program modules will be described.

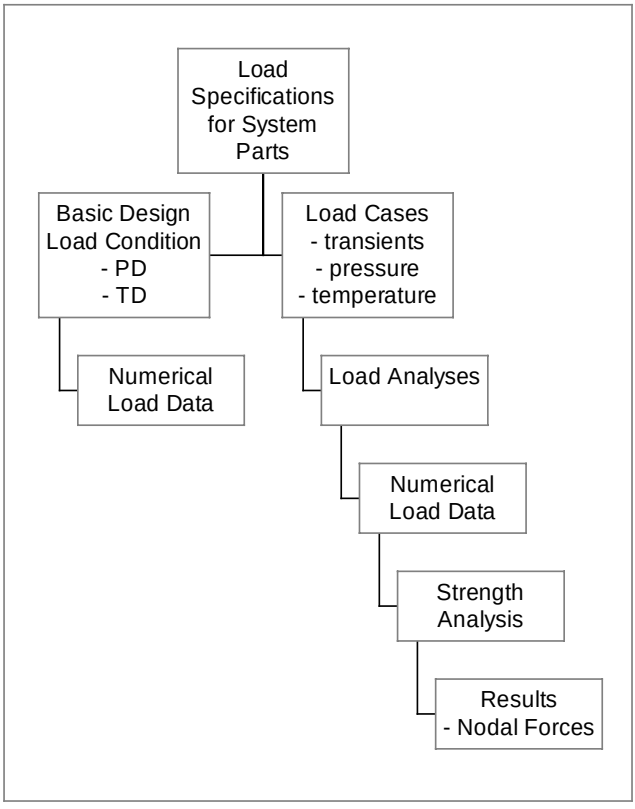

Figure 5. Load specifications for piping sections and system parts, the hierarchy of load cases, load analyses, load data, strength analysis and nodal results from the strength analysis.

3.4 The document database

In order to find easily documents, a document database was developed. All documents that are related to any of the items within the TVO pipeline analysis and monitoring system will be gathered into this database as will all other documents that are related to strength and vibration. Once a document is part of the document database, it can be logically associated to any of the other databases. An example of a main form corresponding to an analysis report is shown in Fig. 6. For instance, a load analysis report can be coupled to the load of the system (part) that it is related to. Also input data that was retrieved from an isometric can be coupled to the applicable revision of the isometric. In this way

data in the database will always be accompanied by an exact trace to the data source. In case the database document is available in electronic format even this file can be coupled to the document database and will thus be readily available from the PC. An extra option in the document database is that activities and deadlines may be associated to the documents and reports can be produced showing future activities and deadlines.

After making the associations that are described before it is possible to automatically add information with regard to the data sources to the documentation that is produced by the system. For instance the crack growth analysis that is mentioned later on is performed as a batch analysis and will automatically generate a complete report.

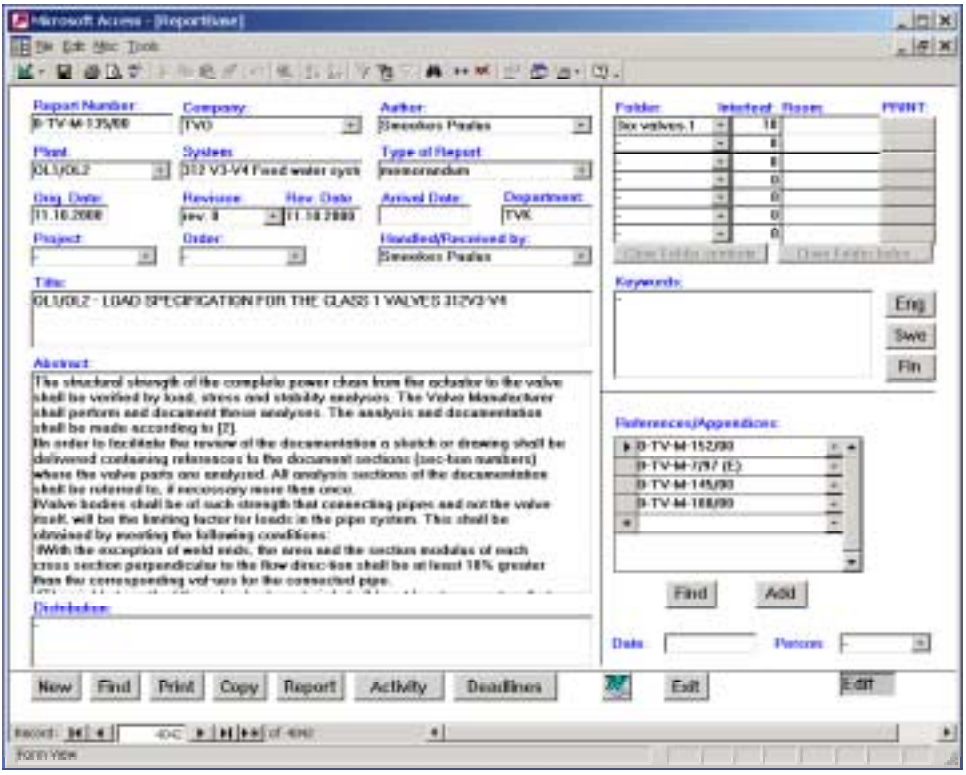

Figure 6. An example of the main form of the document database.

3.5 The result database

The significant analysis results will be saved into the result database. Due to the fact that results are computed for loads the organization of the result database will be similar to that of the loading database.

4. Analyses and application programs

4.1 Organization of data exchange

The data exchange between the databases and the application programs will be done via neutral files. For the time being the neutral files are equal to the batch input and standard output files of the application programs. So they are not yet true neutral files. As this project is a stand-alone project, it is not worthwhile to develop true neutral files. It is however important to follow the international development in this field. True neutral files would be a huge step forward as the same file could be used to perform analysis with different application programs and again the results would be readable with only one tool.

4.2 Piping strength analysis

The piping strength analysis will be carried out with a commercially available piping analysis program. For the moment FPIPE [6] is chosen. It shall use the geometry and material properties as described in section 3.1 and the loading as described in section 3.3. Compared to a basic piping calculation program, some of the following additional features may be necessary:

- The loading to be directly defined from the events (measured temperature or vibration data).
- Automatic model improvement for a dynamic analysis (see section 3.1).
- A transient analysis capability.
- The shape and welding coefficients according to ASME shall be included.
- Analysis with nonlinear supports, gaps and friction.

- A capability to use integrated supporting structures or a matrix (from FEM-analysis) as boundary condition.
- A general linear elastic element with mass (valve, tank, etc.) shall be available.
- A dedicated bellow element, linear and/or non-linear, shall be available.
- A capability to give shape factors for pipe-bends, T- and Y-joints, reducers and welds (from FEM-analysis).

Loading for these analysis may be temperature, mechanical or of any other nature. For the moment, two analysis types, which may be either static or dynamic, will still be handled separately:

- Linear elastic analysis for load cases or combinations. The results will be used for documentation, post processing or written back into the result database for later post processing. In case the results are written back into the database, the structure of the result database will be very similar to the structure of the load database. The development of the result database is planned for the year 2001.
- Non-linear analysis for load cases or combinations. The results will typically be used for immediate documentation and post processing.

4.3 Fatigue analysis

A fatigue analysis may be done according to the ASME, the materials' Wöhler diagram or any other method. The system contains a program that performs fatigue analysis according to the ASME III -standard [5] for class 1 piping. The input for this program shall be taken from the input data and results of many of the programs mentioned in chapters 1 and 2. This analysis shall be performed for materials like ferritic and austenitic steel and INCONEL. Events causing loading shall be taken from either the design event database or from the event counter database. The strength analysis results for all locations analyzed must be available to perform other analysis like for instance crack sensitivity analysis. In the design phase of the program the feed water system, system 312, will be used as a pilot system.

4.4 Fracture analysis

When performing fracture analysis, several crack growth mechanisms have to be considered, like crack growth due to cyclic mechanical loading or IGSCC [6]. As these mechanisms are dependent upon the material and the environment these method(s) can be chosen automatically. These analyses may be performed using one of the following methods:

- According to the simplified ASME method,
- Using the VTT developed MASI-PIPE program,
- Or other programs using batch type input.

A conservative way to estimate the usage status of the piping may be made through the assumption of a postulated initial crack equal to maximum non-detectable crack at the least favorable location or the worst detected crack. This crack shall, while including an appropriate safety factor, not grow to a critical crack during lifetime. These cracks are assumed to grow from the last periodical inspection. The crack growth is estimated using the actual events at the station. Thus the best estimate or worst possible crack growth can be predicted and necessary actions can be specified in due time.

4.5 Other development

The following topics will be studied in the future:

- Flow induce loads, like water hammer or pump transients and pipe break loads
- Back coupling of pressure and temperature measurements. The inside temperature transients to be determined from the measured outside temperature transients.
- Bimetallic weld analysis
- Transient temperature- and flow analysis
- Transient and event monitoring based on events and/or measurements.

5. Bookkeeping and validation

As the database will be quite complex, a good design and bookkeeping is very important. Records shall be kept for piping, equipment and other significant parts. The records shall contain such information as date of installation and possible exchange, as-build geometry and properties, welding, inspection and repair. Also the validity of the data shall be indicated. Thus analysis can be performed based on reliable and up-to-date information.

All information comprised in the database shall be accompanied by significant information related to date of installation and reference documents. The date is important as for instance thermal cyclic loading that has occurred before a part was replaced shall be ignored with regard to the fatigue of the replaced part. Reference documents are important, as, in order to be significant, input data to analyses shall be traceable. Reports that are produced with help of the database shall contain references to the source of the information contained.

6. Project organization and time schedule

During the first years, TVO was the sole contributor to the project. During this period, the material database and the document database were developed, as was the base of the pipeline database. Up to this time, the interface was still alphanumerical. As test project, a pipeline geometry transfer was performed to a general purpose FEM-program. Since a few years, the project is a joint effort of TVO, VTT and FEMDATA. In the project "Lifetime of pressure retaining components" [3] a practical toolbox consisting of computational and experimental tools is generated for effective condition monitoring of process piping and estimation of its remaining lifetime. New features to the pipeline database are the development of the visual interfaces to the database, the input and visualization of cracks and the loading database. Application programs that have been coupled to the database are the finite element method (FEM) based piping analysis program FPIPE developed at FEMdata Oy and the MASI-PIPE program system, which has been developed at VTT to estimate fatigue crack growth and integrity of flawed piping. As a part of the project, both application program systems are further extended and tailored to optimally fit the monitoring needs.

Developments for the near future are the result database and the bookkeeping features. Feasibility studies will be performed with regard to interfaces to one-dimensional pipe loading analysis programs, CFD-programs, modal analysis and update, general-purpose FEM programs and true neutral files.

Acknowledgements

The work reported here is part of the project Plant Life Management (XVO), which is coordinated by VTT Manufacturing Technology. The work has been funded by the National Technology Agency (TEKES) of Finland, VTT Manufacturing Technology and Teollisuuden Voima Oy (TVO). Their funding is gratefully acknowledged.

References

1. Smeekes, P., Lipponen, A., Raiko, H. & Talja, H. 2001. Pipeline analysis and monitoring system. SMiRT 16 Paper 1868.

2. Smeekes, P., Talja, H., Saarenheimo, A. & Haapaniemi, H. Numerical Simulation of Piping Vibrations Using Modal Correlation. SMiRT 16 Paper 1866, 2001.

3. Raiko, H., Lipponen, A., Smeekes, P. & Talja, H. Load-Case, and -Combination Database. SMiRT 16 Paper 1869, 2001.

4. Talja, H., Smeekes, P., Torkkeli, E., Laaksonen, J., Rostedt, J., Haapaniemi, H., Lipponen, A., Saarenheimo, A. & Solin, J. Lifetime of pressure retaining components (PUKK). Espoo: VTT Manufacturing Technology. Report VAL64-001549. 2000. 22 p.

5. ASME BOILER AND PRESSURE VESSEL CODE, SECTION III, Nuclear Power Plant Components, Division 1, Subsection NB, Class 1 Components.

6. FPIPE, a finite element method (FEM) based piping analysis program developed at FEMdata Oy, Finland

7. MASI-PIPE, a fracture mechanics analysis program to make quick crack growth and residual lifetime assessments for cracked piping, developed by VTT Manufacturing Technology, Finland

Piping Vibration Management Combining Measurements and Numerical Simulation

P. Smeekes
Teollisuuden Voima Oy, Olkiluoto, Finland
H. Talja, A. Saarenheimo and H. Haapaniemi
VTT Manufacturing Technology, Espoo, Finland

Abstract

In an ongoing project a practical method is being developed to monitor the condition and remaining lifetime of process piping. This method combines both measurements - using a minimum number of fixed continuous measurements - and an adequate computational model. Relatively simple piping was chosen as the first pilot analysis case. This paper outlines the contents of the project and describes the finite element analyses, based on design documents, detailed observation of the piping geometry and supports and results obtained by updated FE (finite element) model.

1. Introduction

It is essential that developing piping failures can be anticipated and/or monitored and that any repair work is carefully planned ahead and carried out during regular outages. Traditional design and condition monitoring of piping is mainly based on postulated events and on the application of allowable vibration levels. This approach gives only indirect information on the loading at the critical locations and generally leads to over conservative assessments.

More relevant information about the actual loading state and condition of the piping is obtained by direct measurements, which can be accompanied by detailed finite element (FE) analyses. In practical cases the amount of measurement points is very limited. Many actual structural details can be rather difficult to model or they may deviate significantly from design documents. So, often an iterative process is needed to obtain adequate agreement between

computational and experimental results. This goal may be achieved using special purpose tools designed to update Finite Element analysis models with experimental data (modal correlation).

The main aim of this project is to find a practical method based both on measurements – using a minimum number of fixed continuous measurements – and on an adequate numerical model. This method is then used to monitor the condition and remaining lifetime. In the model updating and development phase a somewhat larger amount of measurements will probably be necessary than is possible in normal condition monitoring. Probably several iteration cycles are needed to come up to an adequately working FE model, Fig. 1.

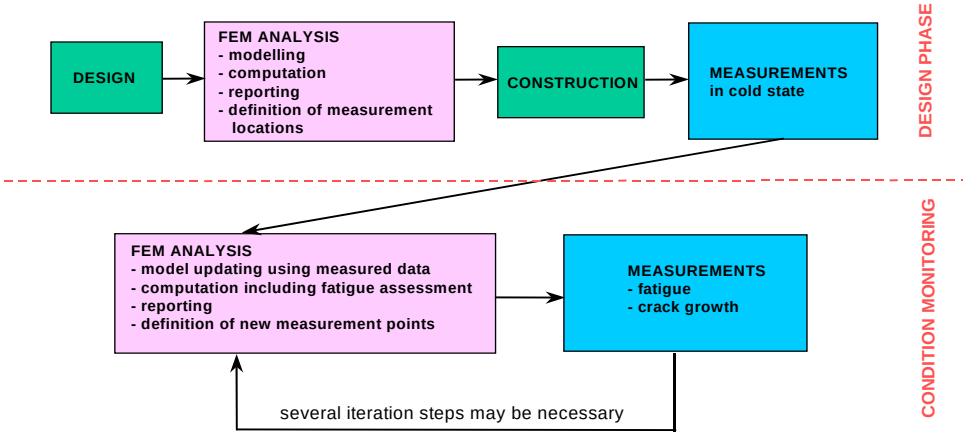

Figure 1. The approach to come to an adequate model to monitor the vibration behavior of a piping system, starting from the piping design phase.

One special feature of the work is that the modelling work will utilize the piping and loading database systems developed as a co-operation task between TVO and VTT as described in paper [1] in the BALTICA conference. The work performed during the first project year has been described in [2].

2. Studies with the pilot piping

There are several issues causing uncertainties to the dynamic piping analysis. The most important ones are the difficulties in determining the actual in-service loads and in describing certain structural features, especially the functioning of the piping supports. This may differ significantly from the original design documents. It is essential to keep the first studied case as simple as possible. However, it was decided to perform the study using an actual process plant pipe line instead of a laboratory experiment.

The first pilot system, part of the auxiliary feed water system piping at the OL1 plant was chosen based upon the following requirements:

- Cold in operation condition, no temperature effects nor insulation,
- Easy to access and measure in both operational and standstill condition (modal analysis),
- A clearly defined excitation (reciprocating pump).

During normal operation the auxiliary feed water system is not in use except for the periodically performed tests lasting for five minutes each month. The expected - and measured - vibration amplitudes were so small that no integrity problems are anticipated due to this vibration.

The part of the piping system being under consideration is located on the outside of the containment between the containment penetration and the auxiliary feed water system pumps. The pumps are 3 piston plunger pumps running at a frequency of 4 Hz. The pipeline has a total length of about 40 meters and has two major branches. There are 17 supports and the pump is equipped with three different pressure accumulators. Main dimensions of the pipe line are shown in Fig. 2a. This pipeline is made from a DN 100 stainless steel pipe. The design pressure, which is effective while operating the pump, is 90 bar and the design temperature is 100ºC. However, the piping is filled with water that does not exceed the room temperature during any anticipated transient. This means that the piping is not insulated and that temperature is not an issue.

3. Modal testing

Mode shapes and eigenfrequencies of the pipe were evaluated using both impact hammer and shaker. Both operational and modal animations of the actual pipe have been reported in [3]. Measurements were performed in 29 measurement locations mostly measured in 3 directions. Measurement locations are shown in Fig. 2c. However, the measurements to the pipe axial direction are missing at the measurement points located at the straight pipe sections. These values are predicted by interpolation. Modal testing was performed to experimentally characterize the dynamic behavior of the piping. The mode shapes and associated frequencies were determined both during operation and in standstill condition.

The natural mode shapes were excited with hammer impacts causing short time impulses with more or less uniform energy input over the significant frequency band. The mode shapes themselves were then recorded but the data immediately after the impulses is neglected. The data, after the direct influence of the excitation has become negligible, is used to determine the modes and associated frequencies. Later on, also shaker excited mode shapes have been studied.

4. FE analyses

4.1 Model and analyzed cases

The first FE analysis was carried out with models based solely upon the design documents. In the following this model is referred to as Case 1. This would also be the normal approach in the design phase and this model would also be used to plan the first measurements. Of course, it was clear from the beginning that there are always differences between the actual structure and the ideal design drawing.

Properties of the FE model were varied in order to find out how different modifications affect the behavior of the model. Because it was known on beforehand that the critical aspect was to find suitable stiffness values for the piping supports, mainly their spring constants were modified. The stiffness values for the supports were estimated by using simple FE models loaded by unit forces and moments. Also more relevant information concerning the actual

piping geometry was obtained by direct measurement and applied in analysed based on updated input data.

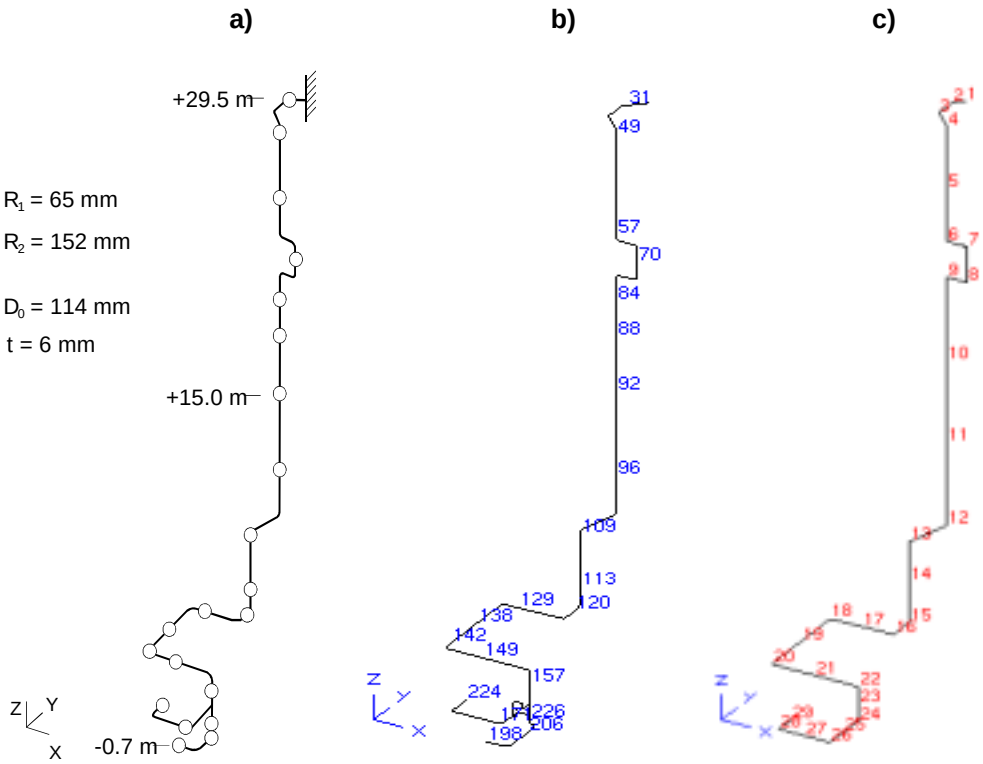

Figure 2. a) FE model and the support locations, b) node numbers at supports and c) vibration test model and measurement points.

The FE model used in the ABAQUS analyses [4], main dimensions of the pipe line and support locations are shown in Fig. 2a. Corresponding nodal numbers at support locations are shown in Fig. 2b. The model consists of 181 elbow and pipe elements. Both pipe bends and adjacent straight segments are modeled with ELBOW31 elements. There are 5 integration points through the wall thickness and 20 integration points around the circumference of the section; six ovalization modes are used. The middle segments of long, straight pipe runs are modeled with PIPE31 type elements. To join the pipe segments modeled with different element types, warping of the straight PIPE31 elements is prohibited at the connecting node. 1-dimensional spring elements are used in the appropriate

directions to model the supports. Six spring elements with different stiffness values (one for each degree of freedom) are needed to describe one pipe support.

The locations and stiffness values of the supports as well as the pipe wall thickness values were modified according to inspection and measurements in Cases 2 and 3. In Cases 1 and 2 the pipe is assumed to be completely filled with water whereas in Case 3 the pipe is assumed to be filled only up to +15.00 m (see Fig. 2a). This is done because one may assume that the isolation valve at the top of the piping is closed and there will be a vacuum in the upper part of the piping.

Case 4 was obtained by updating the support stiffness values of Case 3 model using the FEMtools program [5]. However, it should be noted that the automatic updating procedure was not yet applied. Instead, FEMtools was applied first to identify the critical spring elements and evaluate the effect of changes in these elements. FEMtools was also applied to to study the sensitivity of the FE model to changes in material properties and evaluate the effect of these changes.

The main differences between Cases 1–4 are summarized in Table 1 and the material properties used in these analyses are summarized in Table 2. In Case 4 the same values were applied except for Youngs modulus, which was increased by 2.5% for the elements filled by water (up to level +15 m).

Table 1. Analyzed cases.

Property	**Case 1**	**Case 2**	**Case 3**	**Case 4**
Support locations	as designed	as measured	as measured	as measured
Support stiffness	simple FE	simple FE [1)]	simple FE	simple FE[3)]
Gaps	low stiffness[1)]	updated[2)]	updated[2)]	updated[2)]
Wall thickness	nominal	measured	measured	measured
Water level	full	full	level +15 m	level +15 m

[1)] Gaps in supports according to design documents are described using spring elements with low stiffness value

[2)] Observed gaps in supports are described using spring elements with low stiffness value

[3)] Supports stiffness updated by FEMTools program

Table 2. Material property values used in analyses 1 to 3.

Property	Value
Young's modulus	206 GPa
Steel density	7850 kg/m^3
Water density	1000 kg/m^3
Poisson's ratio	0.3

4.2 Results

Numerical FE results of the four different analysis models are compared to experimental data. The comparison presented below is based on hammer excited mode shape measurements. The results are compared in terms of eigenmodes and eigenfrequencies as well as the modal assurance criterion (MAC) values [5]

$$MAC(\psi_a, \psi_e) = \frac{\left|\left(\{\psi_a\}^t \{\psi_e\}\right)\right|^2}{\left(\{\psi_a\}^t \{\psi_a\}\right)\left(\{\psi_e\}^t \{\psi_e\}\right)} \quad (1)$$

where Ψ_a and Ψ_e are computed and measured eigenmode vectors.

The second, fourth and seveth measured vibration mode and the corresponding numerical modes of Case 4 are shown in Fig. 3. A selection of measured and corresponding calculated results in Cases 1 and 2 are shown in Table 3 and those for Cases 3 and 4 in Table 4. The comparison is done for lowest nine measured modes and frequencies, up to 82 Hz. The measured data is filtered when calculating the MAC values so that the eigenvector components less than 17.5% of the maximum value are ignored. This is done because due to the definition of the MAC value an eigenvector component with relatively small amplitude may still dominate the MAC value. Corresponding calculated modes were selected based on visual inspection of results, proportional eigenfrequency error values (see columns 5 and 9) and MAC values (columns 6 and 10). In performing the Error and MAC value computations for the first mode, only the upper part of the FE model (above point 10, Fig. 2b) was considered. It should also be noted that

for Case 1 the supports were located as shown in the design drawings, i.e. there are differences compared to the as build structure.

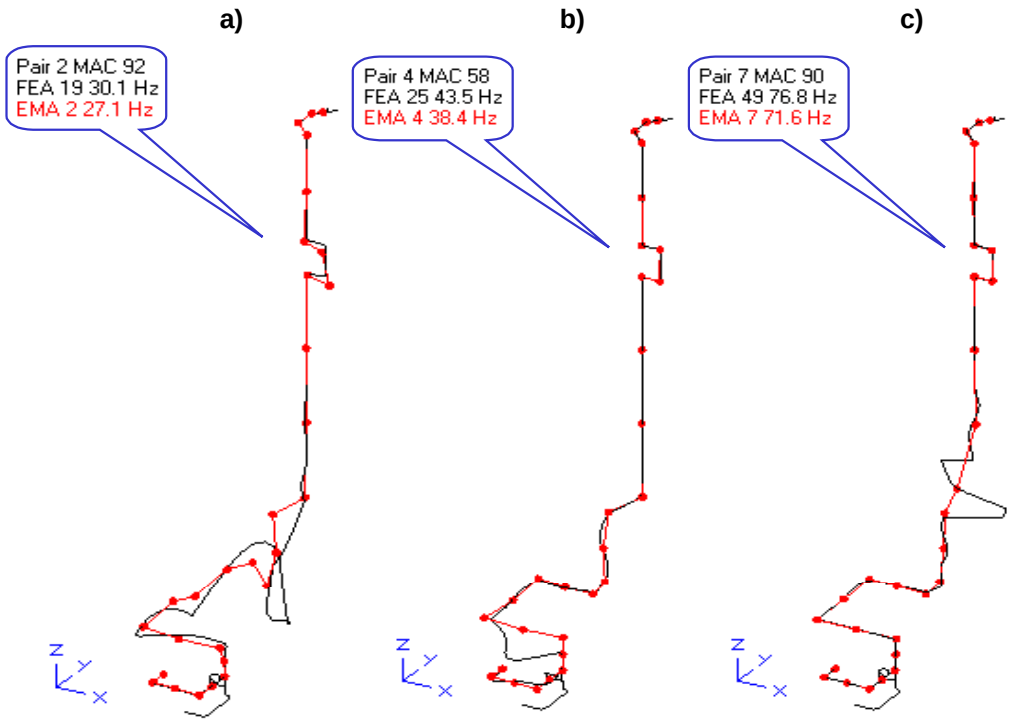

Figure 3. Measured mode numbers 2 (a), 4 (b) and 7 (c) together with the corresponding calculated Case 4 modes.

The water level in the piping hardly affects the lowest 14 calculated eigenmodes (Cases 2 and 3, see Table 1). The eigenmodes in Cases 2 and 3 are essentially similar, but the frequencies in Case 3 are higher due to the lower mass of the upper part of the pipeline.

The percentual change in stiffness values due to the FEMTools updating process is presented in Table 5. It should be noted that the relative high values in this table are due to the originally very low stiffness values which were simulating possible gaps in supports.

According to the latter experiment with the shaker, the lowest eigenfrequency is 27.2 Hz. Compared to the impact hammer excitation there are a few more frequencies between 27.2 and 72 Hz (27.2, 32.7, 33.5, 39.2, 40.8, 42.3, 56.4, 57.8 and 71.2 Hz). Analysis of these, quite recently obtained results is at present an ongoing process. All the numerical and experimental results will be reported in [6].

Table 3. Mode shape pairs between experimental data and Cases 1 & 2 with 17.5 % filtering.

EMA	[Hz]	FEA Case 1	[Hz]	Error [%]	MAC [%]	FEA Case 2	[Hz]	Error [%]	MAC [%]
1	19.00	12	22.36	17.7	54.5	14	24.34	28.1	66.6
2	27.13	17	25.13	-7.4	92.4	19	27.84	2.6	93.8
3	32.38	33	50.15	54.9	54.8	29	43.05	33.0	50.6
4	38.38	33	50.15	30.7	52.7	39	56.53	47.3	85.4
5	40.88	31	43.27	5.8	51.5	28	40.76	-0.3	69.7
6	56.50	30	41.07	-27.3	34.4	37	54.65	-3.3	64.3
7	71.63	46	65.23	-8.9	95.1	61	94.25	31.6	94.8
8	77.64	82	144.62	86.3	46.2	43	58.03	-25.3	81.2
9	82.00	80	142.64	74.0	57.0	68	112.64	37.4	46.2

Table 4. Mode shape pairs between experimental data and Cases 3 & 4 with 17.5 % filtering.

EMA	[Hz]	FEA Case 3	[Hz]	Error [%]	MAC [%]	FEA Case 4	[Hz]	Error [%]	MAC [%]
1	19.00	14	24.34	28.1	44.1	7	17.11	-9.9	67.4
2	27.13	17	28.02	3.3	93.9	19	30.11	11.0	91.5
3	32.38	28	43.68	34.9	50.6	20	31.8	-1.8	53.8
4	38.38	30	44.48	15.9	57.5	25	43.46	13.2	58.1
5	40.88	28	43.68	6.8	75.6	27	44.78	9.5	80.7
6	56.50	45	66.16	17.1	75.3	36	55.47	-1.8	69.1
7	71.63	59	91.99	28.4	94.7	49	76.8	7.2	89.9
8	77.64	54	80.57	3.8	86.4	51	79.88	2.9	86.2
9	82.00	63	101.02	23.2	79.4	53	80.87	-1.4	70.7

Table 5. Percentual changes in support stiffness values due to the updating process (node numbers are shown in Fig. 2b).

Translational supports			
Support Node	**Support direction**		
	KX	**KY**	**KZ**
31	137.50 %	190.00 %	87.50 %
49	57.07 %	100.00 %	415.76 %
57	(rigid)	(rigid)	(rigid)
70	0.00 %	20.00 %	0.00 %
84	0.00 %	0.00 %	0.00 %
88	0.00 %	0.00 %	0.00 %
92	(rigid)	(rigid)	(rigid)
96	0.00 %	0.00 %	0.00 %
109	20.04 %	399900 %	20.35 %
113	19.94 %	1200 %	20.12
120	0.00 %	1800 %	0.00 %
129	499900 %	6.95 %	400.00 %
138	22.81 %	15.01 %	399900 %
142	10.02 %	9.68 %	13900 %
149	11900 %	9.97 %	9.98 %
157	24.31 %	19.09 %	80.12 %
171	150.00 %	375.00 %	150.00 %
198	0.00 %	0.00 %	0.00 %
206	0.00 %	0.00 %	0.00 %
226	92.31 %	900.00 %	129.87 %

5. Summary and conclusions

Operational modes and eigenmodes of a pipeline were measured using an impact hammer excitation. Even shaker excitation was used for comparative vibration testing. The modes and frequency values determined with these methods were similar.

Finite element analyses were carried out using the ABAQUS code. The first model, Case 1, was built according to the available design drawings. In Cases 2 and 3 the geometry of the model was modified according to the observations and measurements carried out at the plant. For Case 3 the water level was corrected to correspond to the expected vacuum. The FEMtools code was used to compare the measured and calculated results and in updating the model, Case 4 but the automatic updating procedure was not yet used.

FEMtools is found to be an effective tool in comparing and studying measured and numerical data. The modeling of the supports according to the inspection clearly improved the numerical results whereas the effect of the measured wall thickness variation was of minor importance.

The manual updating improved the results further. The use of the automatic updating available in FEMtools is successfull only when the original model is relatively close to the measured data.

One possible reason for differences is that at certain measurement points only the displacements in both horizontal directions were measured and the vertical ones had to be interpolated. Further, the effect of the mesh used in the model should be carefully studied before any further updating. E.g. the number of elements in pipe bends may affect the result. In this FE model pipe bends are modeled with two elbow type elements only.

Obviously it is necessary to continue the work by describing the supports in the model with beam elements instead of springs so that their vibration properties can be desribed more realistically. The final updated model will be loaded using the excitation calculated by a special purpose code. These numerical results will be compared with the measurements carried out during the operation of the pump. Further work will be performed with two other piping cases.

Acknowledgements

This work is part of the project Plant life management (XVO), which is coordinated by VTT Manufacturing Technology. The work has been funded by the National Technology Agency (TEKES), Teollisuuden Voima Oy (TVO),

FEMdata Oy, Fortum Engineering, Neste Engineering and VTT Manufacturing Technology. Their funding is gratefully acknowledged. Special thanks are due to Mr. Jaakko Rostedt for his contribution in performing the vibration measurements and in analyzing the measured results.

References

1. Smeekes, P., Lipponen, A., Talja, H. & Raiko, H.2001. Integrated approach and database system for managing load cases and integrity of piping. Baltica Conference 2001.

2. Talja, H., Smeekes, P., Torkkeli, E., Laaksonen, J., Rostedt, J., Haapaniemi, H., Lipponen, A., Saarenheimo, A. & Solin, J. Lifetime of pressure retaining components (PUKK). Espoo: VTT Manufacturing Technology. Report VAL64-001549. 2000. 22 p.

3. Rostedt, J. 2000. Description of the dynamic properties of pipeline 327 with help of vibration animation. Kankaanpää: J. Rostedt Oy. Report RR000712.Doc. 5 p. + app. 21 p. (in Finnish)

4. ABAQUS Theory Manual, Version 5.8. 1998. Hibbit, Karlsson & Sorensen, Inc. RI.

5. FEMtools Users Guide. Version 2.0, 2000. Dynamic Design Solutions. Leuven, Belgium.

6. Haapaniemi, H. 2001. A Case Study for Validating and Updating the Dynamic FE Model of a Pipeline. Espoo: Helsinki University of Technology, MSc. Thesis.

Thermal fatigue of NPP components: potential multiaxial, environmental and small cycle effects

Gary Marquis, Jussi Solin
VTT Manufacturing Technology
Espoo, Finland

Abstract

Current fatigue design curves for NPP components are based largely on strain controlled tests of small specimens tested in air at room temperature. Reduction factors of 2 for strain or 20 for fatigue life are applied to the mean data and are intended to account for material, environment, surface finish and loading uncertainties. Pipe failures in recent years have been attributed to high cycle thermomechanical fatigue and have prompted re-evaluation of the fatigue design curves. Research has focussed especially on environmental effects and load sources. Some data also suggests that multiaxial loading and small stress cycles as part of a spectrum may cause significantly more fatigue damage than what is predicted. This paper examines some of these potential sources of fatigue damage.

1. Introduction

Thermomechanical (TM) fatigue has surfaced as a significant contributor to industrial component failure. Components as diverse as automotive brakes, steam turbine disks, railway wheels and metal-forming dies are all subject to combinations of temperature variation and mechanical loading or constraint which may lead to cracking and eventual failure by fatigue. Sehitoglu [1] has proposed the following general definition of TM fatigue *"Fatigue of materials and components subjected to changing strain and temperature"*. In order for the temperature change to become damaging, however, some degree of constraint is also required. Constraint may be either strain controlled where local expansion or contraction is hindered by the surrounding material or displacement controlled where the overall expansion or contraction of a component is limited by

other structures. A wide variety of strain temperature combinations are possible depending on whether the constraint is full-, partial-, or over- and whether the thermal and mechanical strains are in- or out-of-phase.

Fig. 1 illustrates the role of constraint in TM fatigue for a plate or pipe. The upper figure shows the temperature variation with thickness. The three lower figures show three alternate constraint conditions which may be present and which influence the magnitude of surface stress.

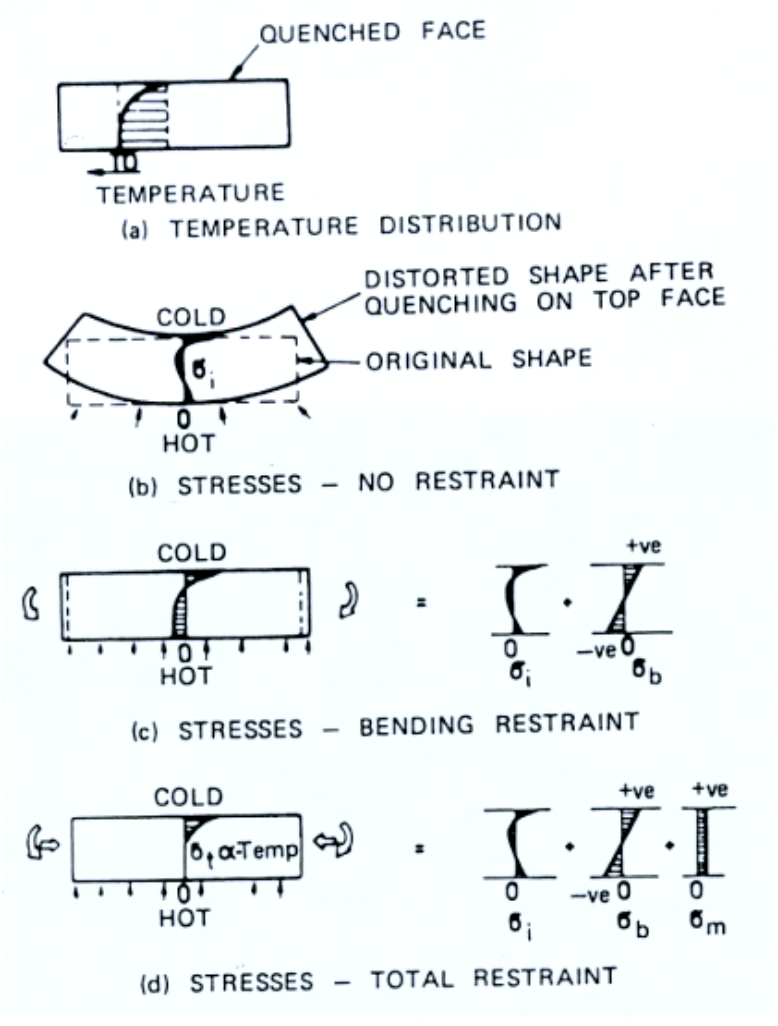

Figure 1. Stress distribution in a quenched plate with varying constraint.

1.1 Bree diagram

Sehitoglu uses the Bree diagram, Fig. 2, to illustrate the various mechanisms that can be attributed to TM fatigue. The vertical axis in represents the ratio of thermal quasi-elastic stress to yield stress and the horizontal axis represents the ratio of applied or constraint induced load to collapse load of the component. Four areas representing four potential failure mechanisms are identified.

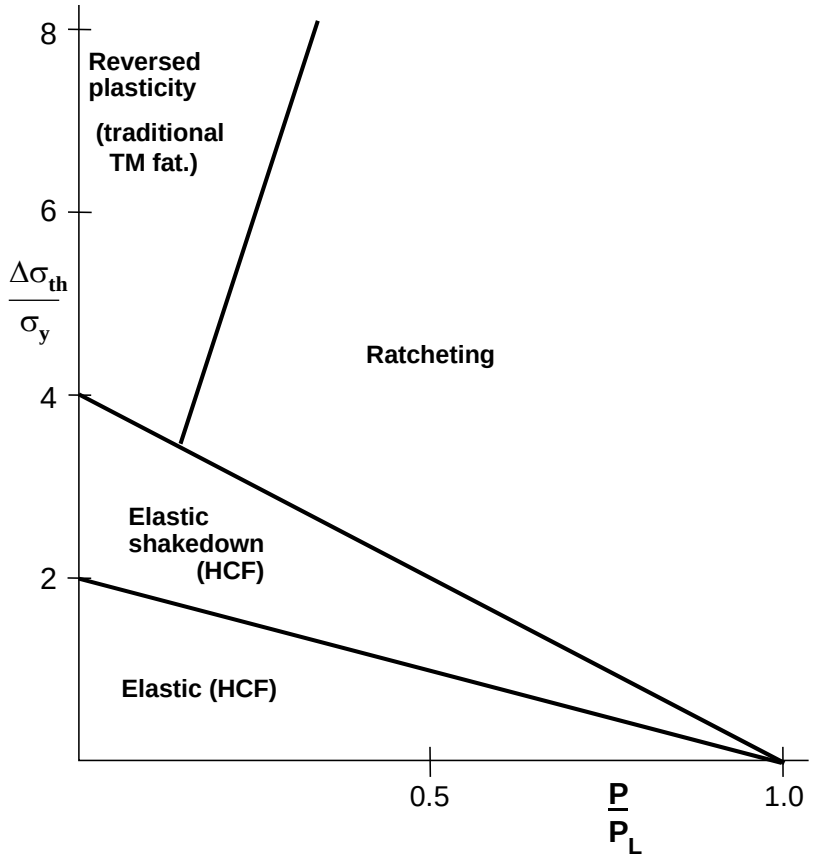

Figure 2. Bree diagram for AISI 304 stainless steel [1].

Bartsch et al. [2] provide an excellent review of TM fatigue research, experimental methods, and mechanisms. They note that, "*Thermal fatigue is usually considered as a low cycle fatigue phenomenon, which is commonly defined as the regime where plastic strain in each cycle exceeds the elastic strain*". This is the region denoted as "reversed plasticity" in Fig 2. and illustrates the region

where most research activity has been directed. This region is characterised by low cycles, large temperature changes, significant temperature dependent changes in mechanical properties, creep fatigue interactions, and possible metallurgical changes like grain growth, oxide formation, precipitation, etc.

1.2 Fatigue mechanisms for NPP components

In the context of nuclear power plant components and especially piping systems, the thermal stresses are usually low to cause significant reversed plasticity and the region in Fig. 2 denoted as "elastic high cycle fatigue (HCF)" is of most concern. The characteristics of this region are large numbers of cycles, low thermal stresses, essentially isothermal mechanical properties, and negligible creep fatigue effects.

In the past 15 years fatigue cracks initiated due to thermomechanical processes have been observed in a variety of components in the nuclear industry in many countries. In many cases the failure mechanism has been identified as high cycle TM fatigue. Environment is considered to have a large effect and in some cases multiaxial and the interaction between large and small fatigue cycles may be of significance. Several authors have considered multiaxial effects in TM fatigue of austenitic stainless steels but in these cases the temperature changes are fairly high and not directly relevant to the current problem [3, 4].

1.3 Aim of this paper

Thermal fatigue of NPP components has been previously studied experimentally and analytically. Certain aspects are, however, not yet clarified and new research efforts are being started in the EU fifth framework programme and the NESC network. On the other hand, the vast majority of thermal and classical fatigue research has been performed for industries other than nuclear power plants.

The aim of this paper was to review the NPP thermal fatigue experience and problems and compare them to the general state of the art in fatigue. A comprehensive literature review was not performed, but the major trends were considered and certain issues of particular interest are raised for discussion.

2. Operating experience

In the late 1980's, primary coolant leakage due to cracks in elbow piping of an emergency core cooling system have been reported in Farley 2 (USA) and Tihange 1 (Belgium). In both cases damage was attributed to high cycle TM fatigue [5, 6]. Civaux 1 (France) had a similar failure in 1998 after 1500 hours of operation near a mixing "T" with a large[1] temperature variation, $\Delta T > 150°$ C [7].

Jansson [8] reports that most Swedish BWRs have about 20 locations where thermal mixing with ΔT greater than 50° C occurs. This ΔT is sufficient to cause thermal fatigue problems. Three to four locations have temperature differences of 100° C or more. The first cases of TM fatigue occurred in "T" joints in the 80s and early 90s. Fig. 3 shows the branch pipe connection between the feedwater and shutdown cooling systems from a Swedish BWR where TM fatigue cracks have been observed.

Thermal cycling due to both high and low frequency temperature transients resulted in the TM failure of a regenerative heat exchanger elbow at Tsurunga-2 (Japan) PWR in 1999 [9]. The combined effect of a relatively high frequency thermal mixing with a low frequency change in the flow behaviour within the heat exchanger due to global thermal distortions. The two loading mechanisms produce one significant cycle every 500s which resulted in failure after about 95000 hours of operation. Failure location and loading is shown in Fig. 4.

Failure of a nozzle assembly at Oconee 2 (USA) in 1997 has been attributed to the combined effect of thermal fatigue and flow induced vibration loading [10].

[1] Large in the category of thermal fatigue loads in NPP piping.

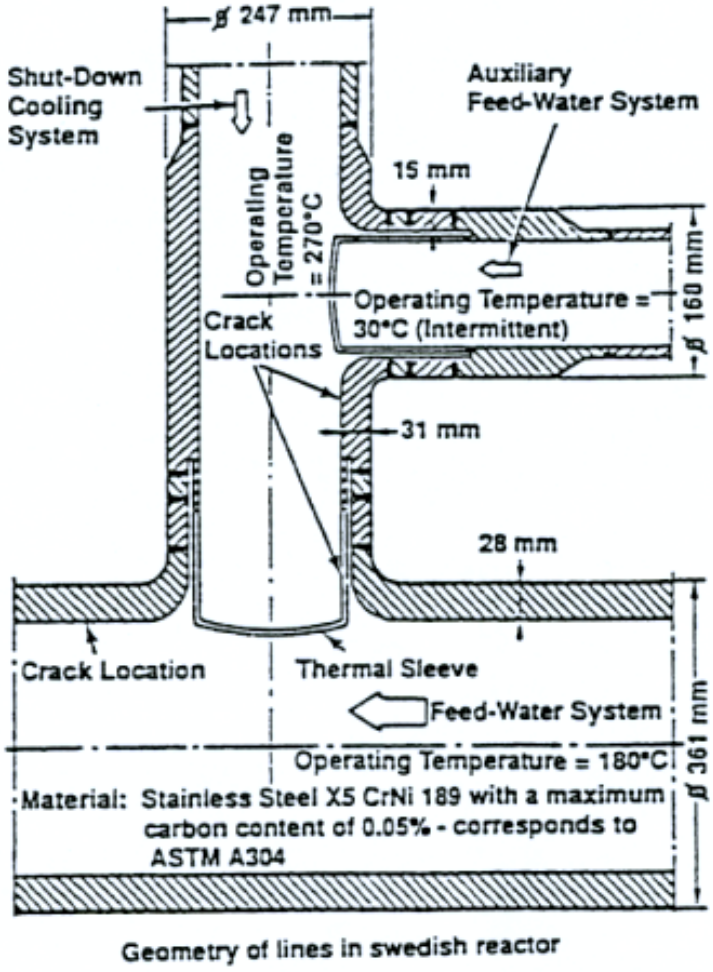

Figure 3. Branch pipe connection that has experienced high cycle TM fatigue failure [8].

In most of these cases thermal stratification at "T"s or elbows has been identified as a major cause of TM fatigue loading. However, leaking valves or seals which results in the intermittent release of cold water may also produce TM fatigue. Seal leakage has been reported as the major cause of a BWR pump shaft failure [11] and a leaking isolation valve at Genkai 1 (Japan) resulted in thermal cycling and cracking in an unisolable pipe section [6].

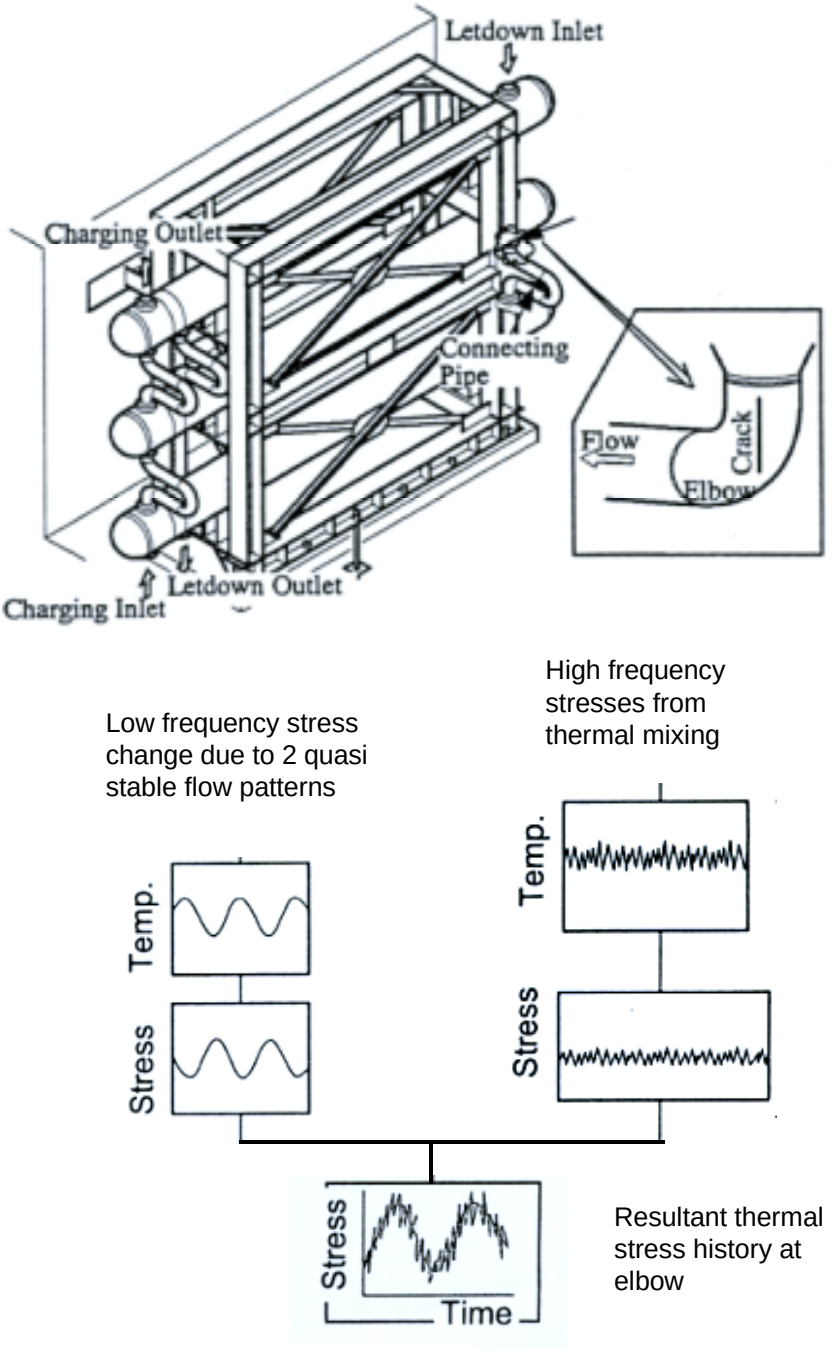

Figure 4. Elbow failure in a heat exchanger at Tsurunga-2, Japan [9].

Hirschlberg et al. [6] report that there have been a total of 14 thermal fatigue leak events in unisolable portions of PWR reactor coolant systems. Aaltonen [12] has reported that fatigue is expected to become a major failure mechanism for small diameter BWR piping systems. Certain classes of thermal fatigue events were not evaluated as part of the original design basis for many plants. Failures like those mentioned in this section have been reported in USA, Europe and Japan and have prompted activity both from the utilities and regulatory authorities. Fatigue will become a more important consideration in the ageing management programs for plants seeking operating license extension.

3. Fatigue

3.1 Thermal and mechanical load

Thermal stratified flow is characterised by three superposed layers: a cold layer along the bottom of the pipe, a hot layer near the upper surface of a pipe and an interface layer between these two which has a vertical temperature gradient. The condition of the intermediate layer changes with flow rate, fluid density and pipe dimensions with result that fatigue cycles are introduced to the inner wall of the piping system with frequencies from 0.1 to 1 Hz. Thermal stratification is closely associated with TM fatigue at elbows or "T" connections.

In some cases leaking valves or seals may intermittently leak cooler water into a hot area producing thermal cycling and TM fatigue [6,11]. In at least one failure case low frequency global thermal distortions produced changes in the fluid flow behaviour within a heat exchanger and lead to TM fatigue [9].

At 300° C the thermal expansion coefficient 316L SS is about 17 $x10^{-4}$ %/°C which means that $\Delta T = 100°$ C would result in a thermal strain range of 0.17%. Jansson [8] reports that $\Delta T = 50°$ C is considered sufficiently severe to cause TM fatigue difficulties.

Thermal stresses do not act in isolation but are often combined with flow induced or mechanical vibration or with global thermal stresses which are present especially during start-up and shut down events. The combination of low fre-

quency global events e.g., start-ups, and relatively high frequency localised thermal cycling can result in a cumulative damage problem that is not well addressed in experimental studies.

3.2 Multiaxial effects

Multiaxial loading can significantly affect the fatigue life of components and materials. This is the case especially when loading is non-proportional. Loading is non-proportional if the stress components change out of phase, i.e., when the direction of principal stress rotates.

3.2.1 Non-proportional hardening

In the case of non-proportional loading multiaxial effects are significantly more remarkable for stainless steels than for other materials. Due to planar slip tendency of austenitic stainless steels, additional stain hardening occurs under non-proportional loading. This dramatically reduces the fatigue life [13].

Fig. 5 shows effective stress strain curves for AISI 304 under both in-phase and 90° out-of-phase loading. The effective stress amplitude in the case of out-of-phase loading is approximately twice that of in-phase loading for the same strain amplitude. For materials like aluminium or low carbon steel the additional hardening due to out-of-phase loading is from zero to only about 30%.

Numerical analyses based purely on strain or failing to account for the additional strain hardening in stainless steels due to non-proportional cycling can greatly underestimate the fatigue damage due to an underprediction of the actual local stresses in the component.

3.2.2 Biaxial stress time histories

The case of cool water impinging on a fully constrained plate or the hot wall of a pipe would produce a proportional equi-biaxial stress field. However, the case of thermal stratification produces a more complicated stress state. It will involve

time varying temperature gradients both in the circumferencial and axial directions along the inner pipe wall.

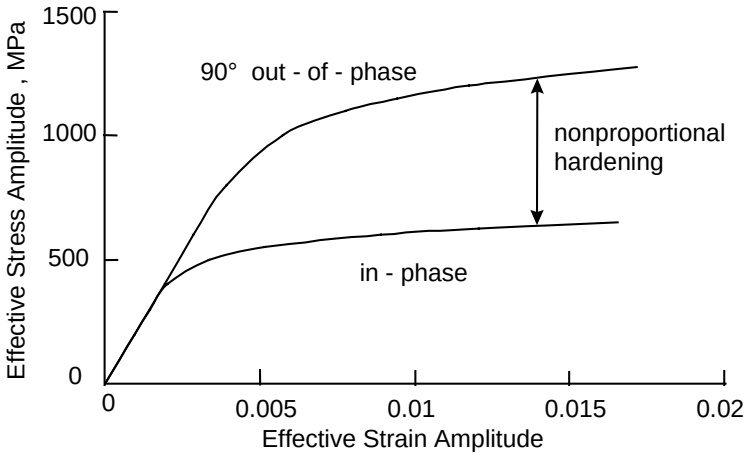

Figure 5. Nonproportional hardening of 304 SS [13].

Fig. 6 shows several simplified biaxial stress time histories. Each involves the same stress range in the σ_x direction, but either mean stresses or the stress paths in the σ_y direction are different. Assuming that the simple uniaxial case shown in Fig. 6a results in a fatigue life of $1x10^6$ cycles and that the S-N curve has a slope of -0.2, fatigue lives of the other multiaxial histories can be predicted. For comparison, three different calculation methods are considered in the following.

3.2.3 Multiaxial damage criteria

Von Mises equivalent strains are obtained using the von Mises yield criterion, which accounts for deviatoric stress. Tresca equivalent strains are obtained using the Tresca yield criterion, which accounts for maximum shear stress.

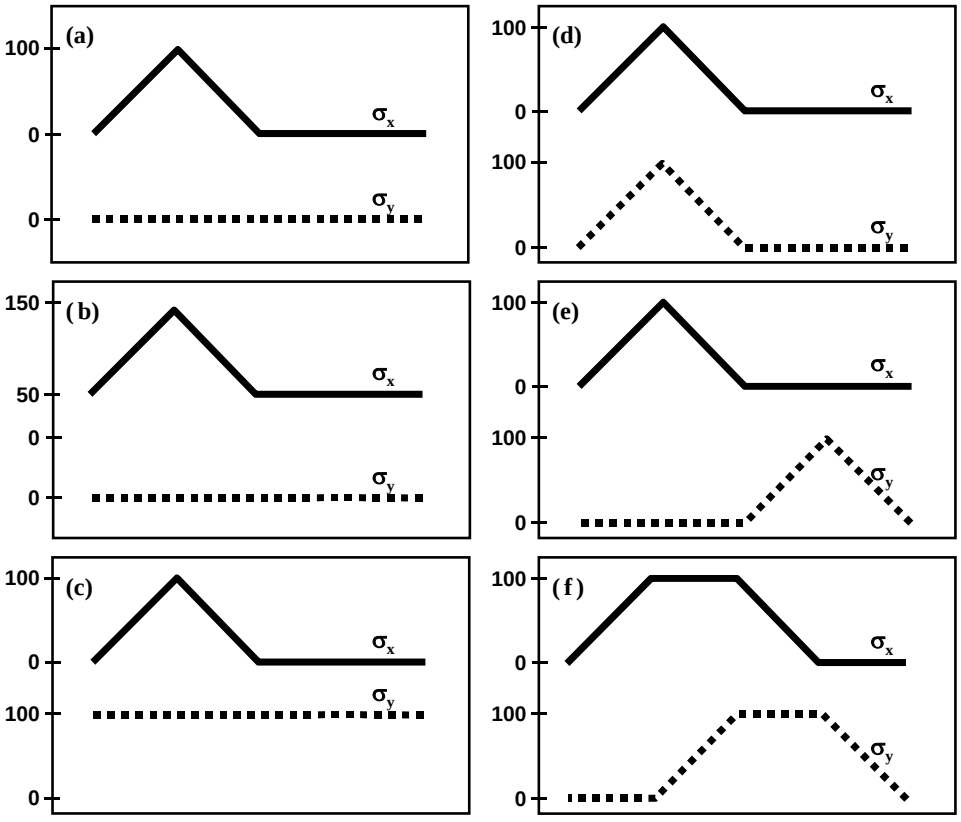

Figure 6. Simplified stress time histories: a) uniaxial, b) uniaxial with mean stress, c) uniaxial with mean stress on the second plane, d) in phase biaxial, e) out-of-phase (alternate) biaxial, and f) out-of-phase biaxial loading.

The Findley critical plane criterion accounts for interaction of shear and normal stresses on a plane where microcracks form. It can be written as

$$\tau^* = \tau + \eta\sigma_n \qquad (1)$$

where τ^* is the effective shear stress used in fatigue life calculations, τ is the maximum shear stress amplitude and σ_n is the normal stress on the plane of maximum shear stress. The critical plane criterion requires an extra material parameter, η, which describes the sensitivity of the material to normal stresses. For many metals this normal stress sensitivity parameter is in the range of 0.2 to 0.3. Because this value tends to be large for stainless steels, a value η=0.3 is chosen in this analysis.

Table 1 shows the computed fatigue lives based on these calculation methods. As seen from Table 1, fatigue life analysis based on von Mises equivalent strain method does not recognise the complex interaction of stresses acting on different planes. In the two out-of-phase cases (e, f), von Mises recognises two cycles, but in case *f* the second cycle is so small that is contributes virtually no damage. Doubled damage in alternate loading remains the only multiaxial effect predicted for these simplified stress time histories.

Also the Tresca method computes equal fatigue damage in cases *a*-*d* but appropriately recognises a significantly larger cycle for the two out-of-phase cases (e, f). The critical plane method is in many ways similar to the Tresca method, but it also incorporates the effects of mean stresses on the plane where fatigue failure is expected. The same fatigue life is computed in cases *a* and *d*, but shorter fatigue lives are predicted in all other cases. Only the critical plane approach recognises between the different mean stresses in the cases a, b, and c, Table 1.

Table 1. Fatigue life calculation for simplified stress time histories in Fig. 6.

	von Mises equivalent strain	Tresca equivalent stress	Findley critical plane
a. Uniaxial	$1x10^6$	$1x10^6$	$1x10^6$
b. Uniaxial with mean	$1x10^6$	$1x10^6$	$5.4x10^5$
c. Uniaxial with mean on second plane	$1x10^6$	$1x10^6$	$4.1x10^5$
d. In-phase biaxial	$1x10^6$	$1x10^6$	$1x10^6$
e. Out-of-phase (alternate) biaxial	$5x10^5$	$3.1x10^4$	$5.4x10^4$
f. Out-of-phase biaxial	$1x10^6$	$3.1x10^4$	$3.6x10^4$

It is interesting to note that all three calculation methods judge cases *a* and *d* to be equally damaging. The in-phase biaxial stress state (d) would be expected to lead to the "elephant skin" type of cracking pattern sometimes associated with thermal fatigue damage. The other cases would be expected to show cracks which grow predominantly in fixed directions.

Specific test data for each of these six load cases is not available for stainless steels. Test data for load cases *a-d* performed on structural steels confirms the value of the critical plane type of approach.

3.2.4 The ASME code and multiaxial fatigue

The Tresca method is outlined in the ASME code [14] as follows:

1) Compute values for each of the six (local) stress components, σ_X, σ_Y, σ_Z, τ_{XY}, τ_{YZ}, and τ_{ZX}, verses time for a complete strain cycle.

2) Choose a point in time at which the conditions are extreme. The stress components at the extreme are designated by the subscript *i*.

3) Subtract the extreme value for all six stress components from the corresponding stress component at each point in time.

$$\sigma_x'(t) = \sigma_x(t) - \sigma_{xi}$$

$$\sigma_y'(t) = \sigma_y(t) - \sigma_{yi}$$

...

$$\tau_{zx}'(t) = \tau_{zx}(t) - \tau_{zxi}$$

4) At each point in time compute the principal stress components derived from $\sigma_X'(t)$, $\sigma_Y'(t)$, ... $\tau_{ZX}'(t)$. These are designated $\sigma_1'(t)$, $\sigma_2'(t)$, and $\sigma_3'(t)$. The principal directions may change direction during a cycle, in these computations, however, each principal stress retains its identity as it rotates.

5) The three components of Tresca equivalent stress are computed at each point in time during the cycle,

$$S_{12}''(t) = \sigma_1'(t) - \sigma_2'(t),$$

$$S_{23}''(t) = \sigma_2'(t) - \sigma_3'(t), \text{ and}$$

$$S_{31}''(t) = \sigma_3'(t) - \sigma_1'(t).$$

6) Find the largest absolute magnitude of any stress difference, i.e., consider the largest difference between any two of the $S_{12}''(t)$, $S_{23}''(t)$, or $S_{31}''(t)$. The alternating stress value during one cycle used in life prediction is half this magnitude.

The following problems with the ASME method have been identified [13].

- No cycle counting method is presented and therefore the method is suitable only for fairly simple load paths and cannot be used for general random load histories.

- The proposed method defines stress or strain range only in terms of two extreme values that occur during a cycle. It is known from experiments, however, that the strain path between the two extreme points has a significant influence on fatigue life.

- As with all equivalent stress or strain criteria, this method computes an average shear value over many slip systems. Experimentally, fatigue cracks are consistently observed on planes having the most severe condition for shear slip. If average shear stress were the correct damage parameter, crack orientation would be a random value.

- The model considers only stress or strain ranges without any mean stress term.

- Complex interactions between different stress components in different planes are not taken into account.

3.3 Environmental effects

The fatigue design curves given in appendix I section III of the ASME code are based on strain controlled tests of small polished specimens tested in air at room temperature. Best fit curves from the experimental data were determined and the design fatigue life curve was computed by adjusting the mean curve by a factor of 2 for strain or 20 for fatigue life, which ever is more conservative. It was intended that this degree of conservatism would account for heat-to-heat material

variability, mean stress effects, load history effects, surface roughness and size effects. The factors of 2 and 20 are not safety factors but are instead data conversion factors intended to obtain reasonable estimates of the fatigue lives of reactor components. Data on which the design curves are based specifically did not include the presence of corrosive environment that might accelerate fatigue failure.

Numerous failure events over the past 20 years have been attributed to fatigue and have led to a re-assessment of the ASME fatigue design curves. Test data obtained over the past 10 years from material tests in LWR environments has shown that some environmental conditions can reduce fatigue lives by one or more decades with the result that the code curves may be far less conservative than previously considered. Some of the available data suggests that environmental effects for stainless steel are more pronounced in low dissolved oxygen content water than in high dissolved oxygen conditions [15–19].

Fig. 7, for example, shows the ASME mean curve obtained in air and the resulting design curve obtained by applying factors of 2 for strain or 20 for fatigue life. Also shown in this figure is test data for austenitic steels tested in LWR environments. A significant portion of the data set falls below the design curve, especially data obtained for PWR environments.

Fig. 8, shows the effect of strain rate and PWR environment on the fatigue strength of 304SS. Open circles represent data for specimens tested in air. In many cases the environment reduces the fatigue life at a given strain amplitude by more than a decade.

EPRI and GE [15] have proposed implementation of an environmental correction factor, F_{en}, which is defined as the ratio of the fatigue life in room temperature air to fatigue life in LWR environment. In the case of stainless steels,

$$F_{en} = \exp\left[0.935 - T^* \cdot O^* \cdot \varepsilon'^*\right] \qquad (2)$$

where T* = T-150 for T > 150, O* = ln(DO/0.04) for 0.05ppm ≤ DO ≤ 0.5ppm, and ε'* = ln(ε'/0.4) for 0.0004 ≤ ε' ≤ 0.4%/s. However, $F_{en} \geq 1$.

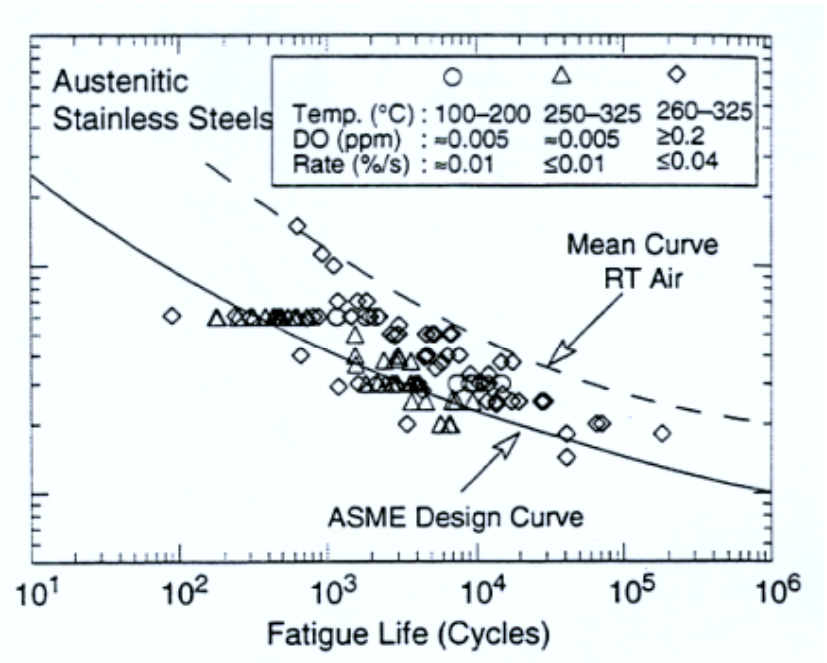

Figure 7. Test data for austenitic steels tested in LWR environments shown with the ASME mean air curve and design curve [17].

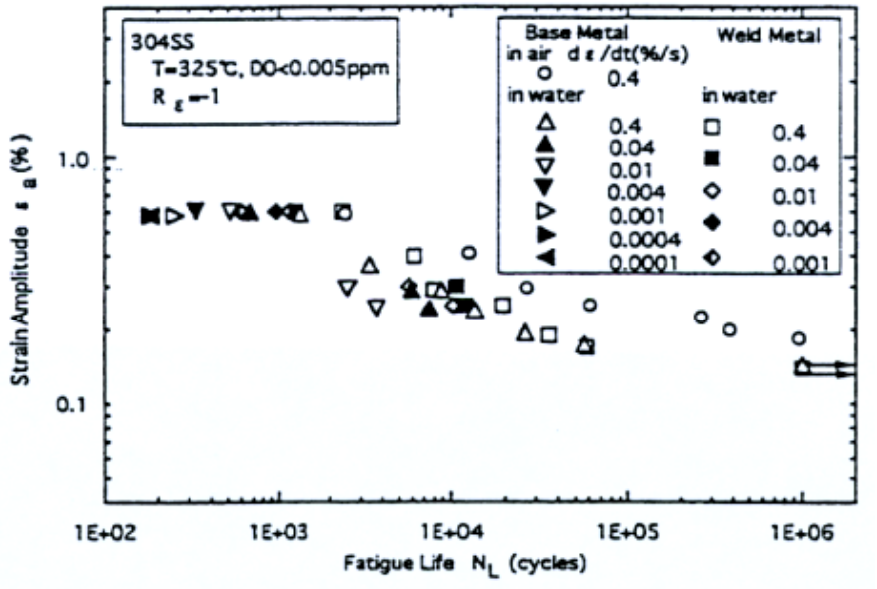

Figure 8. Effect of strain rate on fatigue life in LWR environments [18].

The use of a slightly less conservative "effective" F_{en} has also been proposed. It is intended to take into account some of the environmental effects that are already in the ASME code [15]. For example, surface finish effects are a less severe *additional* effect in LWR environments as compared to in air due to the oxide scale which accumulates in LWR environments even for polished test specimens. However, the US NRC does not recommend the implementation of the less conservative "effective" F_{en} [10].

3.4 Small cycle effects

Very little data is available on the long life load history effects for stainless steels. This is at least partially due to the cyclic stress-strain behaviour of stainless steels which places practical limits on test frequency. Some data on low cycle load effects in austenitic steels is available [20–21], but the load spectra in these cases do not necessarily reflect those expected in NPP components. Of more interest would be data reflecting combinations of large strain cycles, typical of start-up events, and small strain cycles typical of low amplitude TM or mechanical loads.

Constant amplitude test data in air at room temperature suggests a threshold strain amplitude of about 0.16% which, when factors for material variability, mean stress and environment are considered, reduces to a design threshold of about 0.1% [16]. Data for forged and cast materials has shown that cycles 50% or less of the endurance limit stress can still be damaging if they are part of a load history containing a limited number of high strain events.

Several studies on aluminium, low carbon steel, and cast iron specimens have found that a few large cycles in a load history can cause the damage rate of smaller cycles to be greater than that found in constant amplitude loading [22–24]. Large cycles increase the fatigue damage of cycles above the fatigue limit and cause cycles below the threshold to become damaging. An example is given in Fig. 9. Spectrum loading with 3 "start-up" cycles per million exceeding the constant amplitude fatigue limit or causing Miner sums in the order of of 10^{-4} can still lead to failure.

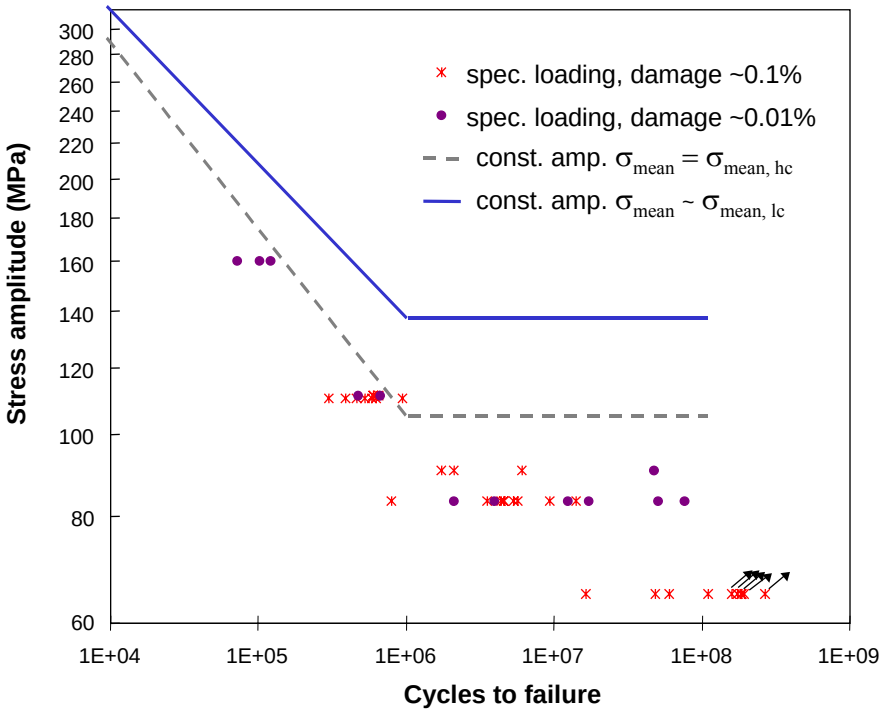

Figure 9. Spectrum fatigue data for a nodular iron [24].

Compressive stresses can also contribute significantly to fatigue life. Fig. 10 shows the effect of single underloads on the fatigue strength of a low carbon steel. Underloads eliminate the fatigue threshold of the material and an increasing frequency of underloads increases the fatigue damage of cycles near or below the threshold.

3.5 Problems in experimental studies

It might be surprising how much essential data is missing. However, as noted before, high cycle fatigue tests for austenitic stainless steels take a long time – even in air. Significant plasticity converts mechanical energy to heat, which would heat up the specimen if a high frequency were be used. This makes critical HCF and spectrum fatigue tests time-consuming, expensive and less attractive.

Relevant corrosion fatigue tests in LWR environments are even more expensive and time-consuming. Realistic environmental effects can be measured only by low strain rates. Furthermore, the experimental problems faced in high temperature water tests has made the test programmes expensive and short.

Strain controlled axial corrosion fatigue tests – as needed for determining the ASME curve – have been made possible only recently when VTT introduced its bellows loaded axial fatigue unit for autoclave use. Previous experiments have utilised a complicated and indirect companion specimen method [17]. Even in constant amplitude tests, the companion specimen method is questionable for nuclear grade stainless steels which may experience both cyclic hardening and softening during the same test. Variable amplitude tests or thermal transient simulations would have been quite impossible before the direct strain control technology was available.

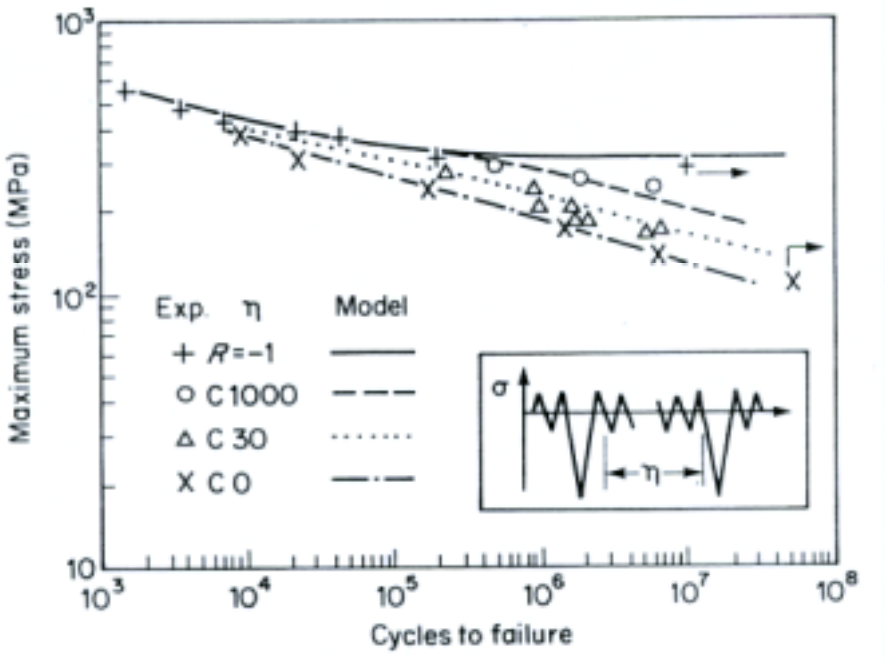

Figure 10. Fatigue damage observed for cycles below the fatigue limit when part of a variable amplitude load history [23].

4. Concluding remarks

This paper has given a brief overview of the current data existing for environmental effects and presented some of the issues of multiaxial fatigue and variable amplitude fatigue that may contribute to deficiencies in current fatigue assessments.

The ASME fatigue design curves for NPP components are based primarily on data obtained from small smooth specimens tested in air using constant amplitude uniaxial loading. Some experimental work to investigate the effects of LWR environment on fatigue of stainless steels has been done in the last decade and these studies have revealed that the existing design curves are non-conservative for some LWR environments.

Several pipe failures in the USA, Japan and Europe have been attributed to high cycle thermomechanical fatigue due to combinations of thermal stratification, mechanical vibration, and global thermal events. Many of these fatigue thermal loads were not considered in the original plant designs. On the other hand, many load cases assumed in the design phase are not observed in service. In reality existing loads require special attention in cases where plant life extension is being considered.

Fatigue life analysis based on von Mises equivalent methods does not recognise the complex interaction of stresses acting on different planes. Fatigue life analysis based on Tresca recognises some of these these interactions but does not account for mean stresses as does, e.g., a Findley critical plane approach.

The fatigue damage contribution of small cycles as part of a variable amplitude spectrum is more severe than the same size cycle during constant amplitude loading. Furthermore, the constant amplitude fatigue limit is not applicable for variable amplitude loading. Stress cycles less than half of the c.a. fatigue limit have been shown to contribute most of the fatigue damage in many load histories containing only few cycles exceeding the c.a. fatigue limit. This has been demonstrated for many materials but has not been examined for nuclear materials in LWR environments.

Well planned experimental studies are recommended to clarify environmental and load spectrum effects on fatigue lives of NPP components. Fatigue critical stress states and time histories should be analysed by in-service monitoring and numerical simulations.

References

1. Sehitoglu, H., "Overview of thermomechanical fatigue", Lecture notes from the Fracture Control Program meeting, Oct, 1996.

2. Bartsch, K., Hänninen, H., and Nieminen, M., "Thermal fatigue: A literature review," Helsinki University of Technology, MTR 3/93, Espoo, 1993. 90 p.

3. Zamrik, S. and Renauld, M. "A biaxial fatigue model for thermomechanical strain cycling," Proceedings 5th Int'l Conf on Biaxial/Multiaxial Fat. and Frac., Crakow, 1997. Pp. 338–354.

4. Shi, H.-J., Niu, L.-S., and Wang, Z.-G., "Mixed mode fatigue behavior under inclined loading conditions for an austentic 304L steel," Scripta Materialia, 1999, **40**, 2, pp. 153–158.

5. USNRC, "Thermal stresses in piping connected to reactor coolant systems", Bulletin 88-08 and suppliments 1, 2, and 3, US Nuclear Regulatory Comission, June 1988.

6. Hirschlberg, P., Deardorff, A. and Carey, J. "Operating experience regarding thermal fatigue of unisolable piping connected to PWR reactor coolant systems", International Conf. on Fatigue of Reactor Components, 31.7.–2.8.2000, Napa, California, EPRI. 7 p.

7. Faidy, C., de Fragulier, E., Leduff, J.-A., Lefrancois, A. and Dechelotte, J. "Thermal fatigue in French RHR system", International Conf. on Fatigue of Reactor Components, 31.7.–2.8.2000, Napa, California, EPRI. 10 p.

8. Jansson, C. "Pipe cracking experience in Swedish BWRs". Int. J. Pres. Ves. & Piping, 1996, **65**, pp. 277–282.

9. Sakai, T. "Leakage from CVCS pipe of regenerative heat exchanger induced by high-cycle thermal fatigue at Tsuruga nuclear power station unit 2", International Conf. on Fatigue of Reactor Components, 31.7.–2.8.2000, Napa, California, EPRI. 21 p.

10. Kalinousky, D. and Muscara, J. "Fatigue of reactor components: NRC Activities", International Conf. on Fatigue of Reactor Components, 31.7.–2.8.2000, Napa, California, EPRI. 16 p.

11. Lancha, A.M., Lapena, J., Serrano, M. and Gorrochategui, I. "Metallurgical failure analysis of a BWR recirculation pump shaft", Engineering Failure Analysis, 2000, **7**, pp. 333–346.

12. Aaltonen, P. "Statistical analysis of cracking in small diameter piping of BWR" in Statistical aspects of fatigue and fracture. I. Virkkunen, G. Marquis, K. Wallin and H. Hänninen, eds., TKK-MTR-1/2000, Helsinki University of Technology. Pp. 123–132.

13. Socie, D. and Marquis, G. "Multiaxial fatigue." Society of Automotive Engineers, Warrendale, 2000. 484 p.

14. ASME Boiler and Pressure Vessel Code, Section III, Div. 1, Subsection NB, Class 1 Components, ASME, New York, 1986.

15. Mehta, H.S. "An update on the consideration of reactor water effects in code fatigue initiation evaluations for pressure vessels and piping", International Conf. on Fatigue of Reactor Components, 31.7.–2.8.2000, Napa, California, EPRI. 7 p.

16. Chopra, O. K. "Environmental effects on fatigue crack initiation in piping and pressure vessel steels", International Conf. on Fatigue of Reactor Components, 31.7.–2.8.2000, Napa, California, EPRI. 13 p.

17. Chopra, O. K. "Effects of LWR coolant environments on fatigue design curves of austenitic stainless steels", NUREG/CR-5704, Washington, 1999. 42 p.

18. Tsutsumi, K., Kanasaki, H., Umakoshi, T., Nakamura, T., Urata, S., Mizuta, H. and Nomoto, S. "Fatigue life reduction in PWR water environment for stainless steels", International Conf. on Fatigue of Reactor Components, 31.7.–2.8.2000, Napa, California, EPRI. 12 p.

19. Roos, E., Herter, K.-H. and Issler, S. "Remarks to the different factors influencing fatigue analysis and fatigue design curves", International Conf. on Fatigue of Reactor Components, 31.7.–2.8.2000, Napa, California, EPRI. 13 p.

20. Polák, J., Vašek A. and Obrtlík, K. "Short crack growth and fatigue life in variable amplitude loading of 316L steel." In: Fatigue Design 1998. Vol. I. G. Marquis and J. Solin, eds. VTT Symposium 181, Espoo, 1998, Pp. 299–308.

21. Gauthier, J.-P., Amzallag, C., Le Duff, J.-A. and Diaz, E.-S. "High-cycle fatigue of auestenitic (316L) and ferritic (A508) steels under Gaussian random loading." In: ASTM STP 1231 Automation in Fatigue and Fracture: Testing and Analysis. C. Amzallag, ed. ASTM, Philadfelphia, 1994. Pp. 286–310.

22. Jurcevic, R., DuQuesnay, D., Topper, T. and Pompetzki, M. "Fatigue damage accumulation in 2024-T351 aluminum subjected to periodic reversed overloads," Int. J. of Fatigue, 1990, **12** No 4, pp. 259–266.

23. Pompetzki, M., Topper, T. and DuQuesnay, D. "The effect of compressive underloads and tensile overloads on fatigue damage accumulation in SAE 1045 steel," Int. J. of Fatigue, 1990, **12** No 3, pp. 207–213.

24. Marquis G. and Solin J. "Long-life fatigue design of GRP 500 nodular cast iron components", VTT Research Notes 2043, Technical Research Centre of Finland, Espoo, 2000. 71 p.

Developments in mechanised ultrasonic inspection and qualification of NDE

P. Kauppinen, J. Pitkänen, P. Kuusinen
VTT Manufacturing Technology
Espoo, Finland

Abstract

1. Introduction

Reliability of non-destructive testing results has a direct influence on structural integrity assessment and safety of the inspected structures, e.g., NPP primary circuit pressure boundaries. Advanced technology together with highly skilled and experienced personnel is required.

One of the current trends is automation. Mechanised equipment can replace tedious manual work in positioning and moving of the transducers. Large areas can be scanned, analysed and numerically documented for direct comparison of eventual later repeated inspections.

Another major trend is qualification, which aims to ensure that the inspection results are correct and fit for the purpose. The suitability and proper operation of equipment, methods and personnel, i.e. the whole chain, shall be proven.

This presentation summarises the advances in automation and qualification of non-destructive inspection during the second project year. Monitoring of material degradation was included in the studied topics and will also be shortly described.

2. Mechanised scanner for ultrasonic inspection

The long term motivation and main objectives of this development work are the following:

- Reduction in irradiation doses during inservice inspections at NPPs.
- Development of scanners for different components.
- Increased reliability of inspection.
- Enhanced possibilities for analysing the results.
- Qualification of the inspection.

2.1 Background

In 1999 a new type of mechanised scanner for ultrasonic inspection of piping welds was constructed and first pilot inspections were performed at the Olkiluoto plant. Based on the experience gained in the inspection of piping welds the development of the scanner was continued in 2000. The target of the work was to develop further the applicability of the scanner to different inspection areas where the access is limited and the working conditions in manual inspection are difficult.

2.2 Novel features of the SC 2000 scanner

The novelty of the new scanner design is the positioning system that allows very rapid positioning on the inspection object. Furthermore, the height of the scanner was again reduced to enhance the applicability on inspection items where free space around the piping is lacking and the height of the scanner is a critical dimension limiting the access. Due to the lightness, compact structure and easy assembly of the scanner on inspection area the SC2000 scanner provides substantial benefits in environments where access or working time is restricted, e.g., due to irradiation doses in "hot parts of" NPP's. Different types of sensors can be attached to the scanner and also adaptation to various NDT-methods is possible. The new scanner with its positioning system is shown in Fig. 1.

Figure 1. SC2000 scanner for mechanised ultrasonic inspection of pipings.

2.3 Pilot inspections

As targeted, the scanner SC2000 was used in pilot inservice inspections of piping welds in Olkiluoto plant. In addition, the scanner was adapted to the inspection of safe-end welds in the emergency cooling nozzles of reactor pressure vessel in the Loviisa plant. Both inspections were successful and demonstrated that the main targets set for the development of the scanner have been achieved.

2.4 Qualification of mechanised inspection

In order to improve the reliability of inspection the complete inspection system (equipment, personnel, procedure) was qualified following the Finnish Qualification practise described in the document The qualification of inservice inspections. This document is based on the European Methodology for Inspection Qualification (ENIQ). The inspection procedure and its technical

justifications were evaluated by Qualification Body formed by several experts of ultrasonic testing. Furthermore, the capability of the inspection technique was demonstrated in practise by arranging an open test with test block containing representative reference reflectors.

The SC2000 scanner was introduced to the NDT-experts world wide in the 15th NDT World Conference in Rome in October 2000.

3. Capabilities and qualification of NDT-techniques

3.1 Development of the Finnish practise

The development of the Finnish practise for inspection qualification was continued in co-operation with the utilities and major inspection companies. First pilot-qualifications were carried out connected to the inservice inspections of Finnish NPPs. One of these was the qualification of the mechanised inspection of piping welds in Olkiluoto plant.

In the Finnish Steering Committee for inspection qualification the work continued by preparing several documents supporting the basic strategy document, The qualification of inservice inspections. Especially a document describing the structure of the qualification examination and the validity of qualification was prepared. This document gives the general outlines of the qualification examinations (content of theoretical and practical examinations) and describes the rules according which a qualification successfully performed for certain inspection item can be accepted to cover other inspection items of the same type.. This practise is an important approach to reduce the number of expensive qualifications without reducing the reliability of the inspection.

3.2 Inspection of reactor pressure vessel shell welds

As a pilot qualification the mechanised ultrasonic inspection of the shell welds of reactor pressure vessel of Loviisa NPP was performed. For this inspection a detailed inspection procedure and technical justifications were drafted. These

documents were the first complete qualification documents prepared for Finnish NPPs and form a basis for further qualifications in the future. The documents are still under evaluation in Inspection Validation Centre (IVC) in UK. Based on the comments received these documents will be finalised.

The qualification of the inspection of reactor pressure vessel welds at Loviisa NPP was reported in the 15th World Conference on Non-Destructive Testing in Rome (Elsing et al. 2000).

3.3 European ENIQ-network

In the European ENIQ-network the preparations for the 2nd pilot study continued. It was decided that the component which will be used for this study will be a BWR nozzle to shell weld. An important issue in this second pilot study will be the use of technical justifications and the possibility to reduce the need for test piece data to qualify the inspections.

The Task Group 4 on Risk Informed In-service Inspection of the European Network for Inspection Qualification (ENIQ) was again activated and VTT participated the group as an observer. The group issued a Discussion Document on Risk Informed In-Service Inspection of Nuclear Power Plants in Europe.

4. Monitoring of material degradation

In the 5th framework programme of EC a new GRETE-project (Evaluation of NDT techniques for monitoring of material degradation) was started in late 2000. In this project the capabilities of different NDE-methods in assessing the degradation of material will be studied in a round robin exercise. The degradation mechanisms considered are irradiation embrittlement of reactor pressure vessel steel and thermal ageing of stainless steel piping. In the kick-off meeting the detailed time schedule for the project was prepared and the matrix of test specimens to be used in the round robin test was specified.

Thermal fatigue of stailess steel will be studied in Work-Package 6 of the project by circulating 58 samples containing different levels of fatigue damage in 8

research laboratories where measurements by different NDE techniques will be performed. The techniques involved are: Magnetic Barkhausen Noise and micromagnetic measurements, Non Linear Harmonic Analysis, SQUID magnetometer and ultrasonic back-scattering. The test samples will be hour-glass specimens of AISI 321 that will be mechanically tested before NDE measurements.

Ultrasonic inspection of a reactor pressure vessel from outside surface

Raimo Paussu
Fortum Nuclear Services Ltd, Vantaa, Finland
Jorma Pitkänen, Pauli Särkiniemi, Harri Jeskanen
VTT Manufacturing Technology, Espoo, Finland
Bernhard Elsing
Fortum Power and Heat Ltd, Loviisa NPP, Finland

Abstract

Welds are one of the main objects in inservice inspections of reactor pressure vessel (RPV). Circumferential core region weld is most critical for RPV integrity and therefore complementary ultrasonic inspection from the outside surface is found necessary.

In reactor pressure vessel inspection, there are some factors that have an effect on the ultrasonic inspection. It is important to know the temperature of outside vessel wall during inspection. Temperature changes the angles of incidence and affects on the detection capability of defects. The state of cladding is important also for detection of the defects at the interface between cladding and base material.

The basic inspection techniques and the measurement of transducer contact will be discussed in this overview. It is very important to have similar noise level in the validation block as in the cladding of the component. By this way, the best verification of the technique for real situation will be achieved.

The crack detection is depending on orientation, skew and tilt angle of the crack. The optimisation for detection of smaller defects requires certain angle of incidence. Noise from the cladding can enlarge the size of detectable defect. These factors are handled in the qualification of ultrasonic inspection of pressure vessel at Loviisa NPP performed from the outside surface.

1. Introduction

Fortum Power and Heat operates at Loviisa two Russian designed PWR units of type VVER 440/213.

Inservice inspections (ISI) of Loviisa NPP are based on the requirements of ASME Code Section XI (inspection scope, objects, methods and interval) following the guides of Finnish regulator. The applied inspection interval is ten years for ISI inspections at Loviisa NPP. Practically, the reactor pressure vessel (RPV) will be totally inspected every eight years from the inside surface through the cladding.

An additional ultrasonic inspection of the critical core section weld from the outside surface will be carried out between the inside inspections of RPV. The specified volumes of inner and outer near surface areas of this core section weld are to be covered by this outside inspection.

The objective of this complementary inspection of core weld is to detect surface breaking defects in the outer surface area, and also, underclad defects and defects penetrating the cladding and growing into the ferritic steel in the inner surface area.

2. Qualification

2.1 Qualification approach in Finland

Finnish Regulator (STUK) has in 1996 set requirements for the qualification of inservice inspections following the “Common position” document of European Nuclear Regulators (NRWG).

The Finnish Utilities together with inspection companies and VTT Manufacturing Technology, as a national qualification Steering Committee, have started to outline and organise the Finnish approach for qualification of inspection systems following the principles of the “European methodology” document and published ENIQ recommendations.

The steering committee will nominate a task-based qualification body formed by independent NDT level 3 experts, and with complementary experts of other fields when necessary, for qualifications of separate inspection cases.

Additional education and training for detection and sizing of cracks in austenitic stainless steel welds has started in 1982 for Finnish level 2 and 3 inspectors participating in the pre- and inservice inspections. Blind tests of personnel for crack detection after training courses have been implemented since 1997.

2.2 Qualification Body

Key tasks of the qualification body are to assess inspection procedure, technical justification and documentation of laboratory trials, and to supervise practical trials with test blocks and their defects, and evaluate the results versus defined qualification requirements. The statement of qualification body summarises the implementation of inspection qualification.

2.3 Level of Qualification

The utility together with the vendor will prepare the document specifying qualification level for approval of steering committee. The basic level of qualification (normal, medium or high) depends on the safety importance of the inspection object and on the safety importance of the inspection to be performed for the integrity of the inspection object. In Finnish approach, the level & rigour of different activities in the process of inspection qualification may deviate from the basic level.

In the case of RPV inspection, normal qualification level & rigour is given for personnel and equipment qualification activities, medium for procedure qualification and technical justification and high for grouping of items.

2.4 Qualification plan

The utility will prepare the qualification plan giving the input data for component, defects and inspection conditions, and the objectives for inspection qualification (capability requirements for inspection system and inspection personnel).

In this inspection task the volumes to be covered are:

- Outer surface area up to 30 mm thickness and 100 mm on both sides of core weld
- Inner surface area up to 40 mm thickness and 100 mm on both sides of core weld.

The defect types and orientations (skew ±10° and tilt ±15°) to be detected in outer and inner surface areas of core weld are defined as follows:

- Axial and circumferential surface breaking cracks in outer surface area
- Circumferential subsurface defects of core weld in outer surface area
- Circumferential subsurface defects of core weld in inner surface area
- Circumferential, but also axial, surface breaking cracks penetrating cladding and grown into ferrite base or weld metal in inner surface area.
- Underclad cracks in inner surface area.

Detectable defect size is defined based on the crack size used in the deterministic safety analysis of RPV divided with the applied safety factor.

Detection capability of inspection system is qualified if the defect size 5 mm * 10 mm (depth * length) will be detected with over 6dB signal-to-noise ratio in the open trials.

3. Inspection procedure

ENIQ Recommendations are considered in the content and structure of inspection procedure. The mechanised ultrasonic equipment Sumiad III with

Masera analysing software (Tecnatom, Spain) is used for defect detection and characterisation. SAFT equipment (IzfP, Germany) is available for accurate analysing of indications and sizing of defects.

Inspection is carried out in assembly of 4 probes in two separate scans, see figure 1. Scanning steps in rotation direction are 5 mm for outer surface inspection and 8 mm for inner surface inspection. The measurement step in scanning direction is 1 mm.

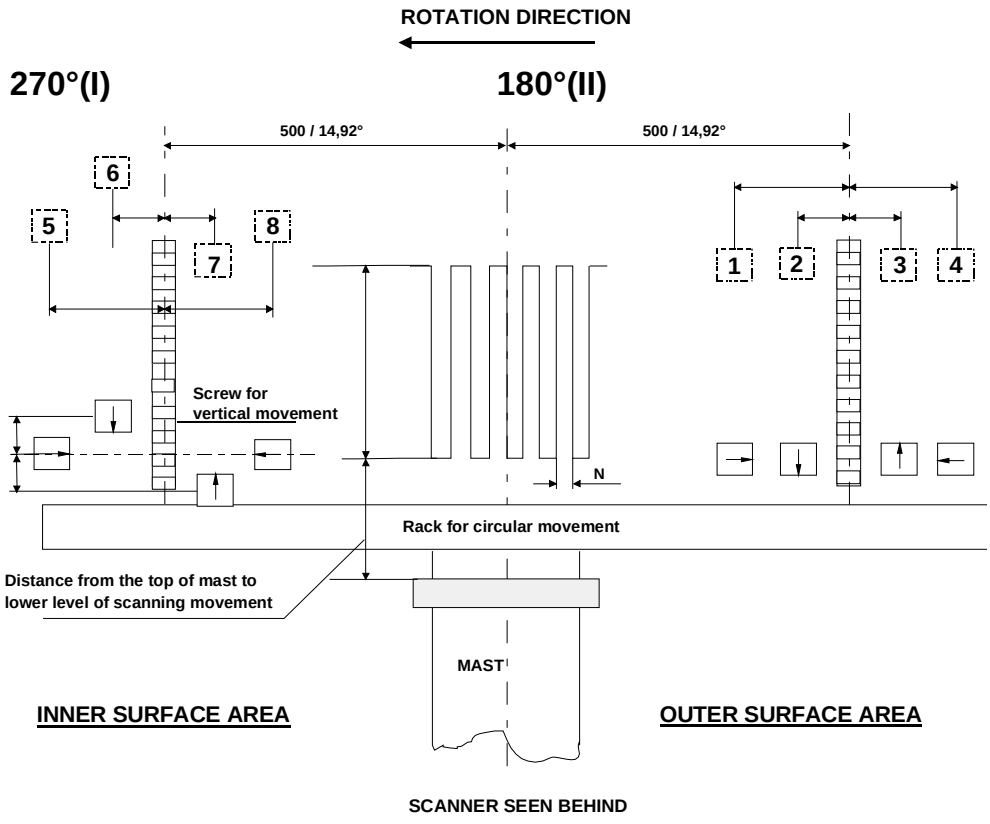

Figure 1. RPV inspection assembly for scanning from outside surface.

Figure 2 shows the different defect size levels (based on standard EN 12062) and how the indications and defects are handled during site inspection.

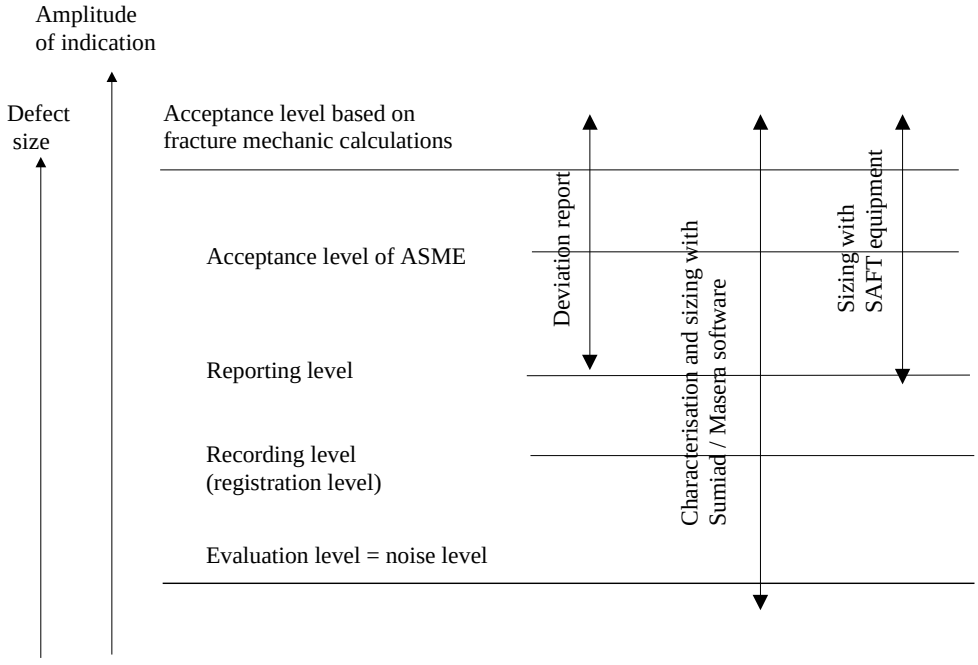

Figure 2. The principles of recording and reporting of indications.

3.1 Inspection technique of outer surface area

The inspection technique for outer surface area is validated first time in 1994 using old probes and old inspection system of VTT, and validation was renewed in 1996 with today's inspection system and optimised probes of VTT.

Twin crystal 70°TRL-St probes are selected for inspection of outer surface area. Surface breaking defects and near surface defects up to 30 mm depth can be clearly detected and analysed with this probe (Särkiniemi, 1994). Two gates are used during scanning – gate 1 for detection and gate 2 for contact control of probes, see figure 3. Multiple peaks with sound path information are stored in both gates from the measured data.

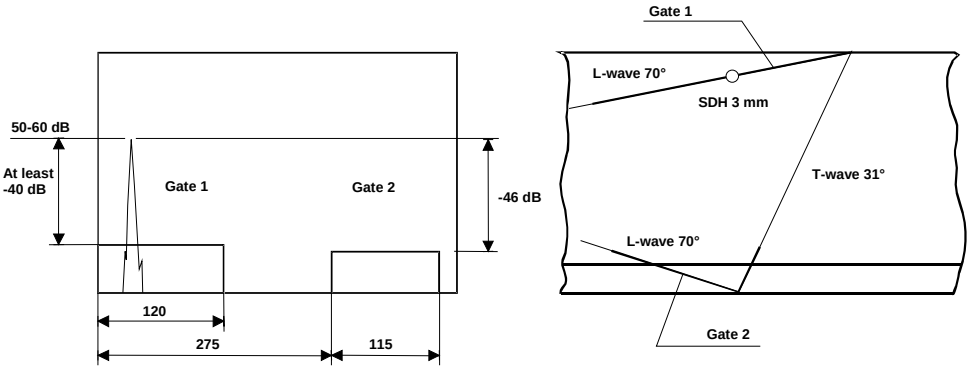

Figure 3. Scanning of outer surface area.

3.2 Inspection technique of inner surface area

The inspection technique to be used for inner surface area is developed in 1994-1996 for outside inspection of core weld and fixing welds of radial supports welded to RPV cladding.

Transversal probes 41° T1-St are selected for inspection of inner surface area. The noise from cladding is applied for contact control of probes. This incidence angle gives an excellent S/N ratio. This 41° T1-St probe is sensitive for detection of both small and large defects. According to Wüstenberg (1972) with angles just below 40° the sensitivity is better than 45° for smaller notches. Similar results were gained also from practical experience, NESC and open trial in 1994, see figure 4. The same probe type were used for scanning of both axial and circumferential defects.

The validation of inspection system and personnel for core weld, for defect detection in inner surface area, is implemented just before site inspection in 1999 under the supervision of qualification body. This open trial is performed using one test block of Loviisa NPP with machined underclad reflectors of qualification size and orientations.

The whole A-Scan is stored from measured signals coming from inspection area.

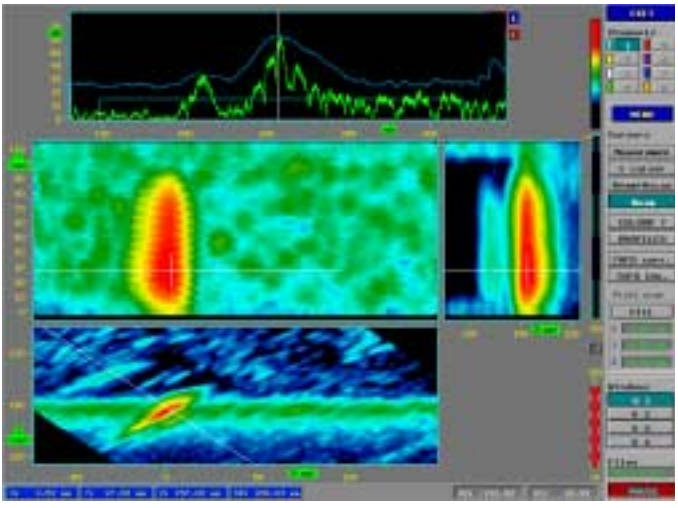

Figure 4. Indication from an underclad fatigue crack in test block PS13. The best S/N ratio was about 30 dB.

4. Technical justification

Technical Justification (TJ) is based on physical reasoning, results of laboratory trials, round robin and field experience and on the results of open trial. The variables of component, defects, procedure, equipment, scanner and analysis of results are defined, assessed and justified in this TJ according to ENIQ recommendations.

Effects of some inspection conditions are studied in more details in this TJ as new aspects. The temperature of RPV outer wall can be about 60°C when starting UT inspection. The significance of that temperature for capability of specified UT inspections is studied and measured with laboratory trials.

Increased angle of incidence of 70° TRL probe due to higher temperature causes better sensitivity for detection of surface breaking defects, and decreased sensitivity for detection of defects located deeper in outer surface area. That temperature has no relevant effect on UT inspection of inner surface area.

The inspection systems of inner and surface areas are optimised and validated using Finnish and Czech fabricated test blocks simulating the real base material cladding structure. Inner surface cladding has a clear noise effect on UT inspection decreasing detection capability of defects. Noise levels of all test blocks applied and the real cladding in RPV are measured and evaluated. The noise levels are confirmed as similar in all cases and the test blocks can be considered representative. So the implemented open trial gives a reliable verificationg of detection capability of inspection system.

5. Experiences on inspection and qualification

The smoothness of outer surface guarantees proper scanning contact for inspections. In local grinding areas, the contact surface can produce extra indications because of swinging of the probe on the surface. The slag inclusions and slag lines of cladding are slightly disturbing the analysis of inspection results of inner surface area.

UT inspection of outer surface area should be performed first during the outage for getting the best sensitivity for defect detection of surface breaking defects.

The qualification activities of the utility and vendor started too late and time enough was not reserved for preparing necessary documentation and open trials. Nomination of the members of qualification body happened so late that their real contribution for selection of test blocks and reflectors to be used in open trial was limited.

Inspection procedure, technical justification and results of laboratory and open trials could be assessed after site inspections some months later. On the other hand, qualification body was able, time to time to supervise the site inspections and analysis of inspection results, and see how the inspection procedure was really followed.

Also the vendor performed more additional laboratory trials before delivering technical justification with the results of trials. The positive statement of qualification body summarised the succeeded implementation of inspection qualification.

6. Summary

When a cladding is present in the inspection area of a component, it is really important for validation of detection capabilities of inspection system, that the properties and noise levels of test block cladding fully simulate the real component cladding.

Like in this specific case, the number of defects in the test blocks is quite limited and not sufficient as an evidence for statistical assessment of detection capability.

The inspection of RPV core weld is one of the first cases for breaking-in Finnish approach of qualification in practice. One of the challenges was to create proper and practical ways for each organisation to work together. The whole qualification documentation together with the statement of qualification body is now delivered for approval process of Finnish regulator.

References

Wüstenberg, H. & Mundry, E., 1972. Nuten und Kanten als Bezugsreflektoren in der Materialprüfung mit Ultraschall, Materialprüfung 14 (1972) 2, pp. 58–61.

Särkiniemi, P. & Pitkänen, J. 1999. Technical Justification; Mechanized ultrasonic inspection of the RPV weld of the cylinder part.

Jeskanen, H. 1999. Inspection Procedure; Mechanized ultrasonic inspection of the RPV weld of the cylinder part.

Särkiniemi, P. & Jeskanen, H. 1994. Document LO1-K311-961-21. Lo1 Mechanized UT-inspection of RPV, Outage 1994 Technical assesment and Open trial, 12.7.1994.

Innovations on life management of VVER reactor pressure vessels

Jyrki Kohopää[1] and Antero Tamminen
Fortum
Vantaa, Finland

Matti Valo and Jussi Solin
VTT Manufacturing Technology
Espoo, Finland

Abstract

The embrittlement rate of the pressure vessel weld material is a dominating factor in life management of VVER reactor pressure vessels. In order to maintain adequate safety level, several backfitting measures have been performed in Loviisa. The neutron flux and embrittlement rate was reduced after receiving the first indications of anticipated problems. An increase of emergency core cooling water temperature and other process related changes followed to eliminate and reduce potential transients. Finally, the core weld of Loviisa 1 was successfully annealed in 1996. A current concern is to verify the post-annealing embrittlement rate in order to enable safe and economic life management of the RPV.

Post-annealing re-embrittlement is governed by somewhat different mechanisms than the embrittlement of the first irradiation cycle. A new tentative approach for predicting the re-embrittlement rate has been proposed.

[1] Corresponding author at Fortum Nuclear Services, Vantaa, Finland

1. Introduction

The Loviisa Nuclear Power Plant operated by Fortum Power and Heat Ltd consists of two VVER-440 units. The first unit was commissioned in 1977 and the second unit in 1980, see Fig. 1.

The issue of neutron radiation embrittlement of the reactor pressure vessel (RPV) and its potential effect on safety margin during postulated thermal transients was raised during the plant design and build-up phase. This led Fortum to design and install material surveillance capsules inside the RPV. The capsules are located such that the neutron dose rate is higher than it for the pressure vessel and that the end-of-life (EOL) condition can be reached during a shorter period.

Higher than expected embrittlement rate of the weld material was observed already when the first surveillance test results of Loviisa 1 RPV were available in 1980. Since that, several plant modifications and other measures have been carried out by the utility in order to mitigate embrittlement and to ensure integrity of the reactor pressure vessel during its entire service.

This presentation gives an overview on the main measures taken to ensure sufficient safety margins and discusses the current models predicting the future embrittlement behaviour after recovery annealing of the core weld area in 1986.

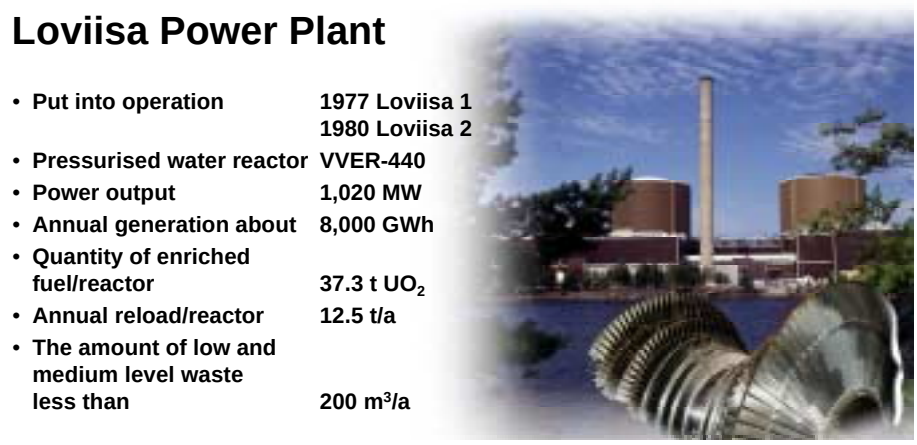

Figure. 1. The Loviisa Power Plant.

1.1 Radiation embrittlement

In light water reactors part of the fast neutrons escape outside the reactor core and hit the reactor pressure vessel (RPV) wall. These fast neutrons cause atomic scale defects in the crystallographic structure of the steel. The formed vacancies and displaced atoms may migrate and/or interact with the alloying elements and impurities present in the solution. Small precipitates, impurity clusters and grain boundary segregation may result. The detailed mechanisms are complex and not completely clarified, but the changes in macroscopic properties are clearly measurable. The microstuctural changes increase the hardness and strength of the steel. But, as expected, this hardening is accompanied by decreased ductility, i.e., radiation embrittlement of the RPV steel.

Embrittlement is a common problem in many pressurised water reactors (PWR), in particular in the Russian VVER designs from 70'ies. If suitable countermeasures were not introduced, embrittlement would become a life limiting factor for safe operation of the plant.

At the time of design and building of the plant, the role and influence of impurities – copper and phosphorus in particular – was not clear. The circumferential welds in the vessel have significantly higher copper and phosphorus contents than the base metal. Unfortunately, one of these welds is near the reactor core area and gets a notable fluence of neutrons during normal operation, see Fig. 2.

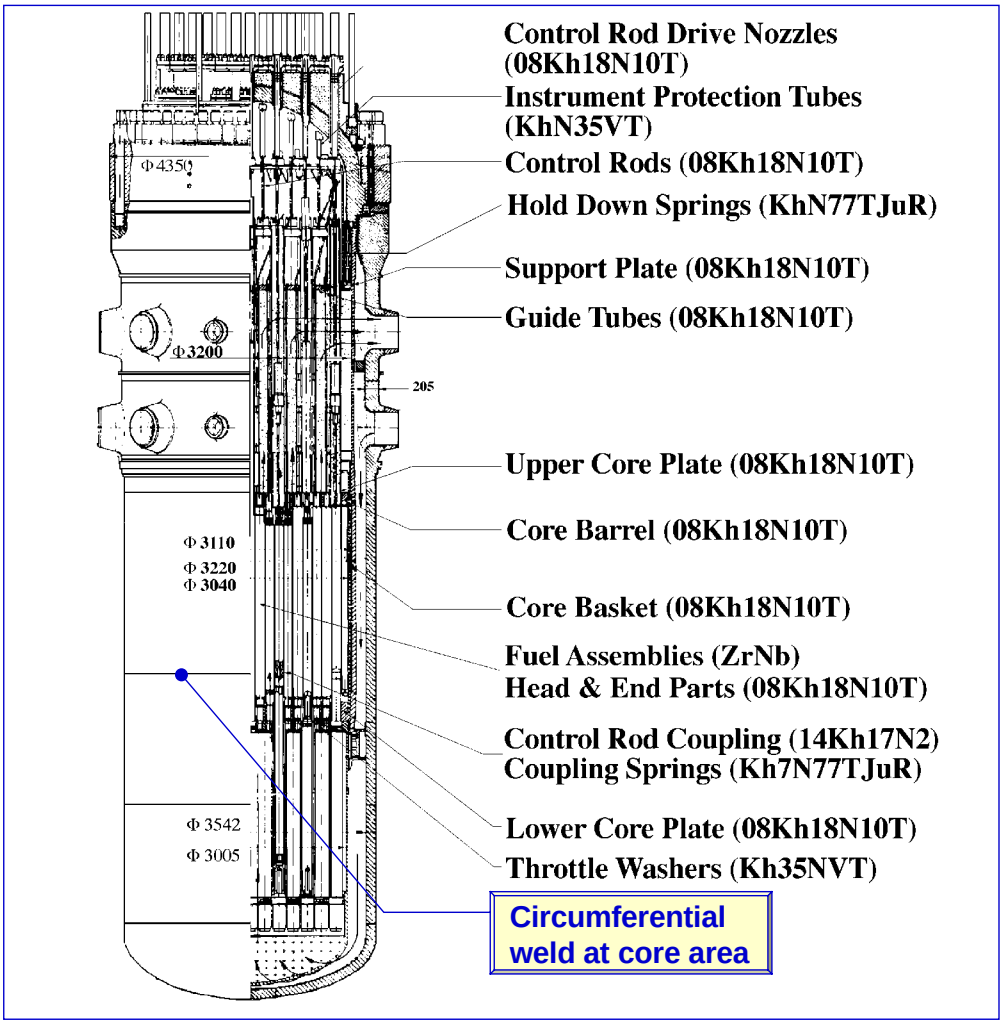

Figure 2. VVER 440 Reactor pressure vessel and location of the critical weld.

1.2 Nuclear safety principles

The western nuclear safety relies on multiple barrier philosophy. The probability of abnormal transients is minimised as close to zero as possible. However, the plant must still be designed and maintained to tolerate even such events without causing a severe accident. In addition to its normal operational function, the RPV also acts as a physical barrier in case of accidents. Both functions set high

requirements on the RPV integrity and ageing management. The abnormal loading function is more sensitive to radiation embrittlement. There are still more barriers, e.g. the steel containment, which fall outside the scope of this presentation. The containment and many other safety features were introduced to the VVER designs for the first time in Loviisa.

The idea of continuous improvement was adopted to the nuclear regulation principles in Finland. In stead of getting a licence for 30 or 40 years in a time, the Finnish NPP's operate on shorter operation licences. Each renewal of operation licence is based on a safety review. The regulatory body requires the utilities to follow the international state of the art and adopt all feasibly available means to maintain and improve the safety.

The Finnish practice has already proven its benefits from both safety and operability points of view. Handling of the Loviisa RPV safety case is a good example of this.

2. Safety requirements

2.1 Acceptance criteria

According to the nuclear safety authority, STUK's regulatory guides ASME III rules are to be applied for Class l Components of Finnish NPP's. The embrittlement of the Loviisa 1 RPV, however, is handled on a different basis by making detailed plant specific studies, where more accurate assessment methods and alternative criteria are used for minimising the uncertainties in the safety assessment. The assurance of the safety of a RPV is based on a deterministic analysis supported by probabilistic evaluations.

The acceptance criterion for the deterministic analysis is that initiation of fast growth of a crack located in the RPV wall is not allowed to take place during the worst postulated transient. The assumed crack size is based on the non-destructive testing capabilities. The transients to be analysed must cover situations, which are expected to cause maximum stresses in the RPV wall due to pressure and temperature variations.

2.2 Analysed transients

At Loviisa the selection of the accidents to be analysed is primarily based on the results of the probabilistic safety analyses. Pressurised thermal shock (PTS) of a reactor pressure vessel caused by injection of cold water from emergency core cooling system (ECCS) into the vessel has been under intense study for more than a decade.

Lately it was realized that - in addition to the internal injection of cold water - a PTS can also be caused by submergence of the RPV in cold water from outside. The reactor cavity may be flooded due to melting of the ice-conderser during some accidents or by a spurious start of the containment spray system. For that reason also thermal shock on the outer surface of the pressure vessel has been analysed. In the deterministic analyses the following classes of accidents were analysed:

- Large loss of coolant accident, LOCA with low pressure.
- Stuck-open pressurizer safety valve in hot standby conditions (after an unspecified occurrence), which leads to flow stagnation and cold plumes, and later reclosing of the safety valve and re-pressurization.
- Pressurizing of a cold RPV.
- Thermal shock on the outer surface of the pressure vessel. This loading case was also combined with the two first cases.

2.3 Assumed cracks

All the estimated transients are severe. Large LOCA has the lowest safety factor when brittle fracture initiation is concerned but in that case the crack will arrest in the pressure vessel wall. Crack arrest calculations were applied only in the large LOCA transient.

In all cases the core weld is the most critical position for a crack. However, the vertical base metal cracks must also be carefully analysed since they might become critical later during the long operation period, which is a target for both of the units.

3. Structural safety analyses

The structural safety analysis of the RPV is a comprehensive process leading to a fracture mechanics based integrity assessment. All input data and methodologies must be carefully verified as shown in Fig. 3.

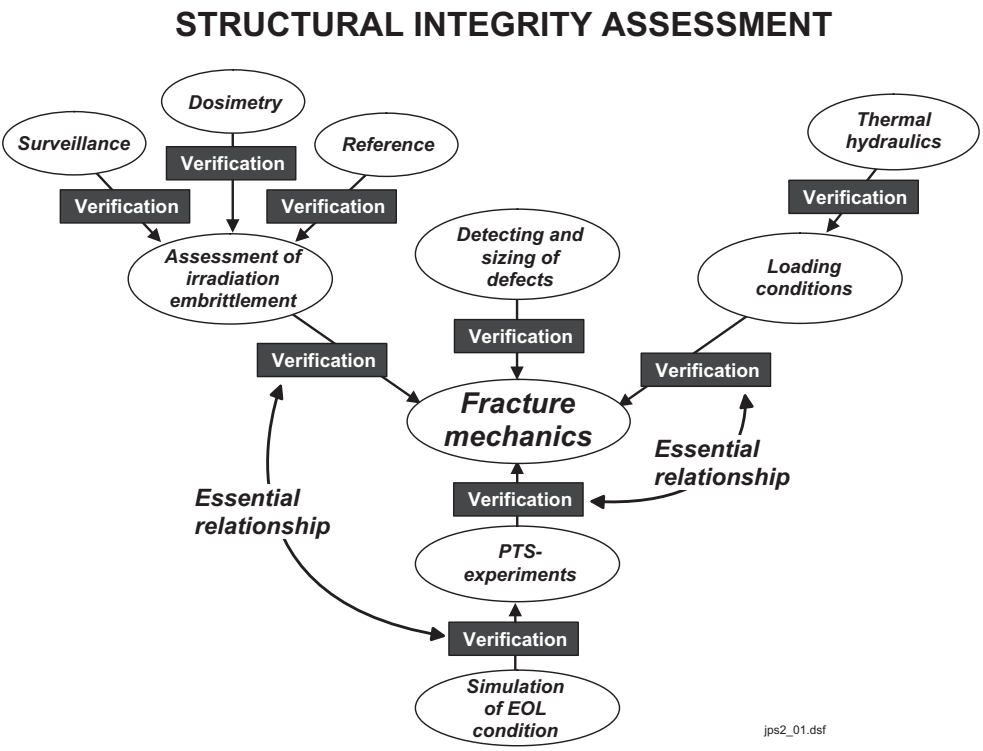

Figure 3. Methods and data for the RPV structural safety analysis.

3.1 Material properties

A comprehensive VVER-440 specific surveillance database has not been available. The material properties used in safety analyses have primarily been based on the plant specific surveillance test results. Fracture toughness K_{IC}-transition curves for irradiated material condition are a key element for the fracture mechanics assessment. Their determination by reliable methods brought both theoretical and technical challenges, which were successfully solved at

VTT. The developed methodology is illustrated in Fig. 4. By the way, the Master Curve approach [ASTM E1921-1997] is also a spin-off result of the Loviisa RPV safety case.

Fracture toughness K_{IC}-transition curves for irradiated material condition have been determined by two different methods. A standard reference K_{IC}-curve for unirradiated material was shifted in the temperature scale by the transition temperature shift measured by Charpy impact testing. K_{JC} values were also measured directly with irradiated pre-cracked Charpy-sized specimens using static three point bending testing. Both methods gave practically the same brittle fracture transition curve for the irradiated weld material.

The properties of the irradiated base material have also been ascertained by taking samples from the outer surface of the RPV. Samples were investigated by carrying out mechanical tests and several microscopic analyses. Chemical composition and neutron fluence of the samples were also determined. The results showed that the methods used for determining transition temperature shifts of the base material are adequately accurate.

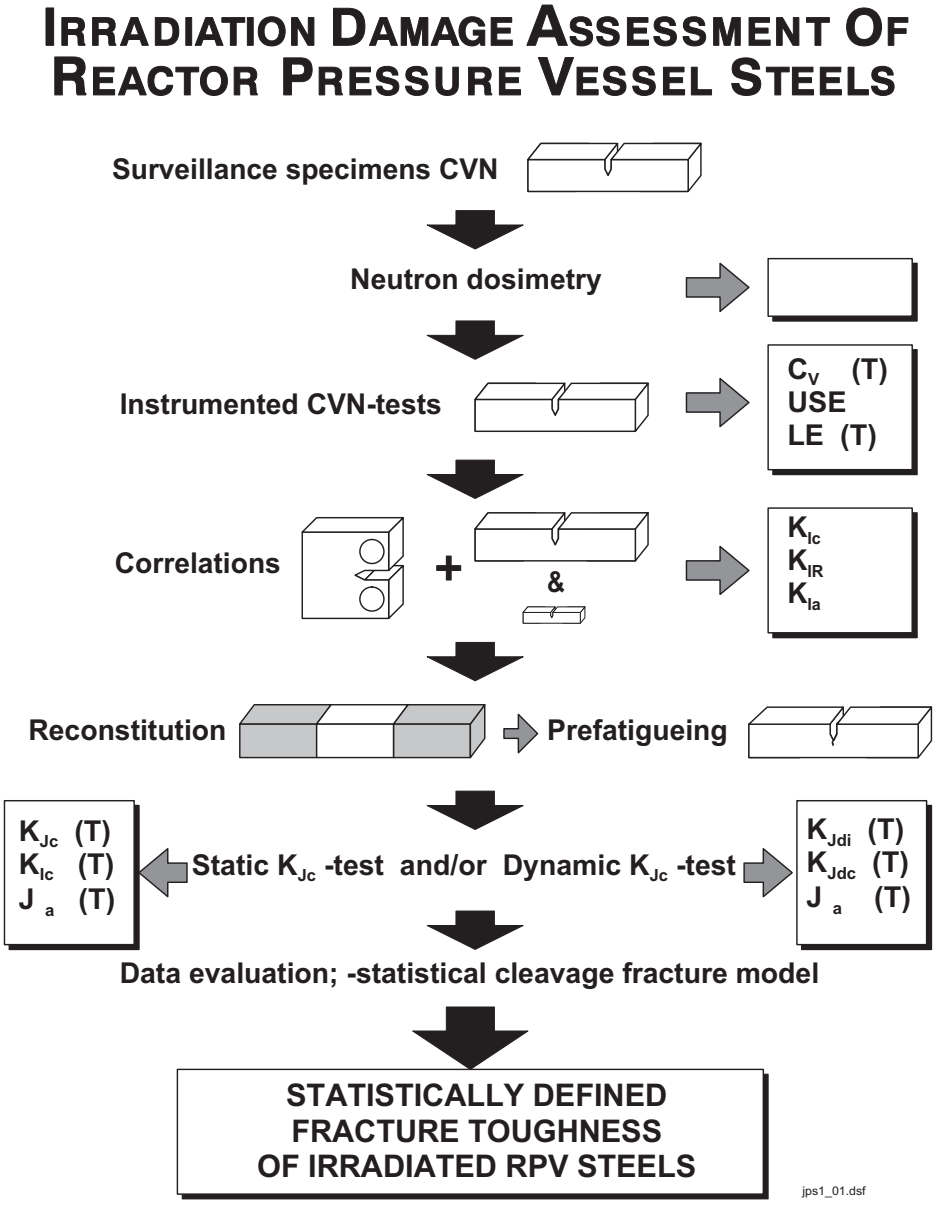

Figure 4. Irradiation damage assessment of RPV steels.

3.2 Neutron fluence

The neutron fluence distribution on the vessel wall has been calculated by the computer program "PREVIEW". For verification purposes altogether 23 material samples were ground from vessel inner surface and 15 samples from vessel outer surface. Also dosimetry wires were spanned on the outer surface of the RPV in horizontal and vertical lines. The consistency with fluence calculations and activity measurements has been found excellent.

3.3 NDE and crack size

The size of the postulated crack in the RPV wall must exceed the minimum crack sizes that can be found with high reliability using modern non-destructive inspection techniques. Beltline zones of the reactor vessels have undergone 100% NDT testing with advanced technique every 8 years. No flaws or cracks have been detected.

The detection limit for a crack has been evaluated to be 5 × 10 mm with more than 90% probability. A safety factor of 3 was introduced. This gave a postulated elliptic crack of 15 mm × 30 mm, which has been used in the analyses. Because the reactor pressure vessel has only circumferential weld seams, only horizontal cracks were postulated in the weld. In the base material also vertical cracks were taken into account in the fracture mechanics calculations.

3.4 Finite element modelling

The analysed stresses were determined as realistically as possible. In addition to normal mechanical and thermal stresses also residual stresses of the main weld seam and the cladding were included in the analyses. The magnitude of residual stresses in cladding was determined by simulating the last heat treatment and hydrotest pressure load of the RPV with finite element methods (FEM).

Elastic-plastic J-integral values are calculated with 3-dimensional finite element methods and converted to stress intensity factor (K_I) values. Material properties applied like stress-strain curve, thermal expansion and thermal diffusivity are

temperature dependent. In the case of cold plumes the heat transfer coefficient is higher in the plume area than outside of the plume.

4. Applied mitigation methods

In order to reach adequate safety level and redundancy, the utility has performed several backfitting measures. The first measures were adopted immediately after receiving the first indications of the anticipated problems in life management of the RPV. Continuous research and development of practical solutions has continued since the early 1980's, and will continue. For example, prediction of post-annealing re-embrittlement will be gradually refined after testing surveillance samples with increasing doses. Fig. 5 illustrates a combination of observed and further predicted ageing behaviour of Loviisa 1 RPV.

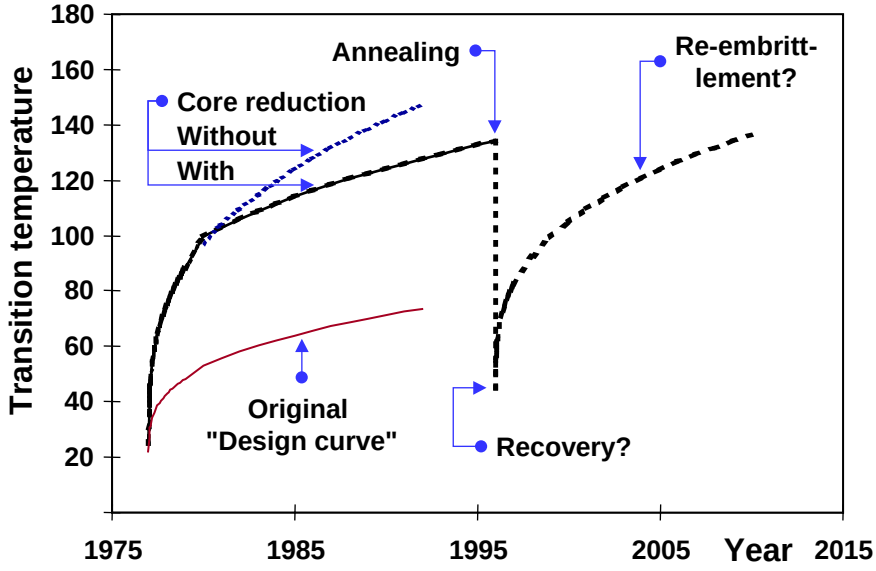

Figure 5. Measured and predicted transition temperature shift of Loviisa 1 RPV.

4.1 Reduction of neutron fluence to RPV

Core reduction was performed in both Loviisa units after the first surveillance results were available. This was the main measure to prevent RPV's from

excessive embrittlement. The neutron flux on the critical circumferential direction was reduced by 83%.

The modification of the core could be implemented without any loss in energy production. A low neutron leakage core design was later adopted by replacing fresh fuel elements in the peripheral positions of the core with used fuel elements. The neutron flux in the peak flux direction was additionally reduced by 18%.

4.2 Elimination and reduction of severe transients

Among the process related changes made are the temperature increase emergency core cooling (ECC) water. This does not reduce the core cooling capacity, but significantly reduces the thermal stresses on the RPV inner surface in case of an emergency cooling situation. The temperature of the two pressurised (ECC) accumulators, which inject directly to the downcomer, was rised to 100°C and the temperature of the ECC water storage tank was increased to 55°C.

The flow capacity and the shut-off head of the high pressure injection pumps was reduced, and the flow capacity of the relief line from the pressuriser was increased. The main steam line and feed-water line isolation criteria were totally modified to be sensitive for the whole spectrum of main steam leaks.

To avoid cold pressurisation, the pressure vessel is not allowed to be in a pressure tight condition at the temperatures below 60°C.

The scope of the emergency operating procedures and the training programme of operators have been extended with regard to the postulated pressurised thermal shock (PTS) transients. Consequently, a large LOCA with high pressure could be left out of the scope of the deterministic analysis, because isolation of primary circuit leaks after severe cooling is not allowed according to operating instructions.

4.3 Annealing of Loviisa 1 RPV

In 1993 the utility decided to anneal the core weld of Loviisa 1. The annealing parameters were established based on material investigations and stress analysis. A target value for the annealing temperature range was 465–505°C and for heating/cooling rate 20°C/h. According to the results of the material investigations about 80% recovery of transition temperature shift caused by irradiation embrittlement can be achieved using the above mentioned annealing parameters.

Temperature distribution during the annealing was monitored with thermo-couples installed on the inside and outside surfaces of the RPV. Stresses caused by local heating of the weld area were calculated on-line by means of 3 dimensional Finite Element model. The measured temperature data were used as an input information for the stress analysis.

Annealing of Loviisa 1 including heating and cooling phases took place between 4.8.1996 and 11.8.1996. The work was carried out according to the plans practically with no delays or deviations. The total time that the annealing related works kept RPV occupied was 12 days. The measured temperature on the inside surface of the weld was 485–500°C and on the outside surface 475–480°C. According to the on-line stress monitoring system stresses in the RPV wall caused by local heating of the weld area were less than 100 MPa including heating and cooling periods.

5. RPV life management

5.1 Material data base for annealing and re-irradiation behaviour

It is clear that shortage of time and relevant materials limits the creation of a data base for post-annealing material behaviour. Because the irradiation history of the vessel wall materials can not be reproduced one to one, extrapolations concerning the applied fluences and fluence rates have to be made. The operating licence is also issued for a limited time span, which means, that the requirements on material data will change in time.

As a first stage, vessel annealing required sufficient data on the material annealing behaviour. Later on re-irradiation behaviour has been the dominating goal for defining the material properties. The material research programmes supporting the annealing and post-annealing operation of Loviisa 1 are described in Table 1.

Table 1. Material research programmes supporting the post-annealing operation of Loviisa-1.

Programme	**Material**	**Irradiation**	**Material conditions**	**Measured properties**
Extended surveillance	Lo-1 surv	Lo-surv	U, I, IA, IAI	CH-V, KLST, K_{JC}
Extended surveillance	Lo-2 surv	Lo-surv	U, I, IA, IAI	CH-V, KLST, K_{JC}
Accelerated surveillance for annealing	Tailored weld	MTR**	U, I, IA, IAI, IAIA, IAIAI	CH-V, K_{JC}
Surveillance for annealing	Tailored weld	Lo-surv	U, I, IA, IAI, IAIA, IAIAI	CH-V, K_{JC}

U	unirradiated reference condition
I	irradiated condition
A	annealing
CH-V	ISO Charpy-V
KLST	subsize Charpy-V
K_{JC}	cleavage fracture initiation toughness measured with ISO CH-V size specimens
**	in Dimitrovgrad by MOHT OTJIG

Since the amount of irradiated material is limited, the research programmes were carefully balanced. The material shortage problem was tackled by two different ways. Reconstitution of the broken surveillance specimens was introduced and used in the annealing and re-embrittlement studies since the middle of 1980's. Additionally, so called "tailored" weld material, which has similar chemical composition and initial transition temperature as the beltline weld of the Loviisa 1 RPV, was purchased.

Other main studies, which were carried out to gain additional information concerning annealing of the RPV, are the following:

- Characterization of a trepan taken from the Novovoronesh 1 RPV by reconstituted Charpy-sized specimens
- Characterization of the cladding of the Novovoronesh trepan
- Study of small "boat samples" taken from Greifswald 1 and 2 RPV's before and after annealing.

5.2 Prediction of re-embrittlement rate

5.2.1 Current models

There are currently three main approaches proposed for predicting the post-annealing re-embrittlement rate: lateral, vertical or conservative shift approach. All three approaches are based on the assumption that the re-embrittlement follows the same path as the embrittlement during the first irradiation cycle. The only difference in the approaches is the way in which the beginning of the re-embrittlement is defined in relation to the original embrittlement path as shown in Fig. 6.

Although, the lateral shift method has been shown to be the most consistent with the experimental test results the currently available results indicate that even the lateral shift approach is not physically correct. It, however, tends to overestimate the re-embrittlement rate, and for this reason, its use for engineering and licensing purposes may be well substantiated.

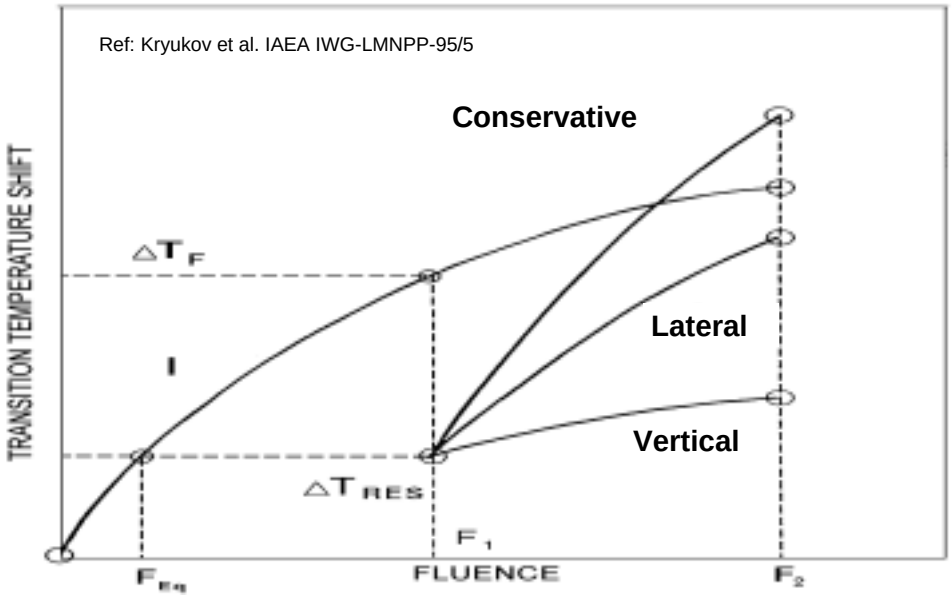

Figure 6. Currently available re-embrittlement models.

5.2.2 New tentative approach

Based on the re-embrittlement results available so far a new tentative approach to describe the post-annealing re-embrittlement behaviour of Cr-Mo-V weld metals has been proposed. This new approach is based on the hypothesis that in the studied weld metals, the solute phosphorus content rather than the copper content is the governing factor in the post-annealing re-embrittlement.

When assuming that phosphorus is mostly dissolved during the thermal annealing, and that copper is still bound in precipitates, the re-embrittlement of Cr-Mo-V steels is governed by the precipitation of phosphorus-rich features. After the saturation of embrittlement due to phosphorus precipitation, the embrittlement probably evolves due to a matrix defect mechanism, but as in very clean steels, at a relatively low rate.

If the above-mentioned mechanism is correct, the total post-annealing embrittlement can be modelled by simply adding the residual embrittlement and the re-embrittlement due to phosphorus precipitation, and possibly also the

embrittlement caused by matrix defect mechanism, see Fig. 7. For this kind of re-embrittlement behaviour a following expression is proposed:

$$\Delta T_{re} = \Delta T_{res} + 2.4 \cdot (F_{re})^{0.5} + 1400 \cdot P \cdot (F_{re})^{0.1} \quad (°C) ,$$

where F_{re} is the post-annealing fluence expressed in 10^{18} n/cm^2 (E > 1 MeV) and P is the phosphorus content of the material (wt-%).

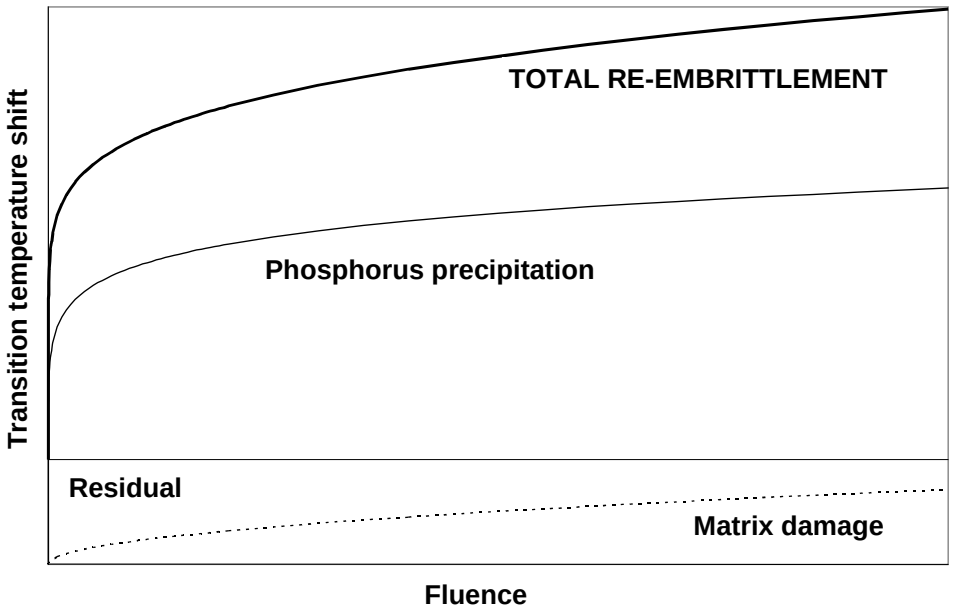

Figure 7. New tentative model for re-embrittlement rate after annealing.

The amount of data available is too limited to allow satisfactory testing of the above-presented tentative re-embrittlement model. Fig. 8 shows comparisons of predicted and measured transition temperature shifts for the currently available data.

More experimental work is required to define the model, as well as for its verification, before it can be used for the actual prediction of the post-annealing re-embrittlement behaviour of VVER-440 RPV welds.

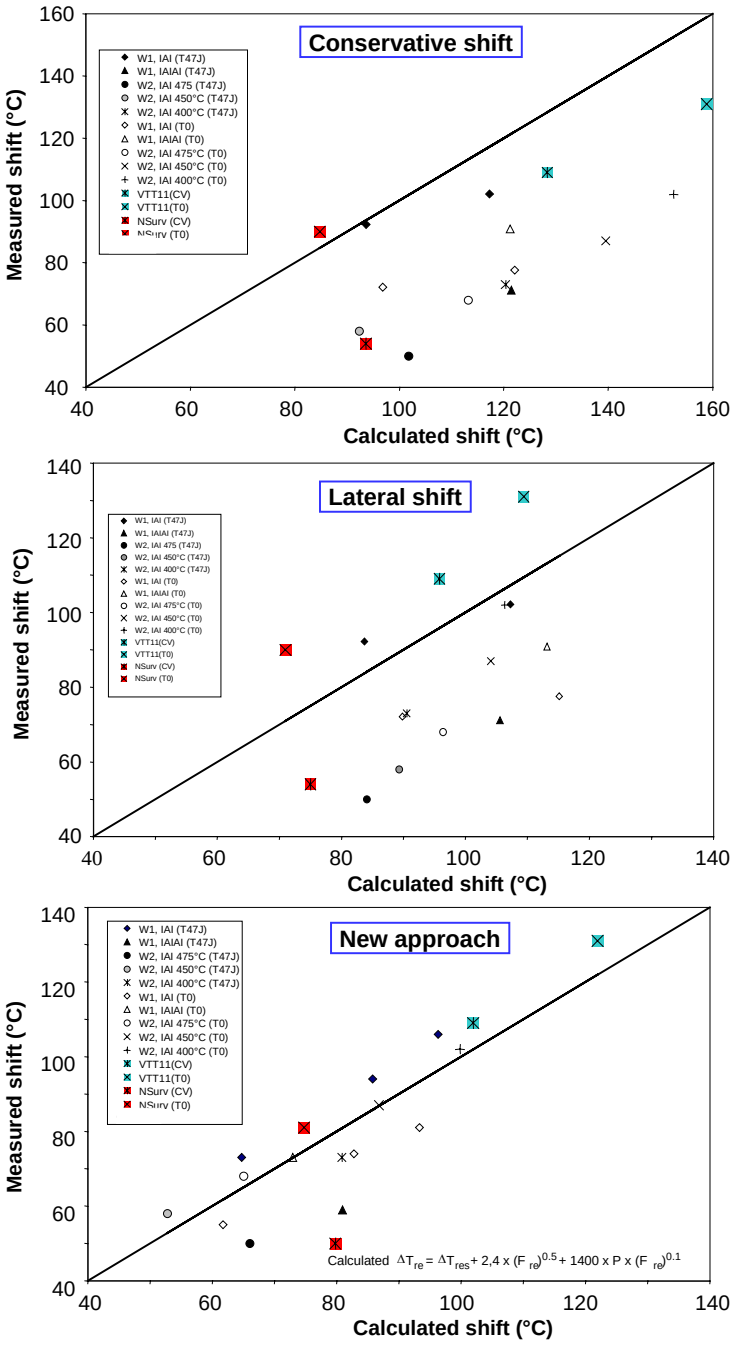

Figure 8. Comparison of predicted and measured re-embrittlement in terms of transition temperature shifts according to the conservative (a), lateral (b) and tentative model (c).

6. Conclusions

Adequate safety level in the postulated transients has been achieved by several measures. Adoption of a low neutron leakage core design has reduced the neutron fluence – and thus also the RPV ageing rate – to a fraction of the original rate. Severe thermal transients potentially subjected to the RPV inner surface have been reduced and/or eliminated by operation and process related modifications. Finally, the Loviisa 1 RPV was successfully annealed to recover its toughness properties.

The current concern is in predicting the future re-embrittlement behaviour of the RPV. The currently available re-embrittlement results allow the following conclusions to be drawn:

1. Thermal annealing treatment is effective in restoring the mechanical properties of weld metals affected by neutron radiation.
2. The impact and fracture toughness transition temperatures of weld metals have similar responses to irradiation as well as to annealing, although no accurate correlation has been found between the transition temperature shifts. The observed changes of the toughness properties have been found to be associated with the changes of the tensile properties.
3. No indications of temper embrittlement have been observed to be associated with the radiation embrittlement of VVER-440 RPV welds.
4. The post-annealing embrittlement rate of the weld metals is not higher than the preannealing embrittlement rate and the increase of the annealing temperature appears to result in a lower post-annealing transition temperature shift.
5. The post-annealing re-embrittlement rate is found to be dependent on the phosphorus content of the weld material.
6. It was observed that the re-embrittlement after thermal annealing at 475°C starts at a relatively high rate, but tends to saturate with increasing post-annealing radiation fluence.
7. The post-annealing re-embrittlement is governed by somewhat different mechanisms than the embrittlement of the first irradiation cycle.

8. The lateral shift approach, currently widely used for predicting the re-embrittlement rate, describes the post-annealing re-embrittlement rate of VVER-440 RPV welds inaccurately, and it tends to give overestimated predictions.
9. A new tentative approach for predicting the post-annealing re-embrittlement rate has been proposed. Much more experimental work is required in order to determine whether the basis of the proposed approach is physically correct.

Acknowledgements

The described results are based on extensive collaboration between Fortum and VTT. The authors wish to point out the contributions of Mr. Ralf Ahlstrand[2], Drs. Rauno Rintamaa[3] and Kim Wallin[3] and many others at Fortum and VTT.

Fortum Power and Heat is thanked for funding of the research and permission to publish these results.

[2] Previously in charge of RPV research at Fortum, currently in IAM/JRC, Petten, the Netherlands

[3] VTT Manufacturing Technology

Tentative re-embrittlement analysis for WWER-440 welds after annealing

M.Valo
VTT Manufacturing Technology, Espoo, Finland
Y. Shtrombakh, A. Kryukov
Russian Research Centre Kurchatov Institute, Moscow, Russia
St. Vodenicharov
Institute of Metal Science, Bulgaria
J.Kohopää
Fortum Nuclear Services Ltd, Vantaa, Finland

Abstract

Re-irradiation data available in RRC-KI and in Fortum Engineering /VTT is analysed in order to identify dependencies of re-irradiation shifts on re-irradiation fluence and flux, Charpy-V specimen size and phosphorus content. The data is considered as a whole and it is well identified that the data is of multi-parameter nature i.e. initial irradiation condition before annealing, re-irradiation condition after annealing, CH-V specimen size, neutron fluence rate, neutron fluence and phosphorus content of welds vary within relatively wide limits. Hence only systematic dependencies on the above mentioned parameters were aimed to be identified. No clear bias in the data based on CH-V specimen size or fluence rate was noticed. When modelling the shift as a function of fluence and phosphorus content, the conservative shift is found to be conservative. The best fit average re-embrittlement rate was found to be less than the upper limit lateral shift model, which is described in the paper.

1. Introduction

Cleavage initiation fracture toughness property of the nuclear pressure vessel materials is required in the safety analyses of the plant. Vessel material properties change due to fast neutron irradiation and possibly due to thermal embrittlement. Currently irradiation effects are monitored with CH-V specimens

and fracture toughness is determined from CH-V data in a correlative manner. In the paper only Charpy-V based re-embrittlement is considered.

The WWER-440 / 230 units have no surveillance programmes and in addition most of them have been annealed in order to mitigate vessel embrittlement. Also Loviisa-1 (type 213) has been annealed. Post-annealing material characterisation for the annealed vessels has been made by vessel wall sampling, by sample re-irradiation in daughter reactors, by enhanced surveillance programmes and by studying tailored materials in supplementary research programmes.

The purpose of the paper is to overview re-irradiation data in a tentative manner. Only re-irradiation data is considered, not the embrittlement in the original irradiation of the materials.

2. Re-irradiation data base

The re-irradiation data available in RRC-KI and in Fortum/VTT is considered. Only re-irradiation shifts measured with Charpy-V type specimens are included. Data on vessel material samples taken from the units Kola-2, Novovoronesh-3 and -4, Kozloduy-1 and -2 and Greifswald-2 is included as well as data on Loviisa-1 and Loviisa-2 surveillance welds and WWER-440 welds 501 and 37. Specimen re-irradiation has been performed in the vessel wall (successive vessel sampling after annealing), in the reduces core surveillance positions in Rovno-1 and Loviisa, in the full core surveillance position in Kola and in the Dimitrovgrad test reactor (equal to full core fluence rate). The respective approximate fluence rates are 10^{10}, 10^{11} and 10^{12} n/cm^{2}s, E> 1MeV. The cross-sectional specimen sizes and the applied transition temperature criteria are as follows: 10mm x 10mm (68J), 5mm x 5mm (8.5J) and 3mm x 4mm (3.1J).

The nominal chemistry contents and neutron fluence values are used. No harmonisation or cross-checking of data or experimental techniques was performed. The applied annealing treatment varied in the range of 465 ^{o}C–490 ^{o}C / 100h–168h.

The ranges of applied environmental and technical parameters are given in Table 1.

Table 1. Approximate ranges of applied parameters.

parameter	range	unit
chemistry		
phosphorus	0.020–0.046	at- %
copper	0.10–0.18	at -%
initial irradiation		
fluence	20–400	10^{18}, n/cm^2, E>0.5 MeV
time	0.5–15	years
fluence rate	10^{10}–10^{12}	n/cm^{2}s, E>1MeV
annealing		
T	465–490	^{o}C
time	100–165	h
cooling rate	not specified	
re-irradiation		
fluence	5–100	10^{18}, n/cm^2, E>0.5 MeV
time	0.3–5	years
fluence rate	10^{10}–10^{12}	n/cm^{2}s, E>1 MeV
CH-V test		
specimen sizes	3x4, 5x5, 10x10	cross-section, mm x mm
trans. temp. criteria	3.1	J (3x4 specimen)
	8.5	J (5x5 specimen)
	68	J (10x10 specimen)

3. Analyses

3.1 Effect of parameter variation

The data is plotted as a function of fluence in Figs. 1 to 3. In Fig. 1 the data is divided into three groups based on the phosphorus content of the material. High phosphorus material shows in general higher re-irradiation shifts as is expected. The main task in the tentative modelling will be the description of the shifts as a

function of phosphorus content and neutron fluence. In Fig. 2 the CH-V specimen sizes are denoted. ISO CH-V data is distributed more tightly on the shift-fluence plane than small specimen data. Hence the models will be fitted into the whole data as well as into the ISO CH-V data. In Fig. 3 the fluence rates are denoted. No clear bias based on the fluence rate is seen in the data.

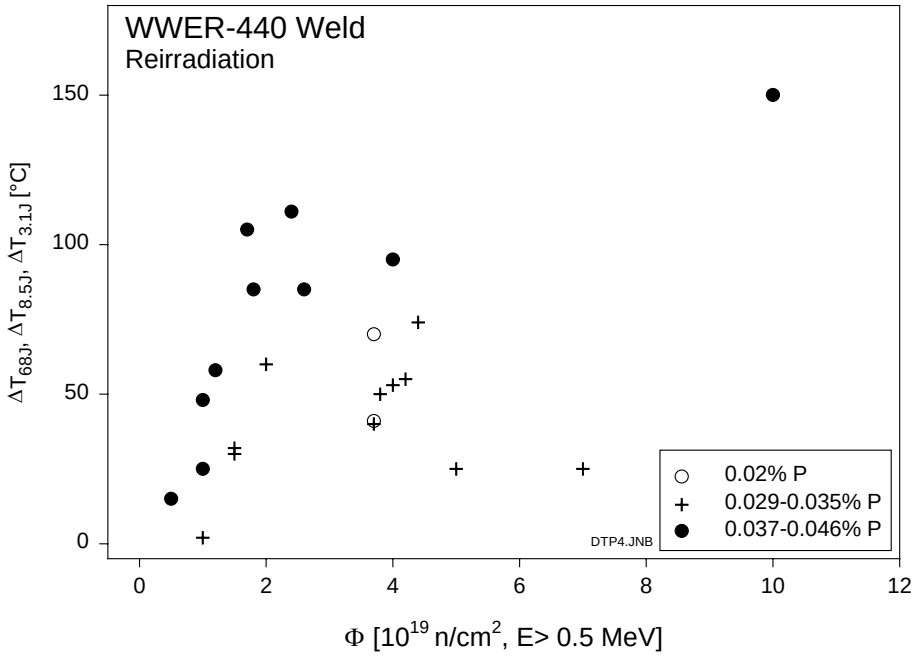

Figure 1. The measured re-irradiation shift as a function of re-irradiation fluence. Approximate phosphorus contents are indicated.

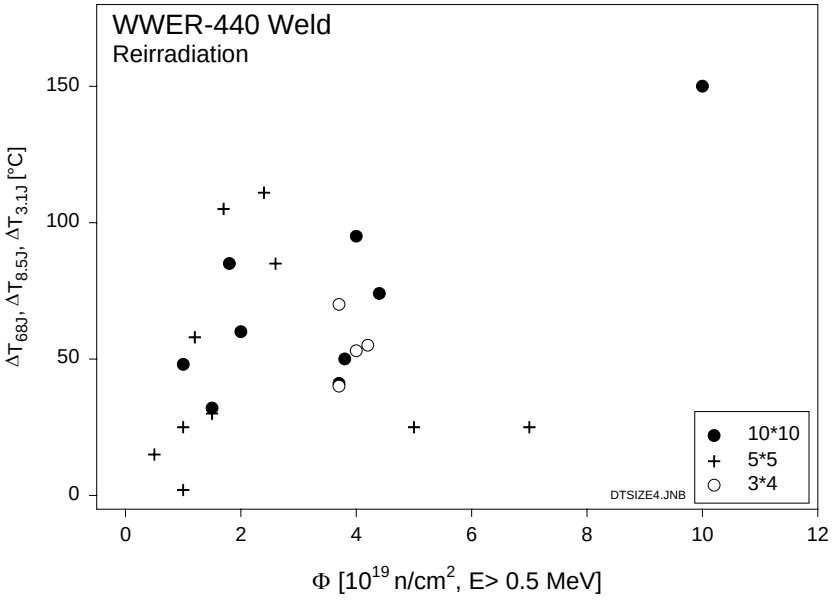

Figure 2. The measured re-irradiation shift as a function of re-irradiation fluence. The CH-V specimen sizes are denoted.

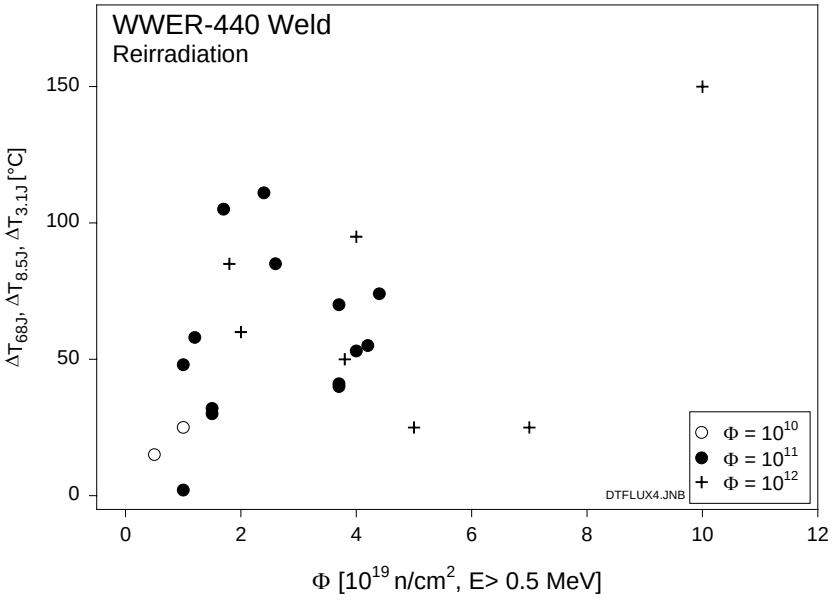

Figure 3. The measured re-irradiation shift as a function of re-irradiation fluence. The applied neutron fluence rates are denoted.

3.2 Modelling of re-embrittlement rate on the bases of phosphorus content and neutron fluence

Traditionally the modelling of re-irradiation embrittlement rate after annealing is derived from the original embrittlement behaviour. The standard models are shown in Fig. 4 and the functional descriptions are given in equations (1) to (3). Currently no verified models on re-irradiation behaviour are available due to small number of re-irradiation data and its diverse character. As irradiation embrittlement data is not considered in the paper the validity of the models can not be checked directly.

Hence only comparisons with the so called upper limit re-irradiation models will be made. It is assumed that the original embrittlement follows the (upper limit) Russian norm function even if in reality the embrittlement rate may be considerably lower. Furthermore it is assumed that the residual shift value is ΔT_{res} = 20 ^{o}C independent of the material. These upper limit functions are defined in equations (4) and (5).

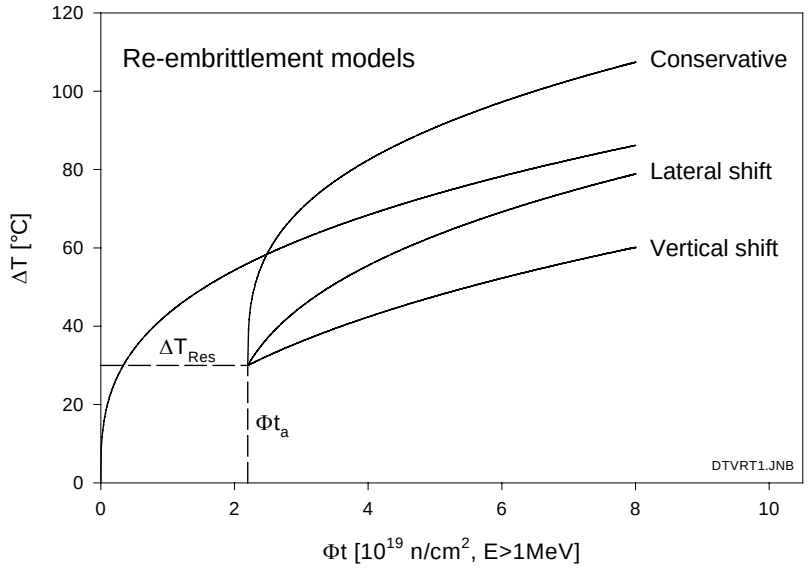

Figure 4. The conservative shift, lateral shift and the vertical shift re-embrittlement models.

In the modelling trial functions are fitted to the data and the model with the smallest standard deviation is considered to be the best estimate. Lateral shift type functions (2) are used as trial functions but the flexibility of the functions is increased by letting the chemistry factor, the value of the residual shift and the fluence exponent to be free parameters. The applied trial functions are defined in Table 2 and the parameter values obtained from fitting are given in Table 3.

$$\Delta T_2^{con} = A*\left(\Phi_2\right)^n, \qquad \textit{conservative shift} \quad (1)$$

$$\Delta T_2^{lat} = A*\left[\left(\frac{\Delta T_{Res}}{A}\right)^{\frac{1}{n}} + \Phi_2\right]^n - \Delta T_{Res}, \qquad \textit{lateral shift} \quad (2)$$

$$\Delta T_2^{ver} = A*\left(\Phi_a + \Phi_2\right)^n - A*\Phi_a^n, \qquad \textit{vertical shift} \quad (3)$$

where A, n and Φ_a refer to the original irradiation, ΔT_{res} to annealing and Φ_2 to re-irradiation.

$$\Delta T^{conservative} = 800*(P + 0.07*Cu)*(\Phi_2)^{1/3}, \quad \textit{upper limit conserv. shift} \quad (4)$$

$$\Delta T^{lateral} = 800*(P + 0.07*Cu)*\left[\left(\frac{20}{800*(P + 0.07*Cu)}\right)^3 + \Phi_2\right]^{1/3} - 20^0 C$$

$$\textit{upper limit lateral shift} \quad (5)$$

The model function 1 in Table 2 is the upper limit conservative shift (4) and the function 2 is the upper limit lateral shift (5) except that the chemistry factor for re-irradiation is a fitting parameter. The measured shift versus the upper limit conservative shift is shown in Fig. 5. It is seen that all data points shift less than the prediction of the upper limit conservative shift model.

All the models in Table 2 give practically the same standard deviation for equal data groups, i.e. the whole data or ISO CH-V data. This is an indication that inherent scatter in the data is relatively large and material behaviour is not explainable better by chemistry and re-irradiation neutron fluence even when

using the more flexible functions 5-6. Function number 5 shows slightly larger standard deviation than functions 3 and 4, because standard deviation is calculated per degree of freedom of the fit. The fits of the model function number 3 into the whole data and ISO CH-V data are given in Figs. 6 and 7.

In Fig. 8 the fits made to whole data and ISO CH-V data of the model function number 3 are shown as a function of fluence for the phosphorus contents 0.02%, 0.003% and 0.04%. Also the measured data points are shown in the figure. According to Fig. 2 the scatter of data points is larger, when measured with small CH-V specimens than with ISO CH-V specimens. This is reflected in the re-irradiation behaviour in Fig. 8, where also the functions based on the whole data cover a wider range than the functions based on ISO CH-V data only.

Table 2. The model functions.

No	Model function	Free parameters
1	$\Delta T^{re-irradiation} = 800 * (P + 0.07 * Cu) * (10 * I_2)^{1/3} + a$	a
2	$\Delta T^{re-irradiataion} = (a * P + b)\left\{\left[\frac{20}{800 * (P + 0.07 * Cu)}\right]^3 + 10 * I_2\right\}^{1/3} - 20$	a, b
3	$\Delta T^{re-irradiataion} = (a * P + b)\left\{\left[\frac{20}{a * P + b}\right]^3 + 10 * I_2\right\}^{1/3} - 20$	a, b
4	$\Delta T^{re-irradiataion} = (a * P + b)\left\{\left[\frac{30}{a * P + b}\right]^3 + 10 * I_2\right\}^{1/3} - 30$	a, b
5	$\Delta T^{re-irradiataion} = (a * P + b)\left\{\left[\frac{c}{a * P + b}\right]^3 + 10 * I_2\right\}^{1/3} - c$	a, b, c
6	$\Delta T^{re-irradiataion} = (a * P + b)\left\{\left[\frac{c}{a * P + b}\right]^n + 10 * I_2\right\}^{1/n} - c$	a, b, c, n
7	$\Delta T^{re-irradia´tion} = a * (10 * I_2)^{0.5} + b * P * (10 * I_2)^{0.1}$	a, b

Table 3. Parameter values derived from the fits made into the whole data and the ISO CH-V data.

No	all data		ISO CH-V data	
	parameters	stand. dev.	parameters	stand. dev.
1	a = -48 ^{o}C	27.8 ^{o}C	a =-39 ^{o}C	14.3 ^{o}C
2	a = 893 b = -4	27.5 ^{o}C	a = 1095 b = -7	14.1 ^{o}C
3	a = 923 b = -5.2	27.4 ^{o}C	a = 1114 b = -7.4	14.0 ^{o}C
4	a = 979 b = -4.2	27.4 ^{o}C	a = 1113 b = -4.6	13.8 ^{o}C
5	a = 966 b = -4.4 c = 28	28.1 ^{o}C	a = 1114 b = -4.1 c = 32	14.9 ^{o}C
6	a = 2731 b = 151 c = 295 n = 9.5	28.6 ^{o}C	a = 702 b = -7.8 c = 0.0 n = 2.2	16.1 ^{o}C
7	a = 4.6 b = 757	30.3 ^{o}C	a = 7.9 b = 635	22.9 ^{o}C

The functions shown in Fig. 8 are the best fit or nearly best fit descriptions of the data. The derived functions are compared with the upper limit conservative shift model (4) and the upper limit lateral shift model (5) in Figs. 9 and 10.

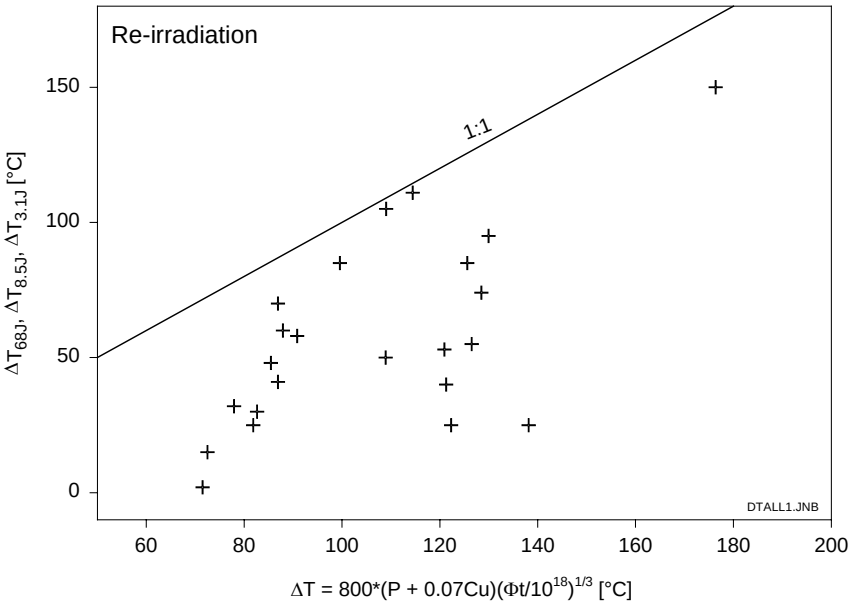

Figure 5. The measured re-embrittlement shift versus the upper limit conservative shift.

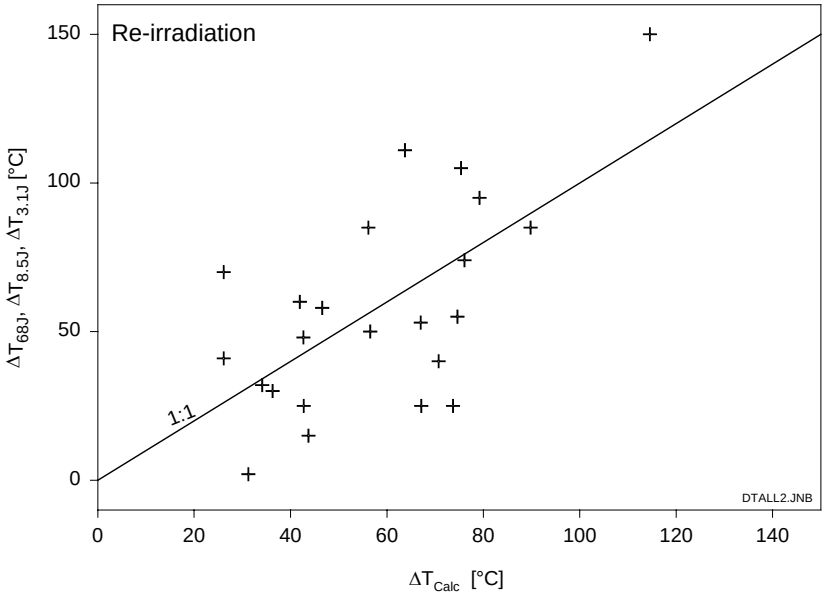

Figure 6. Model function number 3 fitted to the whole data, measured versus calculated shifts.

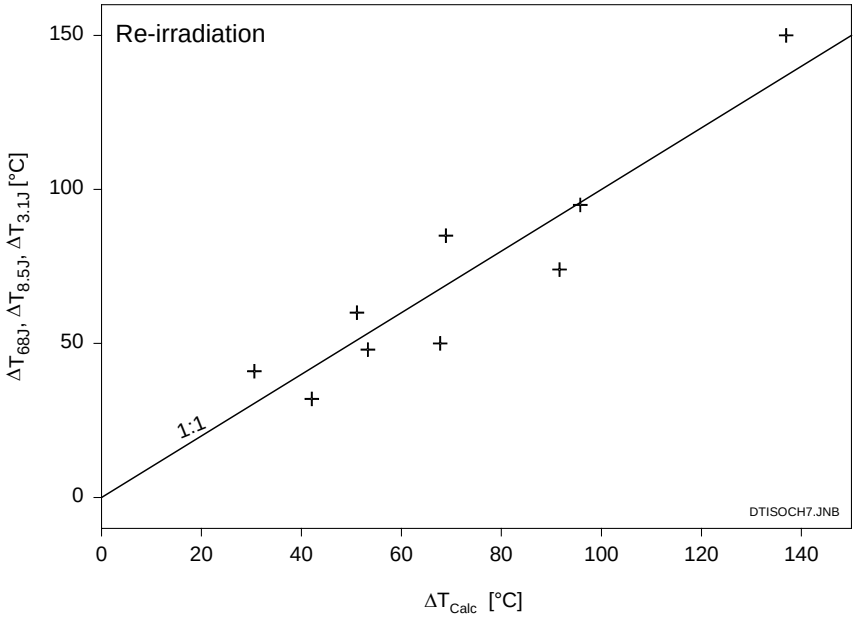

Figure 7. Model function number 3 fitted to ISO CH-V data, measured versus calculated shifts.

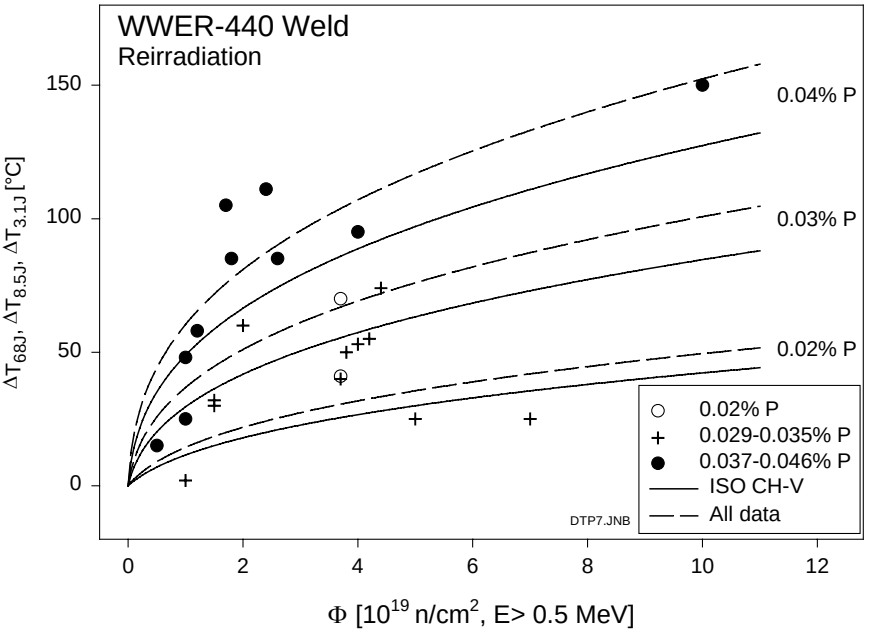

Figure 8. Model function no 3 derived from the ISO CH-V and all data as function of phosphorus content and neutron fluence; measured data included.

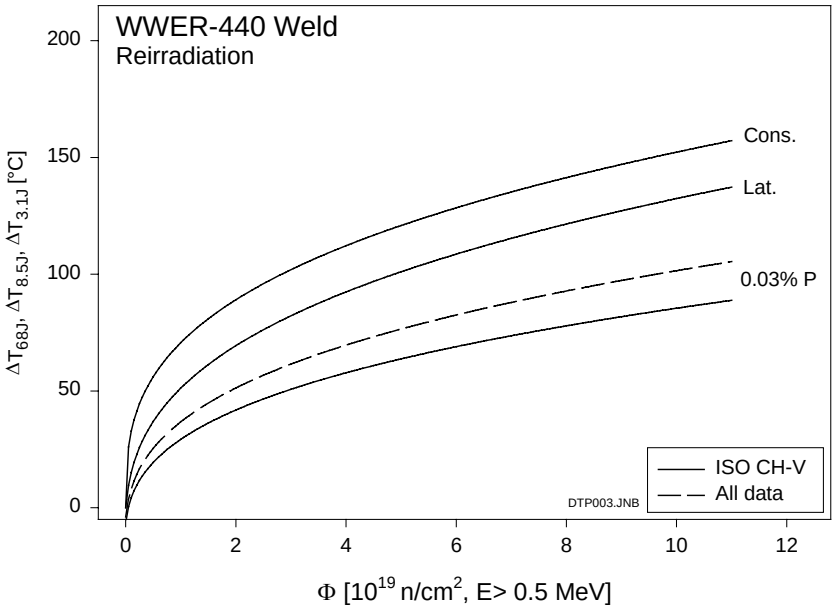

Figure 9. Comparison of the average re-irradiation behaviour with the upper limit lateral and conservative shift models for 0.03% phosphorus content.

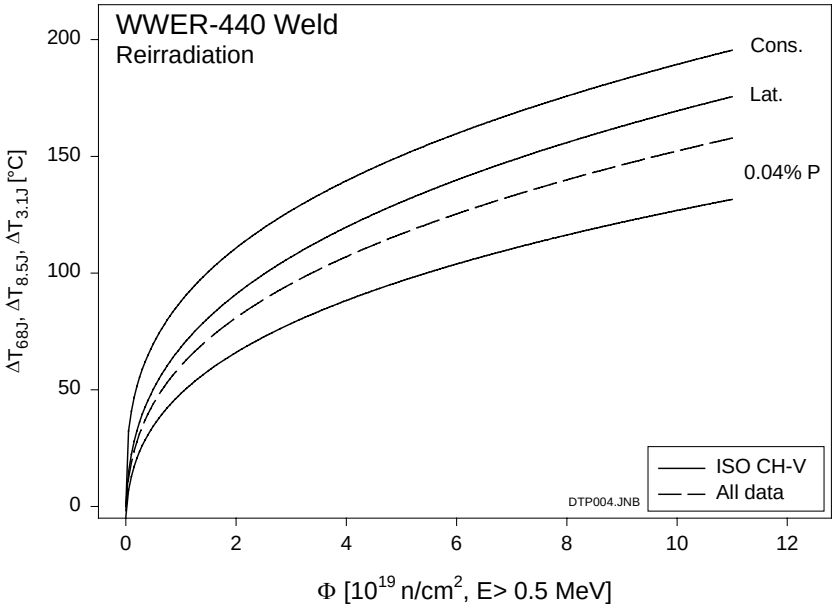

Figure 10. Comparison of the average re-irradiation behaviour with the upper limit lateral and conservative shift models for 0.04% phosphorus content.

4. Discussion

As is indicated in Table 1 the applied irradiation and re-irradiation parameters vary widely. In principle all the parameters in Table 1 may have an important role in re-irradiation behaviour and in the quantitative estimation of embrittlement shifts. Hence it is clear that the data may contain relatively large uncertainties or biases. It is also assumable that small shifts are relatively less accurate than large shifts.

The main trend in the data is assumed to be revealed by the performed analyses.

Fig. 2 and Figs. 6 and 7 suggest that sub-size CH-V data contains more scatter than ISO CH-V data, when toughness changes are monitored. This is understandable as the whole data contains uncertainties due to applied specimen size correlations. Fig. 3 specifies the neutron fluence rates used in re-irradiation and the figure does not reveal any clear trend or bias in the current data based on fluence rate.

The measured data is compared to the upper limit conservative shift model in Fig. 5 and the conservative shift model seems to form an upper limit for the measured shifts. The lateral shift type model function 3 in Table 2 was found to explain the data equally well as the more flexible and complicated functions 5 and 6. The description given by model function 3 is shown in Fig. 8 with the measured data. The model clearly overestimates embrittlement rate at very low fluences and an incubation type threshold fluence may be inherent in the data.

The best estimate shifts are compared with the upper limit lateral shift and the upper limit conservative shift models in Figs. 9 and 10. The best estimate falls below both these models. This conclusion, however, is based on fitted averages and on the norm based upper limit embrittlement assumption. Hence Figs. 9 and 10 do not describe the behaviour of individual materials.

5. Conclusions

The purpose of the paper was to make tentative analyses of re-irradiation behaviour based on multi-parameter data, the nature of which is indicated in Table 1. The findings support current trends i.e. re-irradiation shift is near the lateral shift prediction but this conclusion is based on average behaviour only. Hence the conclusions can not be generalised into individual materials.

The data as a whole has much scatter and some outlying data points. It is clear that progress requires single parameter experiments. The determination of the functional form of re-irradiation requires the use of one material and its re-irradiation into different fluence values.

It is essential that irradiation, annealing and re-irradiation parameters in the experiments are as close as possible to the parameters, which the reactor vessel has experienced. In this respect best material to be used for re-irradiation studies is the vessel material available by the decommissioned Greifswald units.

In the paper tentative re-irradiation models are developed without the original irradiation data. As the creation of original irradiation data is time consuming and expensive, direct modelling of re-irradiation behaviour may be a good and sufficient approach, if only proper irradiated material is available. Direct fracture toughness measurements would give an absolute temperature scale for the re-irradiation data and remove the need to resort to correlations.

Acknowledgements

This study is part of a cluster of joint R&D projects on plant life management and ageing of metallic components, which is realised mainly by VTT in 1999 - 2002. The projects are funded by Tekes, the National Technology Agency, Teollisuuden Voima Oy, Fortum Power and Heat, Fortum Engineering, VTT and to smaller extent also by other energy and process industry in Finland. A significant amount of background information and preparation of the paper originates from the Finnish research programme on nuclear power plant safety (Finnus).

The year 2000 contribution towards quantitative estimation of irradiation and re-irradiation effects on material toughness

Matti Valo
VTT Manufacturing Technology
Espoo, Finland

Abstract

The re-irradiation material studies aim to provide reliable data for the safety analyses of the annealed Loviisa unit 1 pressure vessel. A physical description for the material toughness evolution during re-irradiation should be developed and a clear classification and quantification among the variety of applied toughness parameters should be made. A quantitative re-irradiation model will be approached gradually within the boundary conditions set by the reproducibility of environmental parameters, availability of relevant materials and the required irradiation times. In the current paper data measured with Lo-1 surveillance weld and the simulated weld 501 is given and analysed.

1. Introduction

Middle term annealing and continued operation after annealing of nuclear pressure vessels is a non-standard operation mode, which, however, is the mode by most WWER 440 / 230 plants and by Loviisa unit-1. Quantitative understanding of material behaviour in annealing and re-irradiation is the new challenge by these units.

Embrittlement of the critical weld material is found to depend on phosphorus and copper contents of the weld. This conclusion is based on Charpy-V data. Also re-irradiation behaviour is currently modelled based on these two impurity contents.

In WWER welds phosphorus is the main embrittlement causing impurity. The micro-mechanism behind the phosphorus effect has not been identified and hence material behaviour is derived from mechanical properties without support from micro-mechanistic understanding. Defect evolution in micro-scale proceeds by diffusion and hence environmental parameters may play a important role in the quantitative estimation of material property changes. The most important environmental parameters are the neutron fluence, the irradiation temperature and the neutron fluence rate. Even if not currently clearly identified, the parameters of the initial irradiation may also influence the re-irradiation behaviour of the material. Often the relevant neutron fluence or fluence rate can not be reproduced in surveillance or research work properly and hence an uncertainty due to non-compliance of environmental parameters is inherent in the analyses.

Cleavage initiation fracture toughness is the material property, which is required in the safety analyses (pressurised thermal shock) of the vessel. This property, i.e. K_{JC}, can be directly measured with CH-size fracture toughness specimens but unfortunately most irradiation data is measured with CH-V test. Fracture toughness and impact toughness are different mechanical properties even if sometimes the correlation between them is reasonably good. Often small CH-V specimens are used in the studies, which adds causes additional and sometimes large uncertainty into the data.

The research irradiation programme 11K and other irradiation research programmes (past and future) address to the understanding and reducing of uncertainties in re-embrittlement toughness estimations made for the critical weld. The data has been reported in Finnish in the reports *M.Valo, Säteilytysketju 11K, vuoden 1999 tutkimukset, VAL63-001197, 6.4.2000* and *M.Valo, Säteilytystutkimusketjun 11K lisäkokeet vuonna 2000, VAL63-001974, 14.2.2001*. The current paper is a short English version of the later report.

2. Irradiation embrittlement of weld 501 measured with ISO CH-V test under varying neutron fluence rates

Characteristic for weld 501 is a considerable through-thickness gradient of phosphorus. This gradient is reasonably well characterised and hence by sorting the specimens into equal groups according to phosphorus contents irradiation embrittlement can be measured for several phosphorus contents with one weld. The same weld has been irradiated in Loviisa surveillance position and in the high flux reactor in Petten within the NFS programme REFEREE. Hence the possible effect of neutron fluence rate on embrittlement rate can be estimated with the data. Neutron fluence rates in Loviisa and in Petten are given in Table 1. The measured transition temperatures are given in Table 2 and the measured transition temperature shifts in Table 3.

Upper limit irradiation embrittlement is described in the Russian norm by the function

$$\Delta T = A_f * \left(\frac{\Phi t}{10^{18}} \right)^{n=1/3} \quad (1)$$

where the chemistry factor A_f has the form

$$A_{f,\, E > 0.5MeV} = 800 * (P+0.07*Cu) \quad (2)$$

The numeric value of A_f depends on the applied neutron fluence unit. In Loviisa surveillance position the ratio of the fluence units is [E>0.5 MeV]/[E>1 MeV] = 2.10. The same value is used for Petten Lyra position, because this ratio has not been determined by the JRC personnel. The irradiation shifts calculated from the Russian norm are given in Table 3.

The measured and the norm based transition temperature shifts are compared in Figs. 1–4. The T_{42J} shift follows the norm function well and the shift value is about 70% of the norm prediction (upper limit value). It is noticeable that the Referee-irradiation data point follows the same trend even if it has experienced seven times higher fluence rate as compared to Loviisa irradiation position. The $T_{0.89mm}$ shift is near the norm prediction except the P ~ 0.040% material value,

which clearly exceeds the norm prediction. The reason is the low upper shelf value LE_{US} = 0.98 mm of the material, which is near the conventionally applied transition temperature criterion of 0.89 mm. This data point is an artefact caused by the applied criterion and it does not reflect any abnormal behaviour in material toughness. Embrittlement based on fracture appearance (FA) in Fig. 3 is slightly lower than the norm prediction and the shifts based on the crack arrest load T_{Fa4kN} in Fig. 4 are clearly lower than the norm prediction. The determined crack arrest transition temperatures contain additional uncertainties due to variation of the phosphorus impurity content.

Table 1. Average neutron fluence rates in Loviisa surveillance position and in the JRC Lyra capsule.

Irradiation position	Fluence rate 10^{12} n/cm^{2}s, E > 1 MeV
Loviisa surveillance, 11K	0.24
Loviisa surveillance, 1S1	0.29
JRC Lyra	1.9

Table 2. ISO CH-V based transition temperatures of weld 501.

State	Irradiation	Weld layer	P %	Dose*	T_{41J} °C	$_{0.89mm}$ °C	$T_{FA50\%}$ °C	T_{Fa4kN} °C
ref	-	7–8	~0.028	0	-5	2	-2	-11
I	1S1	2	0.038	2.5	107	146	121	67
I	11K, all	1–8	~0.035	2.0	86	134	89	24
I	11K	1, 6–8	~0.030	2.0	79	112	87	-
I	11K	2–5	~0.040	2.0	106	189	93	70
I	REFEREE	7–8	0.028	0.82	47	66	68	30
					ΔT_{41J} °C	$\Delta T_{0.89mm}$ °C	$\Delta T_{FA50\%}$ °C	ΔT_{Fa4kN} °C
-	1S1	2	0.038	2.5	112	144	123	78
-	11K, all	1–8	~0.035	2.0	91	132	91	35
-	11K	1, 6–8	~0.030	2.0	84	110	89	-
-	11K	2–5	~0.040	2.0	111	187	95	81
-	REFEREE	7–8	0.028	0.82	52	64	70	41

*10^{19} n/cm^2, E > 1MeV

Table 3. Comparison of measured and norm based irradiation shifts. ISO CH-V test. Cu = 0.17% .

	P %	$A_{f,>0.5}$	Dose*	ΔT_{norm} °C	ΔT_{41J} °C	$\Delta T_{0.89mm}$ °C	$\Delta T_{FA50\%}$ °C	ΔT_{Fa4kN} °C
1S1	0.038	40.0	52.5	***150***	112	144	123	78
11K, all	~0.035	37.6	42.0	***131***	91	132	91	35
11K	~0.030	33.6	42.0	***117***	84	110	89	-
11K	~0.040	41.6	42.0	***145***	111	187	95	81
REFEREE	0.028	31.9	17.2	***82***	52	64	70	41

*10^{18} n/cm^2, E> 0.5 MeV

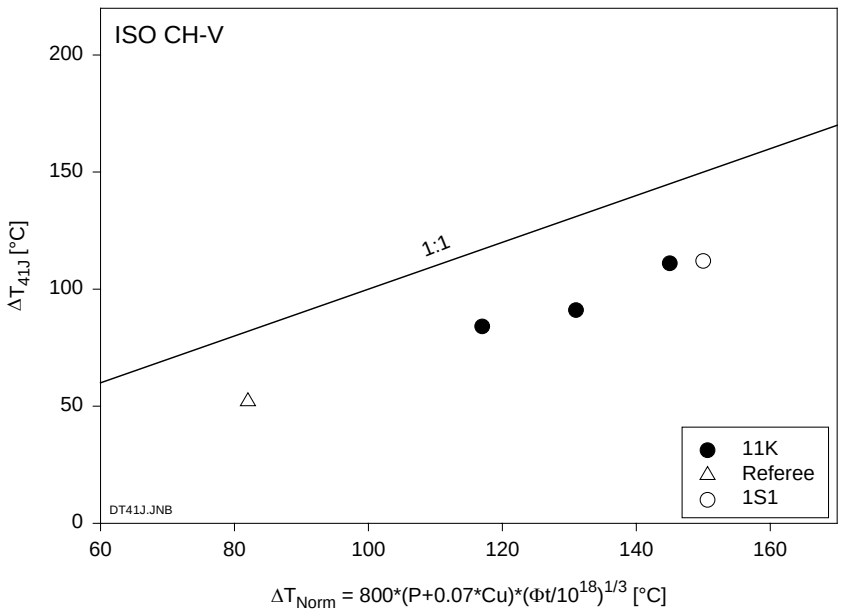

Figure 1. Measured and norm based irradiation shifts. ISO CH-V test, T_{42J} - criterion.

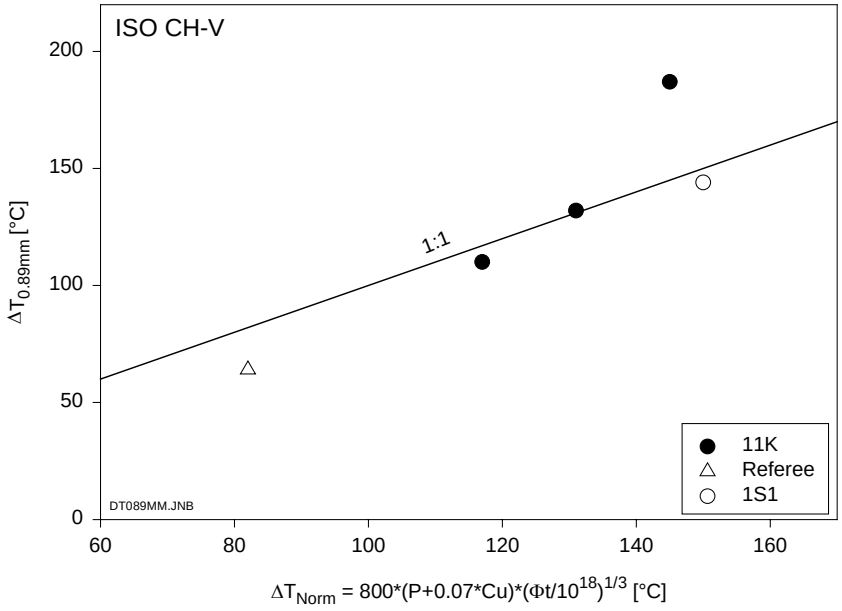

Figure 2. Measured and norm based irradiation shifts. ISO CH-V test, $T_{0.89mm}$ - criterion.

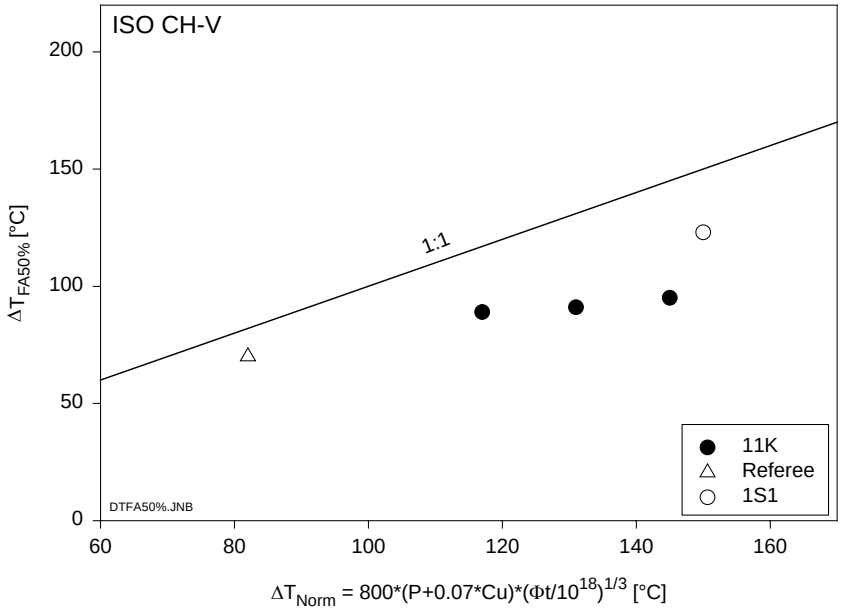

Figure 3. Measured and norm based irradiation shifts. ISO CH-V test, $T_{50\% FA}$ - criterion.

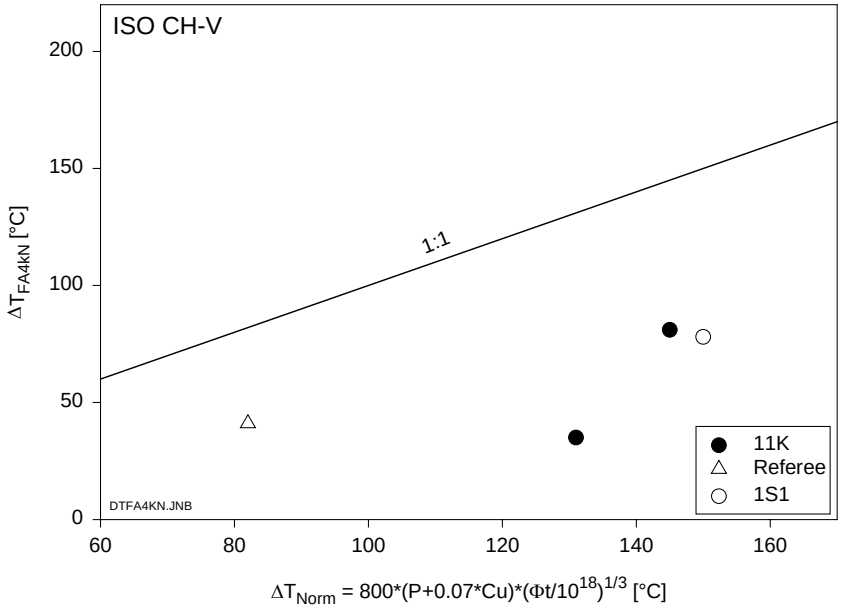

Figure 4. Measured and norm based irradiation shifts. ISO CH-V test, crack-arrest $T_{Fa\ 4kN}$ -criterion.

3. Re-irradiation behaviour of Lo-1 weld measured with KLST-specimens

Summary of toughness of Loviisa-1 weld measured with KLST-specimens for the unirradiated, irradiated, annealed and re-irradiated conditions is given in Table 4. Toughness behaviour is given in Figs. 5–7.

Irradiation embrittlement is described by the function

$$T(\Phi t) = T^{o} + A_{f} * \left(\frac{\Phi t}{10^{18}} \right)^{1/3} \qquad (3)$$

where T^{o} and A_{f} are free parameters. The measured and the norm based embrittlement shifts are compared in Table 5.

Table 4. The measured transition temperatures, KLST-specimen, Lo-1 weld, A = 475°C/100h.

Condition / shift	n	I_1 *	I_2 *	$T_{1.9J}$ °C	$T_{3.1J}$ °C	$T_{0.3mm}$ °C
ref.	18	-	-	**-46**	**-34**	**-43**
I_1	12	5.3	-	**50**	**88**	**60**
I_1A	12	5.3	-	**-19**	**-2**	**-13**
ΔT_{irr}	-	5.3	-	96	122	103
ΔT_{anneal}	-	5.3	-	69	90	73
ΔT_{res}	-	5.3	-	+20	+32	+30
recovery	-	5.3		72%	74%	71%
I_1	12	16.3	-	**113**	**147**	**121**
IA	12	16.5	-	**-18**	**5**	**-6**
ΔT_{anneal}	-	16.3	-	131	142	127
ΔT_{res}	-	16.3	-	28	39	37
ΔT_{irr}	-	16.3	-	159	181	164
recovery	-	16.3	-	82%	78%	77%
$IA_{average}$	-	-	-	**-19**	**2**	**-10**
$\Delta T_{res\text{-}average}$	-	-	-	27	36	33
I_1AI_2 (10K)	18	14.6	1.8	**18**	**42**	**29**
I_1AI_2 (11K)	12	19.5	2.0	**29**	**57**	**30**
$\Delta T_{re\text{-}irr}$ (10K)	-	14.6	1.8	37	40	39
$\Delta T_{re\text{-}irr}$ (11K)	-	19.5	2.0	48	55	40

*10^{19} n/cm^2, E> 1MeV

Table 5. The measured and the norm based embrittlement chemistry factors for Lo-1 weld, KLST-specimens.

Cu	P	$A_{f,\ norm}$		$A_{f,\ measured}$ [E>1MeV]		
at-%	at-%	E>0.5 MeV	E>1MeV	$T_{1.9J}$	$T_{3.1J}$	$T_{0.3mm}$
0.15	0.038	39	**50**	**28**	**33**	**29**

The prediction of the lateral shift model (4) is also shown in Figs. 5–7.

$$\Delta T_2^{lat} = A * \left[\left(\frac{\Delta T_{Res}}{A} \right)^{\frac{1}{n}} + \Phi_2 \right]^n - \Delta T_{Res} \qquad (4)$$

Summary of re-irradiation behaviour of Lo-1 weld measured with fracture toughness, KLST and ISO CH-V specimens is given in Table 6.

Table 6. The measured and the calculated (lateral shift) re-irradiation shifts for Lo-1 weld. The chemistry factors A_f describe measured embrittlement (I) and re-embrittlement (IAI) values. Fracture toughness, ISO CH-V and KLST data.

Criterion	A_f E > 1 MeV		A_f E > 0.5 MeV		ΔT-reirradiation °C		
	I	IAI	I	IAI	$\Delta T_{meas.}$	$\Delta T_{conserv.}$	$\Delta T_{lateral}$
ISO CH-size specimens							
$T_{4\ kN}$	29	21	23	16	**58**	80	**68**
To	38	28	30	22	**77**	105	**55**
$T_{42\ J}$	32	27	25	21	**75**	88	**56**
$T_{0.89\ mm}$	36	31	28	24	**84**	99	**64**
$T_{50\%SA}$	29	21	23	16	**58**	80	**44**
KLST specimens							
10K							
$T_{1.9\ J}$	28	14	22	11	**37**	73	**48**
$T_{3.1\ J}$	33	19	26	15	**40**	86	**53**
$T_{0.3\ mm}$	29	15	23	12	**39**	76	**45**
11K							
$T_{1.9\ J}$	28	18	22	14	**48**	76	**50**
$T_{3.1\ J}$	33	20	26	16	**55**	90	**55**
$T_{0.3\ mm}$	29	15	23	12	**40**	79	**48**
10K+11K							
$T_{1.9\ J}$	28	16	22	12	**43***	76	**51***
$T_{3.1\ J}$	33	18	26	14	**49***	90	**55***
$T_{0.3\ mm}$	29	15	23	12	**41***	79	**48***

* shifts corresponding to a dose of $2.0*10^{19}$n/cm^2, E > 1MeV

Re-embrittlement rate of Lo-1 weld, when measured with KLST-specimens, is in all cases lower or equal than the prediction of the lateral shift model contrary to the ISO CH-V behaviour in Table 6, which is faster than the later shift model prediction except the crack arrest behaviour, which is based on the 4 kN crack arrest load.

The initial irradiation embrittlement rate of Lo-1 weld, when measured with KLST specimens, is according to Table 5 clearly slower than the prediction of the upper limit norm behaviour.

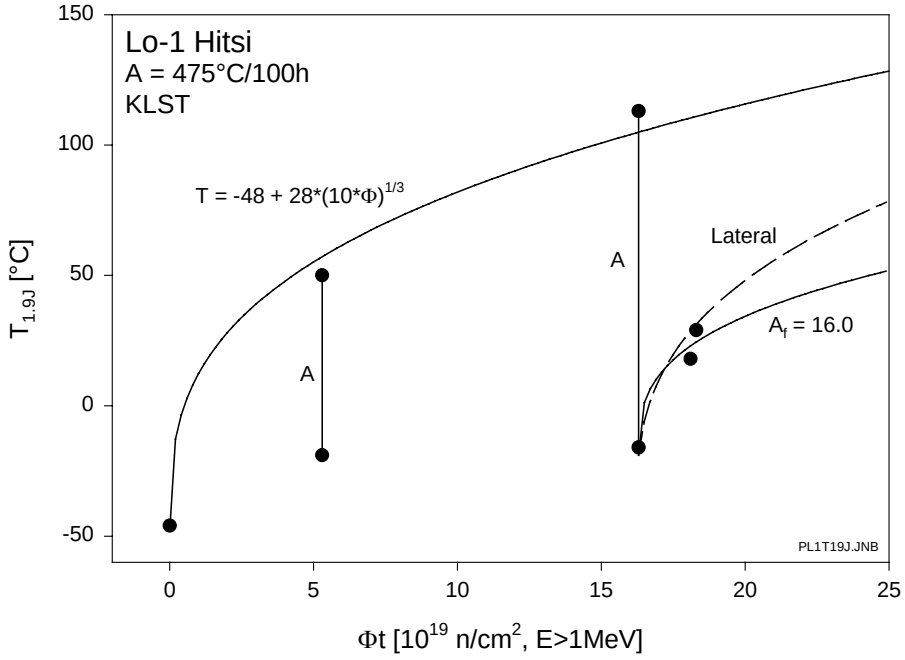

Figure 5. The $T_{1.9J}$ - transition temperatures for Lo-1 weld, KLST-data.

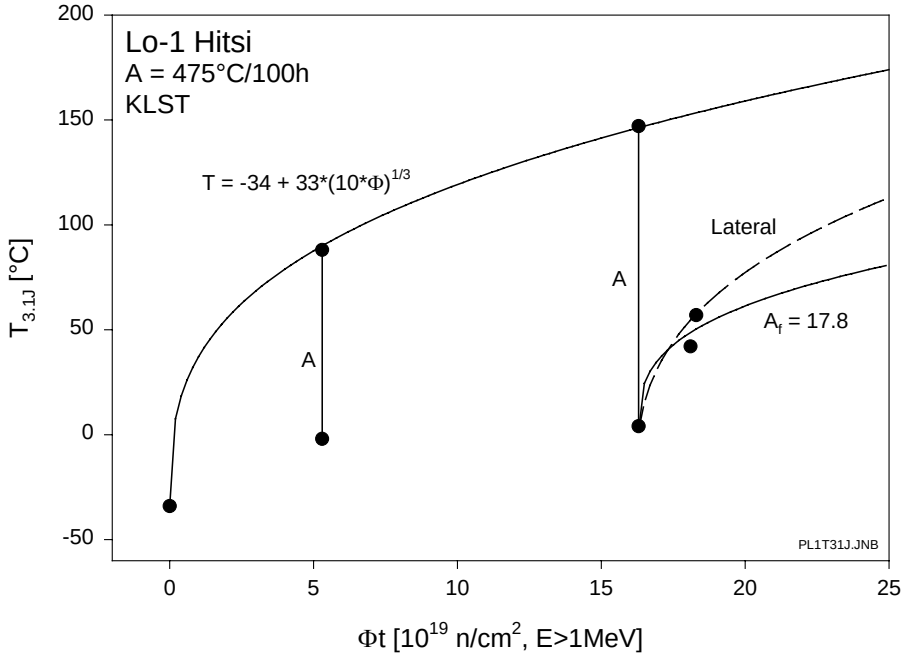

Figure 6. The $T_{3.1J}$ - transition temperatures for Lo-1 weld, KLST-data.

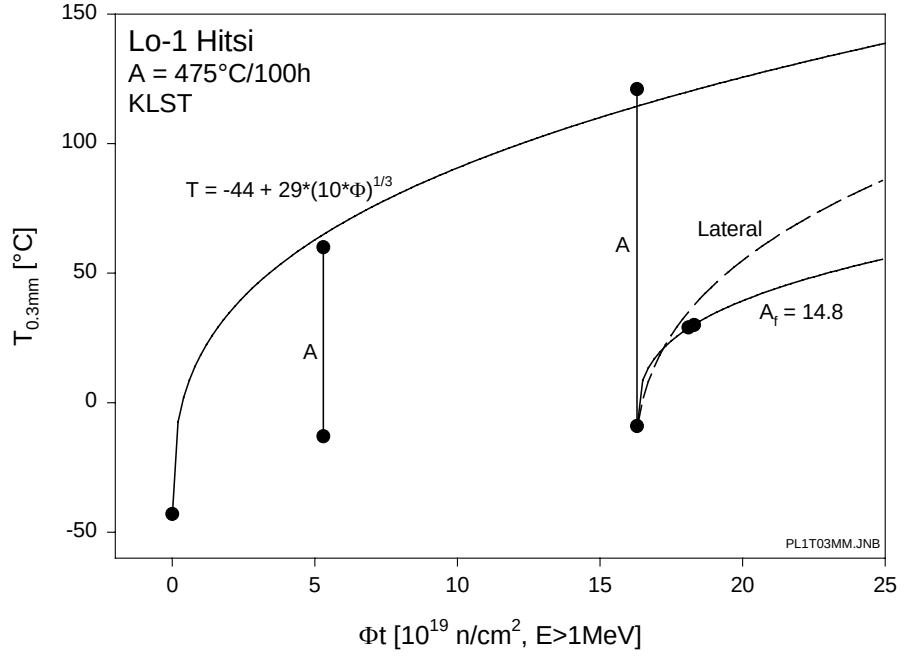

Figure 7. The $T_{0.3mm}$ - transition temperatures for Lo-1 weld, KLST-data.

4. Master curve transition temperature T_0 for Lo-1 weld measured with B = 10 mm and B = 5 mm size specimens, IAI-condition

The Master Curve To transition curves measured with B = 5 mm and B = 10 mm specimens are given in Figs. 8–9. Difference between the measured transition temperatures is 17°C (T_o^{B10} = 91°C and T_o^{B5} = 74°C), which is relatively large. Hence a simple analyses of uncertainties caused by some inhomogeneity factors is given below.

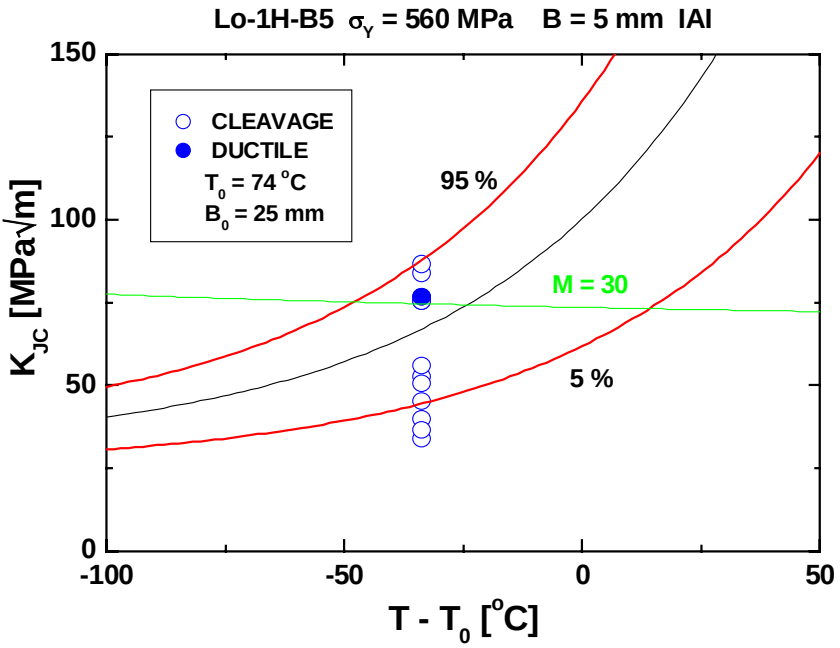

Figure 8. The Master Curve based transition behaviour of Lo-1 weld, IAI-condition, B = 5 mm specimen size.

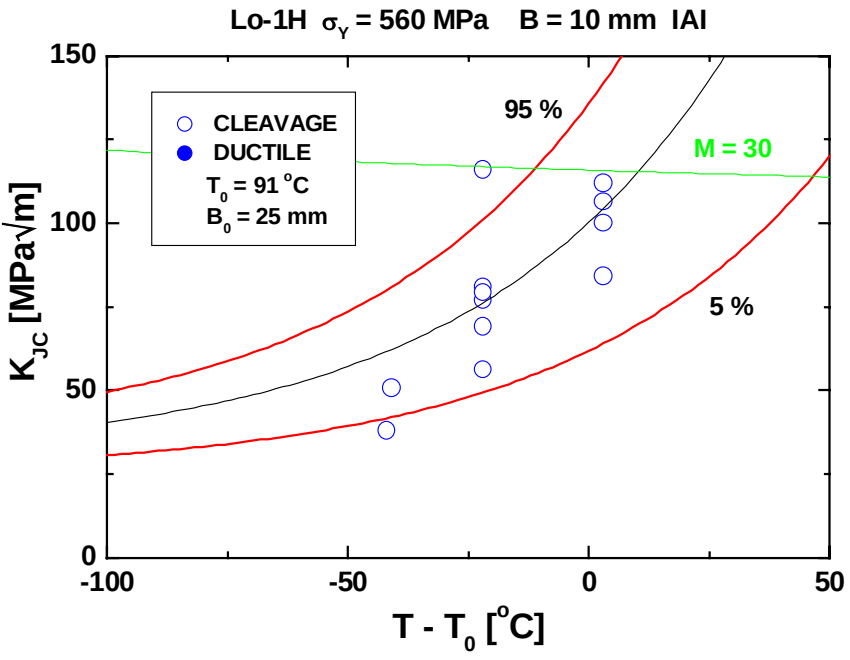

Figure 9. The Master Curve based transition behaviour of Lo-1 weld, IAI-condition, B = 10 mm specimen size.

Uncertainties in the transition temperature values are due to the statistical nature of cleavage fracture and due to the variation of the phosphorus content and the neutron fluence exposure of the specimens. The assumption is that $T_{0,\ reirradiation}$ = 77°C and each specimen gives equal contribution to the value of T_0. Each T_0 value is measured with 12 specimens even if only n = 12 (B = 10 mm) and n = 7 (B5 = mm) specimens fulfil the specimen size criterion (valid values).

Uncertainty of T_0 for a homogeneous material is according to ASTM1921-97

$$\delta T_o = \frac{18^o C}{\sqrt{n}} = 5^oC,\ n = 12 \qquad (5)$$
$$= 7^oC,\ n = 7$$

Neutron fluence gradient in the surveillance position is app. 15%/cm and the radius of the capsule is R = 12.5 mm. Hence upper limit variation of fluence is

app. 19%. It is assumed that the position of individual specimens in the capsule is randomly distributed. Estimation of the uncertainty due to neutron gradient is

$$\delta T_0 = \frac{77^0 C^{\,o}}{\sqrt{n}} * \left[\left(1 + \frac{\Delta \Phi t}{\Phi t} \right)^{1/3} - 1 \right] = 1.3^o C,\ n = 12 \qquad (6)$$

$= 1.7^o C,\ n = 7$

Response to variation of the phosphorus content comes through the chemistry factor of the embrittlement formula. By assuming that for Lo-1 weld Cu = 0.149%, P = 0.0375% and $\Delta P = 0.0041\%$ the following numerical values will be derived.

$$\delta T_0 = \frac{77^0 C}{\sqrt{n}} * \frac{\Delta P}{P + 0.07Cu} \quad = 1.9^o C, \quad n=12 \qquad (7)$$

$$= 2.7^o C, \quad n=6$$

$$= 3.8^o C, \quad n=3$$

The B = 5 mm specimens were prepared from three larger specimens and the B = 10 mm specimen from six larger specimens and hence the values n = 3 and 6 will be applied.

Quadratic summation of the deviations give for the δT_0 (B10mm) = $5.8^o C$ and δT_0 (B5mm) = $8.1^o C$, which leads to $\delta T_0 = 10^o C$ (1σ) for their difference. The measured deviation is 1.7 σ, which is relatively much. The largest contribution originates from the statistical nature of cleavage initiation, the second largest from the variation of phosphorus content and the smallest one from the variation of neutron fluence values. The nature of the variation of the phosphorus content has not been identified but it may also be of deterministic type, which may lead to non-statistical, biased sampling and correspondingly to larger systematic differences.

Parameter variations, which may lead to uncertainties in the determined shift values, are also inherent in the initial specimen irradiation, in annealing and in testing but they are not considered here.

5. Homogeneity of Lo-1, Lo-2 and 501 welds as concerns Cu- and P-contents

Relatively large amount of chemical analyses were made with weld specimens. Diameter of the analysing spot was 8 mm, which is the spatial resolution in the analyses.

The measurements indicate that Lo-1 and Lo-2 welds are homogeneous as concerns the copper and the phosphorus distributions. The weld materials in the surveillance HAZ and weld specimens were proved to be identical as concerns Cu and P contents. Weld 501 is homogeneous as concerns distribution of copper but it has a clear variation of phosphorus in weld depth direction.

Scatter in the measured Cu and P content values is approximately 10%.

Further analyses is required in order to understand the variation and scatter of impurity contents in the welds. Relatively large variations of impurity contents in vessel welds has been recently observed in some decommissioned vessels, i.e. Novovoronesh-1 and -2, Middland weld etc.

6. Homogeneity of weld samples 501-3 and 501-5

Weld 501 material has been delivered as many different blocks. The properties of the blocks 501-3 and 501-5 are compared in Table 7. The differences in strength properties are in line with the differences in the measured toughness properties as indicated in Table 7. Chemical analyses did not reveal any difference between the blocks.

Table 7. Comparison of material blocks 501-3 and 501-5. The unirradiated condition.

Property	Plate	501-3	501-5
hardness [HV1]	"8"	257	208
$R_{p0.2\%}$ [MPa]	"7"	569	502
T_0 [^{o}C]*	"6,7,8"	-18	-42
Cu [at-%]	"8"	0.145	0.143
P [at-%]	"8"	0.034	0.031

* all layers $T_0 = -18 \pm 4$ (1σ) ^{o}C, no variation in depth direction.

Summary

The irradiation chain 11K (1995–1998) included many different materials, which were aimed to be studied during several years. The most important conclusions from the studies performed during 2000 are:

- The relatively large scatter in the original ISO CH-V transition curve (n=12) of irradiated weld 501 is due to phosphorus gradient in the weld. Proper grouping of specimens and preparation of additional specimens from broken specimen halves made it possible to measure transition temperature shifts for two phosphorus contents, i.e. P = 0.03% and P = 0.04%. Comparison of the data with specimens irradiated in REFEREE programme with considerably higher neutron fluence rate indicated no fluence rate effect. Irradiation embrittlement of weld 501 is approximately 70% of the upper limit norm prediction. The fluence rate used in REFEREE irradiation was near the value present in the full core surveillance position. Hence the study suggests that no fluence rate effect exists in the full core or reduced core material irradiations.

- The difference of the Master Curve T_0 values measured with B = 5 mm and B = 10 mm specimens is 17°C, which is approximately equal to 1.7σ offset from the average. The difference is app. 20% of the measured re-irradiation shift. Further conformation of the difference would require additional testing as the number of valid tests was relatively small.

- The re-irradiation data measured with KLST specimens using material, which was irradiated in the 11K-capsule, support older re-irradiation data. KLST specimens measure slower re-irradiation rate than ISO CH-V specimens. Re-irradiation rate measured with KLST specimens is lower than the prediction of the lateral shift model in contrary to the data measured with ISO CH-V specimens.

- In Lo-1 and Lo-2 welds copper and phosphorus are distributed evenly. Weld portion of the HAZ specimens is identical material with the real weld specimens as concerns Cu and P impurity levels. The new analyses confirms the phosphorus distribution in 501 weld in the depth direction. Scatter of phos-

phorus values is relatively large. Further analyses is required in order to characterise the nature of scatter and impurity distributions in the weld.

- Strength level of weld samples 501-3 and 501-5 vary to some extent. The variation is in line with toughness variation. No difference in the impurity content levels was noticed between the blocks.

References

In this report the references identified below were utilised.

[1] Valo, M. Säteilytysketju 11K. Vuoden 1999 tutkimukset. Espoo: VTT Manufacturing Technology. Research Report VAL63-001197. (In Finnish).

[2] Kohopää, J. Effects of post-irradiation thermal annealing on radiation embrittlement behaviour of Cr-Mo-V alloyed weld metals. Acta Polytechnica Scandinavica, Mechanical Engineering Series No. 132. Espoo 1998. 112 p.

[3] Planman, T. and Valo, M. Lo-1:n toivutushehkutuksen seurantaohjelma, referenssitila ja säteilytysketjut 1S1, 1S3 ja 1S4. Espoo: VTT Manufacturing Technology, 2000. Research Report VAL63-001193.

[4] Serén, T. Neutron dosimetry for the surveillance chains 1S1, 1S3 and 1S4 in the new post-annealing surveillance program for Loviisa 1. VTT Chemical Technology, 2001. Research Report KET2057/00.

[5] Serén, T. Loviisa 2:n materiaalinäyteketjujen 9K ja 11K neutronidosimetria. VTT Chemical Technology, 2001. Research Report KET2029/00 .

[6] Valo, M. Toivutushehkutetun tilan (IA) mittaaminen tutkimusketjuun VTT-10 sijoitetuille Loviisan surveillance-materiaaleille. Espoo: VTT, Reactor Laboratory, 1993. Report REA259/93.

[7] Planman, T. and Valo, M. Hitsin 501 homogeenisuus, Murtumissitkeys. Espoo: VTT Manufacturing Technology, 2000. Research Report VAL63-001237.

[8] Valo, M. Loviisan toivutushehkutuksen surveillance-ohjelman säteilytysketju 1S5, IAI-tila, vuosi 2000, Espoo: VTT Manufacturing Technology, 2000. Research Report VAL63-001964.

(three confidential reports not listed above)

Prevention of stress corrosion cracking in piping welds

Erkki Muttilainen
Teollisuuden Voima Oy
Olkiluoto, Finland

Ossi Hietanen
Fortum Nuclear Services Ltd.
Vantaa, Finland

Pertti Aaltonen and Ulla Ehrnstén
VTT Manufacturing Technology
Espoo, Finland

Abstract

Stress corrosion cracking in piping welds in boiling water reactors (BWR's) has been observed in stainless steels as well as in low alloyed ferritic steels. Cracks in welded austenitic stainless steel piping in BWR's have been a serious problem in early operational years of nuclear power plants. Intergranular stress corrosion cracking (IGSCC) incidents of large diameter pipes have had an impact on plant availability and economics and defects are considered also as a safety hazard. The number of welds in connection to large diameter pipes is about 250 per unit, with a large wall thickness, about 30 mm in average, making inspection requirements stringent. SCC has been concentrated in the same systems in the power plants all over the world, namely reactor water cleanup systems, core spray and all lines of main re-circulation lines operating at high temperatures. In order to evaluate the rate of failures and the related safety risk, cracking mechanisms effective in different materials have been analysed and remedial actions have been evaluated.

1. Introduction

Ageing of piping materials in LWR's has been a recurring problem during the forty years operational history of nuclear power plants. Especially welds have shown to be sensitive to the changes caused by ageing, see Fig. 1. In the weld area there is usually a combination of the highest operational loads residual stresses, manufacturing defects and a microstructure sensitive to environmentally assisted cracking. The sensitive microstructure can be in the heat affected zone of the base material or in weld metal itself. Preventive maintenance and in-service inspection have been able to control cracking incidents before any leakage has been observed. At the same time, the knowledge how to prevent stress corrosion cracking in piping welds in general has been increased.

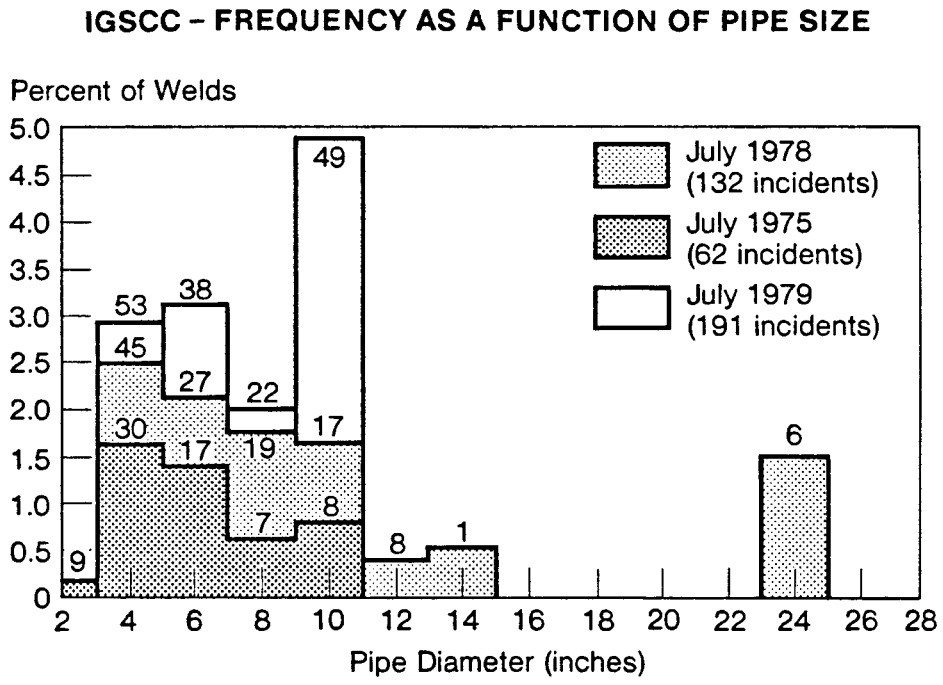

Figure 1. The frequency of IGSCC as a function of pipe size.

2. EAC in AISI 304 stainless steels

The first cracking incidents were observed in AISI 304 stainless steel weld after less that ten years of operation. The mechanism for failures was IGSCC, intergranular stress corrosion cracking, and the main reason for cracking was low temperature sensitisation, LTS, see Fig. 2.

Figure 2. IGSCC in sensitised AISI 304-type stainless steel.

During welding chromium carbide nuclei precipitated in the heat affected zone of high carbon stainless steel and these were able to grow in the operational temperature, i.e., at about 300°C causing sensitisation of the material. In order to prevent cracking incidents due to the LTS mechanism, low carbon stainless steels were developed. Reduction in the carbon content of the stainless steels reduced also their yield strength. On the other hand, nitrogen alloyed stainless steel grades with higher yield strength were introduced.

Today power plants usually use AISI 316NG type, nitrogen and molybdenum alloyed, low carbon stainless steels as piping material. However, also these grades have suffered from IGSCC. The narrow gap welding technique has been developed in order to reduce residual stresses close to weld root at the pipe inner surface. By using this method the residual stress near the pipe inner surface have been reduced and even changed to compressive.

3. EAC in stabilised stainless steels

Sensitisation of stainless steels during welding was a well known phenomena for decades before the first nuclear reactors were constructed. Stabilisation by titanium or niobium is one mean of reducing the amount of free carbon and thus suppress the risk for sensitisation and IGSCC. Stabilised stainless steel grades have been applied in some plants in order to prevent this problem.

Manufacturing of pipes and elbows in desired dimensions require heavy deformation which unavoidable causes very fine grain size, ASTM grain size 7 or even smaller, in the material. During welding of fine grained stabilised stainless steel grain growth in the vicinity of fusion line takes place and large grains are formed close to the fusion line. Cracking during plant operation has been observed to take place within this coarse grain zone. Cracks have grown along the grain boundaries but the location is closer to the fusion line that was observed in the LTS phenomena in AISI 304 type stainless steels.

The cracking is typically within less than 0.5 mm from the fusion line in the case of stabilised stainless steels as shown in Fig. 3, while the typical distance is 3…5 mm from the fusion line in the case of sensitised AISI 304 type stainless steels.

The role of stabilisation grade and sensitisation, segregation during welding and grain growth as well as the role of deformation due to heat expansion during welding have not yet finally clarified.

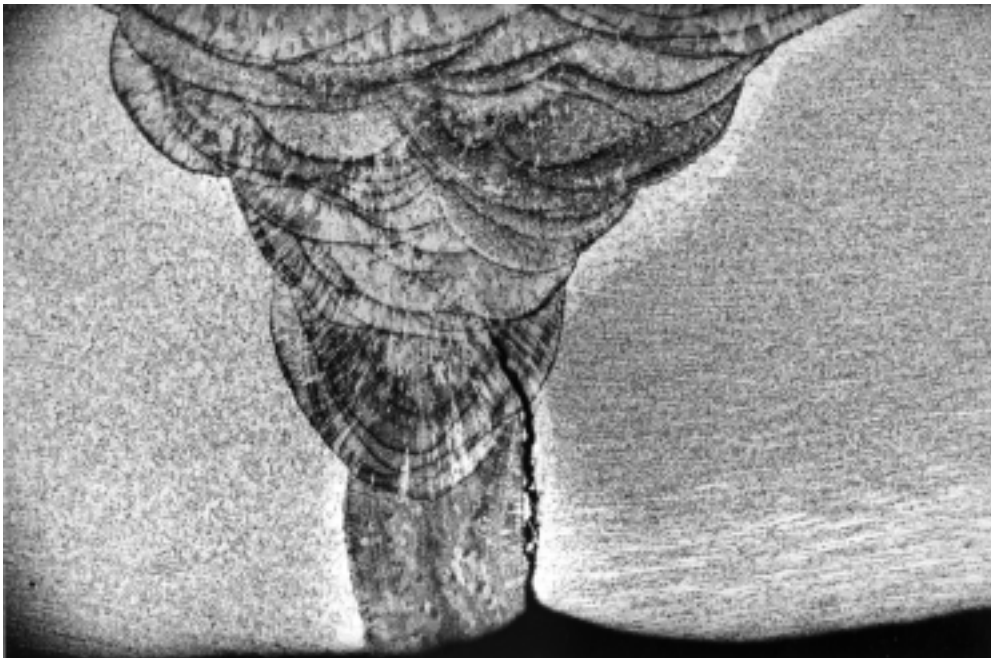

Figure 3. IGSCC in a Ti-stabilised stainless steel.

4. EAC in cold worked AISI 316NG stainless steels

Lately there has been a few IGSCC incidents observed in non-sensitised AISI 316NG material which has been used in replacement of old AISI 304 stainless steel in many plants, see Fig. 4. Even if this low carbon stainless steel is not sensitive to LTS in connection to aged welds, IGSCC has been observed in the HAZ. Similar to the IGSCC in stabilised stainless steels, the cracking in AISI 316NG material has been observed to occur in the coarse grained zone close to the fusion line.

Figure 4. IGSCC in a non-sensitised, deformed AISI 316NG type stainless steel.

The deformation of the material during welding seems to play an important role for the cracking. During welding the thermal heat expansion is limited and causes high local plastic strains next to fusion line as shown in Fig. 5. How these strains modify the properties of material and whether (and how) long term operation in BWR environment increases the cracking susceptibility is not clear at the moment.

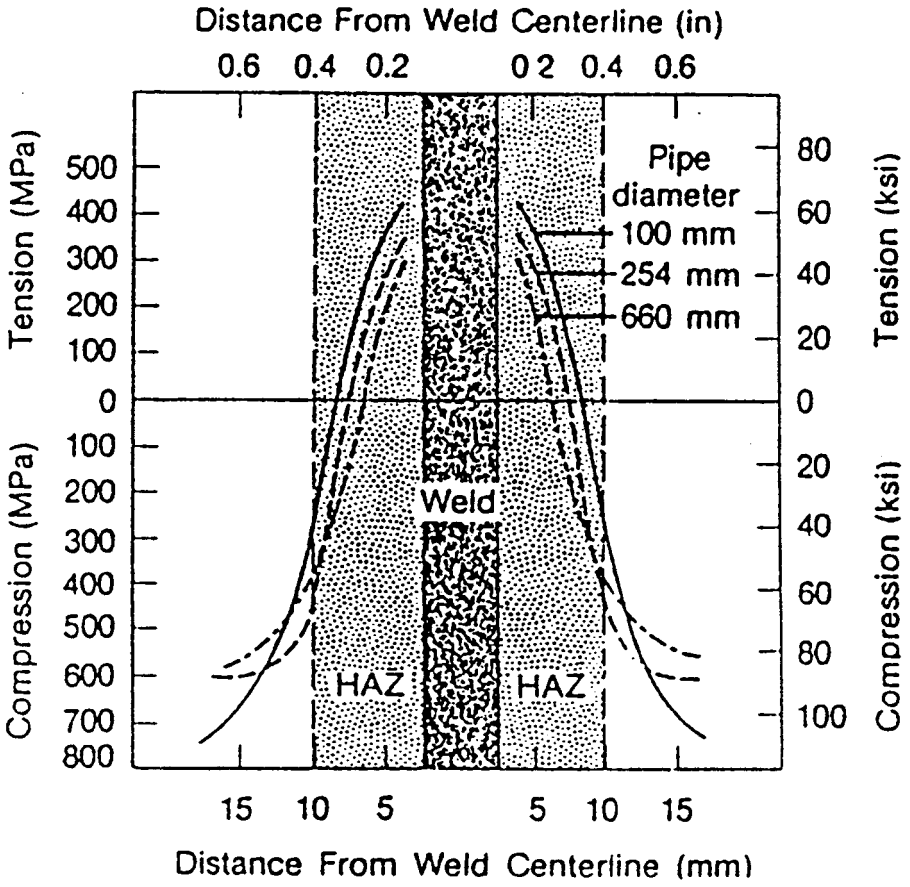

Figure 5. Peak axial surface residual stresses in welded AISI 304 type stainless steel pipe of different diameter.

5. EAC in ferritic low alloyed steels

In some plants low alloyed ferritic steels has been employed in the feed water lines. After several years operation transverse cracking incidents in the pipe weld metal have been found. Usually these cracks have initiated at the positions were pitting corrosion, mainly originating from shut down periods, has occurred. The cracking mechanism has been reported to be strain induced stress corrosion cracking, SICC.

The main parameters affecting the cracking has been the lower yield strength in the weld material compared to the adjacent base material providing yielding of the weld metal at operational temperatures. Remedy for this type of cracking has been replacement of the low strength weld metal with an new filler material having slightly higher strength.

6. Effect of water chemistry

The risk for stress corrosion cracking as well as the crack growth rate increases as a function of the oxidising power of the environment. In order to reduce the risk of stress corrosion cracking, some power plants have started to apply hydrogen water chemistry (HWC) instead the conventional water chemistry where radiolysis maintains an oxygen content of about 200 ppb in the piping of the boiling water reactors. By adding hydrogen into the coolant, the oxygen content can be suppressed and by that way the risk of cracking reduced.

Later on HWC has been modified to a so called noble metal water chemistry. This was introduced in order to reduce the amount of hydrogen needed to prevent cracking in piping welds. By addition of noble metals in soluble form in the coolant they can be precipitated all over the piping surfaces in the reactor loops. Noble metal on the piping surface makes it possible to make the environment reducing with smaller amounts of hydrogen additions in the coolant. The amount of power plants adopting noble metal water chemistry is increasing, especially in USA.

7. Welding technology

Welding related techniques to prevent IGSCC in piping weld are based on the ideas to limit heat input during welding and to minimise residual stresses on the pipe inner surface in contact with the coolant. Heat input has been lowered by welding method- and weld seam design modifications. Narrow gap welding provides a very small heat input and by extended weld beads on the outer surface, the residual stresses on pipe inner surface can be even compressive, see Fig. 6.

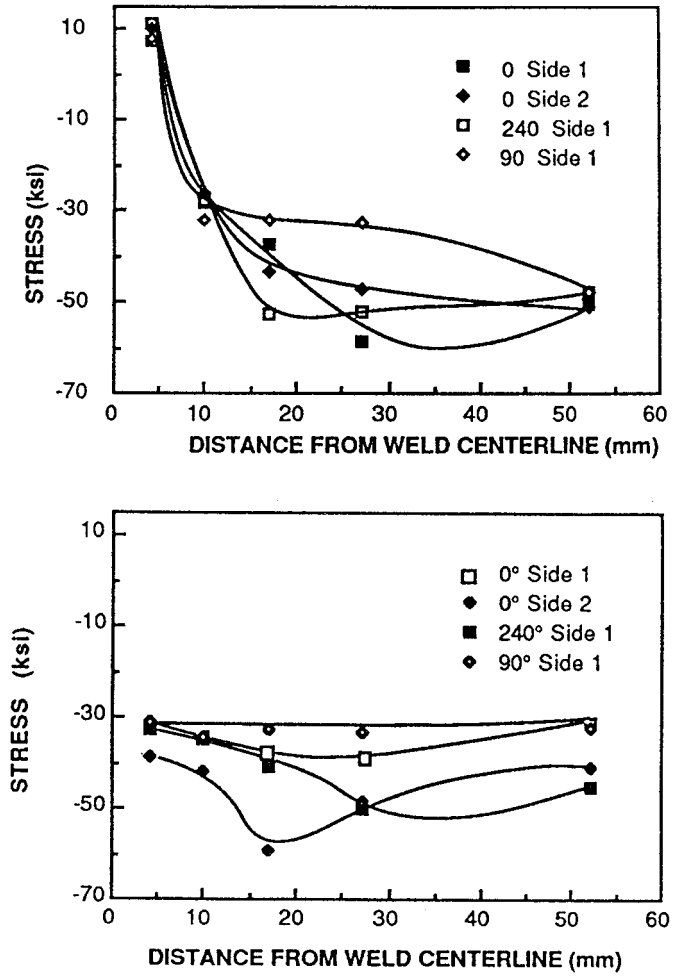

Figure 6. Residual stress distribution in narrow gap welded pipe joint in axial (above) and circumferential (below) directions.

In connection to the failure analyses repair welds have been learned to have a pronounced role. Whatever the reason for repair welding has been originally, repair welding performed on the pipe inner surface modifies the residual stresses markedly and increase the risk of IGSCC.

As an interim repair method providing safe operation until the following shut down, overlay welding has been applied on the pipe outer surface on both sides of the cracked weld seam. By welding additional material, the solid pipe wall thickness can be increased but the main effect is caused by the modification of stresses at the existing crack tip. Obtained compressive residual stresses can prevent crack advance even the crack still remains in the material.

8. Acknowledgements

This presentation is based on long term follow-up and research in collaboration between the Finnish NPP utilities the nuclear safety authority, STUK and VTT. The international experience has been obtained through the international networks (TVO – Swedish utilities as well as VTT's international partners).

Protectiveness of oxide films in simulated BWR crack conditions, SO_4^{2-} enrichment and cracking susceptibility

M. Bojinov, T. Laitinen, K. Mäkelä, T. Saario, P. Sirkiä and A. Toivonen
VTT Manufacturing Technology, Espoo, Finland
E. Muttilainen, A. Reinvall
Teollisuuden Voima Oy, Olkiluoto, Finland
I. Balachov
SRI International, Menlo Park, California, USA

Abstract

Sulphate ions in the BWR coolant dissolved e.g. from ion exchange resins increase the risk of environmentally assisted cracking (EAC). Influence of sulphate is likely to be related to the properties and behaviour of oxide films formed on material surfaces within a crack. For this purpose, the influence of sulphate ion content on the protectiveness of oxide films forming on AISI 316NG stainless steel, Inconel alloys 182 and 82 was characterised in simulated BWR crack chemistry conditions.

The crack propagation rates for Inconel 182 and AISI 316NG have been found to depend on the sulphate content, being higher at higher sulphate contents. The results of the present work show that the electrochemical protectiveness of the crack wall oxide film decreases with increasing sulphate content. Thus a correlation between the protectiveness of the crack wall oxide film and susceptibility to environmentally assisted cracking is indicated. This correlation can be used to assess the susceptibility of a given material to EAC in different environments. However, a comparison of the EAC susceptibility of different materials only by comparing the protectiveness of the crack wall oxides is not recommended.

1. Introduction

Anions are the most important impurities that may contribute to stress corrosion cracking in BWR environments. Presence of sulphate ions in the coolant increases the risk of environmentally assisted cracking (EAC) in structural materials such as AISI 304 stainless steel [1, 2]. In most cases the ion exchange resins provide a source of sulphate into BWR coolant. The breakdown risk of ion exchangers increases with increasing temperature.

1.1 Assumed rate-controlling factor for EAC

Oxide films grow also on the new surfaces of crack walls. Transport of species through these oxide films is one of the possible rate-controlling factors for crack growth. This may be the case if the crack propagates via accumulation of vacancies in the metal. These vacancies (V_m) can be generated at the metal/film interface as follows:

$$m + V_M^{3-} \rightarrow M^{III}{}_M + 3e^- + V_m \qquad (1)$$

In other words, a cation vacancy in the oxide film reacts with a metal atom, resulting in the formation of a cation in the oxide film and a metal vacancy in the metal substrate. For this reaction to occur, cation vacancies generated at the film/solution interface have to be transported through the oxide film to the metal/film interface.

Another possible route for the formation of vacancies in the metal can be written as:

$$m \rightarrow M^{x+}{}_i + xe^- + V_m \qquad (2)$$

In reaction (2), an interstitial cation is formed in the oxide film, while a metal vacancy is left in the metal substrate.

Assuming that the transport of cation vacancies or interstitial cations through the oxide film on the crack walls contributes to the crack growth rate, a correlation should exist between the crack growth rate and the oxide film properties.

Generally, the transport of ionic species through an oxide film is the faster, the more ionic defects the film contains. The transport is thus faster in less stable films.

1.2 Aim of the study

The aim of this work is to investigate the influence of sulphate content on EAC susceptibility in the BWR coolant. For this purpose the influence of sulphate ion content on the protectiveness, i.e. on the transport rate of ionic defects in oxide films forming on AISI 316NG stainless steel, Inconel alloys 182 and 82, was characterised in simulated BWR crack chemistry conditions. A further aim was to correlate these results with crack growth data.

2. Experimental

2.1 Test materials and environment

The composition of the materials used in the study is given in Table 1.

Table 1. Composition of the materials used in the investigations in w-%.

	AISI 316NG	Inconel 182	Inconel 82
C	0.015	0.03	0.036
Cr	16.5	15.2	20.2
Cu	0.26	0.01	0.03
Fe	remainder	8.07	0.71
Mn	1.73	7.57	2.92
Ni	10.5	66.4	73.1*
S	0.002	0.001	0.001
Si	0.54		0.05
Mo	2.55		
Others	N 0.056		Nb 2.48

* Including cobalt

The influence of sulphate ions on surface oxide films was studied in simulated conditions corresponding to the water chemistry within a crack. The tests were performed in a Ti-cladded static autoclave in water purified in a Milli-Q® water purification system (Millipore) and in H_2SO_4 solutions containing 1000, 3000, 6000, 8000 and 10000 ppb sulphate ions. The test temperature was 273°C and the solution was de-oxygenated before each experiment using N_2 of 99.999% purity. The room temperature pH of the five sulphate solutions was measured to be 4.4, 4.1, 3.8, 3.7 and 3.7. The corresponding ranges of high-temperature pH values and corrosion potentials of the samples are given in Table 2.

Table 2. The corrosion potentials of the materials and the corresponding high-temperature pH values in simulated BWR crack chemistry conditions. Given as ranges of values in sulphate contents of 0 ppb ... 10 000 ppb.

	AISI 316NG	**Inconel 182**	**Inconel 82**
$\mathbf{E_{corr}}$ (mV_{SHE})	-470...-390	-370...-340	-450...-340
$\mathbf{E_{redox}}$ (mV_{SHE})	-380...-260		
$\mathbf{pH_T}$ (measured)	5.6...4.1		

2.2 Electrochemical measurements

The films formed on material surfaces during an exposure of ca. 24 h to simulated crack conditions were characterised using a controlled-distance electrochemistry (CDE) arrangement [3]. This arrangement was used for thin-layer electrochemical impedance measurements. They were carried out with a Solartron 1287 ECI/1260 FRA system controlled by CorrWare/ZPlot software (Scribner Associates), while a Wenking LB 81M potentiostat was used to monitor the corrosion potential of the alloys.

2.3 Estimation of sulphate enrichment

In order to define the simulated crack chemistry conditions, the relation between the content of sulphate ions in a BWR bulk coolant and within a crack was

assessed. This was done by modelling diffusion and electromigration of species in the crack. These estimations were carried out for the following three crack geometries:

- Semi-elliptical thumb nail crack in an infinite plate
- Crack in a bend specimen; crack opening angle 0°
- Crack in a bend specimen; crack opening angle 1°

It was found out that the enrichment factor of sulphate ions depends strongly on the exact composition of the coolant and only weakly on the crack geometry. As an example, the estimated enrichment factor for a semi-elliptical crack is shown in Fig. 1 as a function of crack depth. The enrichment factor at the crack tip is about 100, and the maximum value may reach 300 or even more. The simulated sulphate contents of 1000, 3000, 6000, 8000 and 10000 ppb can thus be estimated to correspond crack conditions when sulphate contents of the bulk coolant are as low as 3, 10, 20, 27 and 33 ppb.

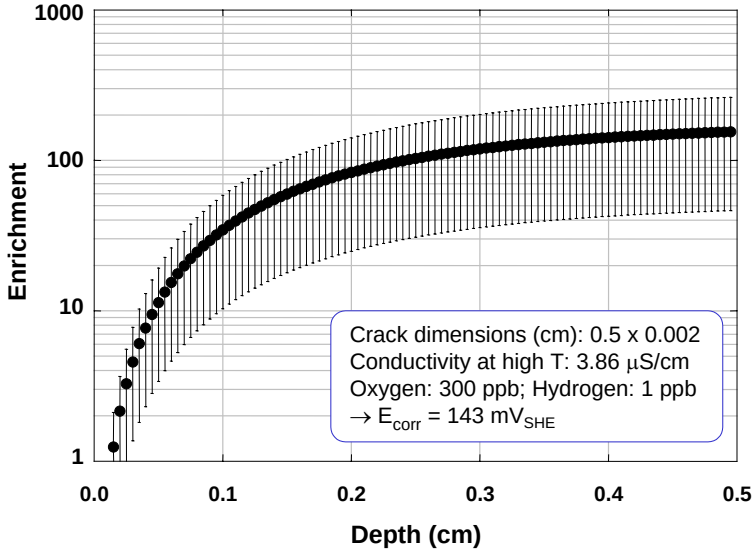

Figure 1. Enrichment of sulphate (C(x)/C(bulk)) in a semi-elliptical crack. Error bars correspond to uncertainties in chemical composition and conductivity at high temperature.

3. Experimental results and discussion

Electrochemical impedance spectra were measured for all three materials at all the sulphate contents after an exposure of ca. 24 h to simulated crack conditions. As an example, the spectra obtained for the materials in the coolant with ≅0 and 10000 ppb SO_4^{2-} ions are shown in Fig. 2.

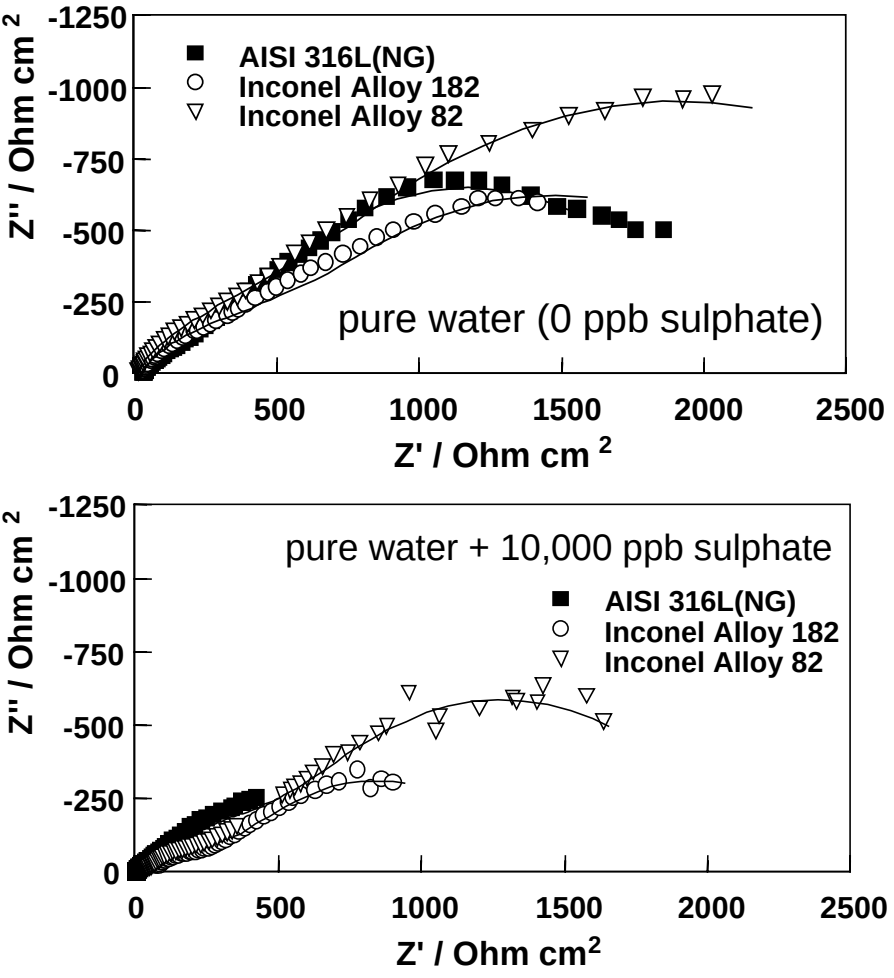

Figure 2. Electrochemical impedance spectra of AISI 316NG stainless steel, Inconel 182 and Inconel 82 in the presence of 0 and 10000 ppb sulphate ions in simulated crack conditions at 273 ℃. The lines are fitted to experimental points.

Qualitatively, the spectra for all the materials in all the sulphate contents exhibit a low-frequency linear part that transforms into a semicircle at very low frequencies. In addition, a small high-frequency impedance loop can be observed in several cases. This kind of spectra are typical for a situation in which both a charge transfer reaction (e.g. oxidation of metal) and a transport process under a concentration gradient contribute to the behaviour. Accordingly, the low-frequency part can most likely be attributed to a transport process in the film, while the high-frequency impedance loop is probably due to the charge transfer of the corrosion reaction.

The impedance, i.e. the electrical transfer function, of an electrochemical system, can be described either by means of an equivalent circuit or an analytical expression. The results obtained in the present work were fitted using the following transfer function, which takes into account the features discussed above:

$$Z = R_{el} + \{j\omega C_{hf} + [R_{hf} + R_D \tanh (j\omega \tau_D)^{n_D} / (j\omega \tau_D)^{n_D}]^{-1}\}^{-1} \qquad (2)$$

The most important parameters of this equation in the present case are the charge transfer resistance (R_{hf}) and the transport resistance for ions and ionic defects (R_D). The relative magnitudes of R_{hf} and R_D determine, whether charge transfer or the transport of ions or ionic defects controls the overall rate of metal oxidation. If $R_{hf} >> R_D$, charge transfer controls the oxidation rate, while if $R_{hf} << R_D$, transport of ions or ionic defects controls the oxidation rate. The rate of transport of ions or ionic defects in the film can be interpreted as a measure for the protectiveness or stability of the film: the slower the transport rate, the more protective or stable towards corrosion the film is. The values obtained for the resistances R_{hf} and R_D as a result of the fitting of the impedance spectra showed that in all the cases $R_{hf} << R_D$. This means that the transport of ions or ionic defects controls the overall rate of metal oxidation. The values of R_D are shown in Fig. 3 for the three materials as a function of sulphate content.

The results given in Fig. 3 show that the value of R_D decreases with increasing sulphate content at low SO_4^{2-} contents and stabilises at higher contents for all the materials. The protectiveness of the oxide film thus decreases when SO_4^{2-} is added, but this influence is observed only at SO_4^{2-} contents $\leq$ 5000 ppb. For AISI 316NG, however, the curve exhibits a minimum at 1000 ppb.

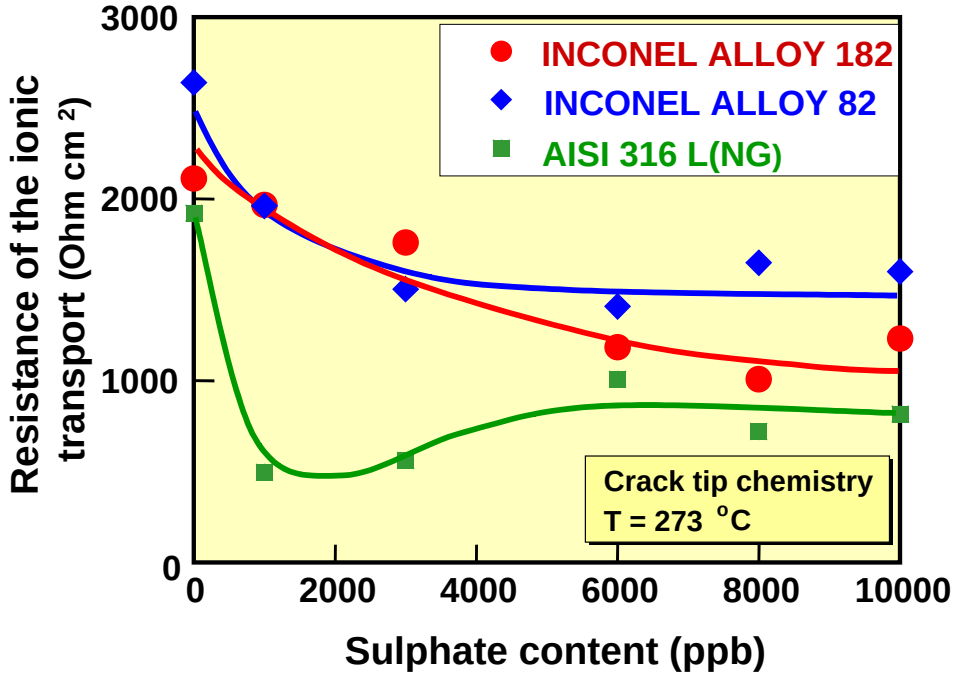

Figure 3. The value of the resistance R_D for the transport of ions or ionic defects through the oxide film on AISI 316NG and Inconel alloys 182 & 82 as a function of sulphate ion content in simulated crack chemistry conditions.

4. Conclusions

The results of this work show that the protectiveness of the films formed in simulated crack tip conditions on AISI 316NG, Inconel alloy 182 and Inconel alloy 82 decreases with increasing sulphate content. The results also suggest that the oxide films in simulated crack chemistry conditions are the most protective on Inconel alloy 82, the second protective on Inconel alloy 182 and the least protective on AISI 316NG.

A comparison of these results with empirical crack growth data indicates that there is a correlation between the protectiveness of the oxide film on the crack walls and susceptibility of the material to stress corrosion cracking. A stress corrosion crack growth test series on the same materials [4] has shown that the crack propagation rates in Inconel alloy 182 and AISI 316NG is dependent on the bulk water sulphate content, being higher at higher contents. The dependence

of crack propagation rates on sulphate ion content has been reported by other authors as well, see for instance refs. 5 and 6. The results reported in ref. 4 also indicate that Inconel alloy 82 is the least susceptible to EAC as no or negligible stress corrosion cracking was observed at any of the applied bulk coolant sulphate contents of ~0, 10, 30 and 100 ppb.

It thus seems possible that a measurable quantity (R_D), describing the transport of ions or ionic defects in the oxide film and thus providing a measure for the protectiveness of the film, can be used to assess the susceptibility of a given material to cracking in different environments. This quantity can be determined in relatively short experiments. However, also the material condition, e.g. the degree of cold work, has been found to have an impact on the actual crack growth rates [4]. The oxide film properties cannot thus be used as the only criterion when ranking different materials with respect to their susceptibility to environmentally assisted cracking.

Acknowledgements

This paper is part of a cluster of joint R&D projects on plant life management and ageing of metallic components, which is realised mainly by VTT in 1999–2002. The projects are funded by Tekes, the National Technology Agency, Teollisuuden Voima Oy, Fortum Power and Heat, Fortum Engineering, VTT and to smaller extent also by other energy and process industry in Finland. A significant amount of background information originates from the Finnish research programme on nuclear power plant safety (Finnus).

The authors are grateful for the provided funding and for the open and fruitful co-operation within the project.

References

1. Aaltonen P., Ehrnstén, U. and Hänninen, H. The effect of sulphate on crack growth rates in stainless steel and Alloy 182 weld metal in BWR environment. VTT Report VALC456, 10.3.1998. Espoo, Finland: VTT Manufacturing Technology.

2. Andresen, P. Effect of Specific Anionic Impurities on Environmental Cracking of Austenitic Stainless Materials in 288 oC Water, International Symposium on Environmental Degradation of Materials in Nuclear Power Systems – Water Reactors, August 25–29, 1991, Monterey, California. Pp. 209–218.

3. Bojinov, M., Hinttala, J., Laitinen, T., Mäkelä, K., Mäkelä, M., Saario T. and Sirkiä P. Solid state processes and release of soluble products during aqueous corrosion of structural materials in simulated NPP coolant conditions, Water Chemistry of Nuclear Reactor Systems 7, Bournemouth, BNES, 2000.

4. Toivonen, A., Moilanen, P., Aaltonen, P., Ehrnstén, U., Taivalaho L. and Muttilainen E. Effects of BWR coolant sulphate ion concentration on SCC propagation in AISI 304, in AISI 316NG and in Inconel weld metals 82 and 182. To be published.

5. Andresen, P.L. Observation and Prediction of the Effects of Water Chemistry and Mechanics on Environmentally Assisted Cracking of Inconels 182 Weld Metal and 600, Corrosion 44 (1988) 376.

6. McMinn, A. and Page, R. A. Stress Corrosion Cracking of Inconel Alloys and Weldments in High-Temperature Water – The Effects of Sulfuric Acid Addition, Corrosion 44 (1988) 239.

Monitoring of BWR water chemistry and oxide films at Olkiluoto 1

Martin Bojinov, Petri Kinnunen, Timo Laitinen,
Kari Mäkelä, Timo Saario, Pekka Sirkiä
VTT Manufacturing Technology, Espoo, Finland

Mika Helin, Erkki Muttilainen, Pekka Nousiainen, Anneli Reinvall
Teollisuuden Voima Oy, Olkiluoto, Finland

Abstract

Flow-through cells for monitoring high-temperature water chemistry have been designed and installed in the shutdown cooling system at Olkiluoto unit 1. The aim is to find correlations between water chemistry data and oxide film properties in the BWR coolant, susceptibility to stress corrosion cracking and other forms of corrosion and the rate of activity incorporation.

The employed monitoring unit has been in operation for one year. It provides relevant information that can be used both for assessing long-term trends and for sensitive detection of rapid changes in the coolant environment. High-temperature conductivity of the coolant has proven to be a sensitive indicator of changes in anionic impurity content and temperature variation of the coolant.

1. Introduction

The susceptibility to stress corrosion cracking and to other forms of corrosion, as well as the extent of activity incorporation on primary circuit surfaces, are closely connected to the chemical parameters of the coolant water and to the properties of surface oxide films in a nuclear power plant [1]. Changes in operational conditions are likely to induce changes in corrosion susceptibility and rate of activity incorporation. To predict these changes, experimental correlations between water chemistry, oxide films, corrosion behaviour and activity

incorporation, as well as mechanistic understanding of the related phenomena need to be established.

A flow-through cell unit has been installed in the Olkiluoto 1 BWR unit in order to collect the data needed when searching for such correlations. The unit is used for monitoring of corrosion potentials of relevant material samples, the redox potential, the conductivity and the pH_T of the primary coolant at high temperature, as well as for observation of the oxide films formed on material samples.

The monitoring of high-temperature water chemistry was started after the refuelling outage of Olkiluoto 1 in 2000. This report summarises the results of high-temperature water chemistry monitoring until March 2001.

2. Experimental

2.1 High-temperature cells and sensors

The flow-through cells for monitoring the corrosion and redox potentials, conductivity and pH_T at high-temperature and for exposing material samples to the primary coolant have been connected to the shutdown cooling system 321 at Olkiluoto 1, Fig. 1. The system has been thermally insulated to ensure a relevant and constant temperature in the cells.

The coolant enters the lower cell and flows further through the upper cells. The flow-rate through the cells is about 0.4 kg/s. The lower cell contains two AgCl/Ag reference electrodes filled with 0.005 M KCl, one conductivity electrode, one pH_T electrode, two Pt samples for measuring the redox potential and eight separate samples for measuring the corrosion potential (ECP) of AISI 316 L(NG) and AISI 304 stainless steels, as well as that of Inconel alloys 182 and 82.

The four-plate high-temperature conductivity sensor has been recently developed at VTT to improve the quality of conductivity measurements in plant conditions, Fig. 2. Alternating current is fed between the two outermost platinum plates, and the voltage is measured between the two inner platinum plates. Zirconium oxide washer rings act as insulators between the platinum plates. The

body of the sensor extending to the water is made of zirconium metal and oxidised in an air oven prior to use to minimise possible interference of the electronically conductive flow-through cell with the conductivity measurement.

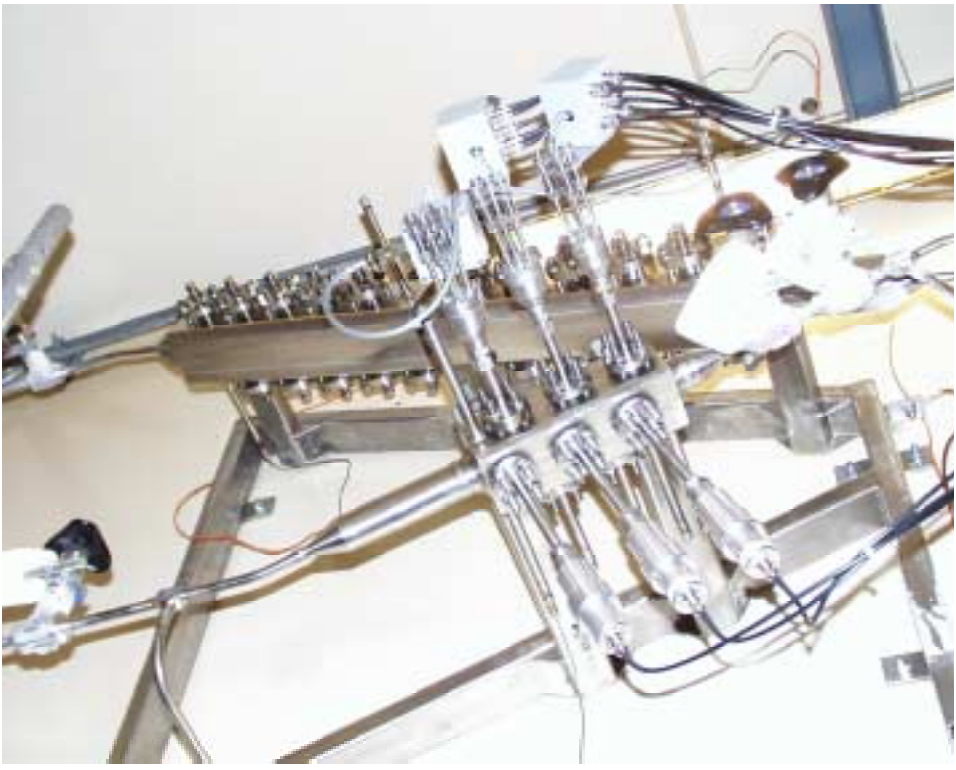

Figure 1. The flow-through cells with high temperature water chemistry sensors and 80 material samples in the shutdown cooling system at Olkiluoto 1.

2.2 Material samples

Material samples made of AISI 316L(NG) stainless steel, AISI 304 stainless steel, Inconel alloy 182 and Inconel alloy 82 have been installed in the two upper cells in order to simulate the exposure of plant component surfaces to the primary coolant. The samples will be removed from the cell at certain intervals, and the oxide films formed on their surfaces will be analysed and the results will be correlated with other observations of the plant operation. The two material sample cells contain altogether 80 samples, whose composition is given in Table 1.

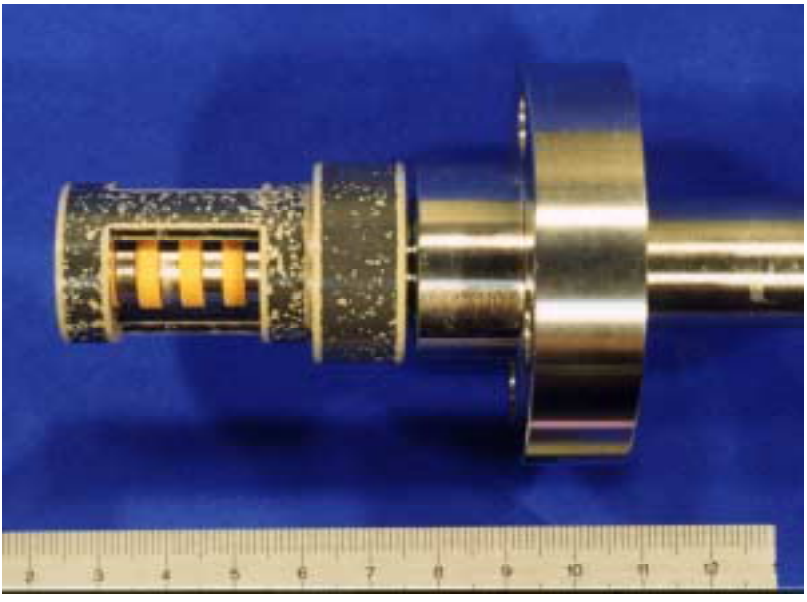

Figure 2. Four-plate high-temperature conductivity sensor.

Table 1. Composition of the materials used in the investigations (weight-%).

Material	C	Cr	Cu	Fe	Mn	*Ni	S	Si	Mo	Other
AISI 316L(NG) [i)]	0.015	16.5	0.26	bal.	1.73	10.5	0.002	0.54	2.55	N: 0.056
AISI 304 [ii)]	0.08	19		bal.	2	9.3	0.03	1		N: 0.1
Inconel 182 [iii)]	0.03	15.24	0.01	8.07	7.57	66.36	0.001			
Inconel 82 [iii)]	0.036	20.23	0.03	0.71	2.92	73.05	0.001	0.05		Nb: 2.48

[i)] Determined using optical emission spectrometer (Spectrolab S)

[ii)] Nominal composition

[iii)] As reported by the supplier.

* including cobalt for Inconel 82

The samples were ground with 600 grade emery paper, washed with demineralised water and placed in 20 sample holders, one sample of each material in each holder, Fig. 3. The samples are electronically insulated from the body of the cell and from each other. The sample holder and the flow-through cell have been carefully designed such that the flow conditions on the 80 sample surfaces are identical.

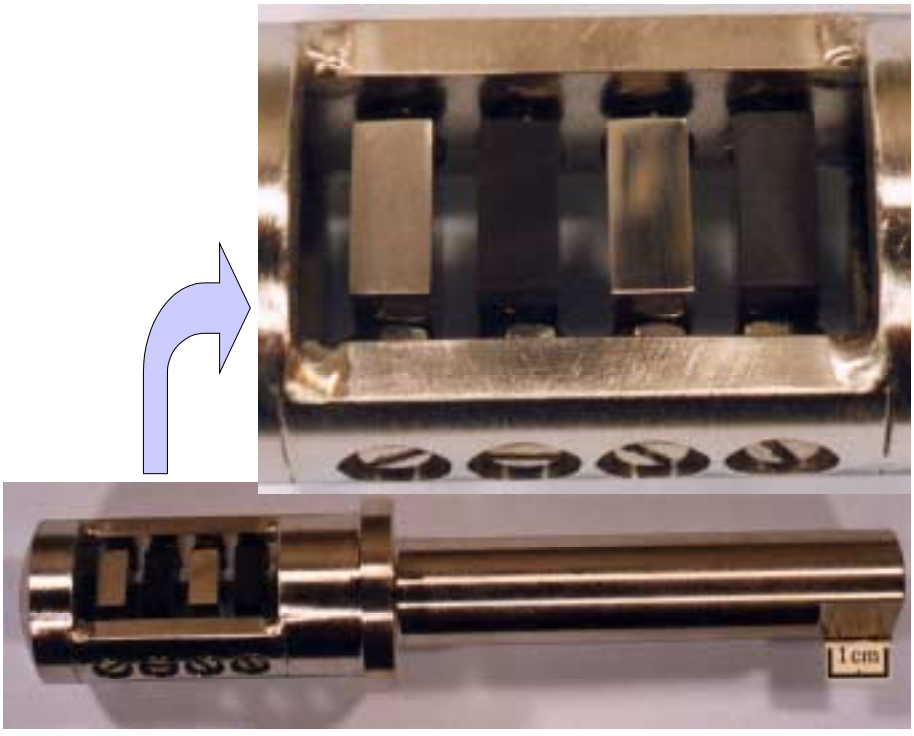

Figure 3. A sample holder with four electrically insulated material samples.

The first sets of samples have been removed from the material sample cell in May 2001 before and after the cool-down for the refuelling outage. The activity levels of most of the samples in the cells have been measured during the outage to ensure a statistical significance of the activity measurements in the future. Later on, samples will be removed also in middle of the fuel cycle and after eventual transients.

2.3 Data acquisition

A sketch of the data acquisition system used to collect the monitoring data for further processing at VTT is shown in Fig. 4. A considerable amount of data points were lost towards the end of March 2001. This problem was resolved by installing an industrial PC computer to enhance data logging at Olkiluoto. Since that the quality of data is good again.

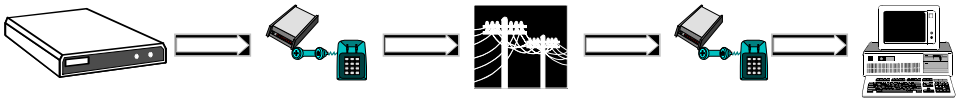

Figure 4. The system applied to collect the monitoring data at Olkiluoto and to transmit it to Espoo for evaluation at VTT. Since 11.4.2001 an industrial PC is installed in between the data logger and modem at Olkiluoto.

2.4 Oxide film analysis

The pickup of activity on the sample surfaces is linked to the composition, structure and thickness of the oxide film. To be able to establish correlations between the structure and measured activity levels, the following techniques will be used to characterise the oxide films after the exposure to the BWR coolant:

- Gamma spectrometry,
- Scanning electron microscopy (SEM),
- Glow-discharge optical emission spectroscopy (GDOES),
- X-ray diffraction measurements (XRD) and
- Secondary ion mass spectrometry (SIMS).

The activity measurements will concentrate on four nuclides (^{60}Co, ^{58}Co, ^{54}Mn, ^{51}Cr). SEM micrographs will be recorded from the top and the cross-sections of the oxide films on the different samples. GDOES will be used to estimate the thickness of oxide films and to obtain information of the depth profiles of different elements in the oxide films. XRD will optionally be used to obtain an estimation of the oxide film thicknesses and to have indications of the oxide phases present in the film. SIMS will optionally be used to provide an estimation of the oxide film thicknesses and to determine a depth profile of the elemental composition of the oxide films on selected samples.

3. Results and discussion

3.1 Plant operation during the monitoring period

The reported monitoring period covers most of the plant's operating cycle between annual outages, However, the cool down and outage phases are missing due to the project interim reporting schedule. The plant was operating normally, but some power variations have occurred.

The level of oxygen content was about 300 ppb, which is an expected level. A decreasing trend in oxygen content can be seen in manual measurements performed by TVO, Fig. 5.

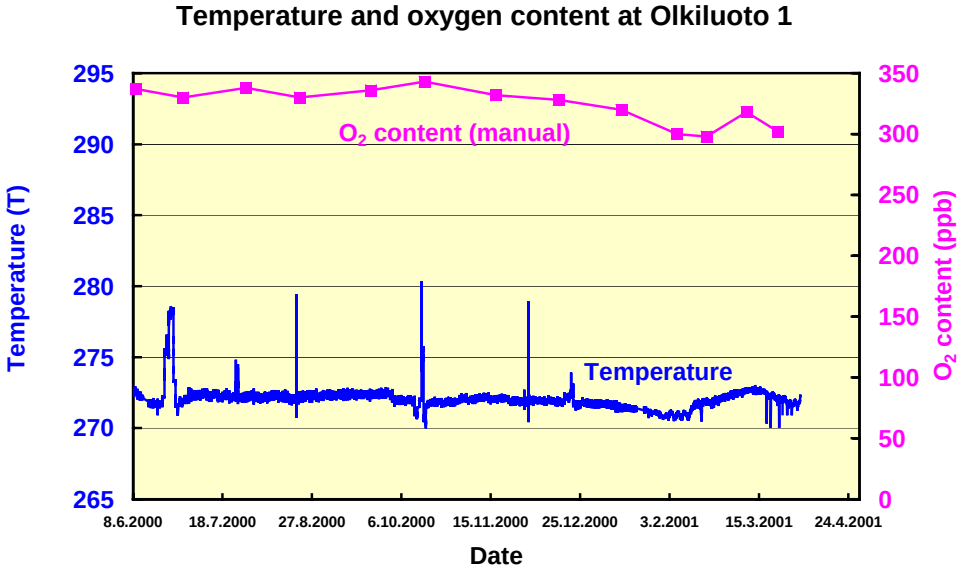

Figure 5. The temperature in the material sample cell in the shutdown cooling system 321 and the oxygen content in the reactor water.

Fig. 5 shows also the temperature of the water flowing through the measurement cells. The temperature of the cell has been in the range 271–273 °C for most of the time. A few excursions to higher temperatures have occurred. According to plant reports, these excursions have taken place during reduced power output. The temperature in the shutdown cooling system 321 increases during a period

of reduced power output because of the reduced cooling effect of the coolant circulation in the primary circuit.

3.2 Impurity contents

The contents of the most important cationic and anionic impurities in the reactor water have been studied on the basis of analyses performed by TVO.

The total Fe content in the coolant was in the range 0–0.25 ppb for most of the monitoring period. Excursions up to 0.8 ppb occurred during the early part of the cycle.

Both the content of total Cr and the activity of ^{51}Cr show a clear decreasing trend with time during the cycle. This may be due to a continuous decrease of chromate ion (CrO_4^{2}) content in the coolant. As the speciation of CrO_4^{2-} during the whole monitoring period is not available, the trends in the content of total Cr and its activity product ^{51}Cr are used as possible indications of the chromate content. However, the correlation is not linear, which causes some uncertainty in the interpretation of the results. Cromium is to a great extent retained in the crud in the core area, while the CrO_4^{2-} content represents the equilibrium between the coolant and the crud. The CrO_4^{2-} content of the coolant may influence both the potential values and the conductivity of the coolant and is thus an interesting factor. It is currently being followed by TVO and the results can be correlated with the high-temperature monitoring data in the next reporting period.

The content of SO_4^{2-} ions varies in the range 3–8 ppb during the whole monitoring period, the mean value being about 5 ppb. The content of NO_3^- ions remains for the most part of the period at about 1.5 ppb, but high peaks up to even 30 ppb are occasionally observed. The periodic variations and peaks in the contents of SO_4^{2-} and NO_3^- ions are ascribed to the behaviour of ion exchange resins used for condensate clean-up at the plant. The contents of both Cl^- and F^- ions remained below 0.5 ppb during the whole monitoring period.

3.3 Corrosion and redox potentials

The measured corrosion potentials (ECP) of the studied materials together with the redox potential are depicted in Fig. 6. The ECP values of AISI 316 L(NG) and AISI 304 are in the range 80–180 mV during the whole cycle, being very close to each other. The ECP values of Inconel alloys 182 and 82 are in the range 40–140 mV. These values are in agreement with observations reported in the literature under simulated and in plant measurements [2].

The redox potentials measured with the two Pt sensors differ considerably from each other. The sensors are situated in closely similar flow conditions and the difference cannot be attributed to different flow rates. This demonstrates the poor reproducibility of the redox potential measurement that has often been observed in earlier experiments. The most probable reason for the difference is the difficulty to provide a reproducible surface condition on the Pt sensor before starting the measurement.

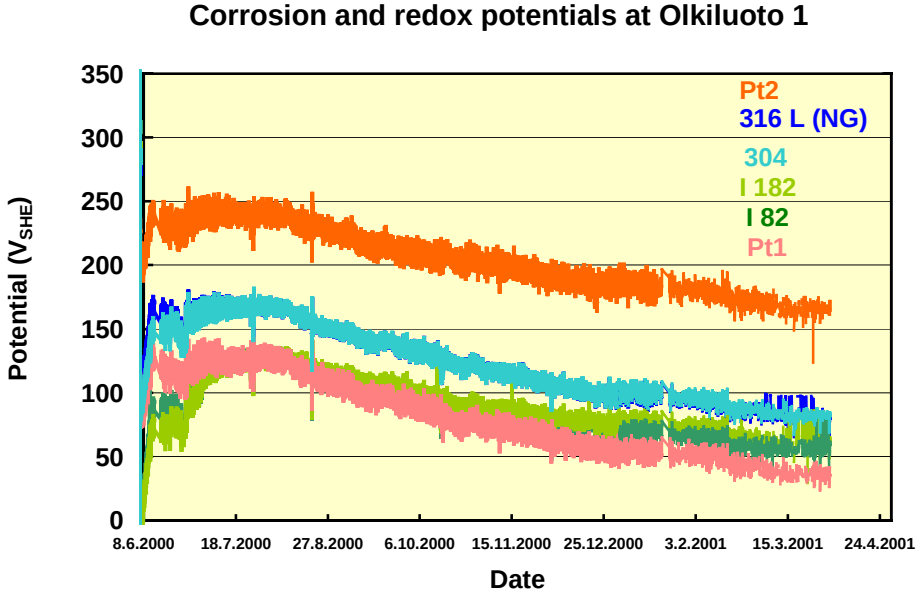

Figure 6. The corrosion potential of AISI 316 L(NG) stainless steel, AISI 304 stainless steel, Inconel alloys 182 and 82, and the redox potential of the coolant measured with two different Pt sensors in the monitoring cell.

Conceivable reasons for the decreasing trend of all the measured potential values during the fuel cycle may be a decrease in the oxygen content or in the chromate content of the coolant, or theoretically even increasing thickness of the oxide film. Fig. 7 shows the potential values together with the oxygen contents, the contents of total Cr and the activity of ^{51}Cr. Both the oxygen content and the Cr content show a decreasing trend during the cycle, but the decreasing trend of the Cr content is much more pronounced. This might refer to a dominating role of chromate in the decrease of the potential values. Further investigations are, however, needed to confirm this assumption.

The stability of the employed reference electrode needs to be considered when discussing the changes of potential values. But the reference electrode is an unlikely reason for the decreasing potential values, because the same trend is obtained also when the potentials are calculated using the second AgCl/Ag reference electrode installed in the cell. A further proof for this will be obtained after the refuelling outage of 2001 when checking both reference electrodes.

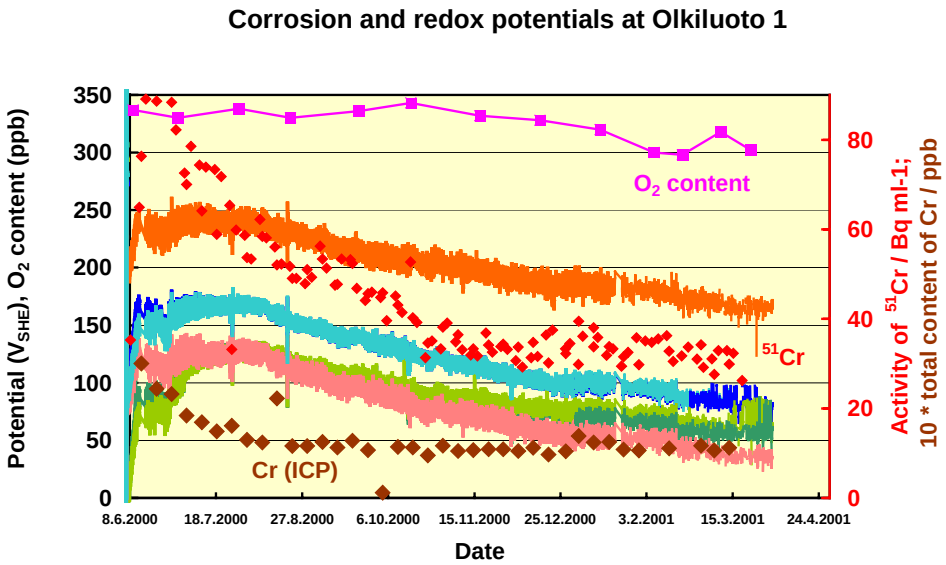

Figure 7. Comparison of oxygen content, total Cr content, activity of ^{51}Cr, redox potential and corrosion potentials of the studied materials.

3.4 High-temperature conductivity

The high temperature conductivity of the coolant in the monitoring cell is shown in Fig. 8 together with the room-temperature conductivity of the reactor water, which is determined on line in the 321 system by TVO. The high-temperature values are in the range 3.5–3.9 μScm^{-1} for the whole monitoring period, except for a few sharp peaks that will be discussed below. The room-temperature values are around 0.1 μScm^{-1} for the whole period.

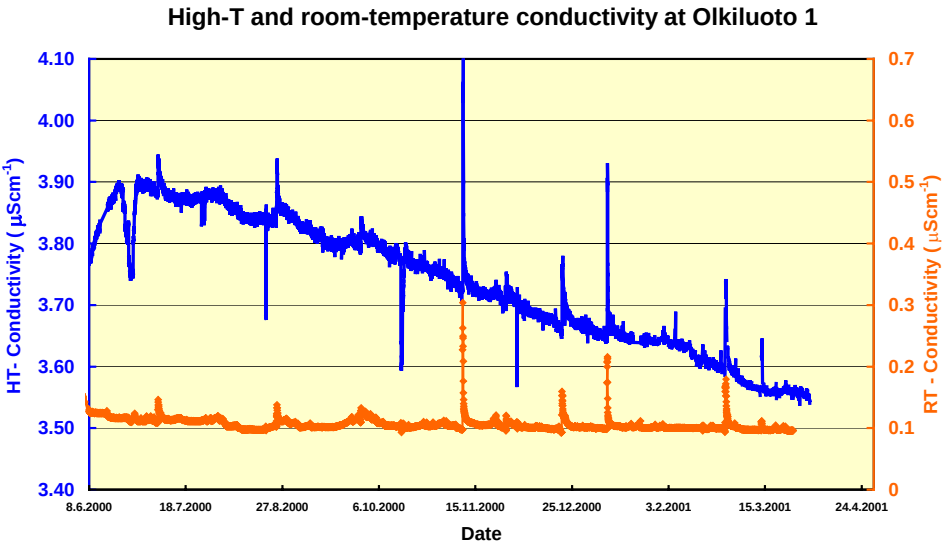

Figure 8. The high-temperature conductivity in the flow-through cell together with the room-temperature conductivity values of the reactor water determined on line in the shutdown cooling system 321.

The results shown in Fig. 8 demonstrate that the high-temperature measurement is much more sensitive to any changes in the conductivity of the coolant than the room-temperature measurement. The theoretical conductivity of pure water at 273 °C is about 3.0 μScm^{-1}. The values in excess of this can be ascribed to the impurities in the coolant.

Four characteristic features can be observed in the curve for high-temperature conductivity:

- The curve shows four relatively sharp minima,
- the curve shows ten sharp maxima,
- the curve shows small hump-like variations, and
- the curve shows a continuously decreasing trend.

3.5 Discussion on high-temperature conductivity results

The minimum observed in the high-temperature conductivity in June 2000 and also the other peaks to lower values are associated with lower power output of the plant and the corresponding increase of the temperature in the shutdown cooling system 321.

The minima of the conductivity correlate well with the theoretically predicted change in the conductivity of pure water with increasing temperature, which explains all the minima in the curve.

A decreasing trend of high-temperature conductivity is clearly seen in Figs. 8 and 9. One possible reason for this trend could have been the decreasing content of chromate ions in the coolant. As shown in Fig. 10, the high-temperature conductivity values seem to follow reasonably well the content of total Cr and the activity of ^{51}Cr.

Theoretically, the decrease of high-temperature conductivity from 3.9 μScm^{-1} to 3.55 μScm^{-1} would require a decrease of the chromate content by 17 ppb. But the total Cr content in the reactor water shows a decrease only from 3 to 1 ppb, which does not seem to explain the observed decrease in high-temperature conductivity. However, as discussed above, the total Cr content in the reactor water is not a quantitative measure for the chromate content, because a lot of Cr is retained in the crud in the reactor core. The chromate content in the solution can be associated with the equilibrium between the coolant and the crud. An additional factor contributing to the uncertainty of the chromate contents is that the contents determined at room temperature may deviate considerably from real high-temperature contents.

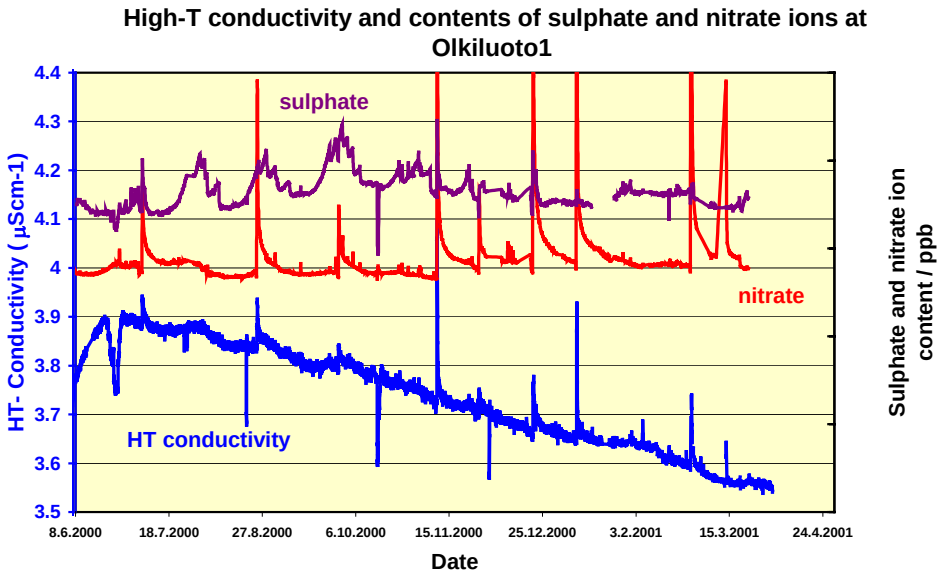

Figure 9. The high-temperature conductivity plotted together with the contents of SO_4^{2-} and NO_3^- ions in the coolant.

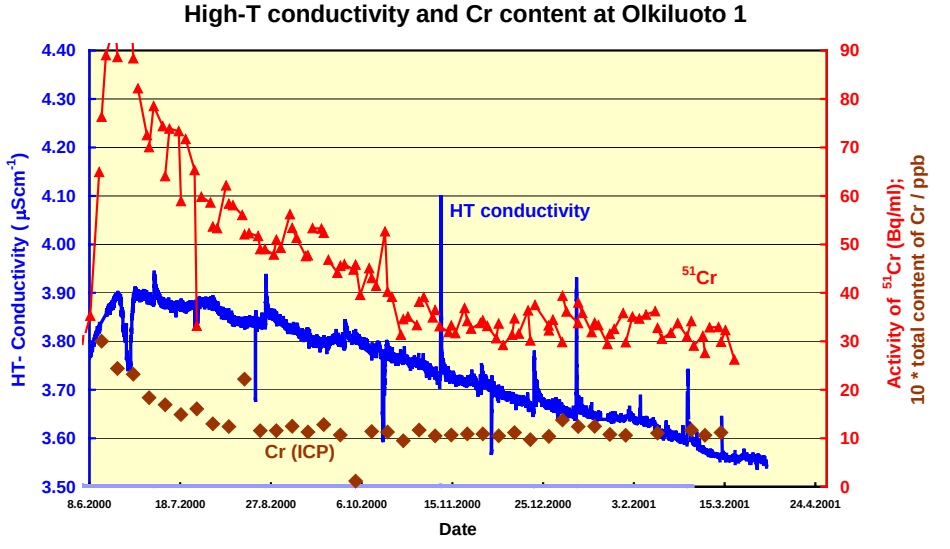

Figure 10. High-temperature conductivity together with the content of total Cr and the activity of ^{51}Cr in the coolant. The latter two can be used as an indicator for the chromate content of the coolant.

The results shown in Fig. 9 demonstrate that the sharp maxima observed in the high-temperature conductivity curve coincide with the peaks in the NO_3^- content, while the hump-like variations follow the SO_4^{2-} content of the coolant. This shows that the high-temperature conductivity measurement can be used as a rapid and sensitive indicator of increased anionic impurity levels in the coolant.

4. Summary of the main observations

The goal of the project is to find correlations between water chemistry data and oxide film properties in the BWR coolant, susceptibility to stress corrosion cracking and other forms of corrosion and the rate of activity incorporation. During the first year of monitoring high-temperature water chemistry in the shutdown cooling system 321 at Olkiluoto unit 1, the following main observations have been made:

- The corrosion potentials of AISI 316 L(NG) stainless steel, AISI 304 stainless steel, Inconel alloy 182 and Inconel alloy 82 are in the range 0–200 mV, which is typical for these materials in BWR plants under normal water chemistry conditions.
- The corrosion potentials are in a range where the materials are subject to a certain risk for environmentally assisted intergranular stress corrosion cracking.
- The corrosion potentials are not very sensitive to the excursions of SO_4^{2-} and NO_3^- contents in the coolant.
- The contents of F^- and Cl^- ions in the coolant are very low. No conclusions on their effect on the corrosion potentials can be drawn.
- The high-temperature conductivity of the coolant has proven to be a sensitive indicator of changes in the anionic impurity content and temperature variation of the coolant.
- A decrease of power output of the plant leads to an increase of the temperature in the cells of the shutdown cooling system 321.
- Repeated maxima in the high-temperature conductivity of the coolant occur because of the release of impurities from ion exchange resins.

- The high-temperature conductivity of the coolant may also partly reflect the changes in the chromate content of the coolant.

During almost the whole monitoring period June 2000 – March 2001, the following general trends have been observed:

- The potentials decrease with time.
- The high-temperature conductivity decreases with time.

It is not yet possible to state definitely which factors cause the observed trends. The decrease of potentials may be related to decreasing oxygen content, and probably also to changes in the chromate content, while the decrease in conductivity could be partly correlated with changes in the chromate content. The checking and maintenance of the electrodes during the refuelling outage in May 2001 will help to find out, whether some of the observed phenomena are caused by improper operation of one of the sensors.

5. Conclusions

The main conclusion of the monitoring at Olkiluoto 1 is that the employed monitoring unit provides relevant information that can be well used both for assessing long-term trends and for sensitive detection of rapid changes in the coolant environment.

Any conclusion about the role of water chemistry and oxide film properties in affecting material susceptibility to different forms of corrosion and activity incorporation on primary circuit surfaces can be drawn only after the removal and analysis of the first sets of samples. This will be the main subject in the second year of the ongoing monitoring period.

Acknowledgements

The work described is part of the subproject "Water chemistry, service reliability and activity levels" within a R&D project on Plant life management (YKK).

References

1. Laitinen T., Bojinov M., Betova, I., Mäkelä K. and Saario, T. The properties of and transport phenomena in oxide films on iron, nickel, chromium and their alloys in aqueous environments, Radiation and Nuclear Safety Authority, STUK-YTO-TR 150, January 1999. 79 p.

2. Lin, C.C. and Smith, F.R. Electrochemical potential measurements under simulated BWR conditions, EPRI NP-6732, March 1990, Palo Alto, USA.

Stability of oxides on stainless steel during simulated PWR shutdown and start-up

M. Bojinov, T. Laitinen, K. Mäkelä, M. Mäkelä, T. Saario, P. Sirkiä
VTT Manufacturing Technology, Espoo, Finland

T. Buddas, M. Halin, K. Tompuri
Fortum Power and Heat Oy, Loviisa, Finland

Abstract

Oxide films formed on OX18H10T Ti-stabilised stainless steel were characterised using the contact electric resistance (CER) technique and electrochemical impedance spectroscopy (EIS). The aim was to determine the effects of H_2O_2 injection temperature on the stability of the oxide films during simulated VVER shutdown and subsequent start-up conditions and to recognise possible changes in the thickness and structure of oxide films as a result of H_2O_2 injection at different temperatures.

Stability of the compact part of the oxide film is not greatly influenced by the injection temperature of hydrogen peroxide during a cool-down period. On the other hand, the injection temperature had a marked influence on the deposited crystals in the outer part of the film.

1. Introduction

The incorporation of activated corrosion products into the surfaces of the primary circuit in nuclear power plants is greatly influenced by the physical and chemical properties of the oxide films growing on the construction materials. A schematic picture of a typical oxide film growing on stainless steel surface in PWR water is shown in fig. 1.

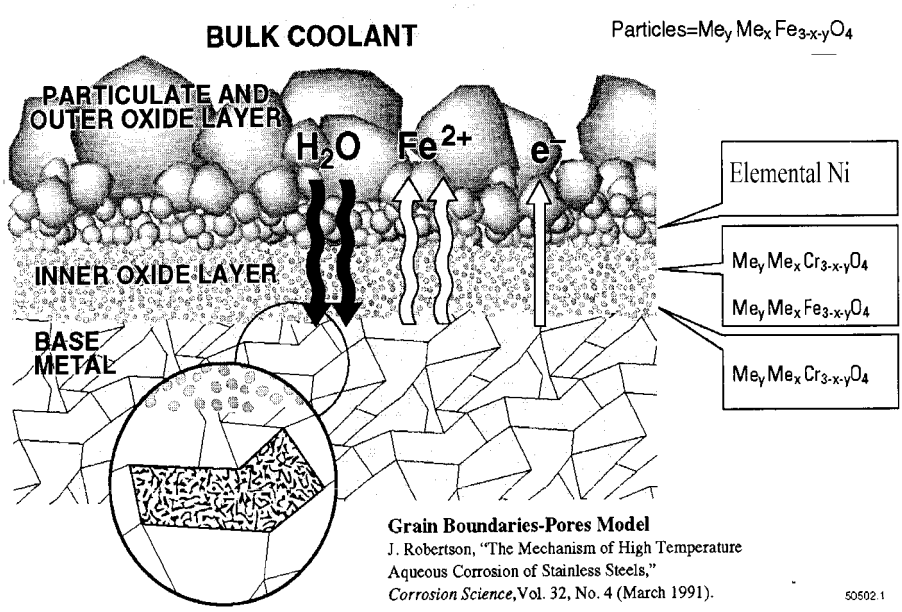

Figure 1. Schematic picture of an oxide film formed on type 316 stainless steel in PWR water. Modified from the figure given in ref. 1.

The outer porous oxide layer on stainless steel has typically a mixed spinel structure with a composition of non-stoichiometric nickel ferrite ($Ni_xFe_{(3-x)}O_4$). The inner part of the duplex oxide film has typically a chromium-rich composition of $Ni_xFe_{(1-x)}Cr_2O_4$ [2, 3, 4]. The outer nickel ferrite layer is typically thicker than the inner layer, but it has been found to incorporate less ^{60}Co on a unit mass basis than the inner layer [3]. The inner chromium-rich oxide layer incorporates ^{60}Co strongly, but since it is rather thin, a relatively small absolute amount of activity is involved. It is thus not straightforward to estimate which part of the oxide film contributes mainly to the total activity levels.

The thickness and composition of the outer layer of these oxide films is likely to be affected mainly by the chemical and physical conditions prevailing during the shutdowns and start-up periods. One typical procedure at operating power plants is to use an acid-oxidising stage during the shutdown period [5]. A hydrogen peroxide injection has been used to provide acid-oxidising conditions during

shutdown procedures as a method to further oxidise the existing oxide film. This is a way to release soluble radioisotopes into the reactor coolant in a controlled manner. The injection of H_2O_2 does not result in an overall increase in the activity released. Instead, the time over which the release occurs is significantly decreased, enabling a more effective removal of activity from the coolant [6].

Since the hydrogen peroxide injections are likely to affect the oxide films, the injection temperature and H_2O_2 concentrations should be defined in such a way that the protective properties of the oxide films formed on the primary circuit surfaces are maintained [6].

The work reported in this paper had two main goals. Firstly, to find out the effects of H_2O_2 injection temperature on the stability of the oxide films formed on the surfaces of stainless steel during simulated VVER shutdown and subsequent start-up conditions. Secondly, to recognise possible changes in the thickness and structure of oxide films as a result of H_2O_2 injection at different temperatures.

2. Experimental

2.1 Tests in a Re-Circulation Loop

The tests were conducted in a high-temperature re-circulation loop. Analytical grade chemicals and water purified in a Milli-Q® water purification system (Millipore) were used in the preparation of the simulated VVER coolant. The hydrogen and oxygen content together with the conductivity of the outlet water were continuously monitored at ambient temperature. The flow rate of the re-circulation loop water was kept constant in all the experiments. H_2O_2 was added into the autoclave water by means of a high-pressure liquid chromatograph (HPLC) pump. Each test was planned to simulate a shutdown and start-up period at the Loviisa NPP (shown in fig. 2). The temperature at which H_2O_2 was added into the autoclave was used as a variable in the test series (50, 90 and 130^{o}C).

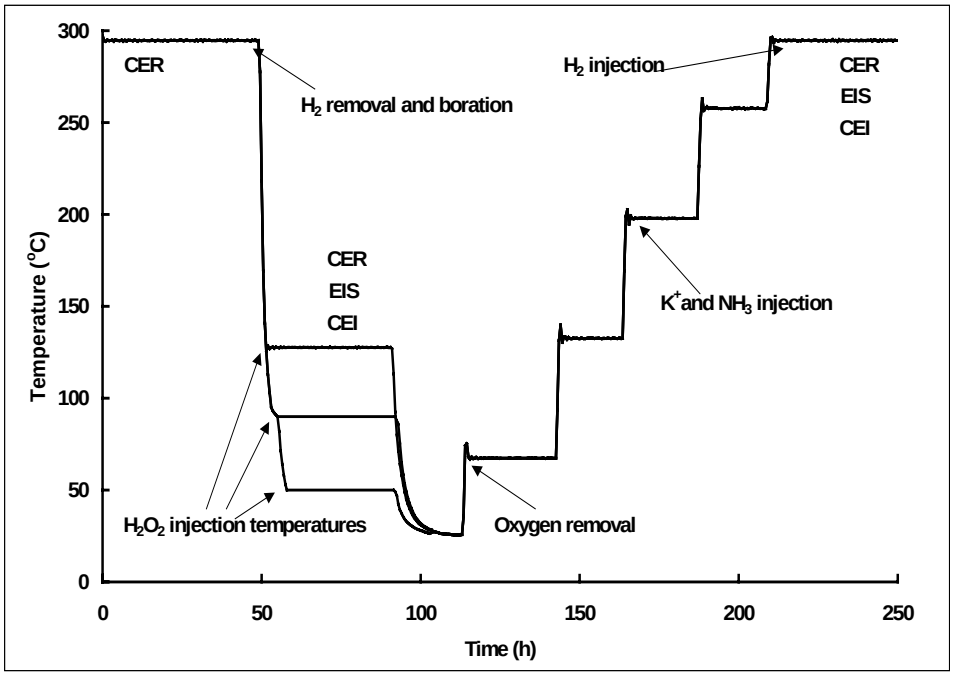

Figure 2. Simulation of the shutdown and start-up in the tests performed to study the influence of H_2O_2 injection on oxide films on stainless steel.

2.2 Measurement Techniques and Equipment

The oxide films formed on the studied samples were characterised using the contact electric resistance (CER) technique and electrochemical impedance spectroscopy (EIS). The CER apparatus was supplied by Cormet Oy, while the EIS measurements were carried out with a Solartron 1287 ECI/1260 FRA system controlled by CorrWare / ZPlot software (Scribner Associates).

A Model 3600 Analyzer (Orbisphere) was used for the room temperature monitoring of the content of dissolved hydrogen in the VVER coolant. The content of dissolved oxygen was monitored at room temperature with an Oxygen Indicator Model 2606 (Orbisphere). The room temperature conductivity measurements were performed using instruments supplied by Contronic. A Shimadzu LC-6A HPLC pump was used for the injection of H_2O_2.

2.3 Materials and Electrodes

The samples used in the experiments were manufactured from an OX18H10T stainless steel rod. OX18H10T is a Ti-stabilised stainless steel, similar to AISI 321SS. They were pre-oxidised for one week in a re-circulation loop in conditions corresponding to typical steady-state conditions in a VVER plant in the middle of a fuel cycle. The estimated contact area of the tips used in the CER measurements was ca. 0.015 cm^2. Separate disk electrodes made of OX18H10T embedded in PTFE (exposed area ca. 0.1 cm^2) were used in the conventional EIS measurements and in the monitoring of corrosion potential, while a Pt electrode was used to measure the redox potential. An external pressure-balanced AgCl/Ag electrode filled with 0.1 M KCl was used as a reference electrode. A Pd wire was employed as a low-impedance quasi-reference electrode in the impedance measurements. Unless otherwise stated, all the potentials given in this paper have been converted to the standard hydrogen electrode (SHE) scale.

3. Results and Discussion

3.1 Corrosion Potential Measurements

The corrosion potential as well as the redox potential increased as a result of the removal of hydrogen from the water and the addition of H_3BO_3 (decrease of pH) as shown in fig. 3. The addition of H_2O_2 increased further the potentials which reached a value (+0.20 V) corresponding to those observed in plant conditions. After the start-up, the potentials were again close to the hydrogen line.

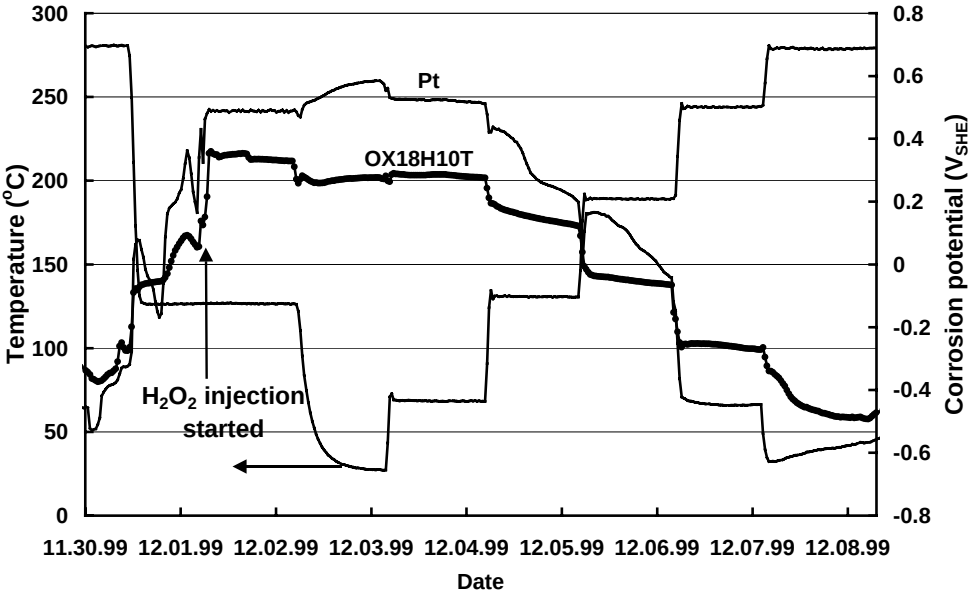

Figure 3. Measured corrosion potential of OX18H10T and the redox potential during the test with H_2O_2 injection at 130°C.

3.2 Scanning Electron Microscopy

To obtain a general view of the changes caused by hydrogen peroxide injection at different temperatures, the oxide films on the CER samples were characterised using a scanning electron microscope after the test period. A set of scanning electron micrographs from the oxide film surfaces is shown in fig. 4. After the pre-oxidation for one week (no H_2O_2 exposure) in a typical VVER coolant, the surface had become covered with a large density of crystals, the sizes of which ranged from 0.2 to 1 μm. After exposing these samples to the test sequence shown in fig. 2 it was found out that the injection temperature of H_2O_2 has an effect on the number and size of the crystals. The samples shown in figs 4b...4d were exposed to the high-temperature water (297°C) for a few days after the injection of hydrogen peroxide and to subsequent cooling before they could be removed from the autoclave. This may have had an influence on the final appearance of the oxide films. The SEM micrographs of the CER samples seem to indicate that the lower the H_2O_2 injection temperature is, the greater is the number of large crystals existing on the surface.

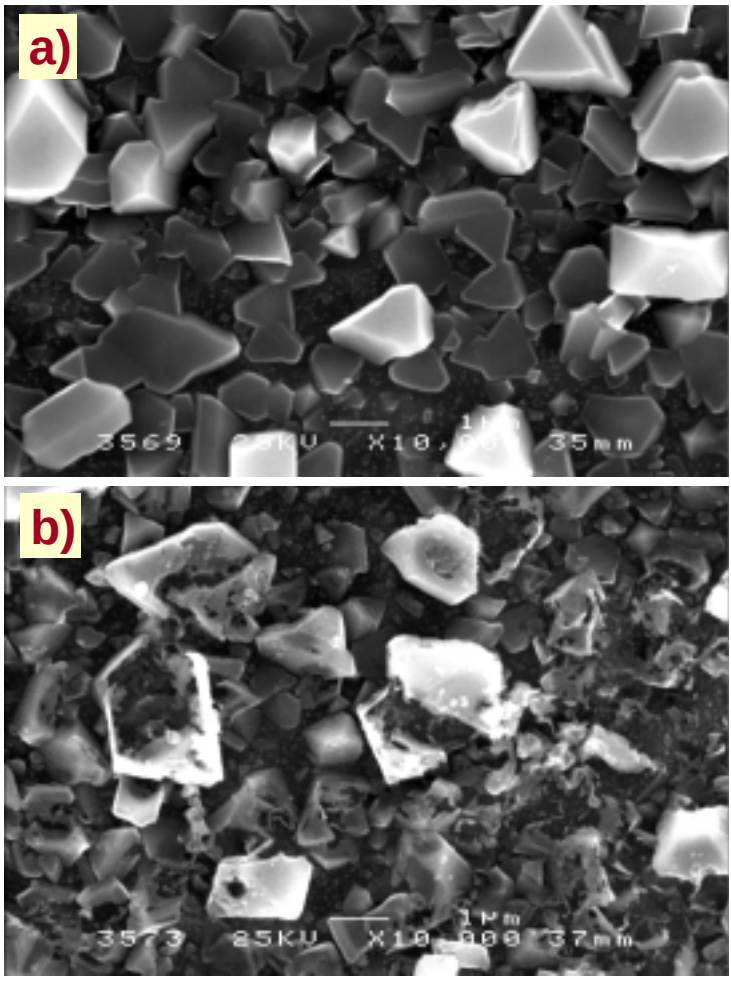

Figure 4. Scanning electron micrographs of the oxide films on the OX18H10T stainless steel. a) before exposure to the H_2O_2 injection test; b) after the test with H_2O_2 injection at 50°C; (continued on next page)

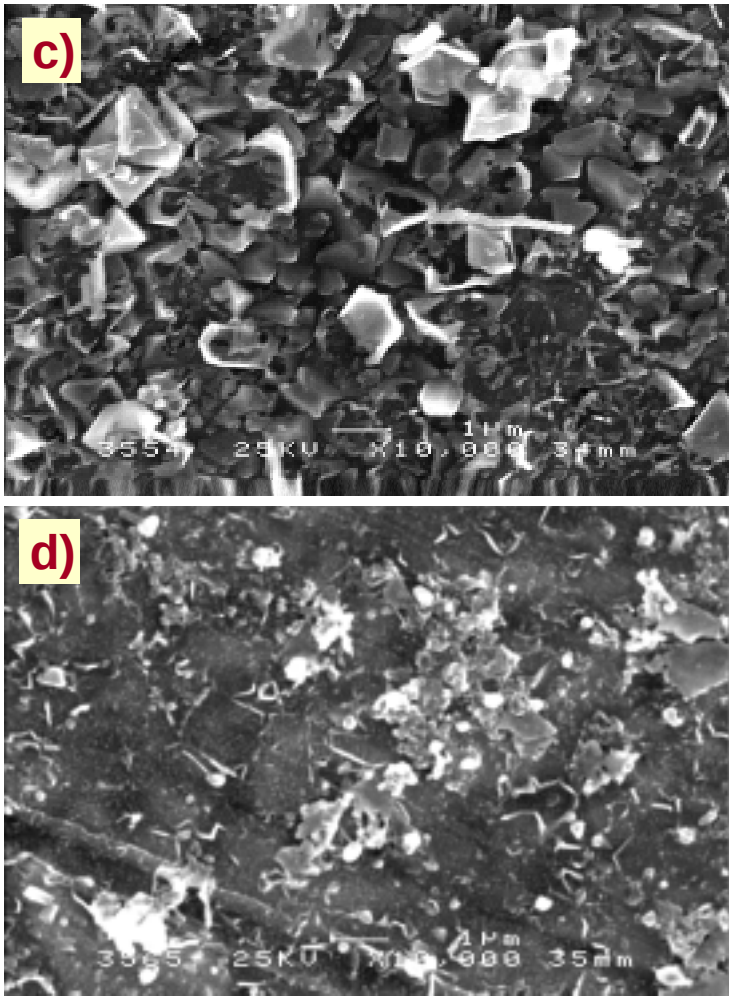

Figure 4. Scanning electron micrographs of the oxide films on the OX18H10T stainless steel. c) after the test with H_2O_2 injection at 90°C; d) after the test with H_2O_2 injection at 130°C.

To obtain an estimate for the oxide thicknesses on different samples, cross section SEM micrographs were taken from these samples. Both after the pre-oxidation and after the tests with hydrogen peroxide injection at 50 and 90°C, the film comprised two layers. The outer layer on these samples consisted of a large number of crystals (also seen in fig. 4) which were loosely attached to the underlayer. The mean thickness of the inner, compact part of the pre-oxidised film was 0.3–0.4 μm. The thickness of the compact part of the film was slightly changed during the tests with hydrogen peroxide injections. The thicknesses

were estimated to be ca. 0.4 μm, 0.4 μm and 0.5 μm after tests with injections at 50, 90 and 130°C, respectively. Thus the examinations indicate that the oxide film on the sample after the test with injection at 130°C has a slightly thicker compact part than the other samples. On the other hand, the lowest number of deposited crystals are found on its surface as shown in Fig. 4d and commented above.

3.3 Contact Electric Resistance Measurements

To obtain information about the effects of H_2O_2 injection on the electronic properties of the oxide films on the studied materials, CER measurements were performed. It is worth noting that the CER technique mainly gives information of the electronic properties of the inner, compact part of the oxide film, which is generally believed to control the rate of the oxidation of the substrate metal. Thus it is also the part that determines the stability of the whole oxide film towards corrosion. The dc resistance (R) of the surface film on the stainless steel sample during the 130°C experiment is shown in fig. 5.

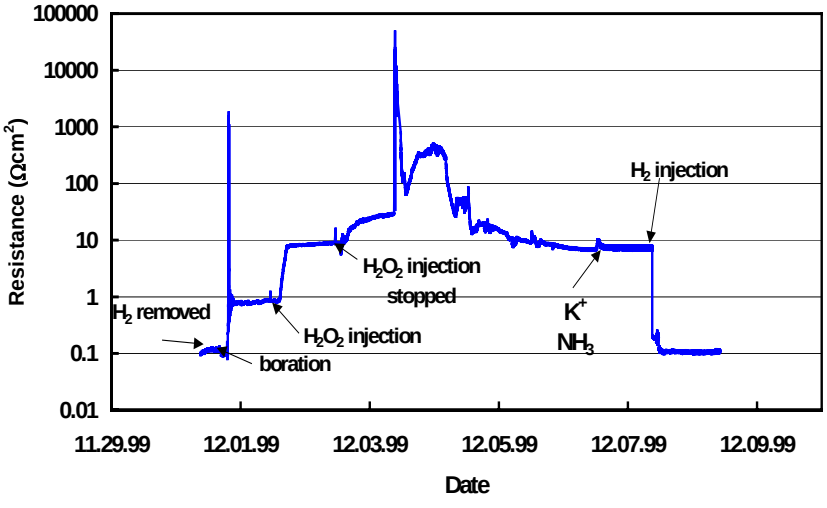

Figure 5. The dc resistance of the surface film on the stainless steel sample in the test during which H_2O_2 was injected into the coolant at 130 °C.

The shapes of the resistance vs. time curves were found to be qualitatively similar to each other at each test temperature. The values of the resistance at the start of the experiment at 297 °C were comparable (ca. 0.08 Ωcm^2). This shows that the electronic properties of the oxide films on the different stainless steel samples were similar after the pre-oxidation period. By the time when the injection of H_2O_2 was started, the resistance had stabilised to values of ca. 11 Ωcm^2, 6 Ωcm^2 and 0.8 Ωcm^2 at 50, 90 and 130°C, respectively. The injection of H_2O_2 resulted in a clear increase of the resistance. The shape of the R vs. t curve resembles that of the potential vs. time curve shown in fig. 3. The value of the resistance was the highest after hydrogen peroxide injection at 50°C (0.8 $k\Omega cm^2$), somewhat lower at 90°C (0.4 $k\Omega cm^2$) and the lowest when the H_2O_2 injection was done at 130°C (0.008 $k\Omega cm^2$). Thus the film after hydrogen peroxide injection at 50°C exhibits the most insulating properties. This may have a retarding effect on the redox reactions of the species in the coolant, and may thus also contribute to a decreased rate of the reduction of hydrogen peroxide.

During the following heat-up, the resistance of the oxide films decreased with increasing temperature (decreasing potential), and during each test a clear fall in the R values was observed as hydrogen was dosed into the coolant. The resistance of the oxide films at 297°C after the start-up was very close to the values measured at 297°C before the cool-down preceding the H_2O_2 injection. Thus the injection of hydrogen peroxide at different temperatures did not seem to influence the electronic conductivity of the oxide film and the rate of redox reactions on its surface on a longer term.

3.4 Electrochemical Impedance Spectroscopic Measurements

In order to obtain more information of the influence of hydrogen peroxide injection on the stability of oxide films and corrosion rate of stainless steel, electrochemical impedance spectra of the samples were measured before and after the H_2O_2 injection as well as after the simulated heat-up. The EIS technique is likely to give information not only of the processes in the inner, compact part of the oxide film, but also at the interface between this inner part and the solution.

Qualitatively, the spectra shown in fig. 6 exhibit a low-frequency linear part, which starts to resemble a semicircle at very low frequencies after exposure to H_2O_2. In addition, a small high frequency impedance loop can be observed in most of the spectra. This kind of spectra are typical for a situation in which both a charge transfer reaction (e.g. oxidation of metal) and a transport process under a concentration gradient contribute to the behaviour. Accordingly, the high-frequency impedance loop is probably due to the charge transfer of the corrosion reaction. The low-frequency part of the spectrum can most likely be linked to a transport process in the film. The results obtained in the present work were fitted using the following transfer function, which takes into account the features discussed above:

$$Z = R_{el} + \{j\omega C_{hf} + [R_{hf} + R_D \tanh (j\omega \tau_D)^{n_D} / (j\omega \tau_D)^{n_D}]^{-1}\}^{-1}$$

The most important parameters of this equation in the present case are the charge transfer resistance (R_{hf}) and the transport resistance for ions and ionic defects (R_D). The relative magnitudes of R_{hf} and R_D determine, whether charge transfer or the transport of ions in the film controls the overall rate of metal oxidation. If $R_{hf} >> R_D$, charge transfer controls the oxidation rate, while if $R_{hf} << R_D$, transport of ions or ionic defects controls the oxidation rate. The rate of transport of ions or ionic defects in the film can be interpreted as a measure for the stability of the film: the slower the transport rate, the more stable the film is. The values obtained for the resistances R_{hf} and R_D as a result of the fitting of the impedance spectra showed that in all the cases $R_{hf} << R_D$. This means that the transport of ions or ionic defects controls the overall rate of metal oxidation. The best-fit results for R_D are summarised in fig. 7. shown below.

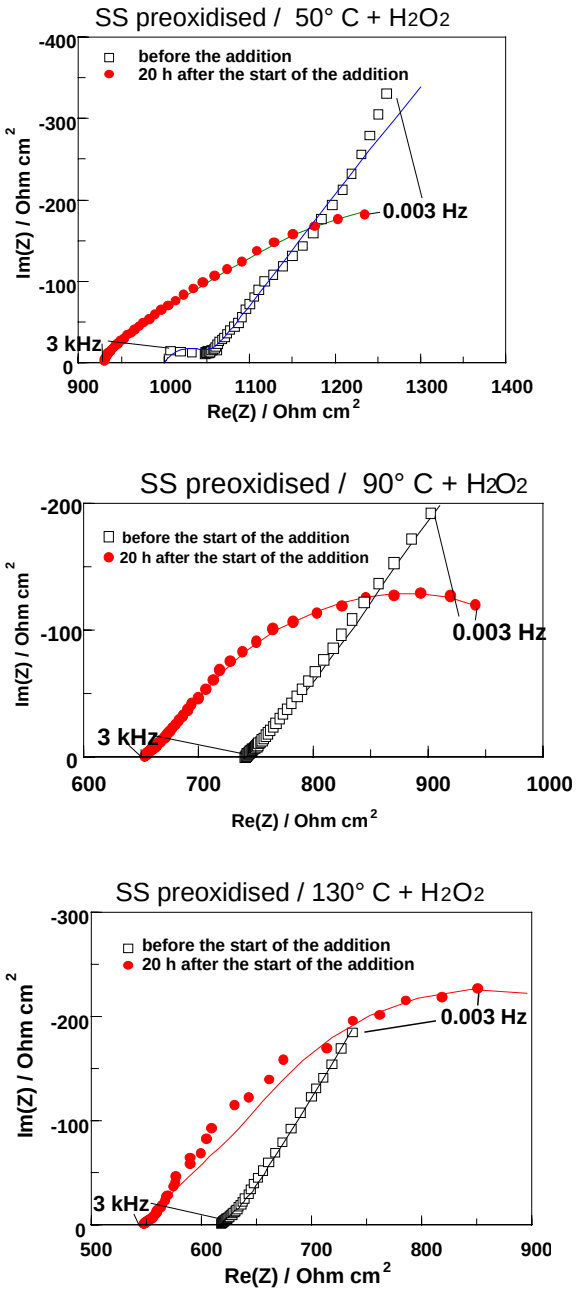

Figure 6. Complex plane plots of the electrochemical impedance spectra for the samples before and after the injection of H_2O_2 at the three test temperatures. Symbols refer to experimental points and the solid lines to the fit to the transfer function given above. Composition of the simulated coolant: 13.5 g/l H_3BO_3. Parameter is frequency in Hz.

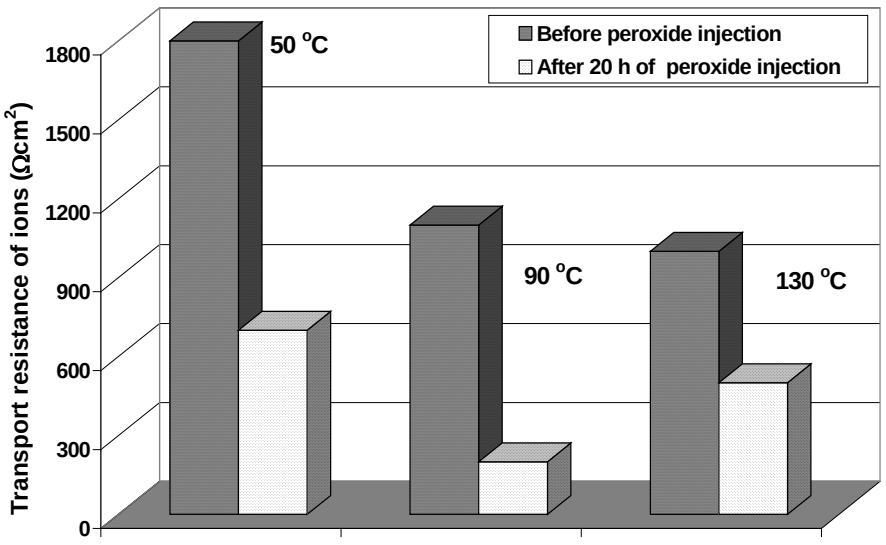

Figure 7. Best-fit results for the transport resistance R_D obtained from the experimental impedance spectra before and after the injection of H_2O_2 at the three different temperatures 50, 90 and 130°C.

The resistance R_D for the transport process decreases at all temperatures as a result of H_2O_2 injection. This can probably be attributed to the fact that the presence of H_2O_2 leads to a more efficient cathodic partial reaction. Therefore, a corresponding increase in the rate of the anodic partial reaction can be expected. As the rate of the anodic reaction is most probably controlled by the rate of transport of defects through the film, the increase of the rate of the anodic reaction should be reflected in the value of the transport resistance. This is exactly what was observed experimentally.

The results show that the value of R_D decreases by 60% as a result of H_2O_2 injection at 50°C, by 80% as a result of injection at 90°C and by 50% at 130°C. This suggests that the injection of hydrogen peroxide at 90 °C causes more pronounced changes in the films than that at 50 or 130°C. The value of R_D after the injection is the highest at 50°C, which in turn suggests that the films are the most stable after injection at this temperature. The second best stability is found at 130°C, while the films exhibit the poorest stability after hydrogen peroxide injection at 90°C. However, a comparison of the influence of hydrogen peroxide

injection on the absolute values of R_D is complicated, because also the difference in temperature alone has an influence on the values of R_D as shown in Fig. 7.

The electrochemical impedance spectra measured for the samples at 297°C after the H_2O_2 injection, the subsequent cool-down and heat-up are shown in fig. 8. The results show no significant differences between the spectra measured for the samples corresponding to the three different injection temperatures. The fitting of the results to the transfer function given above shows that the ionic transport resistance for the three cases is almost the same. This means that the stability of the film in all these cases can be considered the same. In other words, the possible influence of the injection temperature of H_2O_2 on the stability of the oxide films formed on stainless steel in VVER conditions does not seem to extend over the next heat-up.

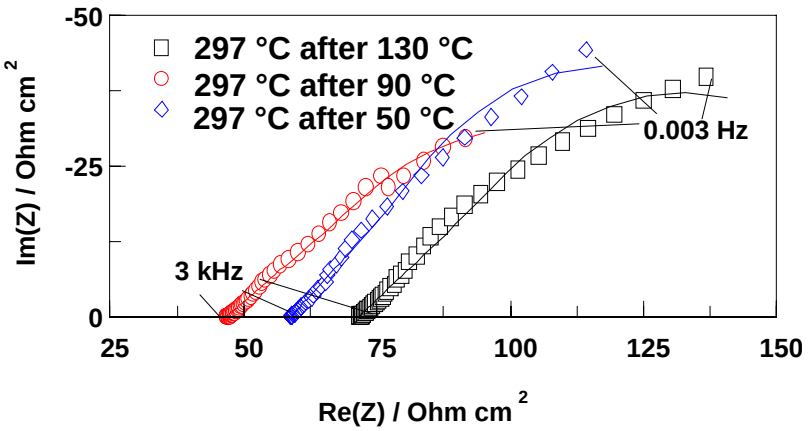

Figure 8. Complex plane plots of the electrochemical impedance spectra measured for the samples exposed to H_2O_2 injection at three different temperatures, subsequent cool-down and heat-up. Symbols refer to experimental points and the solid line to the fit to the transfer function. Parameter is frequency in Hz. Composition of the simulated coolant: 13.5 g/l H_3BO_3, 16 mg/l K^+, 18 mg/l NH_3.

4. Summary of observations

The main observations of this study can be summarised as follows:

- SEM studies showed clearly that the injection of hydrogen peroxide at 130°C results in considerable changes in the appearance of the outer part of the oxide film. The number of large crystals found on the surface before the exposure to the test coolant decreased and/or the crystals were transformed into much smaller ones.
- The dc resistance of the oxide film on stainless steel increased considerably during the hydrogen peroxide injections, which can be attributed to the further oxidation of the film. The influence of the injection of H_2O_2 on the electronic resistance was the larger, the lower the injection temperature. The higher electronic resistance of the film is likely to retard the rate of redox reactions such as the reduction of hydrogen peroxide on the film surface.
- The impedance results suggested that the transport rate of ions or ionic defects in the film is increased as a result of H_2O_2 injection, which is an indication of decreased stability of the compact part of the film and increased corrosion rate of the material.
- The stabilities of the films exposed to hydrogen peroxide injection at 50, 90 and 130°C, subsequent cool-down and heat-up were very similar. This means that the possible influence of the injection temperature on the inner, compact part of the film does not extend beyond the next heat-up.

5. Conclusions

The results of this work show that the stability of the compact part of the oxide film formed on stainless steel in VVER conditions is not greatly influenced by the injection temperature of hydrogen peroxide during a cool-down period. The stability of the film is somewhat higher after injection at 50 and 130 than at 90°C, but these differences are no more observed after the following heat-up period. This suggests that the injection temperature of hydrogen peroxide does not change the steady state corrosion rate of the steel. Therefore, the long term effects of hydrogen peroxide injections may remain rather insignificant.

The injection temperature was on the other hand found to have a marked influence on the deposited crystals in the outer part of the film. Injection at 130°C resulted in the disappearance and/or transformation of these crystals to smaller ones, while injections at other temperatures had no such influence. These changes were found to remain even after the next heat-up. This kind of changes in the deposited layer may have an impact on the rate of incorporation of radioactive species on and in the oxide films.

References

1. Baston, V.F., Garbauskas, M. F. and Ocken, H. Material characterisation of corrosion films on boiling water reactor components exposed to hydrogen water chemistry and zinc injection. Proceedings of the 7th Conference on Water Chemistry of Nuclear Reactor Systems, London, British Nuclear Energy Society, 1996. Pp. 558–565.

2. Lister, D. H. and Davidson, R. D. Corrosion product release in light water reactors, EPRI NP-6512, Palo Alto,1989.

3. Lister, D. H. Activity transport and corrosion processes in PWRs. Proceedings of the 6th Conference on Water Chemistry of Nuclear Reactor Systems, London, British Nuclear Energy Society, 1992. Pp. 49–60.

4. Riess, R. and Stellwag, B. Effects of zinc on the contamination and structure of oxide layers, Proceedings of the 7th Conference on Water Chemistry of Nuclear Reactor Systems, London, British Nuclear Energy Society, 1996. Pp. 573–582.

5. Wood, C. J. PWR primary shutdown and startup chemistry guidelines, EPRI TR-101884, January 1993, Palo Alto, USA.

6. Hansson-Lyyra, L., Laitinen, T. and Mäkelä K. Behaviour of antimony in LWR primary coolant. Espoo, Finland: VTT Manufacturing Technology, Report VALC552, 17.12.1998. 29 p.

Activity incorporation into the oxide films on stainless steel samples exposed to primary coolant in Loviisa 1 unit

Martin Bojinov, Ulla Ehrnstén, Petri Kinnunen, Timo Laitinen,
Kari Mäkelä, Timo Saario, Pekka Sirkiä, Laura Taivalaho
VTT Manufacturing Technology, Espoo, Finland

Thomas Buddas, Magnus Halin, Kimmo Tompuri
Fortum Power and Heat, Loviisa, Finland

Abstract

Changes in operational conditions may induce changes in the oxide films and rate of activity incorporation. To predict these changes and find means to affect activity build-up, experimental correlations between water chemistry, oxide film properties and activity incorporation are sought for. Flow-through cells have been installed in the sampling line of Loviisa unit 1 in order to collect the data needed when looking for such correlations.

The main sources of activity in the samples are ^{110m}Ag and ^{124}Sb. The ^{124}Sb incorporation was highest during the shutdown to refuelling outage and it seems to be a surface related phenomenon. Because of its long half life, ^{60}Co is also an important isotope. The rate of ^{60}Co content increase is highest during the start-up.

1. Introduction

The extent of activity incorporation on primary circuit surfaces in a nuclear power plant is closely connected to the chemical composition of the coolant water and to the structure and properties of oxide films formed on material surfaces. A sketch of a typical oxide film forming on stainless steel surfaces in PWR coolant conditions is shown in Fig. 1.

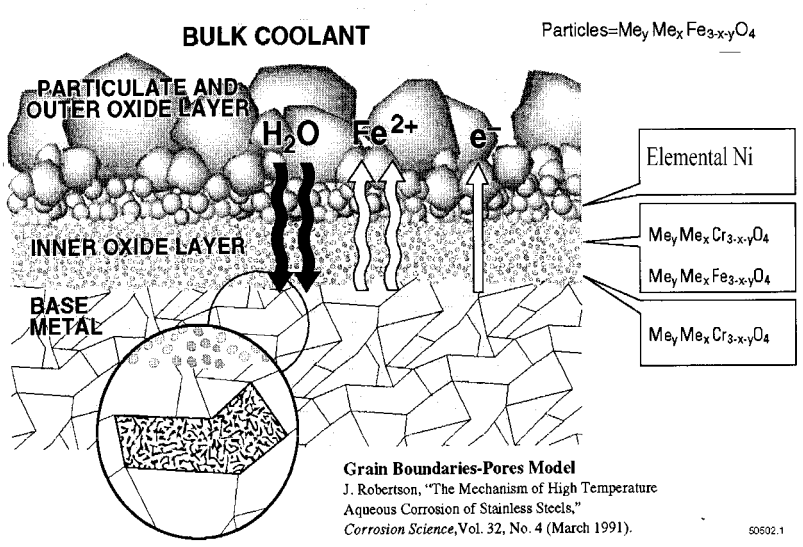

Figure 1. A schematic picture of an oxide film formed on AISI 316 stainless steel in PWR water. Modified on the basis of a figure in ref. 1.

The outer, deposited part of the oxide film has typically a spinel structure with a composition of non-stoichiometric nickel ferrite ($Ni_xFe_{(3-x)}O_4$), while the inner part of the duplex oxide film has typically a chromium-rich composition of ($Ni_xFe_{(1-x)}Cr_2O_4$).

Changes in operational conditions may induce changes in the structure of the oxide films and in the rate of activity incorporation. To predict these changes, experimental correlations between water chemistry, oxide films and activity incorporation, as well as mechanistic understanding of the related phenomena need to be established.

The aim of this work is to establish correlations between the chemical and radiochemical data collected routinely at the Loviisa unit 1, the oxide film properties and the extent of activity incorporation into the films formed on material samples exposed to the primary coolant. These correlations are planned to be used when predicting the evolution of activity incorporation during plant operation, especially if changes in operational conditions occur.

A unit consisting of three flow-through cells has been installed in the sampling line of Loviisa unit 1 in order to collect the data needed when looking for such correlations. The cells are being used for two major purposes:

- Observation of the growth, structure and activity incorporation levels of oxide films formed on material samples exposed to the primary coolant at the cold-leg temperature.

- Correlating these observations with chemical and radiochemical data collected by the plant, as well as with high-temperature water chemistry monitoring data such as the corrosion potentials of relevant material samples, the redox potential and the high-temperature conductivity of the primary coolant.

The exposure of stainless steel samples in the present cell unit and the monitoring of high-temperature water chemistry at the cold-leg temperature has been started at Loviisa unit 1 on the 7th of February, 2000. Since then, three sets of samples have been removed from the cell for activity measurements and oxide film analysis. All the results for the first two sets of samples are available at the moment, while only the activity measurements have been completed for the third set of samples. The data from high-temperature water chemistry monitoring is mainly used to confirm that water chemistry parameters are in the expected range during the exposure period. This report summarises the observations made on the basis of available results on oxide films.

2. Experimental

2.1 High-temperature cells and sensors

The flow-through cells for monitoring the high-temperature water chemistry and for exposing material samples to the primary coolant have been connected to the sampling line of the primary circuit of Loviisa unit 1 as shown in Fig. 2. The flow-rate through the cells is 2 l/min. The photograph shown in Fig. 2 has been taken before the system was insulated thermally to ensure a constant temperature corresponding to the cold-leg temperature of the plant. Due to proper insulation

of the sampling line, there has been no need for extra heating of the cell by the electrical heaters connected to the flow-through cell.

Figure 2. Flow-through cells with high temperature water chemistry sensors (lower cell) and 80 stainless steel samples (two upper cells) at Loviisa unit 1.

The coolant enters first the lower cell that contains two AgCl/Ag reference electrodes filled with 0.1 M KCl, one conductivity electrode, one pH electrode, a Pt sample for measuring the redox potential and two separate samples for measuring the corrosion potential (ECP) of AISI 316L stainless steel. The material samples are in the two upper cells that have been positioned close to each other.

2.2 Data acquisition

A data logger with a computer on site were initially used for data acquisition. However, a break in the data collection occurred between 04.07.2000 and 08.09.2000. It caused a loss of data from the shutdown to the refuelling outage and the subsequent start-up the data. Therefore, a modem connection between the monitoring site and VTT was established in March 2001 to make continuous

observations and data evaluation possible, Fig. 3. In addition, the high-temperature conductivity data at the beginning of the measurement period are not available due to problems in measuring electronics.

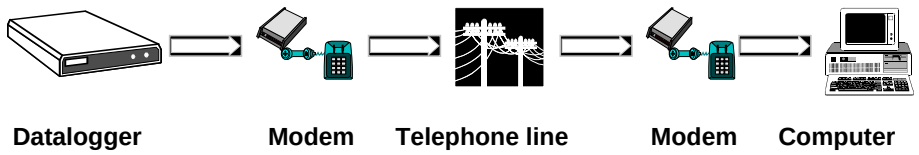

Figure 3. The system applied since March 2001 for collecting the monitoring data at Loviisa unit 1 and transferring it to VTT, Espoo for evaluation.

2.3 Material samples

Material samples made of 08X18H10T stainless steel and of AISI 316L stainless steel have been installed in the two upper cells in order to simulate the exposure of plant components to the primary coolant. Samples are removed from the cell at pre-scheduled intervals, and the oxide films formed on their surfaces are analysed. The results will be correlated with the abundant chemical and radiochemical data such as coolant composition, dose rates etc. measured and collected routinely at the plant over the years. The two material sample cells contain altogether 80 samples.

The elemental composition of 08X18H10T was determined using optical emission spectrometer (Spectrolab S), resulting in the following composition: 18% Cr, 10.4% Ni, 0.05% C, 0.47% Ti, 0.15% Co and balanced with Fe. The composition of AISI 316L is 18% Cr, 10% Ni, 3% Mo, < 0.02% C balanced with Fe.

The samples have been placed in 20 sample holders, Fig. 4, each of which contains two samples of OX18H10T and two samples of AISI 316L with two different pre-treatments. The two different initial surface conditions of the samples - ground and pre-oxidised - were prepared as follows:

- Ground samples were cut from 08X18H10T and AISI 316L rods and were wet ground using 600 grade emery paper and washed with water purified in a Milli-Q® purification system.

- Pre-oxidised samples were first wet ground using 600 grade emery paper and then pre-passivated in high purity water in a re-circulation autoclave. During the one week pre-passivation period at 297^{o}C, the oxygen content in the re-circulation loop was kept at 300 ± 30 ppb.

The samples in the sample holder are electronically insulated from the body and from each other. The design of the sample holder and the flow-through cell has been optimised to guarantee as similar flow conditions on the surfaces of all the 80 samples as possible.

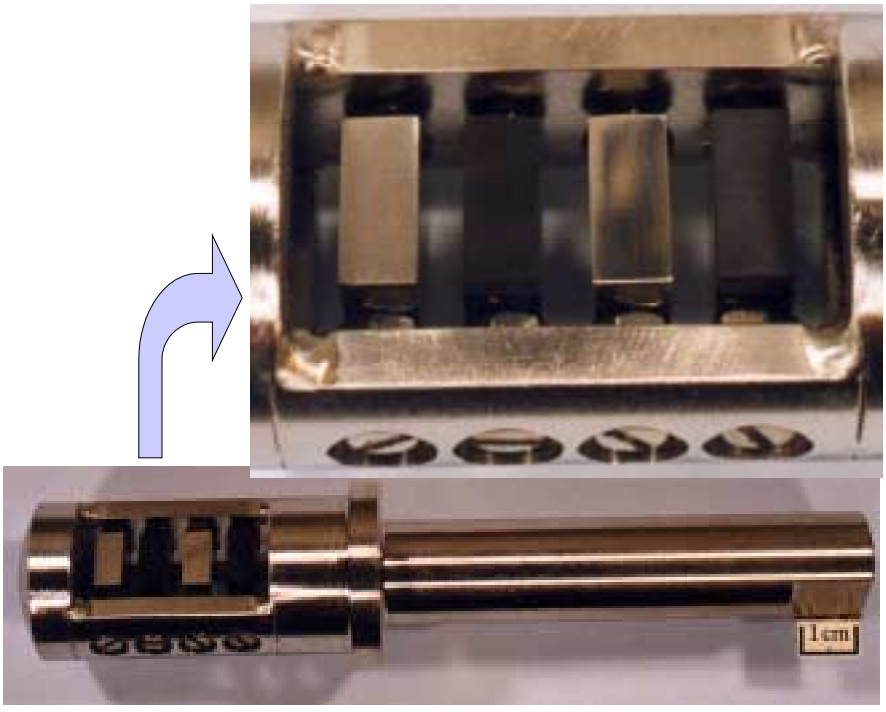

Figure 4. A sample holder containing four material samples.

2.4 Oxide film analysis

As the pickup of activity on the sample surfaces is linked to the composition, structure and thickness of the oxide film, the following techniques have been used to characterise the composition and structure of the oxide films after the exposure to the primary coolant:

- Gamma spectrometry
- Scanning electron microscopy (SEM)
- X-ray diffraction measurements (XRD)
- Secondary ion mass spectrometry (SIMS)

Activity measurements by gamma spectrometry have concentrated mainly on five nuclides, ^{60}Co, ^{58}Co, ^{54}Mn, ^{124}Sb and ^{110m}Ag.

SEM micrographs have been recorded from above the surfaces and from the cross-sections of oxide films on the different samples. XRD has been used to obtain an estimation of the oxide film thicknesses. The measurements have been carried out using a portable XRD equipment.

SIMS has been used to provide an estimate of the oxide film thicknesses and to determine a depth profile of the elemental composition of the oxide films on selected samples. SIMS depth profiling was carried out using a double focusing magnetic sector instrument (VG Ionex IX70S). The current of the 5 keV O_2 primary ions was 400 nA during depth profiling and the ion beam was raster-scanned over an area of 310×420 μm^2. The depth of the crater was measured by a profilometer (Dektak 3030ST) after SIMS analysis. The Dektak 3030ST is a surface texture measuring system which accurately measures surface texture and step heights. Measurements are made electromechanically by moving the sample beneath a diamond-tipped stylus. The high precision stage moves a sample beneath the stylus according to a user-programmed scan length, speed and stylus force.

3. Results and discussion

3.1 Plant operation and water chemistry

Towards the end of the fuel cycle, the stretch-out period started on June 13th, 2000. It lasted approximately one month before the shutdown to refuelling outage. The boration was done and the refuelling outage started on July 22nd. The start-up from the refuelling outage took place on September 4th, 2000.

The results of the routinely at the plant collected chemical analyses of the primary coolant during the monitoring period were carefully analysed for comparison to the current data. The data are presented in more detail in the subproject report and just outlined here.

The concentrations of boric acid and potassium decrease gradually during a fuel cycle. The concentration of ammonium also decreases, except for two periods of increase between 11.1.–10.2.2001 and 3.5.–31.5.2001. The increases in the concentration of ammonium influence the hydrogen content in the coolant. The pH of the coolant increases steadily after the start-up from the refuelling outtake.

The concentrations of Iron and Nickel in the coolant are relatively constant during the whole fuel cycle. Small maxima of Fe content occur at different stages of the cycle. Higher transients at the beginning of the refuelling outage are due to the increase of the boric acid concentration in the coolant. The concentration values indicate that Ni dissolves more slowly than Fe during these transients.

Although the Fe and Ni concentrations do not show significant variations, the results indicate considerable changes in the behaviour of Fe and Ni occurring in April during several fuel cycles. The determined metal contents in ionic form show that the contents of ionic metal species in the primary coolant decrease by several orders of magnitude during the cycle. This observation is worth considering when assessing the factors influencing activity incorporation into the oxide films on primary circuit surfaces. It should also be noted that the content of Ni in the ionic form is considerable smaller than that of total Ni.

3.2 ECP and high temperature conductivity

The corrosion potential of an AISI 316 L sample and the redox potential in the primary coolant are shown together with the cell temperature in Fig. 5. In the beginning of the measurement period, both the corrosion potential of AISI 316 L and the redox potential decreased continuously reaching nearly a steady-state value of about -0.75 V_{SHE}. Since then the potentials have remained low, i.e. close to equilibrium potential of the H^+/H_2 couple throughout the whole monitoring period. These results at Loviisa unit 1 are very similar to those obtained since the start of high-temperature monitoring at the Loviisa units in the 1980's, [2, 3].

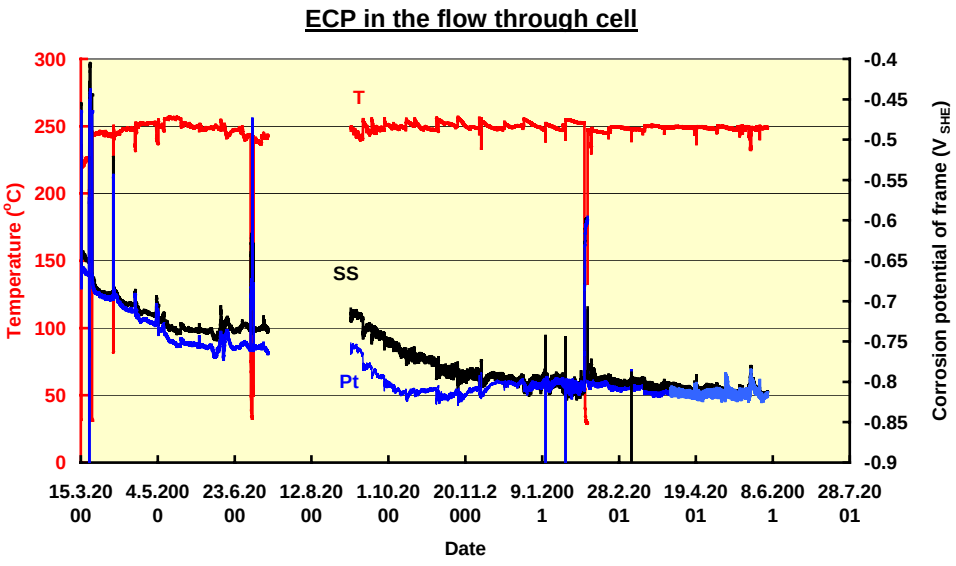

Figure 5. Corrosion potential of AISI 316 L stainless steel (black) and redox potential (blue) along with cell temperature at Loviisa unit 1. Missing data are due to problems in the data logging system.

The results of high-temperature conductivity measurements of the primary coolant during the fuel cycle are shown in Fig. 6, together with the room-temperature conductivity values determined routinely at the plant. Both the room-temperature and the high temperature conductivity values follow the chemical changes in primary coolant composition. The general decrease of the high-temperature conductivity during the fuel cycle is, however, much more pronounced than that of the room-temperature conductivity. This is most probably due to the higher sensitivity of the high-temperature measurement. The generally decreasing trend of the measured conductivity during the fuel cycle and the small conductivity maximum in January–February 2001 can be ascribed mainly to changes in the concentration of ammonia and partly in that of potassium hydroxide during the fuel cycle.

A pH electrode was installed to the cell, but unfortunately the insulation of the electrode was damaged already in the beginning of the monitoring period. Accordingly, no pH data is collected until the pH electrode will be changed to a new one during the refuelling outage in August 2001.

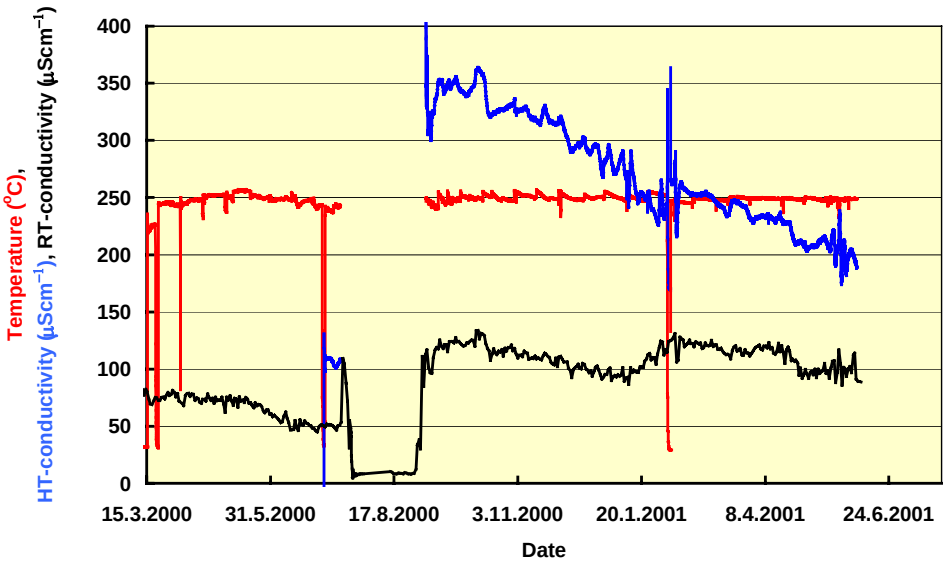

Figure 6. Measured high-temperature and room-temperature conductivities. Missing data are due to problems in the data logging and electronics.

3.3 Activity incorporation into the oxide films

The first set of samples was removed after five months of exposure on 03.07.2000, the second set was removed during the refuelling outage on 8.8.2000 and the third set was removed after another long period of normal operation of the plant on 07.02.2001. The next sample removals have been planned before the chemical transients due to exchange of ion exchange filters and start of stretch-out in summer 2001 and after the shutdown to refuelling outage in August 2001.

The activity data measured routinely at the plant indicate a relatively constant level of activity in the coolant during the most part of the fuel cycle. However, during the stretch-out period (June 15th – July 22nd) preceding the shutdown to refuelling outage the activity levels show a clear increase. These changes correlate with the changes in Fe and Ni concentrations of the coolant, which occur at the same time in every fuel cycle. Additional changes are observed as local

maxima or variations in the levels of ^{60}Co, ^{58}Co, ^{124}Sb and ^{110m}Ag in December 2000, February 2001 and May 2001. These variations coincide fairly well with the small maxima in the Fe content of the coolant and can be explained to be due to power control or mechanical transients.

The activity levels due to five relevant isotopes in the samples removed from the material sample cell after exposures of 5, 6 and 12 months are shown in Fig. 7.

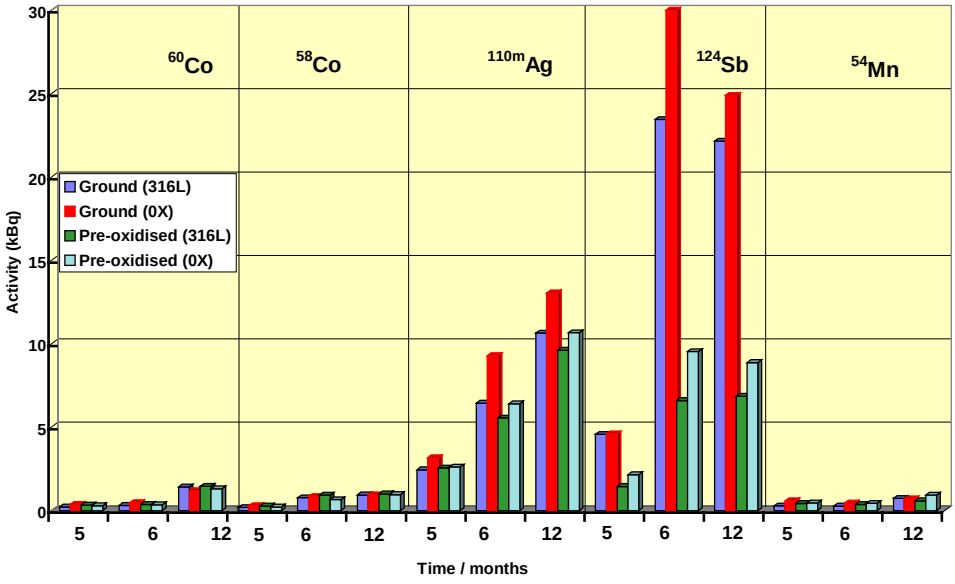

Figure 7. Activity of the major isotopes in samples removed from the material sample cell after an exposure of 5, 6 and 12 months.

3.3.1 Incorporation of different isotopes

Incorporation of ^{60}Co, ^{58}Co, ^{110m}Ag and ^{54}Mn does not seem to depend on the pre-treatment of the sample. On the other hand, the incorporation of ^{124}Sb is much more pronounced into the ground samples than into the pre-oxidised samples for both AISI 316L and 08X18H10T. This may indicate that the outer surface plays an important role in the incorporation of Sb.

Generally, the main contribution to the activity levels in the studied samples is due to the ^{124}Sb and ^{110m}Ag isotopes, while the contributions of ^{60}Co, ^{58}Co and

^{54}Mn are much smaller. However, in the consideration of long-term effects, the different half lives of the different isotopes have to be taken into account. The longest half life is that for ^{60}Co ($t_{1/2}$ = 5.3 years).

A comparison of the absolute activity levels shown in Fig. 7 with those reported earlier for Loviisa unit 2 is not straightforward, because the geometry of the samples is different in the present measurements. However, a qualitative difference is clear. The isotopes ^{124}Sb and ^{110m}Ag have a dominating role over the other isotopes at Loviisa unit 1. At Loviisa unit 2 we observed close to similar contributions of ^{60}Co, ^{110m}Ag and ^{124}Sb [3].

3.3.2 Activity incorporation rates

To obtain an idea of the rate of activity incorporation at different stages of the fuel cycle, the incorporation rates for the different isotopes have been plotted in Figs. 8 and 9. These rates have been calculated simply by dividing the changes in activity levels by the time elapsed between two subsequent sample removals. That the period from 5 to 6 months includes the stretch-out and shutdown to refuelling outage. The period from 6 to 12 months includes start-up of the plant.

For ^{54}Mn, the rate of activity increase is also the lowest in the period including the shutdown. In fact, the activity due to ^{54}Mn decreased during this period, but was relatively constant during the rest of the fuel cycle.

For ^{124}Sb, ^{110m}Ag and ^{58}Co, the rates of activity increase are highest during the period including the shutdown to refuelling outage. This may be related to the high activity levels determined in the coolant during this period.

The differences between the activity increase rates of different isotopes suggest that different mechanisms of activity incorporation may prevail for the different isotopes. The interesting behaviour of Antimony ^{124}Sb and Cobalt ^{60}Co isotopes are described in the following.

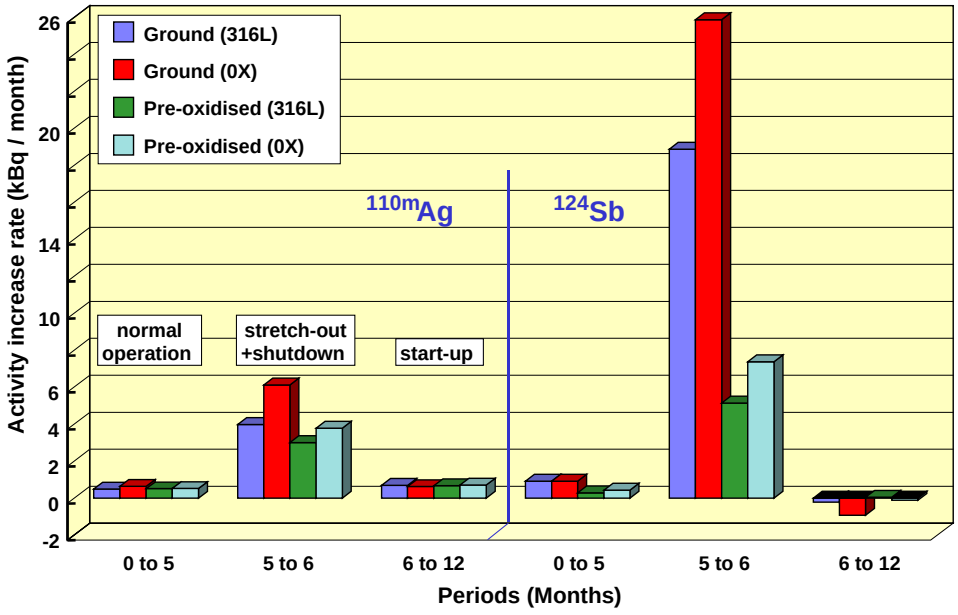

Figure 8. Rates of activity increase on different samples during subsequent exposure periods for ^{110m}Ag and ^{124}Sb.

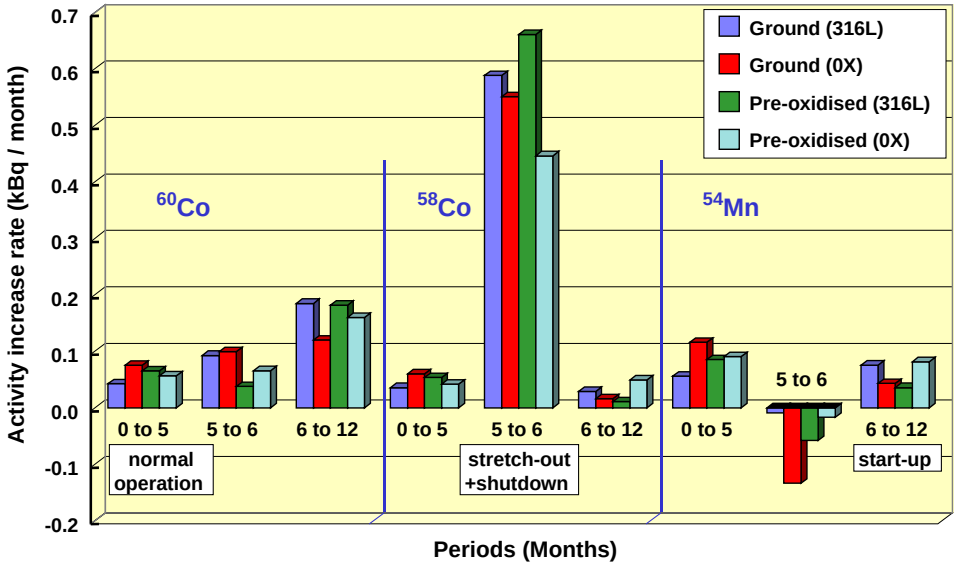

Figure 9. Rates of activity increase on different samples during subsequent exposure periods for ^{60}Co, ^{58}Co and ^{54}Mn.

3.3.3 Behaviour of Antimony

The most significant change in the rate of activity increase during the whole period is observed for ^{124}Sb. The average rate of activity increase of ^{124}Sb on ground samples is several times higher during the period including stretch-out and shutdown than during the other periods.

The coolant activity data show that the increase of the activity in the coolant during the stretch-out is the most pronounced for ^{124}Sb. This indicates that during the stretch-out ^{124}Sb is released in considerable amounts from surfaces such as fuel and reactor pressure vessel to the coolant and subsequently adsorbed or deposited on the sample surfaces. After the relatively rapid decomposition ($t_{1/2}$ = 60 days) of this isotope, no rapid accumulation can be observed during the start-up and normal operation, when a much smaller amount of ^{124}Sb is present in the coolant.

The difference in the ^{124}Sb levels between the samples with different pre-treatments suggests that adsorption or deposition of ^{124}Sb is sensitive to the surface structure.

3.3.4 Behaviour of Cobalt ^{60}Co

Because the ^{60}Co isotope has the highest half life, considerable long-term benefits may result from its behaviour as indicated that the rate of ^{60}Co activity increase is low during the period including the shutdown to refuelling outage. In spite of the high coolant activity level due to ^{60}Co during the shutdown, the shutdown procedure results in a decrease in the rate of incorporation of this isotope.

The activity increase rate is highest during the period including the start-up after the refuelling outage. This high rate of incorporation cannot be attributed to the content of ^{60}Co in the coolant, because the activity due to ^{60}Co is not higher than to the other isotopes during start-up. It is thus probably connected to the oxide films formed on the stainless steel surface. The high rate of activity increase due to ^{60}Co during the period including the start-up has been observed also during the previous measurements at Loviisa unit 2 [3].

It is worth noticing that – due to the long half life of ^{60}Co – the amount incorporated before the refuelling outage still significantly contributes to the activity levels determined after the start-up. This is not the case for the ^{58}Co isotope with a shorter half life.

3.4 Morphology of the oxide films

As described in the introduction, an oxide film formed on stainless steel in cooling systems in typical VVER conditions can be described to consist of two parts: an inner compact layer and an outer porous layer. The compact layer has been formed via solid state oxidation of the metal substrate and the porous layer via deposition form the solution. Usually, the boundary between these two layers is not sharp, but a partly cracked layer exists between them.

Scanning electron microscopy (SEM) can be used to analyse changes in the surface structure such as the different crystal sizes and grain boundaries. Furthermore, by taking a cross-section from a sample surface, estimates of the thickness of the film as well as that of its different layers can be obtained.

At the moment of writing this report, the SEM results for the samples removed after an exposure for 12 months were not yet available. They will be discussed in the next progress report.

3.4.1 SEM micrographs of oxide film surfaces

The top views of the surfaces of 08X18H10T and AISI 316L with the two pretreatments and after exposures for 5 and 6 months are shown in Figs. 10 and 11.

On the basis of the SEM micrographs in Fig. 10, the samples with different pretreatments differ in their macroscopic appearance after an exposure for 5 months during normal operation. The oxide films on the ground surfaces have a smaller number of large crystals than the pre-oxidised sample surfaces. This is clearly seen in the 30 000 fold magnifications.

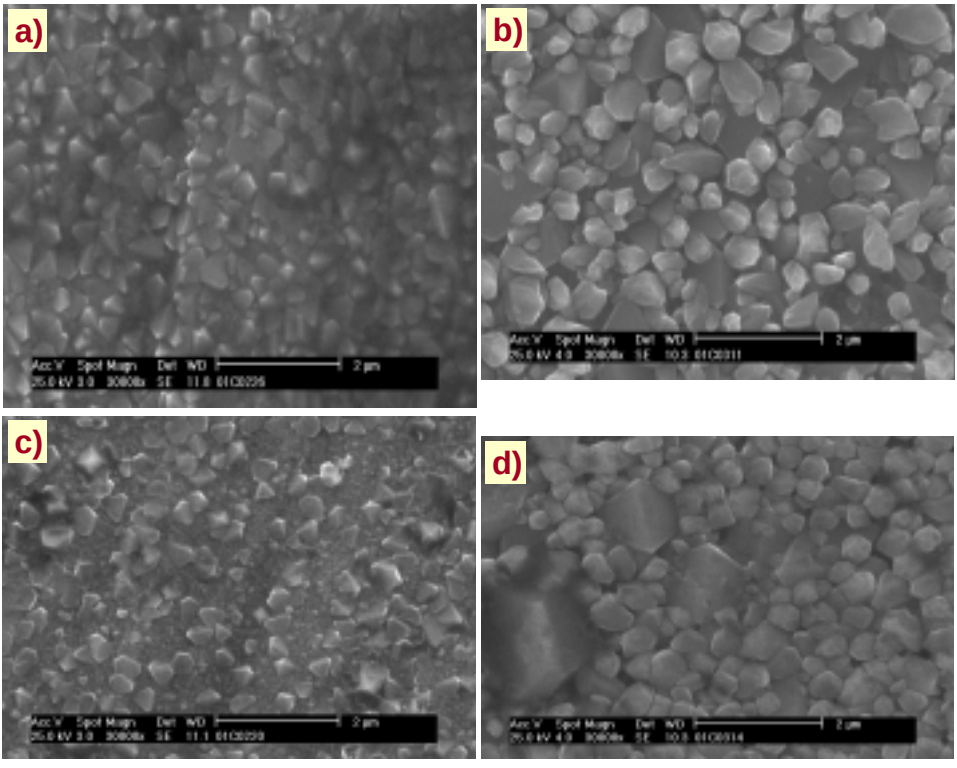

Figure 10. SEM micrographs of the sample surfaces exposed to the primary coolant at Loviisa 1 for 5 months of normal operation; a) 08X18H10T ground, b) 08X18H10T pre-oxidised, c) AISI 316 L ground, d) AISI 316 pre-oxidised.

The surface of a ground AISI 316L sample is covered with a continuous layer of small crystallites with only a relatively small number of crystals with 0.1–0.3 μm size. On the other hand, the surface of a ground 08X18H10T sample is totally covered with crystals of that size. The appearance of these oxide films on both AISI 316L and 08X18H10T are different from those of pre-oxidised samples made of the same materials. The pre-oxidised samples are covered with crystals with 0.2–0.6 μm size. On both AISI 316L and 08X18H10T sample surfaces, some significantly larger crystals also exist. Their diameter is larger than 1 μm.

The SEM micrographs of the samples exposured for 6 months (Fig. 11) indicate that the oxide films seem to have changed only moderately during the further exposure including the stretch-out and the shutdown to refuelling outage. The surfaces of the ground AISI 316L and 08X18H10T samples are totally covered with crystals. Their size seems to be larger for AISI 316 L (up to 0.5 μm).

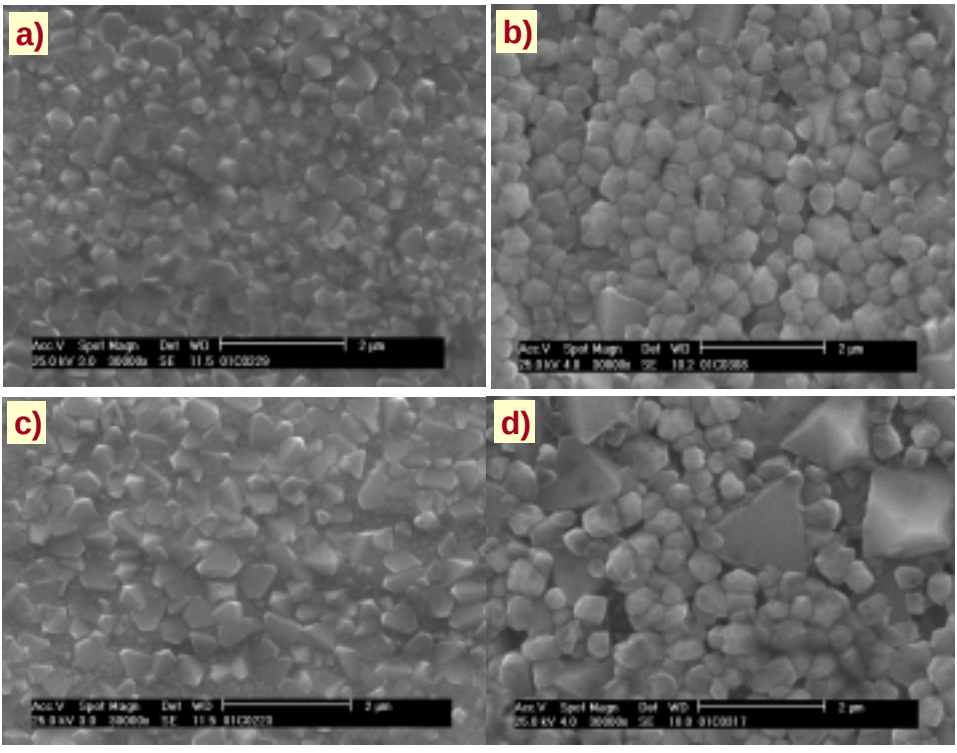

Figure 11. SEM micrographs of the sample surfaces exposed to the primary coolant at Loviisa 1 for 6 months including shutdown; a) 08X18H10T ground, b) 08X18H10T pre-oxidised, c) AISI 316 L ground, d) AISI 316 pre-oxidised.

On the pre-oxidised 08X18H10T surfaces, the number of large crystals seems to have decreased during further exposure from 5 to 6 months. On pre-oxidised AISI 316L surface such change is difficult to estimate. The shape of the crystal edges on the surface has become rounder during the period including the shut-down, i.e. from 5 to 6 months.

A possible explanation to the change in the appearance of the oxide films may be a transformation of the outer film surface as a result of reduction and dissolution processes during the different stages of the shutdown water chemistry.

3.4.2 SEM micrographs of oxide film cross sections

To assess the oxide layer thicknesses, cross-sectional SEM images were prepared. Examples of such images are shown in Fig. 12. The thickness of the different parts of the film, as well as its total thickness show considerable variations. Accordingly, the average thickness of the film was estimated. These values are given in Table 1.

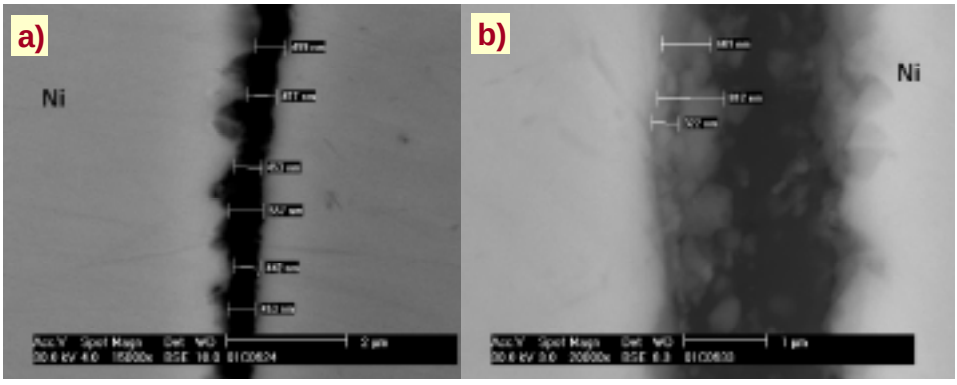

Figure 12. Cross-sectional SEM images of pre-oxidised 08X18H10T with oxide films consisting a) of a compact layer, b) of a porous and a compact layer.

Table 1. Average thicknesses of the whole oxide film as determined from cross-sectional SEM images.

Sample			Thickness
Material	Treatment	Exposure	Average
AISI 316L	ground	5 months	0.38 µm*
08X18H10T	ground	5 months	0.71 µm
AISI 316L	pre-oxidised	5 months	0.54 µm
08X18H10T	pre-oxidised	5 months	0.58 µm
AISI 316L	ground	6 months	0.39 µm
08X18H10T	ground	6 months	0.33 µm
AISI 316L	pre-oxidised	6 months	0.46 µm*
08X18H10T	pre-oxidised	6 months	0.42 µm

*very large variation in thickness

One of the major problems in determination of the film thickness on the basis of SEM images is due to the sample treatment. In order to be able to make a cross-section, a Ni layer has to be coated on the surface of the sample. The oxide will thus be between a Ni layer and the base metal. However, the Ni coating does not always attach to the film surface properly but rips off leaving a crack between the film and the coating. In such cases the boundary between the film surface and the Ni coating is not sharp, which means that the thickness determination can be very difficult. This happens especially if the porous layer of the film is thick. Also, if there are large crystals present at the film surface, proper mounting of the Ni coating can be impossible. Because of these experimental problems, the thicknesses determined with SEM should be viewed with criticism.

3.5 XRD-measurements

X-ray diffraction (XRD) analysis has proven to be a suitable tool to provide an estimation of oxide film thickness and also to obtain tentative information of oxide structures [4]. The fact that the oxides growing on typical structural materials adopt several different lattice structures complicates the interpretation of XRD results. Therefore, XRD cannot give the exact composition of different spinel oxides growing on the studied surfaces. However, a possible composition can be roughly estimated from the determined lattice constants. The first two sets of samples have been analysed using a portable XRD-equipment, and the results are shown in Table 2.

More details like lattice constants and XRD peak areas, which are used in the estimation of the oxide film thickness, are given in the subproject report. The analysis procedure has been reported previously elsewhere [4].

3.6 SIMS-measurements

Secondary ion mass spectrometry (SIMS) and profilometer measurements were performed in order to obtain another estimate for the oxide thickness and to obtain information on how the differences in the distribution of alloying elements in oxide films and the oxide growth rates affect the activity incorporation into the ground samples.

Only six of the eight samples were subjected to SIMS analysis because of the uncertainty in quantifying the results obtained by SIMS. During the ongoing evaluation process of different analysis techniques SIMS analysis will be compared especially with glow discharge optical emission spectroscopic (GDOES) analysis.

Table 2. Estimated oxide film thicknesses and non-stoichiometric formulas giving the best correspondence to measured X-ray diffraction results.

Sample [mat.-treatm.-exp.]	Thickness [µm]	Structures corresponding best to lattice constants
316-grd-5m	0.45	$Ni_xFe_{3-x}O_4$ + $NiCr_2O_4$
0X-grd-5m	0.33	$Ni_xFe_{3-x}O_4$ + $NiCr_2O_4$
316-oxi-5m	0.75	$Ni_xFe_{3-x}O_4$ + $NiCr_2O_4$
0X-oxi-5m	0.64	$Ni_xFe_{3-x}O_4$ + $NiCr_2O_4$
316-grd-6m	0.24	$Ni_xFe_{3-x}O_4$ + $NiCr_2O_4$
0X-grd-6m	0.48	$Ni_xFe_{3-x}O_4$ + $NiCr_2O_4$
316-oxi-6m	0.55	$Ni_xFe_{3-x}O_4$ + $NiCr_2O_4$
0X-oxi-6m	0.58	$Ni_xFe_{3-x}O_4$ + $NiCr_2O_4$

3.6.1 Oxide film thicknesses

The determination of the film thickness by the profilometer was complicated because of the variations in surface roughness. The mean value of the surface roughness in the range between two profilometer markers (R_a) was typically in the range of 30–350 nm. Because of the uncertainty caused by these variations, the profilometer results are not discussed in more detail.

Two to three SIMS analyses were made both into the oxide layer and into the metal substrate, and the sputter rate was determined separately for the oxide and metal substrate. Depth scale in SIMS depth profiles was then calculated. The position of the interface between oxide and bulk material was determined using the Ni signal. The position of the interface was arbitrarily assumed to be at the point where Ni signal is in the middle between the minimum and the maximum, Fig. 13c. Thus obtained oxide thicknesses are given in Table 3. However, as will

be described below, the depth profiles of different elements are not similar. Therefore, it might be reasonable to study the choice of the reference signal and, e.g., Fe and Cr could also be used for the thickness determination in eventual future measurements.

Table 3. Oxide film thickness determined on the basis of Ni signal by SIMS.

Sample [mat.-treatm.-exp.]	Thickness [µm]
316-grd-5m	n.a.
0X-grd-5m	0.22
316-oxi-5m	n.a.
0X-oxi-5m	0.77
316-grd-6m	0.20
0X-grd-6m	0.27
316-oxi-6m	0.54
0X-oxi-6m	0.72

n.a. = not analysed

3.6.2 The SIMS-signal profiles

The SIMS signals of Fe, Cr, Ni, Mo and Co are shown in Fig. 13 as plots of normalised intensity vs. sputtering depth. The signal coming from the substrate has been arbitrarily scaled to 100 for each sample. Because compositions of AISI 316L and 08X18H10T are slightly different, also the scaling of alloying elements in substrate materials has thus been taken into account. It should be noted that the intensities of the different elements do not give any quantitative measure of the contents of the elements in the oxide film or in the substrate. On the other hand, the sputtering depths can be considered to be proportional to the film thickness.

The qualitative shape of the different profiles seems not to be affected by the time of exposure to the coolant. All profiles shown in Fig. 13 describe distributions of isotopes originating from the substrate metal and not from the coolant. The contents of the radioactive isotopes incorporated into the films from

the coolant are at maximum 100 ppb and they are well below the detection limit of the SIMS technique that may in the best cases be of the order of 100 ppm.

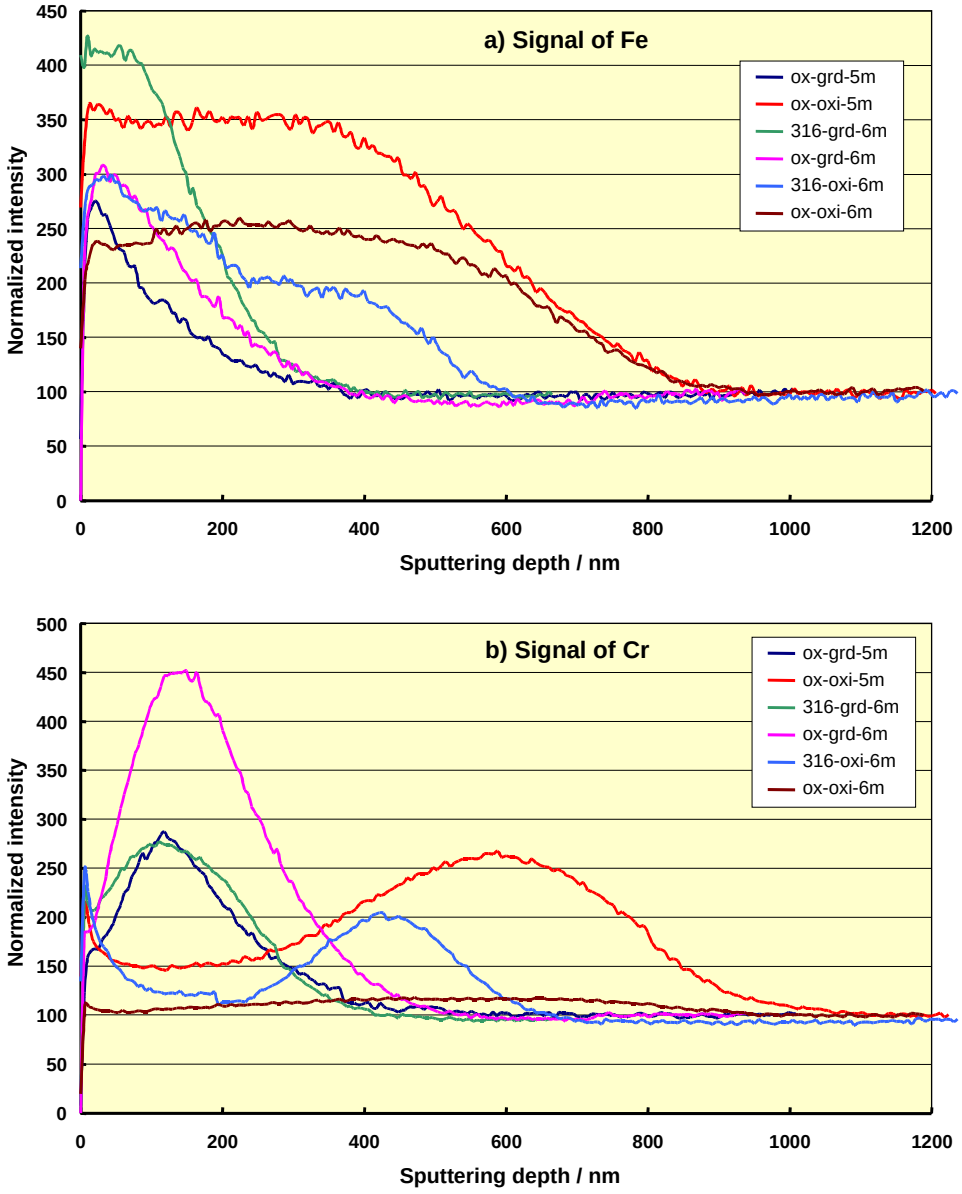

Figure 13 a–b. SIMS depth profiling of Fe and Cr in different samples. (figure continues on next page)

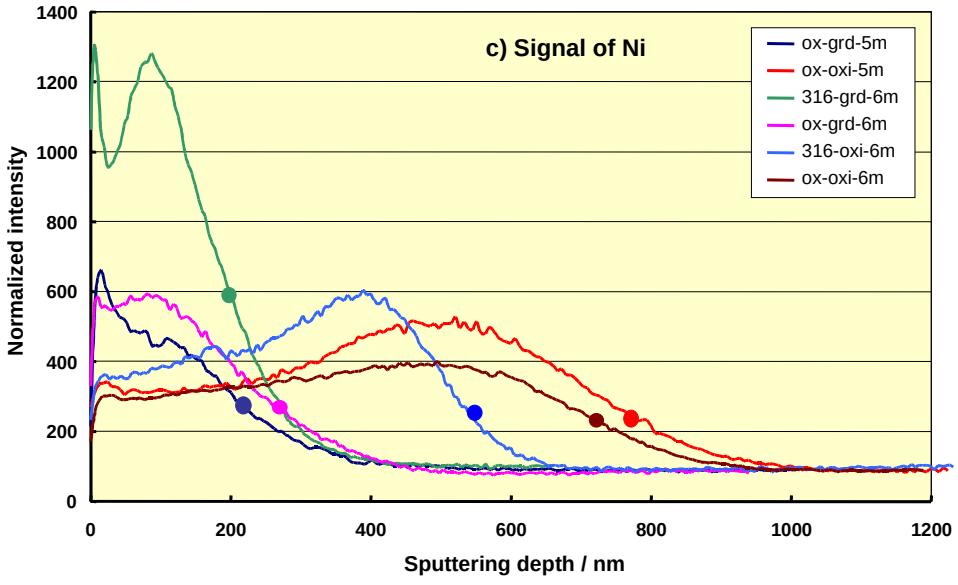

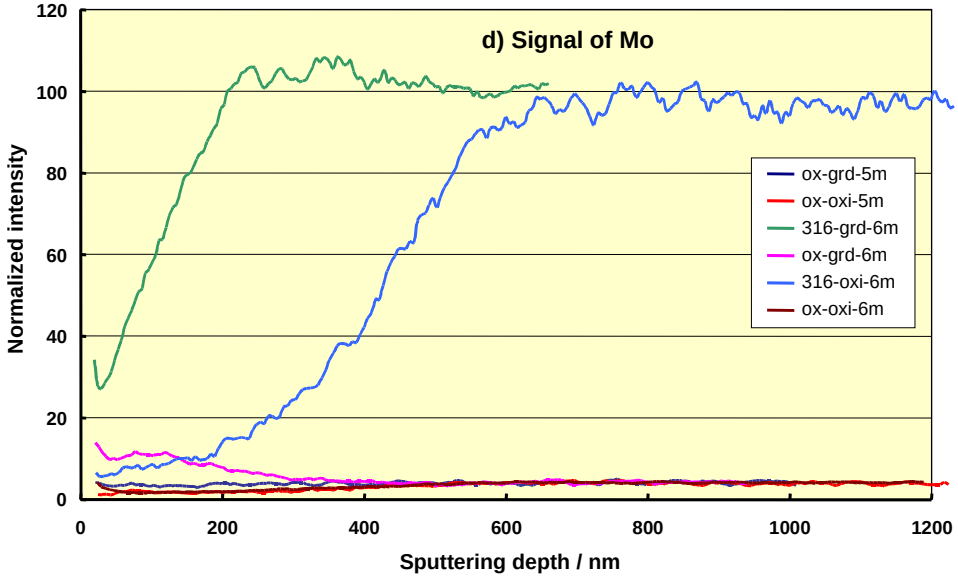

Figure 13 c–d. SIMS depth profiling of Ni and Mo in different samples. The film thicknesses determined on the basis of the Ni signals are marked with balls. The low signal of O8X18H10T is due to the very low content of Mo in this steel and Mo content of AISI 316 L has been used to normalise the scale of Fig. 13d.

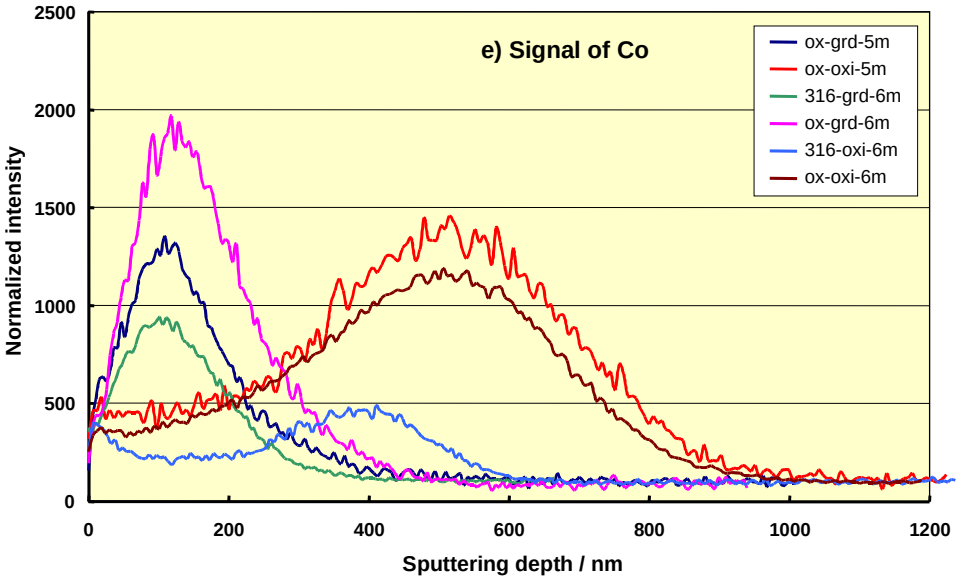

Figure 13 e. SIMS depth profiling of Co in different samples.

Iron (Fe) profiles

On the pre-oxidised O8X18H10T samples Fe seems to be distributed relatively uniformly over the outer part of the oxide films. A continuously decreasing profile is observed in the thinner films on the ground O8X18H10T samples, Fig. 13 a.

On the pre-oxidised AISI 316L sample Fe content seems to show two different plateaus in the film. On the ground AISI 316 L sample, the Fe content shows a short plateau, which is in contrast to the ground O8X18H10T sample. When approaching the film/metal interface, the Fe signals start to decrease as the Cr signals in the film starts to increase.

Cromium (Cr) and Nickel (Ni) profiles

In all samples, the Cr signal exhibits a maximum in the inner part of the oxide, i.e. close to the film/substrate metal interface, Fig. 13 b. It is not justified to draw any quantitative conclusions about the Cr contents in different samples, although the height of the signals seem to differ considerably. This is due to the fact that the results shown in Fig. 13 are not quantitative, but normalised.

The Ni signal shows a qualitatively similar trend to that of Cr. The maximum in the signal of Ni is, however, slightly further away from the inner interface than that of Cr. Some enrichment of Ni can be observed very close to the outer interface, especially in the case of the ground samples, Fig. 13 c.

Molybdenium (Mo) profiles

No enrichment of Mo can be observed in the oxide film formed on the AISI 316 L stainless steel which contains Molybdenium. Pre-treatment of the sample does not seem to affect the signal of Mo to any detectable manner. The low signal of Mo in the oxide films on O8X18H10T is due to the low content of Mo in this steel and the Mo content of AISI 316 L has been used to normalise its scale in Fig. 13 d.

Cobalt (Co) profiles

The profile of the Co signal seems almost similar to those of both Cr and Ni, Fig. 13 e. In other words, it exhibits a maximum in all the samples close to the film/substrate metal interface in the vicinity of the corresponding maxima for Cr and Ni. This means that Co originating from the base metal is most probably located in the same parts of the film as Cr and Ni.

Summary

In summary, the oxide film compositions of the samples were typical for a film formed in PWR primary coolant conditions. The profiles of Cr, Ni and Co show a clear maximum along the depth of the film, while the signal of Fe seems to decrease gradually when approaching the film/metal interface.

3.7 Comparison of oxide thickness measurements

The values of the oxide film thicknesses obtained by SEM-, XRD- and SIMS-measurements are summarised in Table 4 and the mean values are shown also in Fig. 14. In the calculation of the mean values the SEM result for one sample has not been taken into account as an outlier.

Table 4. Comparison of different techniques in determination of oxide film thickness.

Sample [mat.-treatm.-exp.]	Thickness [µm] XRD	SIMS	SEM	Mean value
316-grd-5m	0.45	n.a.	0.38*	0.42
0X-grd-5m	0.33	0.22	0.71 **	0.28
316-oxi-5m	0.75	n.a.	0.54	0.65
0X-oxi-5m	0.64	0.77	0.58	0.66
316-grd-6m	0.24	0.20	0.39	0.28
0X-grd-6m	0.48	0.27	0.33	0.36
316-oxi-6m	0.55	0.54	0.46*	0.52
0X-oxi-6m	0.58	0.72	0.42	0.57

* very high variation in thickness

** excluded from mean calculation

n.a. = not analysed

The values obtained using XRD and SIMS seem to give results in fair agreement with each other, with one clear exception (sample OX-grd-6m). At first sight, the values determined by SEM do not correlate well with the other results. However, if the high thickness value of the sample OX-grd-5m (0.71 µm) is regarded as an outlier, the correlation between the SEM results and the XRD and SIMS results becomes acceptable. The advantage of SEM is that it is the only technique giving a direct image of the film. It is however very sensitive to the exact location in the film where the thickness is determined. The SEM results for a given sample show accordingly very large deviations, which make the assessment of thickness values very uncertain and even subjective. SIMS is also largely dependent on the local variations in thickness. XRD is likely to give an estimate for the average thickness because of the large area from which the signal comes.

Referring to Table 4 and Fig. 14, the oxide films on pre-oxidised samples are found to be thicker than those on ground samples. The thickness of the films has decreased during the shutdown to refuelling outage on almost all the samples, except on the ground 08X18H10T (OX) sample.

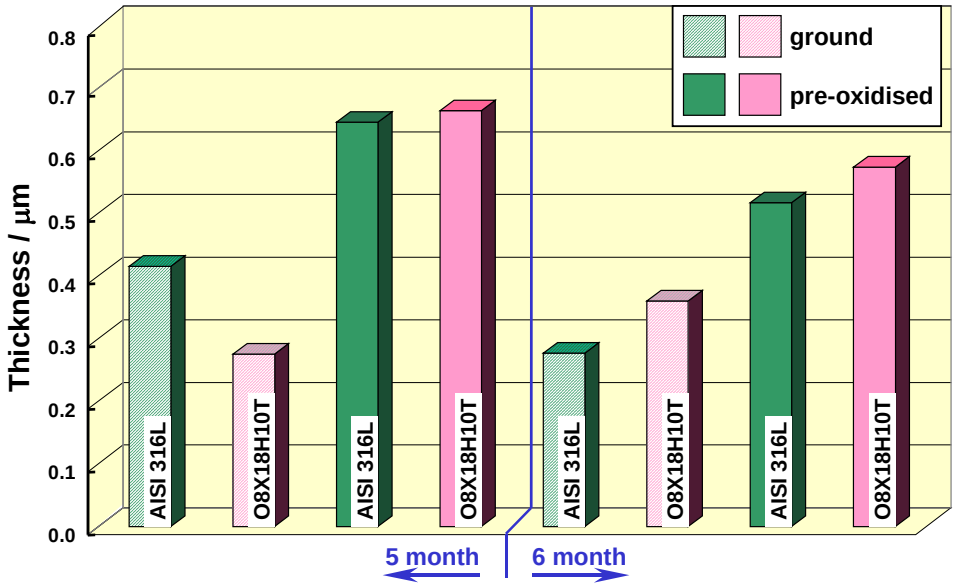

Figure 14. The mean thicknesses of the different samples after 5 and 6 months of exposure to the primary coolant at Loviisa unit 1. Mean values have been calculated from the SIMS, SEM and XRD results given in Table 6.

As it can be seen from Table 2 summarising the XRD measurements, no indications of significant differences in the structure of the surface films are found. It seems that the pre-treatment of the sample does not have large influence on the overall composition of the film but affects only the film thickness.

4. Summary and discussion on activity incorporation

Tentative correlations between activity incorporation and the film properties can be summarised as follows:

- The increase of the activity levels of ^{58}Co, ^{124}Sb and ^{110m}Ag on the material samples during the stretch-out can be associated with higher activity levels in the coolant during this period.

- The activity levels of all the isotopes do not seem to correlate with film thickness at this stage of exposure.

- The measured activity level of ^{124}Sb in the samples removed prior to and after the shutdown to refuelling outage correlates with sample pre-treatment. The activity levels are considerably higher on the ground than on the pre-oxidised samples.

- One possible explanation to the different ^{124}Sb contents in the films can be addressed to structural differences of the outermost part, e.g., differences in "active" surface sites for antimony adsorption. The smaller size of the crystals seen on the ground samples may be associated with a larger available surface area and thus with a higher number of adsorption sites, which may explain a higher rate of activity incorporation of ^{124}Sb.

- Incorporation of ^{60}Co is similar for all the samples. The SIMS results showed that Co, Cr and Ni give a maximum signal at similar distances in the film, indicating that the chromium-rich inner layer that contains also Ni can incorporate Co more readily than the part of the film rich in iron. As the ground samples have a thinner iron rich part of the film, activated cobalt from the coolant has a shorter diffusion barrier to the Cr rich layer than in a case of pre-oxidised samples. This may play a long-term role in the rate of incorporation of ^{60}Co from the coolant.

- The incorporation of ^{60}Co into the oxide films during the period including the start-up seemed to be higher than during the period including the shutdown to refuelling outage. This is supported by the results of previous measurements [3]. If the outer Fe- rich part of the oxide film protects the film to be contaminated with ^{60}Co, as indicated above, the composition of oxide films on pre-oxidised samples can be assumed to have experienced some changes after the shutdown to explain this behaviour.

5. Conclusions and future work

The goal of this still ongoing study is to estimate the factors, which affect activity incorporation into oxide films during the different stages of the fuel cycle. In addition, some effort was put to search for possible correlations between activity build-up and different pre-treatment of the surfaces of different construction

materials. The following tentative conclusions can be drawn on the basis of the existing results:

- The data for the high-temperature water chemistry (HTWC) at Loviisa unit 1 are characteristic of a steady-state operation of a VVER plant and can be used to assess the impact of water chemistry on activity incorporation in such plants.

- A more efficient use of the HTWC monitoring can be obtained during the shutdown and following start-up periods, as well as during possible unscheduled transients. Detailed investigation of HTWC together with on-line measurement of soluble and insoluble species in different time frames of these transients could provide valuable information, because these species determine the amount of activity incorporated into the films.

- The incorporation of ^{60}Co seems to be strongest during the start-up period. A more efficient removal of ^{60}Co at this stage might lead to a decrease of ^{60}Co levels.

- The increase of ^{124}Sb levels are associated with phenomena at the very surface of the oxide film. This can be affected by different surface treatments of the plant components. Samples with, for instance, electropolished surfaces should possibly be incorporated into the test matrix.

- More detailed and reliable information of the composition and thickness of the film is needed to draw conclusions on the mechanism of and factor affecting the incorporation of different species.

- In order to obtain more information of the possible influence of the start-up period and of other stages involving significant changes in the chemistry of the coolant, four to five sample sets are planned to be removed during the next fuel cycle.

Acknowledgements

The reported work is part of the subproject "Water chemistry, service reliability and activity levels" within a R&D project on plant life management (YKK).

References

1. Baston, V.F., Garbauskas, M. F. and Ocken H. Material characterisation of corrosion films on boiling water reactor components exposed to hydrogen water chemistry and zinc injection. Proceedings of the 7th Conference on Water Chemistry of Nuclear Reactor Systems, London, British Nuclear Energy Society, 1996. Pp. 558–565.unit

2. Aaltonen, P., Mäkelä, K., Järnström, R. and Kvarnström, R. Shutdown water chemistry and dissolution of activated corrosion products at Loviisa 1 PWR. Tunturi P. J. (ed.). Proc. of the 12 Scandinavian Corrosion Congress & EUROCORR '92 2, 1992.

3. Sirkiä, P., Saario, T., Mäkelä, K., Laitinen, T. and Bojinov, M. Changes in oxide films on Ti-stabilised stainless steel samples during exposure to primary coolant at Loviisa units, VAL67-001323, 8 May 2000.

4. Mäkelä, K. and Aaltonen, P. X-ray diffraction characterisation of oxide films on primary circuit surfaces at Loviisa unit 2, VTT Research report VAL62-980928/11, 29 October, 1998.

5. Makela, K. The oxide growth and cobalt deposition rates on coupons after Zn addition in typical PWR environments, OECD Halden Project Report, HWR-897, May 1997.

Irradiation assisted stress corrosion cracking of core components

A. Toivonen, P. Aaltonen, P. Nenonen, U. Ehrnstén,
A. Käki, M. Valo, A. Kukkonen
VTT Manufacturing Technology, Espoo, Finland

O. Hietanen
Fortum, Finland

Abstract

A test program on a reactor core material originating from the bottom end of a VVER absorber element is being carried out in aim to characterize the changes in mechanical properties and the occurrence of irradiation assisted stress corrosion cracking in PWR environments by laboratory tests. The mechanical and microstructural properties of the absorber bottom end material have changed due to neutron exposure. However, the material's response to neutron irradiation differs from the usual response of austenitic stainless steels. Yield strength, tensile strength, and dislocation loop density are all lower than expected.

An enhancing effect of Ti-carbide precipitations on the defect density is another new finding of interest. High defect density close to the Ti-carbides is presumed to result from the stress/strain field caused by the precipitations.

1. Introduction

1.1 International research programme

Irradiation assisted stress corrosion cracking (IASCC) of reactor core components is a topic of interest in the international nuclear materials research community. 15 partners from USA, Japan and Europe have joined together in an international group of Co-operative Irradiation Assisted Stress Corrosion

Cracking Research Program (CIR) co-ordinated by EPRI. VTT is participating in the CIR programme through in-kind information exchange.

The Finnish research contribution to CIR is partly realised within this XVO subproject. The objective of this subproject is to investigate whether IASCC can occur in PWR reactor core conditions. Verified evidence was still missing at the time when this project was launched.

1.2 Role of reactor type and coolant chemistry

IASCC has been reported to occur as intergranular cracking in austenitic stainless steels in oxidizing BWR environments at neutron fluences above 5×10^{20} n/cm^2 (E > 1 MeV), corresponding to about 0.7 dpa (displacements per atom). The threshold fluence for increased risk for intergranular irradiation assisted cracking in non-oxidizing PWR environment is suspected to be clearly higher, about 2 dpa.

In oxidizing BWR environment, the role of corrosion in IASCC is evidently important, while in a non-oxidizing environment corrosion should not be as decisive. Possible additional factors affecting intergranular cracking are radiation-induced hardening, radiation-induced creep and hydrogen embrittlement. Also swelling, formation of helium bubbles and radiation-induced precipitates may become an issue, especially at higher irradiation temperatures or at higher doses.

1.3 IASCC susceptibility of Ti-stabilized austenitic stainless steels in PWR reactor conditions

A fuel assembly spacer grid sleeve had failed after three years of operation in the core of a VVER-440 PWR reactor. A careful failure analysis was performed and irradiation assisted cracking was concluded to be the reason for the failure (Ehrnstén et al., 1999). This provided new evidence on the potential of occurence of IASCC in PWR reactor cores.

Fortum Power and Heat has recently provided us with test material irradiated in a VVER reactor core in Loviisa. This material originates from the bottom end of

an absorber element. A comprehensive test program on this reactor core material is currently being carried out. Characterisation of the test material and the changes in mechanical properties due to irradiation was the main task for the project year 2000. Experimental study on the occurrence of IASCC in PWR environments will be carried by laboratory tests in later phases of the project. The first results of the program are described in this report.

2. Analysis of a fuel assembly spacer grid sleeve

2.1 The studied failure case

The analysed fuel assembly spacer grid sleeve had failed after three years of operation in a core of a VVER-440 PWR reactor. Irradiation assisted stress corrosion cracking was suspected and a careful failure analysis was performed (Ehrnstén et al., 1999).

The fuel rod spacer grid is clamped to the central tube with the spacer grid sleeve. The estimated irradiation temperature was 300°C, and the total dose of the failed spacer grid sleeve after three years exposure was estimated to be 4.6×10^{21} n/cm^2, E > 1 MeV, i.e., about 7 dpa, respectively.

The spacer grid with the failed sleeve ($\phi 13 \times 0.55$ mm) was removed for failure analysis and material investigations. In addition, the material of a similar, unirradiated sleeve was investigated. The material is titanium stabilised austenitic stainless steel of type 06X18H10T. The chemical composition is given in Table 1.

Table 1. Chemical composition of the sleeve material (w%).

C	Cr	Ni	Ti	Mn	Si	P	S
0.05	17.50	10.30	0.49	1.50	0.50	0.023	0.010

2.2 Results of the investigations

2.2.1 Hardness measurements, optical microscopy and SEM

The hardness of the irradiated material was 347 HV1, much higher than the hardness of an unirradiated sleeve, 156 HV1. The grain size of the sleeve material was small, corresponding to ASTM 9. The microstructure contained numerous inclusions and precipitates, i.e., sulphides, phosphides and titanium nitrides and carbides. Fractography revealed that the spacer grid sleeve had cracked intergranularly without any detectable plastic deformation, Fig. 1.

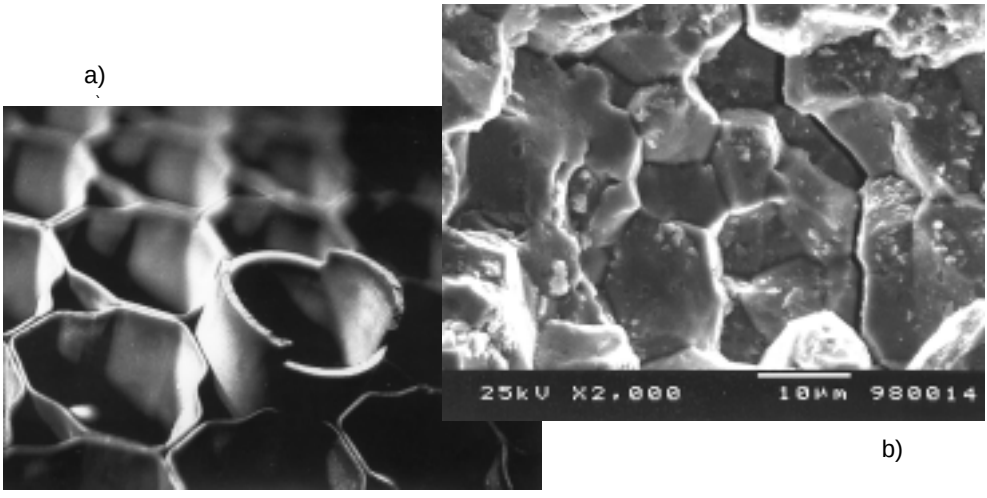

Figure 1. A macrograph (a) and the intergranular fracture surface (b) of the failed spacer grid sleeve.

2.2.2 Transmission microscopy, microstructure and ageing

Both materials were investigated using a Field Emission Gun Scanning Transmission Electron Microscope, FEGSTEM (Philips CM 200). These investigations were focused on the defect structure of the irradiated material as well as on the composition of the grain boundaries. Spot analyses were performed at grain boundaries using a 1 nm beam and at the adjacent grain matrixes using a 20–30 nm beam.

The irradiated sleeve material contained a dense defect structure consisting of mainly interstitial loops and some new precipitates. The main part of the defect structure was found to consist of faulted interstitial loops on {111}-planes. No defect-free zones were observed near the grain boundaries and the average loop size was 10 nm.

2.2.3 Segregation

Clear grain boundary depletion of chromium and iron and enrichment of nickel and silicon was observed at some grain boundaries in the irradiated material, while no compositional changes were observed at others. Segregation had occurred at grain boundaries where the orientation difference between the adjacent grains was large. No segregation was observed at grain boundaries where the orientation difference was small. The average amount of chromium depletion was 4.2%, i.e., from 18.9% to 14.7% Cr. The maximum measured depletion of an individual spot analysis was 6% resulting in a chromium concentration below 12%. No consistent segregation of impurity elements like sulphur and phosphorus was observed.

2.2.4 Assessment of findings

Chromium depletion and nickel enrichment will probably increase the local stacking fault energy and the initiation threshold for dislocation glide. This may allow higher stress concentrations to develop at the grain boundaries. On the other hand, irradiation also causes significant hardening of the matrix due to the heavily defected microstructure.

The hard matrix together with the increased local stacking fault energy may result to much higher stresses at the grain boundaries than in an annealed material, thus promoting intergranular cracking instead of yielding.

2.3 Conclusion

The investigated failure was concluded to be caused by irradiation assisted cracking in the non-oxidizing PWR environment.

3. Investigations of an absorber element material irradiated in a VVER 440

This test program, initiated after the investigations of the spacer grid sleeve, aims to characterize the changes in mechanical properties and the occurrence of IASCC in PWR environments by laboratory tests. The following test plan is a tentative plan and, depending on the results obtained during the program, changes will be made if needed.

3.1 Test plan

3.1.1 Test materials

Test materials are austenitic stainless steel steel 08X18H10T used in reactor of Loviisa NPP owned by Fortum Power and Heat Ltd, Table 2. The irradiated materials originate from the bottom end of an absorber element, Fig. 2. The calculated fluences are ~$1x10^{21}$ n/cm^2 in the thickest part in the middle of the component and ~$2.6x10^{21}$ n/cm^2, E> 1 MeV, in the lowest part of the component, i.e., about 1.5 and 4 dpa, respectively (calculations are based on irradiation history). The estimated irradiation temperature is 300°C.

Table 2. The nominal composition of 08X18H10T, w%.

Fe	C	Cr	Ni	Mn	Si	Ti
Bal.	0.08	17–19	10–11	1.0–2.0	< 0.8	5×C–0.7

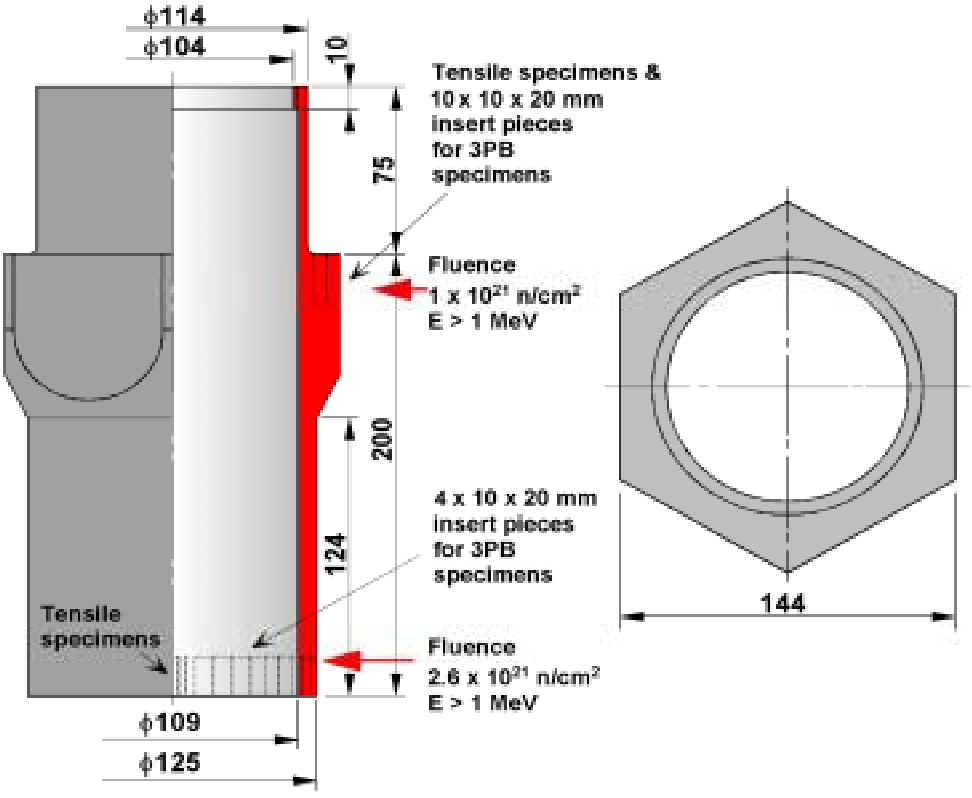

Figure 2. Bottom end of the absorber element.

3.1.2 Microstructural characterization

Metallographic characterization of the materials is conducted by optical and/or electron microscopy. Characterization is also conducted using field emission gun scanning transmission electron microscope, FEGSTEM.

3.1.3 Characterisation of mechanical properties

The mechanical properties of the test materials are characterized by tensile tests, fracture resistance (J-R) test, impact tests and microhardness measurements. The tensile- and J-R tests are conducted at room temperature, 100°C, 200°C and 300°C. Impact tests are conducted at room temperature. Material in both of the calculated fluence levels, 1.5 and 4 dpa, is tested.

Hardness measurements are conducted at room temperature using Vicker's microhardness measurement.

The specimens for the tensile tests are small plate type specimens with the cross-section of 1x2 mm. The specimens for the J-R tests are 3x4x27 mm, 4x10x55 mm and 10x10x55 mm (B x W x length) prefatigued side grooved three point bend specimens. The impact specimens are notched 3x4x27 mm specimens.

3.1.4 Characterization of IASCC susceptibility

The IASCC tests will be conducted in simulated normal operation- and shut-down water chemistries of VVER 440 plants as well as in an inert environment. Also, if the material proves to be IASCC resistant in VVER environments, an optional simulated BWR environment is included into the test plan. The tests are either slow J-R tests or low K_I level constant load tests on prefatigued three point bend specimens. The test matrix is presented in Table 3.

Table 3. Test matrix for IASCC tests in simulated VVER 440 conditions.

Fluence, n/cm^2 (E>1MeV)	**Test environment**
1x10^{21} 2.6x10^{21}	Normal operation, T=300^{o}C
1x10^{21} 2.6x10^{21}	Shutdown, T=200^{o}C
1x10^{21} 2.6x10^{21}	Shutdown, T=100^{o}C + H_2O_2 addition
To be determined To be determined	Inert (argon), temperature to be determined BWR (optional)

Crack propagation rates are measured using potential drop method. After each test the relevance of the resulted fracture morphology is analysed using scanning electron microscope, SEM. If the fracture morphology is relevant, i.e., intergranular, and no interegranular cracking is obtained under slow loading in inert

argon environment, the fracture can be considered to be IASCC and the measured crack propagation rates can also be considered relevant.

3.2 Subproject progress and results in 2000

The following steps were passed during the project year.

- Two sections were cut from the bottom end of the absorber element at Loviisa power plant and transported to VTT.
- Tensile specimens were machined from both sections and tensile tests were conducted at room temperature and at 100^{o}C.
- Hardness was measured by Vicker's microhardness measurement.
- Microstructural characterisation of the material cut from both of the sections of the irradiated absorber element bottom end were conducted by FEGSTEM.
- New specimen preparation method, reducing the volume of the active material near to 1% of the normal case, was developed for energy dispersive x-ray analysis.

3.2.1 Mechanical properties

The tensile test results show that the material has remained very ductile regardless of the exposure to neutron irradiation even though the yield and tensile strengths have increase when compared to the nominal, unirradiated, value for the same material. The hardness measurement results also show that the mechanical properties have changed during the exposure. However, the yield strengths and hardnesses are is lower than expected when compared to other available data. The measurement results are shown in Table 4 together with the nominal unirradiated values. The yield strengths vs. the square root of the fluence are presented in Fig. 3 along with the values of several other studies (Bruemmer et al., 1999).

Table 4. Mechanical properties of the absorber element bottom end and spacer grid materials.

Neutron fluence	Temp., °C	σ_{YS}, MPa	σ_{UTS}, MPa	A_5, %	Hardness HV1
0	23	196	490*	38	156**
	23	367	658	64	210
$1x10^{21}$ (1.5 dpa)	100	326	549	41	
	300	294	472	32	
	23	453	692	65	228
$2.6x10^{21}$ (4 dpa)	100	408	602	43	
	300	387	537	31	
$4.6x10^{21}$ (7 dpa)	23				347**

* Minimum values according to the material supplier.

** Fuel assembly spacer grid sleeve. Grain size corresponding to ASTM 9.

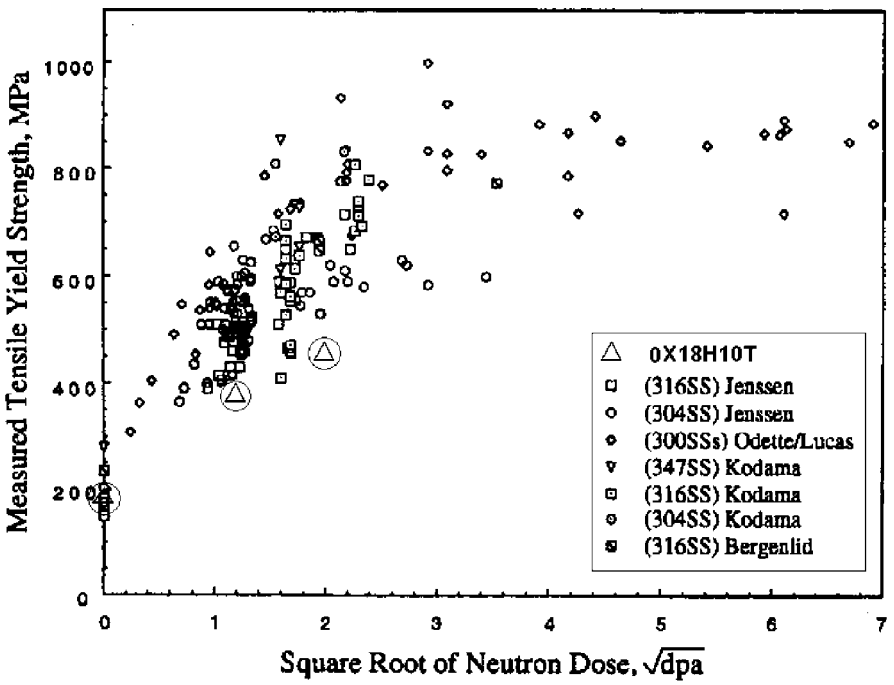

Figure 3. Comparison of the measured and nominal yield strengths vs. square root of the fluence with other studies (original picture: Bruemmer et al., 1999).

3.2.2 Microstructure

FEGSTEM results show defect structure consisting mainly of faulted interstitial loops with the size of a little over 4 nm at both fluences. The total defect density is 4.5×10^{22} m^{-3} in the lower fluence material and 5.5×10^{22} m^{-3} in the higher fluence material. Besides the loops, the material probably contains also small 2 nm voids. The loop densities and loop sizes are smaller than expected. The measured loop densities and sizes both for this material and the irradiated spacer grid material are presented in Fig. 4 with the values of several other studies (Bruemmer et al., 1999). The loop density is clearly higher close to the Ti-carbides than elsewhere, Fig. 5. The loops are also larger, about 8 nm in average. The higher density and larger loop size may be a result from the stress/strain field caused by the precipitation.

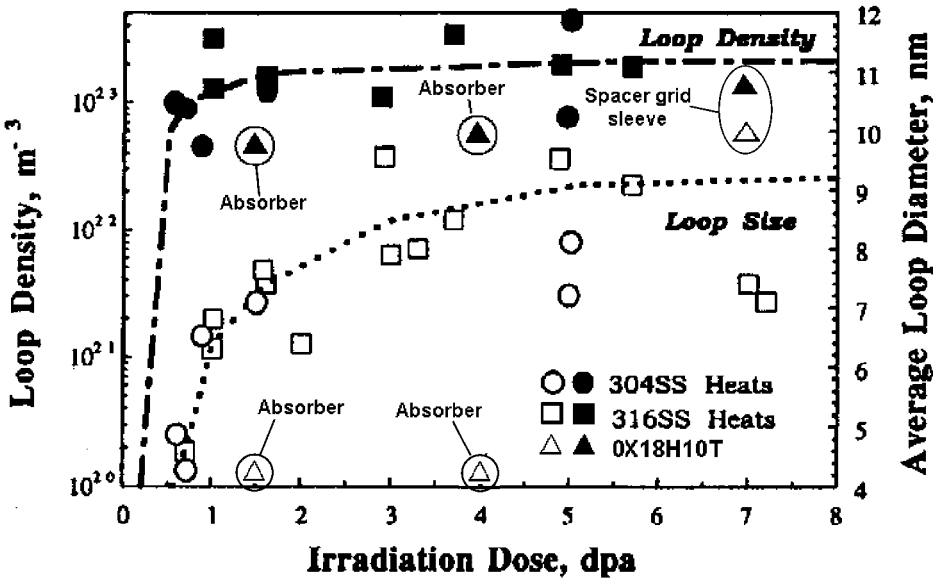

Figure 4. The measured loop densities both for the absorber element bottom end material and the irradiated spacer grid material with the values of several other studies (original picture: Bruemmer et al., 1999). The loop size of the irradiated spacer grid material is also presented.

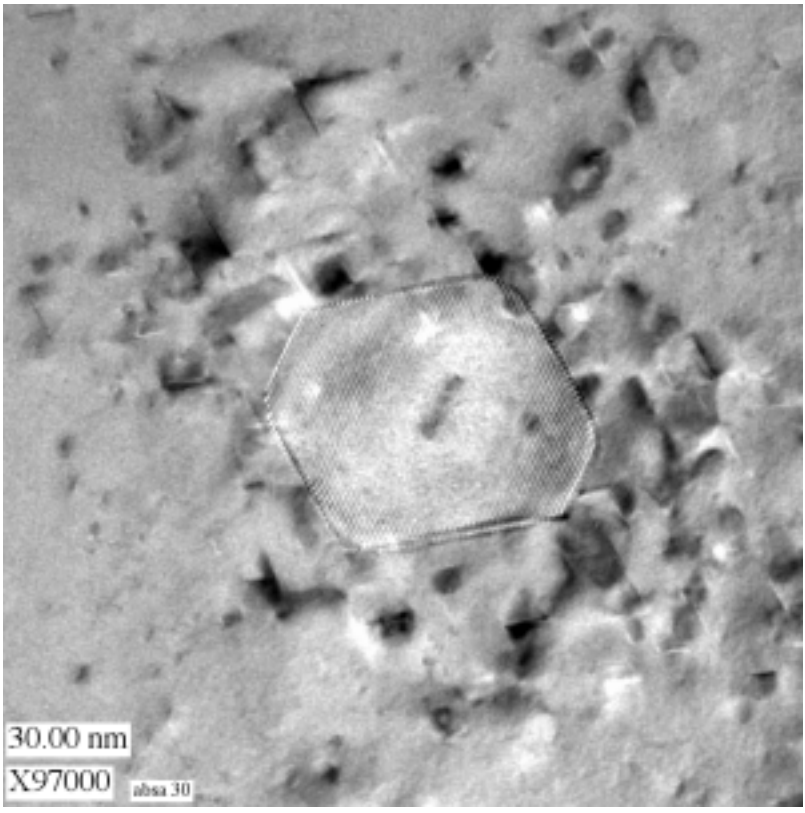

Figure 5. High loop density close to a Ti-carbide propably resulting from the stress/strain field caused by the precipitation.

Initially, energy dispersive x-ray analysis to determine radiation induced grain boundary segregation was prevented by high gamma activity of the material. After the new specimen preparation method was developed, the results showed that there was grain boundary Fe and Cr depletion and Ni, Si, P, Mo and Ti enrichment.

4. Conclusions

The mechanical and microstructural properties of the absorber bottom end material have changed due to neutron exposure but not as much as expected. However, the material's response to neutron irradiation may differ from the usual response of austenitic stainless steels due to Ti-stabilization.

A new result is also the effect of Ti-carbide precipitations on the defect density. If the high defect density close to the Ti-carbides results from the stress/strain field caused by the precipitations, the response of actual structural components under residual or structural stresses to neutron irradiation may differ from the response of non-stressed samples.

Acknowledgements

This paper is part of a cluster of joint R&D projects on plant life management and ageing of metallic components, which is realised mainly by VTT in 1999–2002. The projects are funded by Tekes, the National Technology Agency, Teollisuuden Voima Oy, Fortum Power and Heat, Fortum Engineering, VTT and to smaller extent also by other energy and process industry in Finland.

References

1. Bruemmer, S.M., Simonen, E.P., Scott, P.M., Andresen, P.L., Was, G.L. and Nelson, J.L. Radiation-induced material changes and susceptibility to intergranular failure of light-water-reactor core internals. Journal of Nuclear Materials 274 (1999), pp. 299–314.

2. Ehrnstén, U., Nenonen, P., Aaltonen, P., Teräsvirta, R. and Hietanen, O. Intergranular Cracking of an Irradiated Ti-stabilized Austenitic Stainless Steel Spacer Grid Sleeve from a VVER-440 reactor. Presented at 9th Int. Conf. Environm. Degradation of Materials in Nuclear Power Systems – Water Reactors, Newport Beach, CA, USA, Aug. 1–5, 1999. 8 p.

In-situ Studies of the Oxide Film Properties on BWR Fuel Cladding Materials

M. Bojinov, L. Hansson-Lyyra, T. Laitinen, K. Mäkelä and T. Saario
VTT Manufacturing Technology
Espoo, Finland

Abstract

The corrosion resistance of Zirconium alloys is influenced by the electrical and electrochemical properties of the oxide films. This study searches correlations between these oxide films properties and the second phase particle structures and hydrogen contents of the alloys. The target is to improve capabilities to compare candidate fuel cladding products through experimental techniques.

Three types of Zircaloy-2 specimens with the second phase particle sizes ranging from 0.049 μm to 0.174 μm and two specimens hydrided up to 1000 ppm of hydrogen were used in the experiments. The work consisted of electrochemical impedance spectroscopic, contact electric impedance and contact electric resistance measurements performed using the controlled distance electrochemistry arrangement in simulated BWR coolant conditions at a temperature of 300ºC.

The results obtained up to now do not enable discerning between the transport properties of the oxides formed on the different Zircaloy specimens. Alternative experimental methods are proposed for continued research efforts.

1. Introduction

Zirconium alloys are used as fuel cladding material in light water reactors. High reliability demands are set for the cladding, which acts as a barrier between the fuel and coolant. Alloying elements, such as Fe, Cr, Ni, and Sn, are added to Zircaloy-2 to provide the required corrosion properties. Due to their low solubility the alloying elements form a population of second phase particles, such as hpc-Zr(Fe,Cr)2 and bct-Zr2(Fe,Ni) typical of Zircaloy-2 matrix. An optimum

precipitate size must be attained to have both nodular (non-uniform) and uniform corrosion resistance [1]. Hydrogen content of the material has also been found to affect the rate of corrosion after the thickness of the oxide film is more than a few micrometers [2].

The corrosion resistance of zirconium alloys is influenced by electrical and electrochemical properties of the oxide films formed on these alloys. A proper understanding and modelling of the oxide film properties requires reliable in-situ electrochemical techniques. Such techniques have been developed in recent and parallel projects.

1.1 Controlled Distance Electrochemistry arrangement

Since the conductivity of the boiling water reactor (BWR) coolant is very low, the electrical resistance of the water between the sample, the reference and the counter electrodes in a conventional electrochemical cell arrangement becomes very high, often preventing the use of electrochemical techniques. But a new techniques have been developed to overcome such problems.

The controlled-distance electrochemistry (CDE) arrangement has been developed to perform measurements even in low conductivity media, such as boiling water reactor (BWR) coolants at high temperatures and pressures. This arrangement has already been successfully applied to study and model the behaviour of Fe, Cr, Ni, Fe-Cr alloys and Ni-Cr alloys as well as commercial stainless steels and Ni-based alloys in aqueous high-temperature conditions [3,4].

The gap between the working and reference electrodes is large, typically from 1 to 2 mm in conventional electrochemical measurements. But in the thin layer geometry, it is typically less than 10 μm. Since the gap between the electrodes can be adjusted smoothly, the CDE arrangement can be employed for many purposes. A scheme of the controlled-distance electrochemistry (CDE) arrangement is shown in Fig. 1.

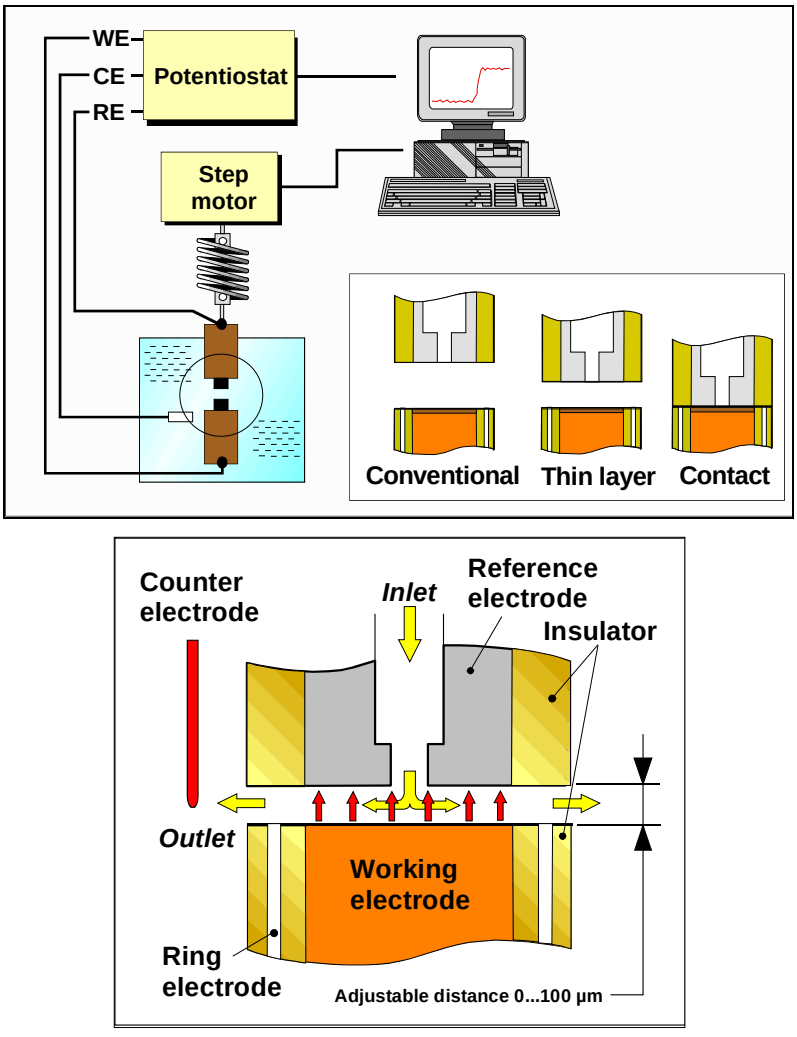

Figure 1. A scheme of the controlled-distance electrochemistry (CDE) arrangement and its different applications.

Electrochemical techniques using CDE have been applied in the solving of plant-specific problems in simulated VVER and BWR conditions. However, their applicability had not been tested for Zircaloy-2 fuel cladding. Furthermore, the chemical composition does not solely determine the corrosion properties of a fuel cladding tube. The manufacturing process is an important factor too. The current project targets on developing and verifying experimental techniques to enhance capabilities for comparing candidate fuel cladding products.

1.2 Aim of the study

The purpose of this work was to clarify whether the differences in the electric and electrochemical properties of the oxide films formed on five different types of Zircaloy-2 alloys can be correlated with their different second phase particle (SPP) structures and hydrogen contents. The work consisted of electrochemical impedance spectroscopic (EIS), contact electric impedance (CEI) and contact electric resistance (CER) measurements. They were performed using the controlled distance electrochemistry (CDE) arrangement in simulated BWR coolant conditions at a temperature of 300ºC.

The study has been thoroughly reported in a separate report. This paper provides an overview of the activities and findings during the project year 2000.

2. Experimental

2.1 Test specimens

The test matrix consisted of five different tube specimens. The initial condition was as-fabricated. Two of the three tubes were heat treated and two were charged with hydrogen. The specimens were finally characterised for the average size and size distribution of the second phase particles and for their hydrogen content by the fuel vendor. The characteristics of the tube materials are shown in Table 1.

2.2 Simulation of coolant conditions

The controlled-distance electrochemistry (CDE) arrangement was inserted into an autoclave. The autoclave was connected to a high-temperature re-circulation loop, which was used to simulate BWR coolant conditions at 300°C and at 10 MPa. The oxygen content of the water was less than 300 ppb and the conductivity lower than 0.1 μScm^{-1}. The autoclave contained a working electrode made of one of the Zircaloy specimens, an Ir reference electrode, a Pt counter electrode and an external pressure-balanced AgCl/Ag reference electrode filled with 0.01 M KCl.

The conditions in the loop after the autoclave were monitored by using a separate high-temperature measurement cell containing sensors for the pH, conductivity and redox potential (Pt) of the water, for the corrosion potentials of Zircaloy-2 and AISI 316 NG stainless steel and a AgCl/Ag reference electrode (0.01 mol/l KCl). The measurements were carried out at an open circuit potential.

Table 1. Characteristics of the studied Zircaloy-2 specimens.

Specimen	Treatment	Annealing / Hydrogen content	Average SPP size (μm)
A	as-fabricated		0.049
B	annealed	2 h in 750 °C	0.122
C	annealed	8 h in 750 °C	0.174
D	hydrogen charged	appr. 500 ppm	
E	hydrogen charged	appr. 1000 ppm	

2.3 Electrochemical measurements in the Controlled-distance electrochemistry (CDE) arrangement

The CDE arrangement was applied to various electrochemical measurements. The thin-layer electrochemical impedance spectrum (TLEIS) was used to characterise the oxidation and reduction kinetics and mechanisms of the Zircaloy specimens, as well as the properties of Zr oxide films even in the low-conductivity aqueous environment. The CDE arrangement was also used to measure the contact electric resistance (CER) and contact electric impedance (CEI) spectra of the oxide films alone.

In the beginning of these experiments the surface of the working electrode, i.e. the Zr specimen, and an Ir quasi reference electrode were brought into tight contact with each other to prevent the exposure of the specimen to the water during heating up of the autoclave. After the temperature was increased up to 300ºC the CER measurement was started and continued during each test run.

The specimens remained in the autoclave for 3 to 4 days after which the electrochemical impedance spectra were measured. The TLEIS of the combined system of the electrolyte and the Zr oxide film were measured by reducing the distance between the electrodes from approximately 20 μm to less than 0.3 μm. The electrochemical impedance measurements in the contact mode (CEI) were carried out after the TLEIS measurements.

3. Results and discussion

After removing the specimens from the autoclave their oxide thickness values were determined from metallographic samples by using a scanning electron microscope (SEM). After the three to four-day exposures at 300°C the oxide film thickness of the specimens was around 0.4 μm, except for one specimen which exhibited an uneven, over 1 μm thick oxide.

The CER measurements showed that the resistance of the growing oxide layers generally decreased sharply after reaching a maximum for the first time. This may be an indication of an electrical short-circuit of a very thin oxide layer. A comparison between the resistance vs. time curves during the first two hours of oxidation for the studied alloys is shown in Fig. 2.

The electrochemical impedance measurements performed in a thin-layer configuration (i.e. the TLEIS measurements) turned out to provide basically similar information of the corrosion reactions and transport processes of the zirconia layers as the CEI measurements, as shown in Figs. 3 and 4 for specimen A. The close correspondence between these spectra may indicate that in the case of oxide covered Zr alloys, the two types of impedance responses are largely controlled by same phenomena.

The similarity between the two spectra may also be due to the high resistance of the zirconia, which leads to a situation where the current passes mainly through the solution phase. It is probable that this water remaining between the sample and the Ir tip in the contact situation acts as a thin solution layer through which the current passes because of the high resistance at the solid contact points.

If this is true, the measurements in the CEI configuration were actually measurements in a thin-layer configuration. The corrosion process of these Zr alloys is not blocked in the contact mode because of the fact that the contact area between two rough solid surfaces is considerably smaller than their nominal geometrical area. This means that the space between the contact surfaces is filled with the water phase.

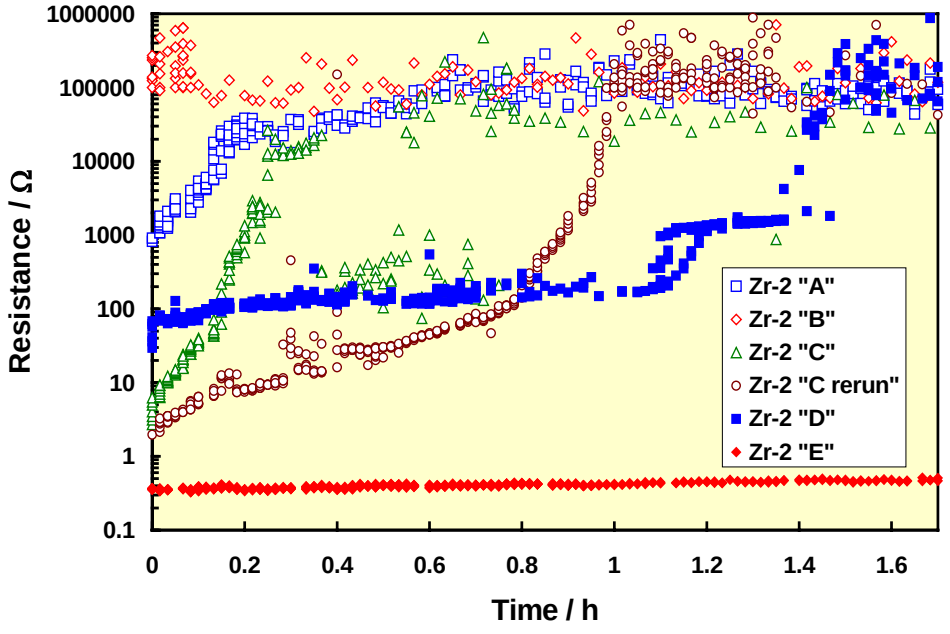

Figure 2. Dependence of the resistance of the oxide film on the studied Zr-2 alloys on time, as measured by the CER technique during the initial period of oxidation at 300°C.

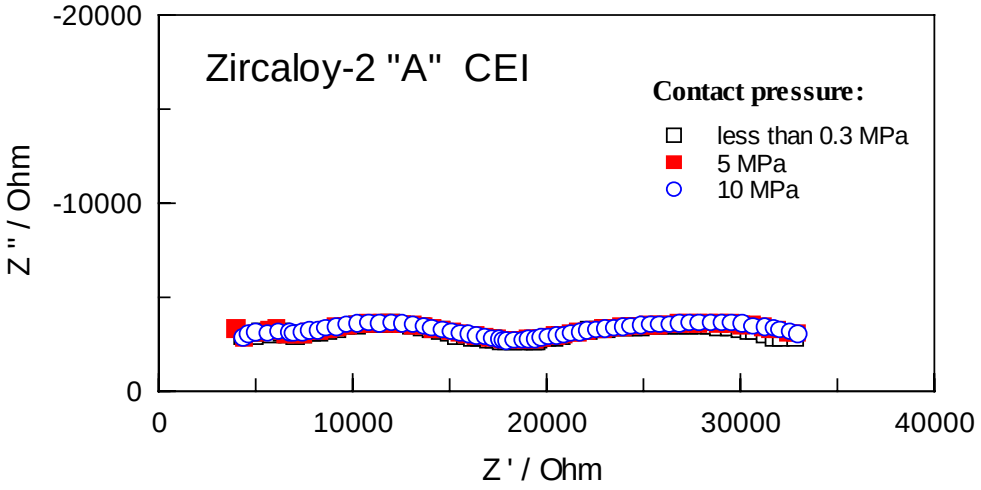

Figure 3. Contact electrochemical impedance spectra (CEI mode) of sample "A" at different contact pressures between the Zr-2 specimen and the Ir quasi reference electrode

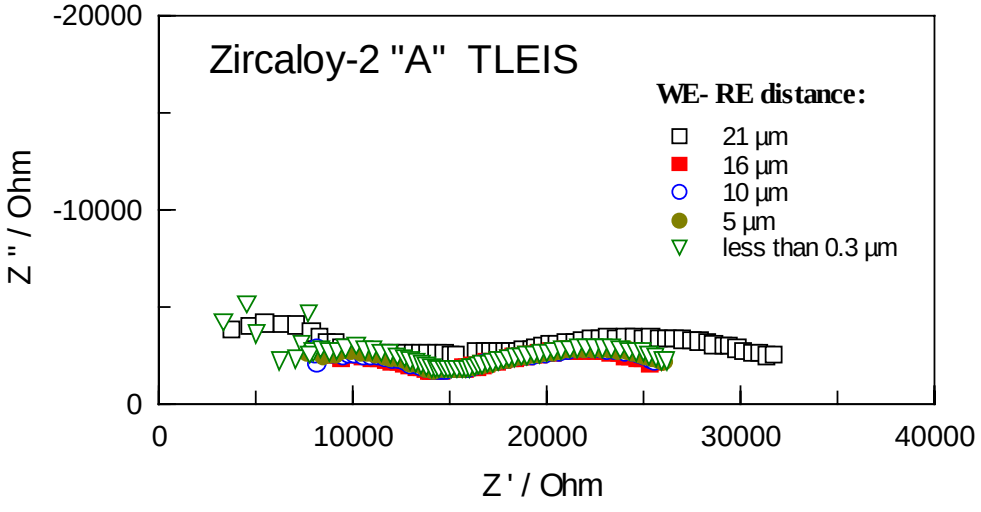

Figure 4. Thin-layer electrochemical impedance spectra (TLEIS) of sample "A" at different distances between the Zr-2 specimen and the Ir quasi reference electrode.

4. Conclusions

The results obtained so far do not enable discerning between the transport properties of the oxides formed on the different Zircaloy specimens. This would have required data measured both in the thin-layer (TLEIS) mode and in a real contact mode (CEI). Because of shortcomings of the current system, the latter condition was not reached in these experiments. Consequently, the obtained information is no sufficient to be used as input data for the planned modelling procedure.

To gain complementary information on the zirconia corrosion layers, an alternative measurement configuration should be used in order to eliminate the effects of the corrosion reaction, which takes place in BWR water. Contact electric impedance measurements in gaseous atmospheres up to 300°C or a conventional impedance measurements in a neutral electrolyte at room temperature are proposed as the next step.

References

1. Garzarolli, F., Schumann, R. and Steinberg, E. 1994. Corrosion optimised Zircaloy for BWR fuel elements. Proc. 10th Int. Symp. on Zirconium in Nuclear Industry, PAIKKA 1994, ASTM-STP 1245. Pp. 709–723.

2. Blat, M. and Noel, D. 1996. Proc. 11th Int. Symp. on Zirconium in Nuclear Industry, Garmisch-Partenkirchen, Germany 1996. ASTM-STP 1295. Pp. 319–335.

3. Bojinov, M., Hinttala, J., Laitinen, T., Muttilainen, E., Mäkelä, K., Reinvall, A., Saario, T. and Suksi, S. Development of electrochemical techniques to study oxide films on construction materials in high temperature water. JAIF International Conference on Water Chemistry in Nuclear Power Plants, 13–16 Oct. 1998, Kashiwazaki, Japan. P. 111.

4. Bojinov, M., Fabricius, G., Kinnunen, P., Laitinen, T., Mäkelä, K., Saario, T. and Sundholm, G. EIS and CER study of the passivity of Ni-Cr alloys in a neutral solution at 200°C, 7th International Symposium on Electrochemical Methods in Corrosion Research, 28.–31. May 2000, Budapest, Hungary, p. 91.

Modelling of Material Ageing

Yu. Jagodzinski, H. Hänninen
Helsinki University of Technology
Espoo, Finland

1. Introduction

Within the frameworks of the project ”Rakenteellisen käyttöiän hallinta” in 2000, Laboratory of Engineering Materials has been conducting research in the field of degradation of mechanical properties of metals and alloys resulting from the interaction with environment in accordance with the outlined directions.

2. TGSCC mechanism

Further analyses of the TGSCC mechanism were performed. OFHC copper was used as a research material for this study. The analysis of the creep data of OFHC copper after electrochemical polarization in NaNO2 solution has shown that:

- For the studied temperature range of 20–80°C the obtained creep curves can be qualitatively described by the Van der Vekken’s model. The quantitative agreement, has not, however, been obtained;
- Activation analysis of environmentally assisted creep of OFHC copper in $NaNO_2$ solution gives the value of 0,2–0,3 eV for the activation energy, which is significantly smaller than the energy of self-diffusion in copper (0,7 eV);
- The observed quantitative discrepancy on the environmentally assisted creep in OFHC demands for the development of a new model, which will take correctly the interaction between the defects in the subsurface layers of copper and the growing oxide scale into account.

An X-ray study of the stresses induced in the subsurface layers by oxide scale growth is in progress.

3. Hydrogen in Inconel 600 alloys

The behavior of hydrogen in Inconel 600 alloys with controlled carbon content was studied. Total number of measurements 65+. It was shown that carbon and hydrogen occupy different interstitial positions in the crystal lattice of Inconel 600 alloys – carbon prefers high-chromium sites, while hydrogen – high-iron positions. A presentation was made at 5th Workshop "Hydrogen isotopes in solids", Stockholm, May, 2000.

4. Internal friction of low alloy steels

The low-temperature internal friction of low alloy steels was studied in WB36 and MF342 steels. Total number of measurements 20. The measurements were also performed on cold-worked and hydrogen charged steels and revealed several additional peaks. A set of measurements of amplitude dependent internal friction was undertaken. The frequency dependences of ADIF were obtained. Time dependent internal friction was measured at different strain amplitudes. Abnormal behavior of internal friction – growth with time – was detected in MF342 LAS at the strain of 2.75×10^{-4}, while at all other measured strains, both smaller and larger, internal friction decreases with time. The phenomenon will be studied more attentively. The experiments on WB36 samples, prepared from the components been in service are in preparation.

5. Thermal desorption of hydrogen

As a result of the study of hydrogen effects, a new method for studying thermal desorption of hydrogen from metals, based on internal friction technique, has been developed. The method is based on the kinetics study of internal friction peaks related to the hydrogen outgassing. A presentation was made at 5th Workshop "Hydrogen isotopes in solids", Stockholm, May, 2000. A publication in the proceedings of the Workshop in Physica Scripta is in preparation.

Acknowledgements

This paper is part of a cluster of joint R&D projects on plant life management and ageing of metallic components, which is realised mainly by VTT in 1999–2002. The projects are funded by Tekes, the National Technology Agency, Teollisuuden Voima Oy, Fortum Power and Heat, Fortum Engineering, VTT and to smaller extent also by other energy and process industry in Finland. A significant amount of background information originates from the Finnish research programme on nuclear power plant safety (Finnus).

References

1. Jagodzinski, Yu., Hänninen, H., Tarasenko, O. and Smuk, S. Interaction of Hydrogen with Dislocation Pile-Ups and Vacancy Generation at Plastic Deformation. Scripta Materialia (43), 2000, No. 3, pp. 245–251.

2. Smuk, S., Hänninen, H., Jagodzinski, Yu., Tarasenko, O. and Aaltonen, P., Hydrogen Distribution and its Interaction with Lattice Defects in Inconel 600 Alloy Studied by Internal Friction. Presented at 5th International Workshop “Hydrogen Isotopes in Solids”, May, 17–19, 2000, Stockholm, Sweden. 9 p. (joint report, part of Finnus)

3. Jagodzinski, Yu., Hänninen, H. and Tarasenko, O. A new method for studying thermal desorption of hydrogen from metals based on internal friction technique. Presented at 5th International Workshop “Hydrogen Isotopes in Solids”, May, 17–19, 2000, Stockholm, Sweden. 17 p. (joint report, part of Finnus)

4. Jagodzinski, Yu., Hänninen, H., Smuk, S. and Tarasenko, O. Hydrogen-Probe Mechanical Spectroscopy for Studying Local Ordering in Concentrated Substitutional Alloys. Presented at ICIFUAS-12, Buenos Aires, Argentine, July 19–23, 1999. Journal of Alloys and Compounds 2000, 310, No. 1–2, pp. 200–204.

5. Jagodzinski, Yu., Aaltonen, P., Smuk, S., Tarasenko, O. and Hänninen, H. Internal friction study of environmental effects on metals and alloys. Presented at ICIFUAS-12, Buenos Aires, Argentine, July 19–23, 1999. Journal of Alloys and Compounds, 2000, 310, No. 1–2, pp. 256–260.

6. Tähtinen, S., Jagodzinski, Y., Tarasenko, O., Smuk S. and Hänninen H. Application of the internal friction method to studying microstructural effects in fusion materials. J. Nuclear Materials, 2000, (283–287), pp. 255–258.

Appendix A:
List of publications 1999–2001

Balachov, I., Bojinov, M., Laitinen, T., Muttilainen, E., Mäkelä, K. Reinvall, A., Saario, T. & Sirkiä, P. Correlations between the stability of oxide films in simulated BWR crack conditions, $SO_4$2-enrichment and cracking susceptibility. 8th Int. Conference on Water Chemistry of Nuclear Reactor Systems. Bournemouth, UK. October 22–26, 2000.

Bojinov, M., Buddas, T., Halin, M., Laitinen, T., Mäkelä, K., Mäkelä, M., Saario, T., Sirkiä, P. & Tompuri, K. Stability of oxide films on stainless steel during simulated PWR shutdown and start-up conditions. 8th Int. Conference on Water Chemistry of Nuclear Reactor Systems. Bournemouth, UK. October 22–26, 2000.

Bojinov, M., Hansson-Lyyra, L., Laitinen, T., Mäkelä, K., Saario, T. & Sirkiä, P. Development of the structural integrity of nuclear power plants. Zircaloy-2 cladding materials - effect of microstructure on corrosion properties. Research Report BVAL62-001086 prepared for Teollisuuden Voima Oy and Tekes. VTT Manufacturing Technology. 11 p. + app.

Bojinov, M., Hansson-Lyyra, L., Laitinen, T., Mäkelä, K. & Saario, T. In-situ studies of the oxide film properties on BWR fuel cladding materials. 13th International Symposium on Zirconium in the Nuclear Industry. Annecy, France. June 10–14, 2001.

Bojinov, M., Kinnunen, P., Laitinen, T., Mäkelä, K., Saario, T. & Sirkiä, P. Monitoring of high-temperature water chemistry and characterisation of oxide films on material samples exposed to BWR coolant at Olkiluoto 1. VTT Manufacturing Technology. Research Report BVAL67-011125 prepared for Teollisuuden Voima Oy and Tekes. 19 p.

Bojinov, M., Kinnunen, P., Laitinen, T., Mäkelä, K., Saario, T. & Sirkiä, P. Corrosion behaviour of steam generator tube materials inside the sludge pile material. VTT Manufacturing Technology. Research Report BVAL67-011112 prepared for Fortum Power and Heat Oy, Loviisa. 26 p.

Bojinov, M., Ehrnstén, U., Kinnunen, P., Laitinen, T., Mäkelä, K., Saario, T., Sirkiä, P. & Taivalaho, L. Activity incorporation into the oxide films on stainless steel samples exposed to primary coolant in Loviisa 1 unit. Research Report BVAL67-011113 prepared for Fortum Power and Heat Oy, Loviisa. 29 p.

Bojinov, M., Ehrnstén, U., Kinnunen, P., Laitinen, T., Mäkelä, K., Saario, T., Sirkiä, P. & Toivonen, A. Influence of sulphate ions on the oxide films on AISI 316 L(NG), Inconel alloy 182 and Inconel alloy 82 in simulated BWR crack conditions. Ex situ analysis of oxide films formed in simulated crack chemistry conditions. Research Report BVAL67-011131 prepared for Teollisuuden Voima Oy.

Bojinov, M., Ehrnstén, U., Kinnunen, P., Laitinen, T., Mäkelä, K., Saario, T., Sirkiä, P., Taivalaho, L., Buddas, T., Halin, M. & Tompuri, K. Activity incorporation into the oxide films on stainless steel samples exposed to primary coolant in Loviisa 1 unit. In this book. P. 211–240.

Bojinov, M., Kinnunen, P., Laitinen, T., Mäkelä, K., Saario, T., Sirkiä, P., Helin, M., Muttilainen, E., Nousiainen, P. & Reinvall, A. Monitoring of BWR water chemistry and oxide films at Olkiluoto 1. In this book. P. 179–194.

Bojinov, M., Laitinen, T., Mäkelä, K., Mäkelä, M., Saario, T., Sirkiä, P., Buddas, T., Halin, M. & Tompuri, K. Stability of oxides on stainless steel during simulated PWR shutdown and start-up. In this book. P. 195–210.

Bojinov, M., Laitinen, T., Mäkelä, K., Saario, T., Sirkiä P., Toivonen, A., Muttilainen, E., Reinvall, A. & Balachov, I. Protectiveness of oxide films in simulated BWR crack conditions, SO_4^{2-} enrichment and cracking susceptibility. In this book. P. 169–178.

Bojinov, M.,. Hansson-Lyyra, L., Laitinen, T., Mäkelä, K. & Saario, T. In-situ Studies of the Oxide Film Properties on BWR Fuel Cladding Materials. In this book. P. 255–264.

Ehrnstén, U., Karjalainen-Roikonen, P., Nenonen, P., Ahlstrand, R., Hietanen, O., Timofeev, B. T. & Bloomin, A. A. 2000. Properties of cast ti-stabilised stainless steel after long-term ageing. The 6th Int. Conf. Material issues in design, manufacturing and operations of nuclear power plants equipment. CRISM "Prometey". June 19–23, 2000. 8 p.

Ehrnstén, U., Nenonen, P., Aaltonen, P., Teräsvirta, R. & Hietanen, O. Intergranular Cracking of an Irradiated Ti-stabilized Austenitic Stainless Steel Spacer Grid Sleeve from a VVER-440 reactor. Presented at 9th Int. Conf. Environm. Degradation of Materials in Nuclear Power Systems – Water Reactors, Newport Beach, CA, USA, Aug. 1–5, 1999. 8 p.

Hänninen, H., Aaltonen, P., Jagodzinski, Yu., Tarasenko, O. & Smuk, S. “On the mechanism of environmentally assisted cracking of pure copper in $NaNO_2$ solution”. Presented at Int. Conf. Environ. Degradation of Engineering Materials ´99, Gdansk-Jurata, Poland, Sept. 19–23, 1999.

Hänninen, H., Jagodzinski, Yu., Tarasenko, O., Vilpas, M. & Aaltonen, P. XVO 2000 subproject at TKK: modelling of material ageing. Bulletin. 2 p.

Jagodzinski, Yu., Hänninen, H., Smuk, S. & Tarasenko, O. “Hydrogen effects in FCC metals”. Presented at ICG-SCC seminar, Turku, Finland, May 18–20, 1999.

Jagodzinski, Yu., Hänninen, H., Smuk, S. & Tarasenko, O. “Hydrogen-Probe Mechanical Spectroscopy for Studying Local Ordering in Concentrated Substitutional Alloys”. Presented at ICIFUAS-12, Buenos Aires, Argentine, July 19–23, 1999.

Jagodzinski, Yu., Aaltonen, P., Smuk, S., Tarasenko, O. & Hänninen, H. “Internal friction study of environmental effects on metals and alloys”. Presented at ICIFUAS-12, Buenos Aires, Argentine, July 19–23, 1999.

Jagodzinski, Yu., Hänninen, H., Tarasenko, O. & Smuk, S. “Interaction of Hydrogen with Dislocation Pile-Ups and Vacancy Generation at Plastic Deformation”. Presented at Int. Conf. Environ. Degradation of Engineering Materials ´99, Gdansk-Jurata, Poland, Sept. 19–23, 1999. Article has been submitted to Scripta Materialia.

Jagodzinski, Yu., Hänninen, H. & Tarasenko, O. A new method for studying thermal desorption of hydrogen from metals based on internal friction technique. To be published in Physica Scripta in 2001. 17 p.

Jagodzinski, Yu. & Hänninen, H. Modelling of Material Ageing. In this book. P. 265–268.

Kauppinen, P., Pitkänen, J. & Kuusinen, P. Developments in mechanised ultrasonic inspection and qualification of NDE. In this book. P. 91–96.

Kohopää, J., Tamminen, A., Valo, M. & Solin, J. Innovations on life management of VVER reactor pressure vessels. In this book. P. 107–126.

Laitinen, T., Mäkelä, K., Sirkiä, P. & Mäkelä, M. Olkiluoto 1:n vesikemian monitorointi- ja oksidinäytekennon tarkastusaineisto. VTT Manufacturing Technology research report VAL67-001298 prepared for Teollisuuden Voima Oy. (in Finnish).

Marquis, G. & Solin, J. Thermal fatigue of NPP components: potential multiaxial, environmental and small cycle effects. In this book. P. 67–89.

Moilanen, P., Arilahti, E., Bojinov, M., Laitinen, T., Mäkelä, K., Mäkelä, M., Mäkinen, R., Saario, T., Sirkiä, P. & Toivonen, A. Pneumatic servo-controlled fracture resistance measuring device (PSFM-Device) and contact electric resistance measuring device (CER Device). Enlarged Halden Programme Group Meeting. Loen, NO, 24–29 May 1999, 1999. 16 p.

Muttilainen, E., Hietanen, O., Aaltonen, P. & Ehrnstén, U. 2001. Prevention of stress corrosion cracking in piping welds. In this book. P. 159–168.

Muttilainen, E., Hietanen, O., Aaltonen, P. & Ehrnstén, U. 2001. Prevention of stress corrosion cracking in piping welds. In: Hietanen, S. & Auerkari P., eds., BALTICA V, Condition and Life Management for Power Plants. Espoo, Technical Research Centre of Finland, VTT Symposium 212. Pp. 681–688.

Mäkelä, K., Beverskog, B. & Aaltonen, P. In-core Pd reference electrode to be used in LWRs. Report VALB443, VTT Manufacturing Technology, Espoo, 2000. (draft 13.4.2000). 15 p.

Paussu, R., Pitkänen, J., Särkiniemi, P., Jeskanen, H. & Elsing, B. Ultrasonic inspection of a reactor pressure vessel from outside surface. In this book. P. 97–106.

Pelli, R. Uusia korjaus- ja parannusmenetelmiä ydinvoima-laitosmateriaaleille. Report VALB62-001050, VTT Manufacturing Technology. 23 p.

Pelli, R., Hansson-Lyyra, L. & Taivalaho, L. Characterisation of texture of General Electric NF Triclad and Hife barrier cladding tubes. Reseach Report No. VAL62-012522 PREPARED for TVO. 19 p.

Pelli, R., Hansson-Lyyra, L. & Taivalaho, L. Characterisation of texture of Framatome ANP GmbH cladding tubes. Reseach Report No. VAL62-012573 prepared for TVO. 5 p.

Pelli, R., Hansson-Lyyra, L. & Taivalaho, L. Characterisation of texture of Westinghouse Atom LK3 cladding tubes. Reseach Report No. VAL62-012574 prepared for TVO. 5 p.

Raiko, H., Lipponen, A. & Talja, H. Load-case and -combination database. Paper to be presented at SMiRT 16, Washington, USA, 12.–17.8.2001.

Saarenheimo, A., Talja, H. & Haapaniemi, H. Updating dynamic FE analysis models with experimental data: applications. VTT Manufacturing Technology BVAL64-001033. 32 p.

Saarenheimo, A., Silde, A. & Lindholm, I. A reinforced concrete structure under detonation conditions. 16th SMiRT Conference. Washington DC, USA. August 12–17, 2001. 8 p.

Saario, T., Mäkelä, K., Laitinen, T. & Bojinov, M. Effects of acid-oxidising conditions on oxide films on stainless teel during a simulated shutdown and start-up of a VVER plant. VTT Manufacturing Technology research report VAL67-001316. 27 p.

Saario, T., Sohlberg, S. & Solin, J. (toim.) Ydinvoimalaitosten korroosio ennakoidaan tutkimuksella ja kansainvälisellä yhteistyöllä. Enegia 1/2001, pp. 68–69.

Sirkiä, P., Saario, T., Mäkelä, K., Laitinen, T. & Bojinov, M. Changes in oxide films on Ti-stabilised stainless steel samples during exposure to primary coolants at Loviisa units. VTT Manufacturing Technology research report VAL67-001323. 20 p.

Smeekes, P., Talja, H., Saarenheimo, A. & Haapaniemi, H. 2001. Piping vibration management combining measurements and numerical simulation. In: Hietanen, S. & Auerkari P., eds., BALTICA V, Condition and Life Management for Power Plants. Espoo, Technical Research Centre of Finland, VTT Symposium 212. Pp. 705–714.

Smeekes, P., Lipponen, A., Talja, H. & Raiko, H. 2001. Integrated approach and database system for managing load cases and integrity of piping sysytems. In: Hietanen, S. & Auerkari, P., eds., BALTICA V, Condition and Life Management for Power Plants. Espoo, Technical Research Centre of Finland, VTT Symposium 212. Pp. 689–704.

Smeekes, P., Talja, H., Saarenheimo, A. & Haapaniemi, H. Numerical simulation of piping vibrations using modal correlation. 16th SMiRT, Washington DC, USA. August 12–17, 2001. 8 p.

Smeekes, P., Lipponen, A., Raiko, H. & Talja, H. The TVO pipeline analysis and monitoring system. 16th SMiRT, Washington DC, USA. 12.–17. 8. 2001. 8 p.

Smeekes, P., Lipponen, A., Talja, H. & Raiko, H. Integrated Approach and Database System for Managing Load Cases and Integrity of Piping Systems. In this book. P. 35–54.

Smeekes, P., Talja, H., Saarenheimo, A. & Haapaniemi, H. Piping Vibration Management Combining Measurements and Numerical Simulation. In this book. P. 55–66.

Smuk, S., Hänninen, H., Jagodzinski, Yu., Tarasenko, O. & Aaltonen, P. "Comparison of Hydrogen Effects on Alloy 600 and 690". Presented at 9th Int. Conf. Environm. Degradation of Materials in Nuclear Power Systems – Water Reactors, Newport Beach, CA, USA, Aug. 1–5, 1999.

Smuk, S., Hänninen, H., Jagodzinski, Yu., Tarasenko, O. & Aaltonen, P. "Internal friction study of hydrogen effects in Alloy 600 and 690". Presented at European Structural Integrity Society ESIS TC 10 Hydrogen Degradation committee seminar, Truskavets, Ukraine, Sept. 16–18, 1999.

Smuk, S. Application of Internal Friction Method for Studying Point Defect Behaviour in Engineering Materials. Acta Polytechnica Scandinavica. Mechanical Engineering Series No. 140. Helsinki University of Technology. 100 p.

Smuk, S., Hänninen, H., Yagodzinskyy, Yu., Tarasenko, O. & Aaltonen, P. Hydrogen distribution and its interaction with lattice defects in inconel 600 alloy studied by internal friction. To be published in Physica Scripta in 2001. 9 p.

Solin, J. "R & D for corrosion management." ENERTEC Special Helsinki Fair Issue 2000. Pp. 8–9.

Solin, J. "R & D for plant life management." Energy in Finland 2000. Pp. 76–77. (Annual special issue of the Finnish journal Energia)

Solin, J. (ed.) Plant life managemet (XVO) report 1999. VTT Research Notes 2077, Technical Research Centre of Finland, Espoo 2000. 68 p. + app. 3 p.

Solin, J. & Rintamaa, R. 2001. Joint research for condition and life management of NPP components. In: Hietanen, S. & Auerkari P., eds., BALTICA V, Condition and Life Management for Power Plants. Espoo, Technical Research Centre of Finland, VTT Symposium 212. Pp. 647–663.

Solin, J., Rintamaa, R. Hakala, J. Kohopää, J. & Tamminen, A. Joint research for operability and life management of NPP components. In this book. P. 7–34.

Talja, H., Solin, J. & Rintamaa, R. An approach to systematic structural lifetime management. Paper to presented at Int. Conf. Nuclear Energy in Central Europe 2000. Bled, Slovenia. September 11–14, 2000.

Talja, H., Saarenheimo, A. & Haapaniemi, H. Updating dynamic FE analysis models with experimental data, a literature study. VTT Manufacturing Technology report BVAL64-001017.

Tamminen, A., Kohopää, J., Valo, M. & Solin, J. 2001. Innovations on life management of VVER reactor pressure vessels. In: Hietanen, S. & Auerkari P., eds., BALTICA V, Condition and Life Management for Power Plants. Espoo, Technical Research Centre of Finland, VTT Symposium 212. Pp. 665–680.

Toivonen, A., Moilanen, P., Pyykkönen, M., Tähtinen, S., Rintamaa, R. & Saario, T. The feasibility of small size specimens for testing of environmentally assisted cracking of irradiated materials and of materials under irradiation in reactor core. Nuclear Engineering and Design 193 (1999), pp. 309–316.

Toivonen, A. & Aaltonen, P. Relation between loading parameters and SCC propagation rate in elastic plastic loading conditions on small precracked specimens. ICG/EAC Meeting, Williamsburg, 10.–14.4.2000.

Toivonen, A. Effects of thermal history, BWR coolant sulphate ion concentration, crack orientation and loading type on stress corrosion crack propagation in Inconel Alloys 82 and 182. Interim Report for Teollisuuden Voima Oy. Espoo, 2000. 14 p. (in Finnish)

Toivonen, A., Aaltonen, P., Nenonen, P., Ehrnstén, U., Käki, A., Valo, M., Kukkonen, A. & Hietanen, O. Irradiation assisted stress corrosion cracking of core components. In this book. P. 241–253.

Valo, M., Koukkari, P. & Pitkänen R., 2000. Validation of melting alloy temperature monitors for RPV surveillance. VTT Manufacturing Technology research report VAL63-00xxxx.

Valo, M. The year 2000 contribution towards quantitative estimation of irradiation and re-irradiation effects on material toughness. In this book. P. 141–158.

Valo, M., Shtrombakh, Y., Kryukov, A., Vodenicharov, St. & Kohopää, J. Tentative re-embrittlement analysis for WWER-440 welds after annealing. In this book. P. 127–140.

Published by

Vuorimiehentie 5, P.O.Box 2000, FIN–02044 VTT, Finland
Phone internat. +358 9 4561
Fax +358 9 456 4374

Series title, number and report code of publication

VTT Symposium 218
VTT–SYMP–218

Author(s)
Jussi Solin (Ed.)

Title

Plant Life Management, Midterm status of a R&D project

Abstract

Experimental and analytical research is being carried out in an industrially oriented project cluster dealing with estimating and managing lifetime of critical structures and components in energy industry. The research topics include systematic component lifetime management, lifetime of pressure bearing components, piping vibrations and integrity management, management of materials ageing, non-destructive inspection, water chemistry, oxide films and their role in service reliability and build-up of activity levels, stress corrosion cracking in Inconel welds, irradiation assisted stress corrosion cracking of core components, development of crack growth testing methods as well as the mechanisms of environmentally assisted cracking.

This Symposium is a compilation of selected papers describing the midterm status of the projects after two years of research.

Keywords
nuclear power plants, service life, life (durability), structures, stress corrosion cracking, aging (metallurgy), piping, vibrations, reliability

Activity unit
VTT Manufacturing Technology, Materials and Structural Integrity,
Kemistintie 3, P.O.Box 1704, FIN–02044 VTT, Finland

ISBN	Project number
951–38–5727–1 (soft back ed.) 951–38–5728–X (URL: http://www.inf.vtt.fi/pdf/)	

Date	Language	Pages	Price
October 2001	English	268 p. + app. 9 p.	F

Name of project	Commissioned by
Rakenteiden käytettävyys ja käyttöiän hallinta	TVO, Fortum

Series title and ISSN	Sold by
VTT Symposium 0357–9387 (soft back ed.) 1455–0873 (URL: http://www.inf.vtt.fi/pdf/)	VTT Information Service P.O.Box 2000, FIN–02044 VTT, Finland Phone internat. +358 9 456 4404 Fax +358 9 456 4374